TARGETING THE MTOR SIGNALLING PATHWAY FOR PREVENTION AND THERAPY OF TUBEROUS SCLEROSIS IN MOUSE MODELS

Maria Kalogerou

2013

Thesis submitted to Cardiff University in fulfillment of the requirements for the degree of Doctor of Philosophy

Summary

Tuberous sclerosis is an autosomal dominant genetic disorder characterised by the development of benign tumours in multiple organs. It is caused by mutations in the *TSC1* or *TSC2* tumour suppressor gene, leading to hyperactivation of mTOR signalling in affected tissues. Rapamycin and its analogues are mTOR inhibitors and have been used to treat tuberous sclerosis in both pre-clinical and clinical trials. However, tumours usually relapse after drug withdrawal. The aims of this project were to identify novel agents and strategies for prevention and therapy of tuberous sclerosis using mouse models.

First T2 weighted MRI was evaluated for assessment of renal lesions in *Tsc1*$^{+/-}$ and *Tsc2*$^{+/-}$ mouse models. MRI identified all types of Tsc-associated renal lesions in both Tsc mouse models. The smallest detectable lesions were <0.1 mm^3. Eighty five percent of all renal lesions detected in a first scan at 12 months of age were re-identified in a second scan 2 months later. Between the two scans, MRI revealed a significant increase in the total number and volume of lesions in 9 untreated mice. Compared to histological analysis, MRI detected most cysts and papillary tumours (64%) but only a minority of solid tumours (30%).

Metformin is a mild inhibitor of mTOR. The therapeutic effect of metformin on renal lesions in *Tsc1*$^{+/-}$ mice was investigated using T2 weighted MRI and histological analysis. Metformin treatment for 9 months had no significant effect on renal lesions in these mice.

Finally, the preventive effects on renal lesions in *Tsc2*$^{+/-}$ mice of rapamycin, metformin or both agents in combination were assessed using histological analysis. Treatment started from one month of age and continued for 7 to 9 months. Rapamycin or rapamycin plus metformin but not metformin alone effectively blocked the development of renal lesions including cysts, adenomas and carcinomas through the inhibition of mTOR signalling. These findings suggest that mTOR inhibition may be an effective strategy for preventing emergence of disease manifestations in tuberous sclerosis.

Declaration

This work has not previously been accepted in substance for any degree and is not concurrently submitted in candidature for any degree.

Signed ……..…… (candidate) Date ……

Statement 1

This thesis is being submitted in partial fulfillment of the requirements for the degree of PhD.

Signed ……..……..…… (candidate) Date ……

Statement 2

This thesis is the result of my own independent work/investigation, except where otherwise stated. Other sources are acknowledged by explicit references.

Signed ……..…… (candidate) Date ……

Statement 3

I hereby give consent for my thesis, if accepted, to be available for photocopying and for inter-library loan, and for the title and summary to be made available to outside organisations.

Signed ……..…… (candidate) Date ……

Statement 4

I hereby give consent for my thesis, if accepted, to be available for photocopying and for inter-library loans after expiry of a bar on access previously approved by the Graduate Development Committee.

Signed ……..…… (candidate) Date ……

Acknowledgements

I would like to thank my supervisors Dr Ming Hong Shen and Prof Julian Sampson for their continued guidance and support. In particular, I would like to thank Dr Ming Hong Shen for his patience and invaluable advice and constructive criticism throughout my study.

I would like to thank Dr Yadan Zhang and Dr Paulina Samsel for help in animal work; Dr Jian Yang for help in molecular analysis, and all for their continuous encouragement throughout my project.

I am grateful to Mr Derek Scarborough for technical help in histological analysis; Dr John Potts for help with slide scanning; Dr David Griffiths for help with renal pathology; Prof Jerry Cheadle's team for developing the *Tsc1* mouse model and Prof David Kwiatkowski for provision of the *Tsc2* mouse model.

I would also like to thank all the other people in the Institute of Cancer Genetics who helped me in all ways and made me feel at home in Cardiff, in particular Dr Kayleigh Dodd, JP Hothi, Ellie Rad, Sara Seifan, Becky Harris, Dr Chris Smith, Hannah West and Dr Laura Thomas.

A big thank you is to my mum and dad, family and friends in Cyprus for their unconditional support and encouragement over the last few years. This wouldn't have been possible without you.

The project was supported by the Wales Gene Park and the Tuberous Sclerosis Association UK.

Abbreviations

4E-BP	4E (elF4E)-binding protein
5-aza-2-dC	5-aza-2-deoxycytidine
A	Adenine
aa	Amino acid
ACC	Acetyl-CoA carboxylase
ACTH	Adrenocorticotrophin hormone
ADHD	Attention deficit hyperactivity disorder
ADPKD	Autosomal dominant polycystic kidney disease
AML	Angiomyolipoma
AMPK	5' adenosine monophosphate-activated protein kinase
AP	Alkaline phosphatase
Bp	Base pair
BLI	Bioluminescence imaging
C	Cytosine
CaM	Calmodulin
CDK1	Cyclin-dependent kinase 1
CNS	Central nervous system
CP1	Carboxy-terminal tail of polycystin-1
CR	Cardiac rhabdomyoma
CT	Computed tomography
DEPTOR	DEP domain TOR-binding protein
DHPLC	Denaturing high performance liquid chromatography

DMSO	Dimethyl sulfoxide
DNA	Deoxyribonucleic acid
DPX	Dibutyl phthalate and xylene
DTT	Dithiothreitol
EDTA	Ethylenediaminetetraacetic acid
eIF4B	Eukaryotic translation initiation factor 4B
elF4E	Eukaryotic translation initiation factor 4E
elF4G	Eukaryotic translation initiation factor 4G
ERK	Extracellular signal-regulated kinase
ERM	Ezrin-radixin-moesin
FIT	Farnesyltransferase inhibitor
FKBP12	FK506-binding protein 12
FRAP	FK506 binding protein 12-rapamycin associated protein
G	Guanine
GAP	GTPase activating protein
GAPDH	Glyceraldehyde 3-phosphate dehydrogenase
GDP	Guanosine 5’-diphosphate
GEF	Guanine Exchange Factor
GEM	Genetically engineered model
GFAP	Glial fibrillary acidic protein
GLAST	Glutamate aspartate transporter
Glt-1	Glutamate transporter 1
Grb10	Growth factor receptor-bound protein 10
GSK3	Glycogen synthase kinase 3
GTP	Guanosine 5’-triphosphate

H&E	Haematoxylin and eosin
HA	Histological analysis
HCI	Hydrochloric Acid
HIF	Hypoxia-inducible factor
HRCT	High-resolution computed tomography
HRP	Horse radish peroxidase
IAP	Intracisternal A-particle
IFG	Insulin-like growth factor
IFN-γ	Interferon gamma
IHC	Immunohistochemistry
IKKβ	IκB kinase-β
ip	Intra-peritoneal injection
IQ	Intelligence quotient
IRS	Insulin receptor substrate
Kb	Kilobase
LAM	Lymphangioleiomyomatosis
LOH	Loss of heterozygosity
LeuRS	Leucyl-tRNA synthetase
LKB1	Liver-kinase B1
LTP	Long-term potentiation
MAPK	Mitogen-activated protein kinase
MEF	Mouse embryonic fibroblast
Micro-CT	Micro-computed tomography
MK2	MAPK-activated protein kinase 2
mLST8	Mammalian lethal with Sec-13 protein 8

MMPH	Multinodular multifocal pneumocyte hyperplasia
MRI	Magnetic resonance imaging
mSIN1	Mammalian stress-activated protein kinase-interacting protein 1
mTOR	Mammalian target of rapamycin
mTORC1	Mammalian target of rapamycin complex 1
mTORC2	Mammalian target of rapamycin complex 2
NaCl	Sodium chloride
NAFLD	Non-alcoholic fatty liver disease
NF-L	Neurofilament-Light chain
NMI	No mutation identified
OCT	Organic cation transporter
p90-RSK1	90 kDa Ribosomal protein S6 kinase 1
PCOS	Polycystic ovarian syndrome
PCR	Polymerase chain reaction
PDGF	Platelet derived growth factor
PDGFR	Platelet derived growth factor receptor
PDK1	Phosphoinositide-dependent kinase 1
PEComa	Perivascular epithelioid cell tumour
PEG-400	Polyethylene glycol 400
PET	Positron emission tomography
PFGE	Pulsed field gel electrophoresis
PI3K	Phosphatidylinositide 3-kinase
PIKK	Phosphoinositide 3-kinase-related kinase
PIP2	Phosphatidylinositol-4,5-bisphosphate
PIP3	Phosphatidylinositol-3,4,5-trisphosphate

PKB	Protein Kinase B
PKD	Polycystic kidney disease
PLT	Blood platelet
POF	Premature ovarian failure
PPAR	Peroxisome proliferator-activated receptor
PRAS40	Proline-rich AKT substrate 40 kDa
PROTOR	Protein observed with Rictor
PTEN	Phosphatase and tensin homolog
Q-PCR	Quantitative polymerase chain reaction
RAFT1	Rapamycin and FKBP12 target-1 protein
Raptor	Regulatory associated protein of mTOR
RCC	Renal cell carcinoma
REDD1	Regulated in development and DNA damage responses 1
Rheb	Ras homolog enriched in brain
Rictor	Rapamycin-insensitive companion of mTOR
RNA	Ribonucleic acid
RNase	Ribonuclease
RpS6	Ribosomal protein S6
Rpm	Revolutions per minute
RSK1	Ribosomal S6 kinase 1
SDS	Sodium dodecyl sulfate
SEGA	Subependymal giant cell astrocytoma
SEN	Subependymal nodule
SGCT	Subependymal giant cell tumour
SPECT	Single photon emission computed tomography

SREBP	Sterol Regulatory Element-Binding Protein
STAT3	Signal transducer and activator of transcription 3
T	Thymine
T2D	Type 2 Diabetes
TAE	Tris-acetate-EDTA
TBC1D7	Tre2-Bub2-Cdc16 1 domain family, member 7
TBS	Tris buffered saline
TE	Echo time
TFEB	Transcription factor EB
Tor	Target of rapamycin
TR	Repetition time
TSA	Trichostatin A
TSC	Tuberous sclerosis
TSC1	Tuberous sclerosis complex type 1
TSC2	Tuberous sclerosis complex type 2
UV	Ultraviolet
VEGF	Vascular endothelial growth factor
YY1-PGC1α	Yin Yang 1 peroxisome proliferator-activated receptor gamma coactivator-1α

Contents

List of figures

List of tables

CHAPTER ONE

General Introduction

1.1 Tuberous sclerosis

Tuberous sclerosis (TSC) is an autosomal dominant genetic disorder characterised by the development of hamartomatous growths in multiple organs.

1.1.1 History of the disease

Pierre François Rayer (1835) published an atlas of skin disorders including a drawing of a patient with numerous facial erythematous papules these are now thought to have been TSC associated facial angiofibromas. The first official report of TSC was published by Friedrich Daniel von Recklinghausen in 1862. He described a newborn presenting with cardiac tumours referred to as “myomata” and numerous cerebral “scleroses” (von Recklinghausen, 1862). Désiré-Magloire Bourneville in 1879 first described “sclérose tubéreuse des circonvolutions cérébrales” (“tuberous sclerosis of the cerebral convolutions”) after the death of a 15-year-old mentally subnormal female who suffered seizures and facial angiofibromas (Bourneville, 1880). Two years later, Bourneville and Brissaud (1881) reported a 4-year-old boy with seizures who presented with similar cortical manifestations (later called subependymal nodules) and died. The term “tuberous sclerosis complex” was first coined by Moolten (1942) to define a multi-systemic disorder involving not only the brain but also other organ systems such as the skin, heart, lungs, kidneys and eyes.

In 1905 Gaetano Perusini started to correlate the cardiac, renal, cerebral and dermal lesions observed in patients with TSC and later on, Heinrich Vogt (1908) suggested that the triad of seizures, mental retardation and adenoma sebaceum (facial angiofibromas) be used in the diagnosis of TSC. By 1920, van der Hoeve identified phakomas (retinal hamartomas) which occur in TSC, neurofibromatosis and von Hippel-Lindau diseases. Critchley and Earl (1932) published a detailed clinical review

of TSC, after examination of 29 TSC patients and emphasised the prevalence of hypomelanotic skin macules among the patients.

The invention of computed tomography (CT) for the head (1974), echocardiography and renal ultrasound scanning (1982) and magnetic resonance imaging (1984) provided non-invasive investigation into the pathology of TSC and enhanced its diagnosis, especially in patients not exhibiting Vogt's diagnostic triad (Lagos *et al*. 1967). Gomez (1988) later estimated that only 29% of TSC patients fulfilled Vogt's diagnostic criteria, 45% of patients presented with normal intelligence and 6% of patients analysed had none of the triad's features. By 1987, Fryer and colleagues localised a *TSC* gene, (later termed *TSC1*), chromosome 9q34.3 (Fryer *et al*. 1987), then in 1992; Kandt *et al.* reported the chromosomal localisation of a second *TSC* gene, *TSC2*, linked to chromosome 16p13.3 (Kandt *et al*. 1992). Cloning of the *TSC2* (The European Chromosome 16 Tuberous Sclerosis Consortium, 1993) and *TSC1* genes (van Slegtenhorst *et al*. 1997) revealed 198kDa and 130kDa predicted protein products which were named tuberin and hamartin respectively. A timeline illustrating the history of TSC is indicated in Table 1.1.

Table 1.1 Key events in the history of tuberous sclerosis (adapted from Gomez *et al*. 1999 and Kwiatkowski *et al*. 2010).

Year	Authors	Contribution
1835	Rayer	Published an atlas of facial skin lesions (possibly facial angiofibromas).
1862	Von Recklinghausen	Reported a case of a newborn with cardiac "myomata" and cerebral "scleroses".
1880	Bourneville	Discovered cortical "tuberosities".
1881	Hartdegen	Reported TSC cortical pathology.
1885	Balzer & Menetrier,	Reported and named "adenoma sebaceum".
1890	Pringle	
1901	Pellizzi	Underlined the dysplastic nature of TSC cerebral lesions.
1905	Perusini	Associated cerebral, renal, cardiac and dermal lesions in TSC patients.
1908	Vogt	Suggested the clinical "triad" in diagnosis of TSC.
1910	Kirpicznik,	Reported on the hereditary nature of TSC.
1913	Berg	
1914	Schuster	Found TSC patients lacking pathological characteristics of Vogt's triad (*forme fruste*).
1918	Lutenbacher	Referred to the involvement of the lung in TSC.
1920	Van der Hoeve	Identified TSC retinal phakomas.
1924	Marcus	Radiographic findings.
1932	Critchley & Earl	Reviewed clinical aspects of TSC and discovered hypomelanotic macules.
1942	Moolten	Applied the term "Tuberous Sclerosis Complex".
1967	Lagos & Gomez	38% of TSC patients exhibited normal intelligence.
1974		Development of computed tomography (CT) for the head.
1979	Gomez	Introduced new diagnostic criteria and declined Vogt's triad.
1982		Introduction of renal ultrasound and echocardiography.
1984		Demonstration of cortical tubers by Magnetic resonance imaging (MRI).
1987	Fryer *et al.*	Identification of the first TSC gene (*TSC1*) linked to 9q34.3.
1992	Kandt *et al.*	Identification of the second TSC gene (*TSC2*) linked to 16p13.3.
1993	The European Chromosome 16 TSC Consortium	Cloning of *TSC2*. The 198 kDa protein product named tuberin.
1994	Green *et al*., Carbonara *et al.*	Loss of heterozygosity revealed in renal angiomyolipomas, cardiac rhabdomyoma and giant cell astrocytomas.
1997	Van Slegtenhorst *et al.*	Cloning of *TSC1*. The 130 kDa protein product named hamartin.
2003	Tee *et al.*	Indicated that tuberin and hamartin interact to form a complex that negatively regulates mTOR signalling pathway.
2005	Kenerson *et al.*, Lee *et al.*	Sirolimus suppress the growth of renal lesions in Eker rats and mouse models.
2006	Franz *et al.*	Sirolimus treatment resulted in regression of subependymal giant cell astrocytomas.
2008	Bissler *et al.*	Sirolimus reduced the volume of renal angiomyolipoma.

1.1.2 Epidemiology of the disease

The use of the clinical 'triad' by Heinrich Vogt (1908) for TSC diagnosis resulted in a dramatic under estimation of the frequency of TSC. Based on this clinical 'triad', it was initially estimated to occur at a frequency of 1:100 000 live births. However, the disease extends beyond seizures, mental retardation and facial angiofibromas. Additionally, previous studies focused on TSC patients admitted to hospitals or asylums which would only have included the more severely affected patients (Brushfield and Wyatt, 1926). Further studies attempted to estimate not only the incidence (Ferraro and Doolittle, 1936; Penrose, 1938; Gastaut *et al*. 1965) but also the prevalence of TSC in the general population (Ross and Dickerson, 1943; Dawson, 1954; Paulson and Lyle, 1966; Zaremba, 1968). Gunther and Penrose (1935) found that the incidence of TSC in five hospitals for the mentally handicapped was 1:300 and the estimated prevalence of the disease in the general population was 1:30,000. Gunther and Penrose diagnosed TSC in mentally retarded individuals by looking mainly at facial angiofibromas. Dawson in 1954 and Zaremba in 1968 estimated a prevalence of 1:150,000 and 1:23,000 of TSC cases in the general population, respectively. In 1960, Crome reported diagnostic TSC brain pathology in 7 out of 282 mentally retarded individuals. In another study, Donegani *et al*. (1972) observed TSC cerebral pathologies in 6 out of 49,000 autopsies and estimated the incidence of the disease at 1:10,000.

Stevenson and Fischer (1956), Nevin and Pearce (1968) and Singer (1971) carried out the earliest population-based studies and determined the prevalence of TSC at 1:150,000, 1:100,000 and 1:70,000 respectively. Technological advances in the mid-1970s expanded the diagnostic criteria for the TSC diagnosis and thus increased the reported number of cases. Additionally introduction of major and minor diagnostic criteria by Gomez in 1979 and (revised in 1988) improved diagnosis of TSC and the accuracy of population-based studies (Hunt and Lindenbaum, 1984; Sampson *et al*. 1989, Shepherd *et al*. 1991, Webb *et al*. 1996, Wiederholt *et al*. 1985). The currently estimated prevalence of TSC is 1:6000 to 1:12,500 live births (Osborne *et al*. 1991, O'Callaghan *et al*. 1998).

1.1.3 Clinical manifestations of TSC

The clinical manifestations of TSC are very variable in patients although they usually involve multiple organs. The Central Nervous System (CNS), skin, kidneys and heart are most commonly affected. About 96% of TSC patients have skin lesions, 90% have cerebral pathology, 84% have seizures, 80% have renal pathology and nearly 50% have retinal hamartomas (Gomez *et al*. 1999, Kwiatkowski *et al*. 2010). The age of onset varies in terms of symptoms and complications of TSC. For example cardiac rhabdomyomas (CRs) appear in foetal life and usually disappear in infancy, while renal angiomyolipomas (AMLs) appear later in life, often during the second decade (Roach and Sparagana, 2004).

1.1.3.1 Manifestations in CNS

Tubers, subependymal nodules (SENs) and subependymal giant cell astrocytomas (SEGAs) are hallmark structural malformations found in the brain of TSC patients. Both tubers and SEGAs are included in the diagnostic criteria for TSC. Tubers are hypomyelinated hamartomas usually located on the cerebral cortex and sometimes extending into the underlying white matter (Figure 1.1). Tubers are often numerous with size ranging from a few millimetres to several centimeters. They are firm, smooth, frequently paler than the surrounding cortex and can be restricted to one gyrus or more (Kwiatkowski *et al*. 2010). Cortical tubers can be distinguished prenatally by MRI in 20 week gestation foetuses (Levine *et al*. 2000, Park *et al*. 1997, Wortmann *et al*. 2008). They are associated with autism, epilepsy and cognitive disability in patients with TSC depending upon their size and location (Kwiatkowski *et al*. 2010). They vary in cellularity and feature both neurons and characteristic large cells (Gomez *et al*. 1999).

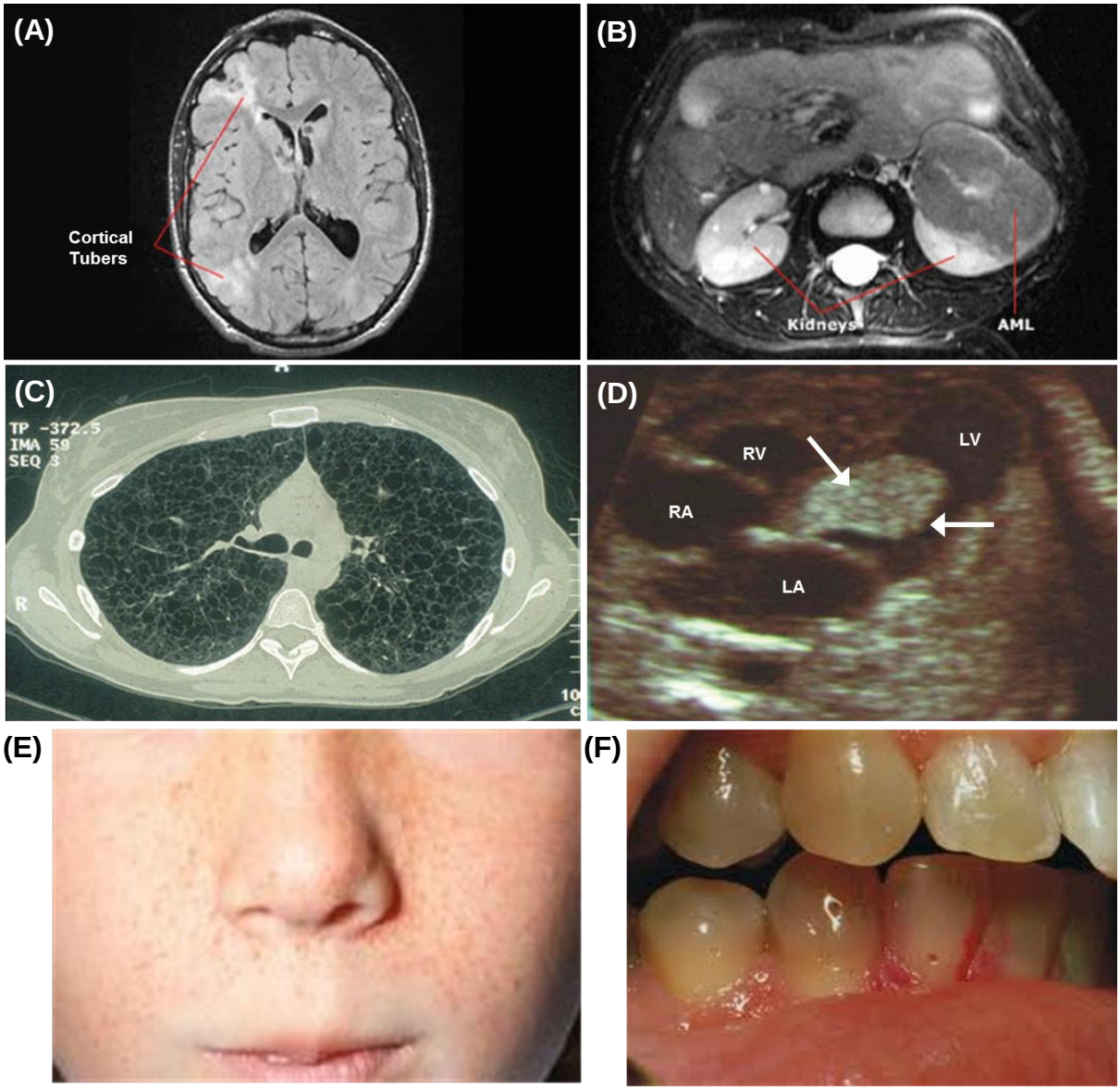

Figure 1.1 Clinical features of TSC. **(A)** Axial brain MRI showing cortical tubers. **(B)** MRI showing renal angiomyolipoma. **(C)** High resolution chest CT showing the lungs of an individual with TSC who has lymphangioleiomyomatosis. **(D)** Fetal echocardiogram showing a cardiac rhabdomyoma (arrows in the left ventricle of the heart of a fetus with TSC). LV, left ventricle; RV, right ventricle; LA, left atrium; RA, right atrium. **(E)** Typical distribution of angiofibromas. **(F)** Dental pits.

SENs are usually asymptomatic lesions of the brain, they occur in approximately 70-80% of individuals with TSC. They are located along the outer walls of the lateral ventricles (Kwiatkowski *et al*. 2010, Mizuguchi and Takashima, 2001; Vinters and Miyata, 2006). Multiple lesions usually develop prenatally and are less than 1 cm in size (Houser and Nixon, 1988). SENs are extensively vascular, covered by a layer of ependymal and are described as “candle gutterings”. SEN degeneration and calcification are frequently observed (Hosoya *et al*. 1999).

SEGAs, also referred to as subependymal giant cell tumours (SGCTs) are present in 5-20% of TSC patients, occur equally in both genders and are histologically identical to SENs but are classified on the basis of their larger size (1-10 cm in size) (Shepherd *et al*. 1991). It is thought that SEGAs develop from the excessive growth of SENs (Kim *et al*. 2001).

The CNS manifestations associated with TSC can be very debilitating. Patients may suffer from epilepsy, behavioural problems, psychiatric, intellectual or neuropsychological abnormalities (Ehninger *et al*. 2009). Intellectual disability affects around 50% of patients and approximately 30% of individuals with TSC develop a very low intelligence quotient (IQ) (severe to profound phenotype) (Joinson *et al*. 2003, Prather and de Vries, 2004). However, TSC patients with normal IQ often exhibit specific neuropsychological impairments, for example, long-term memory and attentional deficits (Ehninger *et al*. 2009, Harrison *et al*. 1999, Prather and de Vries, 2004). Neurodevelopmental disorders such as autism (in 20-60% of patients), attention deficit hyperactivity disorder (ADHD) (in ~50% of patients), and aggressive and disruptive behaviour are common CNS related manifestations of TSC (Bolton *et al*. 2002, de Vries *et al*. 2009, Prather and de Vries, 2004; Smalley, 1998). Epilepsy affects approximately 70-80% of TSC patients during life (Webb *et al*. 1996, Joinson *et al*. 2003). Depressive and anxiety disorders, predisposition to self-harm and psychological distress are also commonly seen in adults with TSC (Ehninger *et al*. 2009).

1.1.3.2 Renal manifestations

The common renal lesions found in TSC include angiomyolipomas (AMLs) and cysts. Oncocytomas and renal cell carcinomas are rare. These renal tumours together were seen in over 80% of patients with TSC (Kwiatkowski *et al*. 2010).

1.1.3.2.1 AMLs

AMLs are the most common renal lesion arising in TSC patients (Figure 1.1). A longitudinal renal surveillance study indicated the development of renal tumours in 80% of 10.5 year-old children with TSC (Ewalt *et al*. 1998). AML and cysts accounted for 75% and 17% (respectively) of renal lesions. Bernstein and Robbins (1991) found AML in 67% of individuals with TSC following post-mortem examination. Similarly, a more recent retrospective review of clinical and radiographic records of TSC patients suggested that approximately 85% of patients develop renal AMLs (Rakowski *et al*. 2006).

AMLs are either classified as hamartomas, choristomas or perivascular epithelioid cell tumours (PEComas) (Dickinson *et al*. 1998; Fischer, 1911). They are mesenchymal tumours probably derived from a single progenitor cell (El-Hashemite *et al*. 2003, Karbowniczek *et al*. 2003), and consist of vascular, smooth muscle and adipose tissue. The composition of the lesions is highly variable, even within the same kidney (Farrow *et al*. 1968, Karbowniczek *et al*. 2003, Kwiatkowski *et al*. 2010, Lin *et al*. 1994, Tweedale *et al*. 1955, Wong *et al*. 1981). Although often developing during childhood in TSC patients (Ewalt *et al*. 1998) AMLs may continue to grow until later life (Kennelly *et al*. 1994, Lemaitre *et al*. 1995, Steiner *et al*. 1993).

Patients with AMLs are at risk of developing life-threatening retroperitoneal haemorrhage as a result of aneurysm rupture (Bissler *et al*. 2002, Chesa Ponce *et al*. 1995, Ou *et al*. 1991) or to chronic renal failure and end-stage renal impairment (Clarke *et al*. 1999, Schillinger and Montagnac, 1996). The risk of haemorrhage is increased in larger AMLs and is proportional to the size of the aneurysm (Yamakado

et al. 2002). According to a survey of the members of the European Dialysis and Transplant Association, 1% of TSC patients of normal intellect required a renal transplant (Clarke *et al*. 1999). Malignant AMLs or even epithelioid AMLs are also reported in TSC. Epithelioid AMLs are lesions with minimal fat accumulation. These are often aggressive and can be fatal (Bjornsson *et al*. 1996, Eble, 1998; Eble *et al*. 1997, Hardman *et al*. 1993).

1.1.3.2.2 Renal cystic disease

Benign epithelial cysts are the second most common renal manifestations in TSC patients (Bernstein *et al*. 1986, Bernstein and Robbins, 1991). At least nine percent of female and 20% of male TSC patients have cysts (Torres *et al*. 1995). In a small proportion of cases severe renal cystic disease develops prenatally or in infants. Cystic disease may cause hypertension or impairment of kidney function (Miller *et al*. 1989, Moss and Henry, 1988). TSC-associated cysts originate in the nephron, form clusters within the renal cortex and then spread into the medulla (Bernstein and Robbins, 1991; Saguem *et al*. 1992). The co-occurrence of cysts and AMLs in the kidneys during adulthood may indicate TSC. Renal cysts are found in patients carrying either *TSC1* or *TSC2* mutations (Dabora *et al*. 2001). Severe and early onset polycystic kidney disease can arise as a result of deletions that involve both *TSC2* and the adjacent polycystic kidney disease (*PKD1*) gene on chromosome 16p13.3 (Brook-Carter *et al*. 1994); contiguous gene syndrome. Twenty three out of 28 patients with both TSC and severe renal cystic disease had genomic deletions affecting the *PKD1* gene in addition to *TSC2* (Sampson *et al*. 1997).

1.1.3.2.3 Oncocytomas

Oncocytomas have been reported in several cases of TSC (Jimenez *et al*. 2001). Renal oncocytomas are benign renal neoplasms that originate from the collecting duct (Eble and Hull, 1984; Zerban *et al*. 1987) and account for 3-5% of renal parenchymal tumours (Siracusano *et al*. 1998).

1.1.3.2.4 Renal cell carcinomas (RCCs)

The exact prevalence of RCCs in patients with TSC is not known yet. It is estimated that less than 2% of TSC patients develop RCC (Kwiatkowski *et al*. 2010). RCCs tend to be present at a younger age in TSC patients than in the general population (Lendvay *et al*. 2002). The average age for the development of TSC-associated RCCs is 28 years old. There have been several reports of RCCs in children (Al-Saleem *et al*. 1998, Robertson *et al*. 1996) and also in a 9-month old infant (Breysem *et al*. 2002). It is thought that these renal lesions arise from the lining of cysts rather than from AMLs (Robertson *et al*. 1996). However sporadic RCCs occur in patients of an average age of 53 years (Al-Saleem *et al*. 1998).

1.1.3.2.5 Imaging renal lesions

Monitoring renal lesions is essential for disease management and control as well as assessment of therapy in TSC patients. At present, there are no non-invasive diagnostic techniques available for reliably differentiating minimal-fat containing AMLs from renal cell carcinomas. Previously, ultrasonography was used for renal imaging in TSC, however it is not effective for detecting solid lesions. CT and MRI scans are now frequently used for detecting and monitoring renal lesions in TSC patients (Kwiatkowski *et al*. 2010).

1.1.3.3 Hepatic manifestations

Hepatic AMLs occur in approximately 16-24% of patients with TSC (Fleury *et al*. 1987, Jóźwiak *et al*. 1992) and at higher incidence during adulthood. Jóźwiak *et al*. (1992) and Fricke *et al*. (2004) reported a higher incidence of multiple hepatic AMLs in women with TSC as opposed to men. Hepatic AMLs are usually asymptomatic. However, Huber *et al*. (1996) reported haemorrhage from a spontaneously ruptured hepatic AML. In addition, some cases of racemose angioma (Feriz, 1930), liver adenomas (Inglis, 1950), lipomyomas (Hallervorden and Krucke, 1956) and fatty mesenchymatous tumours (Cares, 1958) have been found in TSC patients. Yang *et al*. (2008) also found a hepatocellular carcinoma in a female TSC patient with liver

AMLs. Liver AMLs are usually diagnosed using imaging methods such as ultrasound and CT scanning (Kwiatkowski *et al*. 2010).

1.1.3.4 Pulmonary manifestations

The most common pulmonary manifestation affecting TSC patients is lymphangioleiomyomatosis (LAM) (Figure 1.1). LAM is caused by infiltration and proliferation of abnormal smooth muscle cells in the lungs in combination with the development of multiple thin-walled cysts resulting in gradual destruction of the lungs (Kwiatkowski *et al*. 2010). The majority of TSC patients with LAM are women suggesting a link between oestrogen and LAM pathogenesis (Uzzo *et al*. 1994). There are reports of LAM occurring in men with TSC but their presentation appears to be less severe (Aubry *et al*. 2000, Kim *et al*. 2003, Miyake *et al*. 2005). LAM can occur in association with TSC or sporadically and according to the LAM foundation patient records, only 11-15% of individuals with LAM also have TSC. Pulmonary TSC may cause death in young women (Castro *et al*. 1995, Lie, 1991; Shepherd *et al*. 1991). Multinodular multifocal pneumocyte hyperplasia (MMPH) is also seen in both female and male patients with TSC and can occur with or without LAM (Franz *et al*. 2001, Muir *et al*. 1998). High-resolution computed tomography scan (HRCT) of the chest is required to reliably detect any cystic lung changes. Anti-oestrogen therapy and lung transplantation may expand the life span of TSC patients with LAM, however the disease eventually reoccurs even after lung transplantation, suggesting characteristics of malignancy (Castro *et al*. 1995, Taylor *et al*. 1990, Urban *et al*. 1992).

1.1.3.5 Dermatologic manifestations

A cross-sectional study of age-related prevalence of the cutaneous features of TSC reported the incidence of skin lesions in 126 of 131 patients (96%) (Webb *et al*. 1996). The most common dermatologic features of TSC include hypomelanotic macules, facial angiofibromas, forehead plagues, shagreen patches and ungual fibromas (Kwiatkowski *et al*. 2010). Hypomelanotic macules occur in almost all individuals with TSC (Fitzpatrick, 1991; Jimbow, 1997; Jóźwiak *et al*. 1998, Webb *et*

al. 1996) and are often reported in neonates and infants (Fitzpatrick, 1991; Hunt, 1983; Jóźwiak *et al*. 1998). The lesions are 0.5-3 cm diameter, polygonal or oval shape and an off-white colour (white patches) due to reduced pigmentation in the skin (Jimbow, 1997; Kwiatkowski *et al*. 2010). The occurrence of hypomelanotic macules on the scalp, eyelashes and eyebrows may result in poliosis (McWilliam and Stephenson, 1978).

Facial angiofibromas occur less frequently than hypopigmented macules and presented in approximately 75-90% of TSC patients (Figure 1.1) (Kwiatkowski *et al*. 2010, Weiner *et al*. 1998). Angiofibromas start to appear from 2-5 years old and continue to grow in a progressive manner until adulthood (Dabora *et al*. 2001, Hunt, 1983; Jóźwiak *et al*. 1998, Nickel and Reed, 1962; Webb *et al*. 1996). These skin lesions (1-4 mm diameter) are pink to reddish brown papules or nodules with a smooth surface. Patients can present with in excess of 100 angiofibromas, they are usually distributed bilaterally over the centrofacial areas (Jóźwiak *et al*. 1998, Kwiatkowski *et al*. 2010, Webb *et al*. 1996).

Forehead plaques also called fibrous facial plaques, can be present at any age but they occur in the majority of patients at birth or early infancy (Fryer *et al*. 1987, Jóźwiak *et al*. 1998, Nickel and Reed 1962). They affect 20-40% of individuals with TSC and are described as soft or hard lesions with pink to yellowish brown colour (Dabora *et al*. 2001, Jóźwiak *et al*. 1998, Webb *et al*. 1996). These skin lesions appear as plaques with a stable-irregular shape that thickens over time (Jóźwiak *et al*. 1998). Single or multiple fibrous facial plaques may be distributed on the forehead, scalp or on any other region of the face (Kwiatkowski *et al*. 2010).

Shagreen patches affect approximately 50% of patients and frequently occur in individuals within the first decade of life (Dabora *et al*. 2001, Hunt, 1983; Jóźwiak *et al*. 1998, Webb *et al*. 1996). They are firm yellow-brown or pink hamartomatous growth of the connective tissue. They also have an irregular shape and vary in size from few millimetres up to 10 cm. They occur on the dorsal body surfaces, more

often on the lower back (Jóźwiak *et al*. 1998, Nickel and Reed, 1962; Webb *et al*. 1996).

Ungual fibromas appear after the first 10 years of life and gradually increase in size (Jóźwiak *et al*. 1998, Webb *et al*. 1996). Webb *et al*. (1996) reported ungual fibromas in 88% of TSC patients over 30 years old. These characteristic lesions are pink to red papules and nodules that vary in size between 1 mm to 1 cm. They occur adjacent to or underneath the nails but are more frequently located on the toenails (Kwiatkowski *et al*. 2010). Other less common skin lesions present in TSC patients include molluscum fibrosum pendulum, military fibromas and pachydermodactyly (Bardazzi *et al*. 1996, Jóźwiak *et al*. 1998, Lo and Wong, 1993).

1.1.3.6 Cardiac manifestations

Cardiac rhabdomyomas (CRs) are cardiac tumours that are commonly detected in neonates with TSC (Figure 1.1) (Tworetzky *et al*. 2003). Around 50% of TSC patients present with CR at birth (Bass *et al*. 1985, Nir *et al*. 1995, Smith *et al*. 1989). According to Jóźwiak's report, multiple CRs were seen more frequently in children with TSC who are less than 2 years old (66%) or in the 12-15 years age bracket (54%) (Jóźwiak *et al*. 2006). Patients often develop multiple CRs usually 5-15 mm in diameter in any of the four cardiac chambers, most commonly in the ventricles than in the atria (Bass *et al*. 1985, Nir *et al*. 1995). CRs represent the earliest detectable hamartoma in TSC and include the only lesion in TSC that often regress or even disappear completely with time (Curatolo, 2003). CRs are often asymptomatic, with complications arising in no more than 29 out of 74 TSC children with CRs (Jóźwiak *et al*. 2006). Echocardiography including prenatal screening ultrasound has become the standard procedure in the diagnosis of CRs (Czechowski *et al*. 2000, Gushiken *et al*. 1999, Hata *et al*. 2007, Jóźwiak *et al*. 2006). A report also suggested the use of cardiac MRI (T1 and T2 MRI sequences) in detecting CRs (Kiaffas *et al*. 2002).

1.1.3.7 Ophthalmologic manifestations

Angiofibromas of the eye, for example of the eyelids affects an estimated 39% of individuals with TSC (Mencía-Gutiérrez *et al*. 2004, Rowley *et al*. 2001). Hamartomas of the retina are seen in around 30-50% of TSC patients (Au *et al*. 2007, Franz, 2004; Rosser *et al*. 2006). Retinal hamartomas may often develop in utero (Shami *et al*. 1993) and in rare cases can cause loss of vision and increased growth can result in necrosis or haemorrhage (Mennel *et al*. 2007, Rosser *et al*. 2006). Chorioretinal hypopigmented lesions have also been reported in 39% of new-borns and adults with TSC (Franz, 2004; Robertson, 1991; Rowley *et al*. 2001) and in some cases, papilloedema develops as a complication of SEGAs (Chong *et al*. 2007, Goh *et al*. 2004).

1.1.3.8 Gastrointestinal manifestations

Dental enamel pits are very common in TSC patients and develop in both deciduous and permanent teeth (Figure 1.1). Sparling *et al*. (2007) detected dental pits in 56 out of 58 (97%) individuals with TSC. Oral fibromas are also a common manifestation of TSC. Sparling *et al*. (2007) detected oral fibromas in 69% of TSC patients. Fibroadenomatous polyps and AMLs occur rarely in the esophagus and stomach of TSC patients (Hizawa *et al*. 1994, Kim *et al*. 2000). Additionally, an association between TSC and polyps in the small intestine, large intestine and rectum has also been reported (Gould, 1991; Hizawa *et al*. 1994, Kim *et al*. 2000). In another report published by Goh *et al*. (2001), PEComas were found in the large bowel of a 30-years old TSC patient.

1.1.3.9 Additional manifestations of TSC

Other rare manifestations of TSC can be seen in other organs or systems such as the endocrine system (thyroid, pancreas, pituitary) gonads, hypothalamus and the spleen (Gomez *et al*. 1999).

1.1.4 Diagnosis of TSC

Diagnosis of TSC can be difficult due to the variation in phenotypes. Some patients may be diagnosed during late childhood or adolescence if clinical findings are subtle (Au *et al*. 2007, Jóźwiak *et al*. 2000). Gomez (1979) and Roach *et al*. (1992) proposed specific TSC diagnostic criteria. In 1998, a panel of experts at the Tuberous Sclerosis Complex Consensus Conference in Annapolis, Maryland, reported updated consensus diagnostic criteria (Hyman and Whittemore, 2000; Roach *et al*. 1998). In 2004, a revised version was published (Roach and Sparagana, 2004) and a further revision from a 2012 consensus conference is currently in press.

Clinical manifestations of TSC are divided into two categories, the major and minor features (Table 1.2). Clinicians can confirm a definite, probable or possible diagnosis of TSC based upon the clinical manifestations of each individual patient (Roach *et al*. 1998). A definite diagnosis is confirmed if the individual presents with either two major features or one major plus two minor features, probable TSC is diagnosed if the individual has one major plus one minor feature and possible TSC if one major feature or two or more minor features are present. Mutational analysis of the *TSC1* or *TSC2* genes complements the clinical diagnosis of TSC and allows in some cases, prenatal diagnosis. A patient exhibiting TSC-associated manifestations but with no mutation in *TSC1* or *TSC2* genes (no mutation identified- NMI) does not eliminate the possibility of TSC. Possible explanations could be a lack of sensitivity in the mutation detection, mosaicism, or mutation to another undiscovered disease-causing TSC gene.

Table 1.2 Diagnostic criteria for tuberous sclerosis (adapted from Roach *et al*. 1998).

Major Features	Minor Features
Facial angiofibromas or forehead plaque	Multiple randomly distributed pits in dental enamel
Nontraumatic ungual or periungual fibroma	Hamartomatous rectal polyps (histologic confirmation)
Hypomelanotic macules (more than 3)	Bone cysts (radiographic confirmation)
Shagreen patch (connective tissue nevus)	Cerebral white matter radial migration lines (radiographic confirmation)*
Cortical tuber*	Gingival fibromas
Subependymal nodule	Non-renal hamartoma (histologic confirmation)
Subependymal giant cell astrocytoma	Retinal achromic patch
Multiple retinal nodular hamartomas	"Confetti" skin lesions
Cardiac rhabdomyoma, single or multiple	Multiple renal cysts (radiographic confirmation)
Lymphangioleiomyomatosis**	
Renal angiomyolipoma**	

Definite: Either two major features or one major feature plus two minor features.
Probable: One major plus one minor feature.
Suspect: Either one major feature or two or more minor features.

* When cerebral cortical dysplasia and cerebral white matter migration tracts occur together, they should be counted as one rather than two features of tuberous sclerosis.

** When both lymphangiomyomatosis and renal angiomyolipomas are present, other features of tuberous sclerosis should be present before a definite diagnosis is assigned.

1.2 TSC genes

1.2.1 Identification of the TSC genes

In 1890, Pringle and in 1910, Kirpicznik initially identified TSC as a genetic disorder. The autosomal dominant hereditary pattern of TSC was revealed later by Berg (1913) and Gunther and Penrose (1935). However, the genes responsible for TSC were not isolated until the 1990's.

1.2.1.1 TSC1

In 1987, Fryer and colleagues carried out genetic linkage analysis in 19 TSC multigenerational families using 26 polymorphic protein markers. Fryer *et al*. (1987) reported linkage between TSC and the ABO blood group locus on chromosome 9q34. This was the first identification of the TSC locus, later named *TSC1* (tuberous sclerosis complex type 1). Further analyses excluded linkage to 9q34 in some families (locus heterogeneity) and the possible existence of more than one TSC locus (Haines *et al*. 1991, Janssen *et al*. 1990, Northrup *et al*. 1987, Northrup *et al*. 1992, Sampson *et al*. 1989, Sampson *et al*. 1992). The *TSC1* candidate region was a gene-rich region with more than 30 genes (1.4Mb) (Kwiatkowski *et al*. 1996). However, no mutations were detected initially in these candidate genes in cohorts of TSC patients (van Slegtenhorst *et al*. 1997). To detect the TSC gene, comprehensive sequencing of a cosmid contig and heteroduplex analysis of these exons in TSC1-linked families and sporadic cases was used (van Slegtenhorst *et al*. 1997). Mobility shifts were indicated in the 62nd exon screened, presenting mutations in 10 out of 60 patient samples (Gomez *et al*. 1999). Sequence analysis indicated that the mutations in this exon were truncating the *TSC1* gene (van Slegtenhorst *et al*. 1997).

The complete sequence of TSC1 (53 284 nucleotides) was revealed following a comparison of both genomic and cDNA clone sequences. The *TSC1* gene consists of 23 exons of which exon 3 to 23 comprise the coding sequence. The 3492bp coding region of the gene is translated into a 130 kilodaltons (kDa) protein of 1164

amino acids, called hamartin (van Slegtenhorst *et al*. 1997). In addition to the coding region, the *TSC1* gene also contains a 4.5kb 3' untranslated region (3'UTR) and a 221bp 5' untranslated region (5'UTR) (Gomez *et al*. 1999).

1.2.1.2 TSC2

In 1992, Kandt *et al*. revealed linkage between TSC and a polymorphic marker (*D16S283*) close to the ADPKD1 locus on chromosome 16p13 in a set of five multigenerational TSC families unlinked to chromosome 9 (*TSC1*). In 1994, a family was reported with both ADPKD and TSC. Whereas mother and daughter were carriers of a balanced chromosome translocation in 16p13.3 and presented with a typical ADPKD phenotype, the son had an unbalanced karyotype and clinical features of TSC including skin and brain involvement, in addition to renal cysts (European Polycystic Kidney Disease Consortium, 1994). The son's TSC was a result of deletion of the chromosomal region (chromosome 16) containing the TSC gene (The European Chromosome 16 Tuberous Sclerosis Consortium, 1993).

The distal segment of the short arm of chromosome 16 had already been investigated due to it's proximity to both the α-globin (Buckle *et al*. 1988, Simmers *et al*. 1987) and PKD1 genes (Reeders *et al*. 1985). A cosmid spanning the 300kb candidate region was utilised to generate hybridisation probes which were then used to screen the DNA from 260 unrelated TSC patients by pulsed field gel electrophoresis (PFGE) and southern blotting. Five TSC-associated constitutional interstitial deletions of 30kb-75kb were detected in the candidate region of chromosome 16p13.3 by the use of PFGE. These deletions were mapped to the same 120kb segment. Four genes were isolated from which only one was disrupted by all five deletions. Further examination of this candidate gene indicated four additional intragenic mutations (deletions). These findings confirmed the identification of the second TSC locus on chromosome 16p13.3 which was named *TSC2* (tuberous sclerosis complex type 2) (The European Chromosome 16 Tuberous Sclerosis Consortium, 1993). *TSC2* is comprised 40 723 nt and contained 42 exons. The 5474bp coding region of the gene is translated into a 198 kDa protein

product of 1784 amino acids, which is referred to as tuberin. Further multicenter linkage studies indicated that half of the TSC families were linked to chromosome 9q34 and the rest to 16p13 (Janssen *et al*. 1994, Povey *et al*. 1994).

1.2.2 Biochemistry and function of the TSC proteins

The *TSC1* and *TSC2* gene products hamartin and tuberin are evolutionary conserved proteins which do not show significant structural homology between each other but share homology with other vertebrate proteins (Huang *et al*. 2008). These proteins interact with each other forming a functional complex which negatively regulates mTOR signalling (Van Slegtenhorst *et al*. 1998). TSC1-TSC2 complex has a molecular size >450 kDa and is predominantly localised to the cytosol (Nellist *et al*. 1999)

1.2.2.1 Hamartin

Hamartin (TSC1) is a hydrophilic protein comprised of 1164 amino acids (aa). Northern blotting analysis has shown the 8.6kb *TSC1* transcript to be widely expressed (Figure 1.2) (Van Slegtenhorst *et al*. 1997). The existence of a single putative transmembrane domain at residues 127 to 144 is consistent with the reported localisation of hamartin to the cytoplasmic vesicles membranes (Plank *et al*. 1998). Hamartin is also localised to the centrosome (Astrinidis *et al*. 2006). The different regions of hamartin are illustrated in Figure 1.3 and their function is stated in Table 1.3.

At present, the cellular function of hamartin is not completely understood. Hamartin and tuberin directly bind to each other soon after synthesis and inactivation of either the *TSC1* or *TSC2* gene results in TSC, suggesting that both proteins are of similar functional importance and that hamartin is essential for tuberin function (Astrinidis and Henske, 2005; Nellist *et al*. 1999). Hamartin was shown to stabilise tuberin and inhibit its ubiquitination (Benvenuto *et al*. 2000, Chong-Kopera *et al*. 2006). Three kinases have been found to control the activity of hamartin. Hamartin is

phosphorylated and inactivated at residues Thr417, Ser584 and Thr1047 by the cyclin-dependent kinase 1 (CDK1) (Astrinidis *et al*. 2003) and at residues Ser487 and Ser511 by IκB kinase (IKKβ) (Lee *et al*. 2007). Phosphorylation at Thr357 and Thr390 by the glycogen synthase kinase 3 (GSK3) activates hamartin (Mak *et al*. 2005).

Hamartin physically interacts with tuberin through a binding domain at aa 302-430 to form heterodimers. The complex then acts as a GAP towards the mTORC1 activator Rheb (Ras homolog enriched in brain). Binding of tuberin and hamartin may affect the subcellular localisation of tuberin or activate the tuberin's GTPase activating protein (GAP) domain (Astrinidis and Henske, 2005). Hamartin also interacts with the ezrin-radixin-moesin (ERM) family of actin-binding proteins through the ERM interaction domain (aa 881 to 1084). Therefore, any deficiency of hamartin leads to disruption of cell-matrix adhesion (Lamb *et al*. 2000). Oligomerisation of hamartin occurs through the carboxyl terminal coiled-coil domain at aa 719 to 998. Hamartin self-aggregation is prevented by the presence of tuberin (Nellist *et al*. 1999). The fact that hamartin interacts with members of ERM family (Lamb *et al*. 2000), together with evidence that a region spanning aa 674 to 1164 of hamartin binds to neurofilament-Light chain (NF-L) (Haddad *et al*. 2002) could indicate a role of hamartin in the localisation of tuberin.

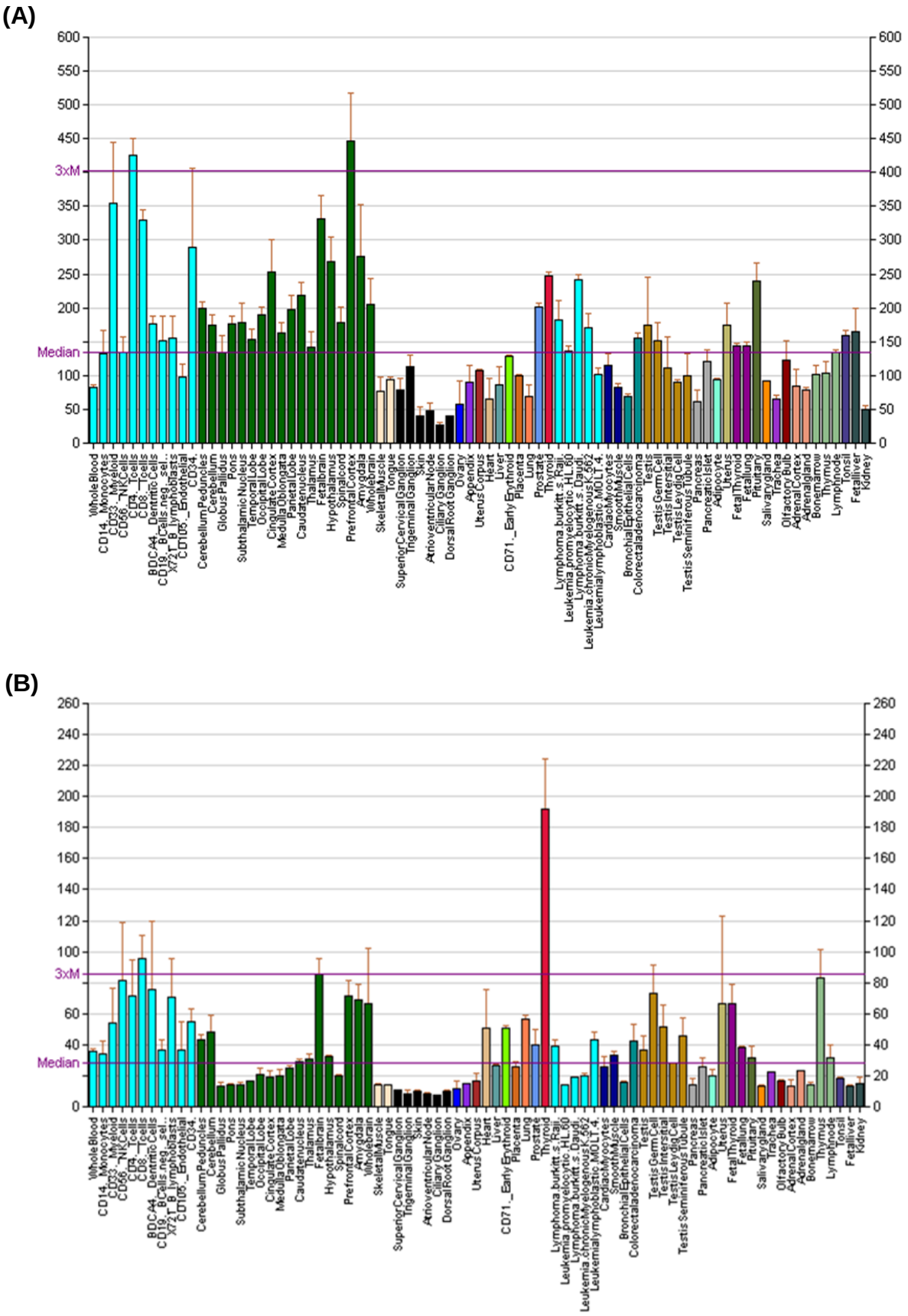

Figure 1.2 Gene expression pattern of the **(A)** *TSC1* and **(B)** *TSC2* gene (created by AndrewGNF at en.wikipedia (Su *et al*. 2004)).

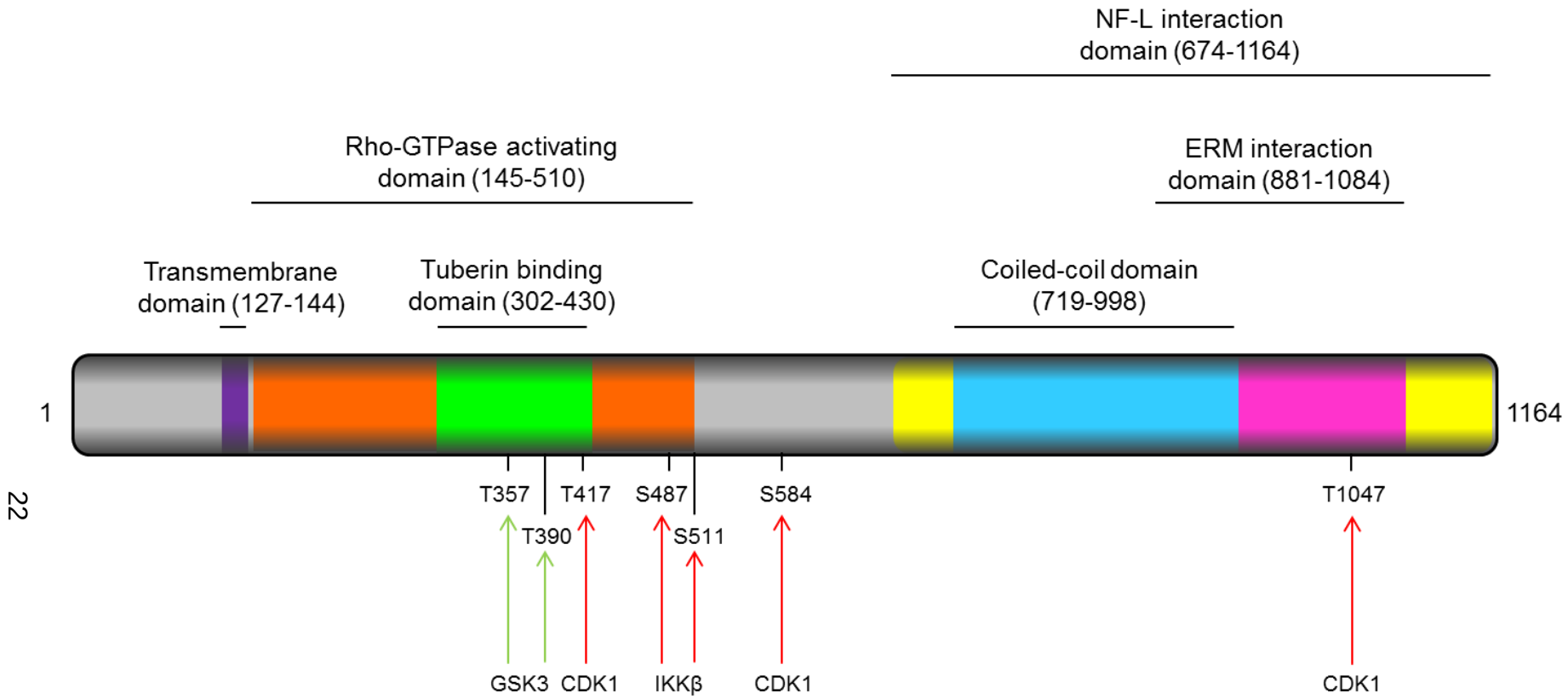

Figure 1.3 Hamartin domain structure. Hamartin is spanning 1164 aa. It is phosphorylated by CDK1 (residues T417, S584 and T1047), GSK3 (T357 and T390) and IKKβ (S487 and S511) kinases. The green arrows indicate activating phosphorylations and the red arrows inhibiting phosphorylations (Rosner *et al*. 2008). The function of each domain is listed in Table 1.3.

Table 1.3 The domains found in hamartin and tuberin proteins.

Hamartin		
Domain	*Location (aa)*	*Function*
Transmembrane	127-144	Induces the localisation of hamartin into the membrane of the cytoplasmic vesicles (Plank *et al*. 1998).
Rho GTPase activating domain	145-510	Activates the small GTP-binding protein Rho which regulates cell adhesion and the actin cytoskeleton (Astrinidis *et al*. 2002, Ridley and Hall, 1992).
Tuberin binding	302-430	Interacts with aa 1-418 of tuberin to form a functional heterodimeric complex that inhibits mTOR (Hodges *et al*. 2001).
NF-L interaction domain	674-1164	Interacts with neurofilament-light chain (NF-L). Allows hamartin to anchor neuronal intermediate filaments to the actin cytoskeleton (Haddad *et al*. 2002).
Coiled coil	719-998	Permits self-aggregation of hamartin. Oligomerisation is prevented by the presence of tuberin (Nellist *et al*. 1999).
ERM interaction domain	881-1084	Interacts with ezrin-radixin-moesin (ERM) family of actin-binding proteins. Hamartin is involved in cell-matrix adhesion pathways (Lamb *et al*. 2000).

Tuberin		
Domain	*Location (aa)*	*Function*
Hamartin binding	1-418	Interacts with hamartin aa 302-430 of hamartin (Hodges *et al*. 2001).
Leucine zipper	75-107	Structural motif implicated in protein-protein interactions (European Chromosome 16 Tuberous Sclerosis Consortium, 1993; Landschulz *et al*. 1988).
Coiled coil domains	346-371 1008-1021	Mediate the interaction with hamartin (van Slegtenhorst *et al*. 1998).
Transcriptional activation domains	1163-1259 1690-1743	Allow tuberin to act as a transcriptional activator. The first domain at residues 1163-1259 exhibit stronger activity level than the second one (Tsuchiya *et al*. 1996).
GTPase activating protein	1517-1674	Inactivates Rheb through increasing its intrinsic GTPase activity (European Chromosome 16 Tuberous Sclerosis Consortium, 1993; Tee *et al*. 2003).
PATJ interaction domain	1538-1763	Interacts with PATJ which regulate the polarity of the epithelial cell and the adhesion between cells (Massey-Harroche *et al*. 2007).
Calmodulin binding	1740-1758	Binding site for calmodulin (CaM). Essential for regulation of transcription events (Noonan *et al*. 2002).

1.2.2.2 Tuberin

The total length of tuberin (TSC2) is estimated to be 1807 aa. Northern blot analysis demonstrated the wide expression of the 5.5kb *TSC2* transcript in human and rodent tissues. Tuberin is highly expressed in the heart, renal tissue and in the central nervous system (cerebellum and developing spinal cord) (Figure 1.2) (The European Chromosome 16 Tuberous Sclerosis Consortium, 1993; Geist and Gutmann, 1995; Yeung *et al*. 1994). The distribution of tuberin and hamartin is identical in some organs whereas in some others the distribution of these proteins is overlapping but not identical (Fukuda *et al*. 2000). The level of expression of hamartin is also higher within some tissues including the distal nephron and the endocrine pancreas (Johnson *et al*. 2001). Tuberin localisation to the cytoplasm, especially within the stacks of the Golgi apparatus, was reported (Wienecke *et al*. 1996). TSC2 translocation to the nucleus has also been reported (Lou *et al*. 2001).

Several kinases have been found to control the activity of tuberin. Phosphorylation at Ser1337 and Ser1341 by GSK3 (Inoki *et al*. 2006) and at Ser1345 by AMP kinase (AMPK) activates tuberin (Inoki *et al*. 2003). In contrast, phosphorylation at Ser1798 by the ribosomal S6 kinase 1 (RSK1) (Roux *et al*. 2004), at Ser1210 by the MAPK-activated protein kinase 2 (MK2) (Li *et al*. 2003), at Ser664 by the extracellular signal-regulated kinase (ERK) (Ma *et al*. 2005) and at Ser939, Ser981 and Thr1462 by AKT (Protein Kinase B (PKB)) (Inoki *et al*. 2002), inactivates tuberin. The structure and function of tuberin's domains are listed in Figure 1.4 and Table 1.3.

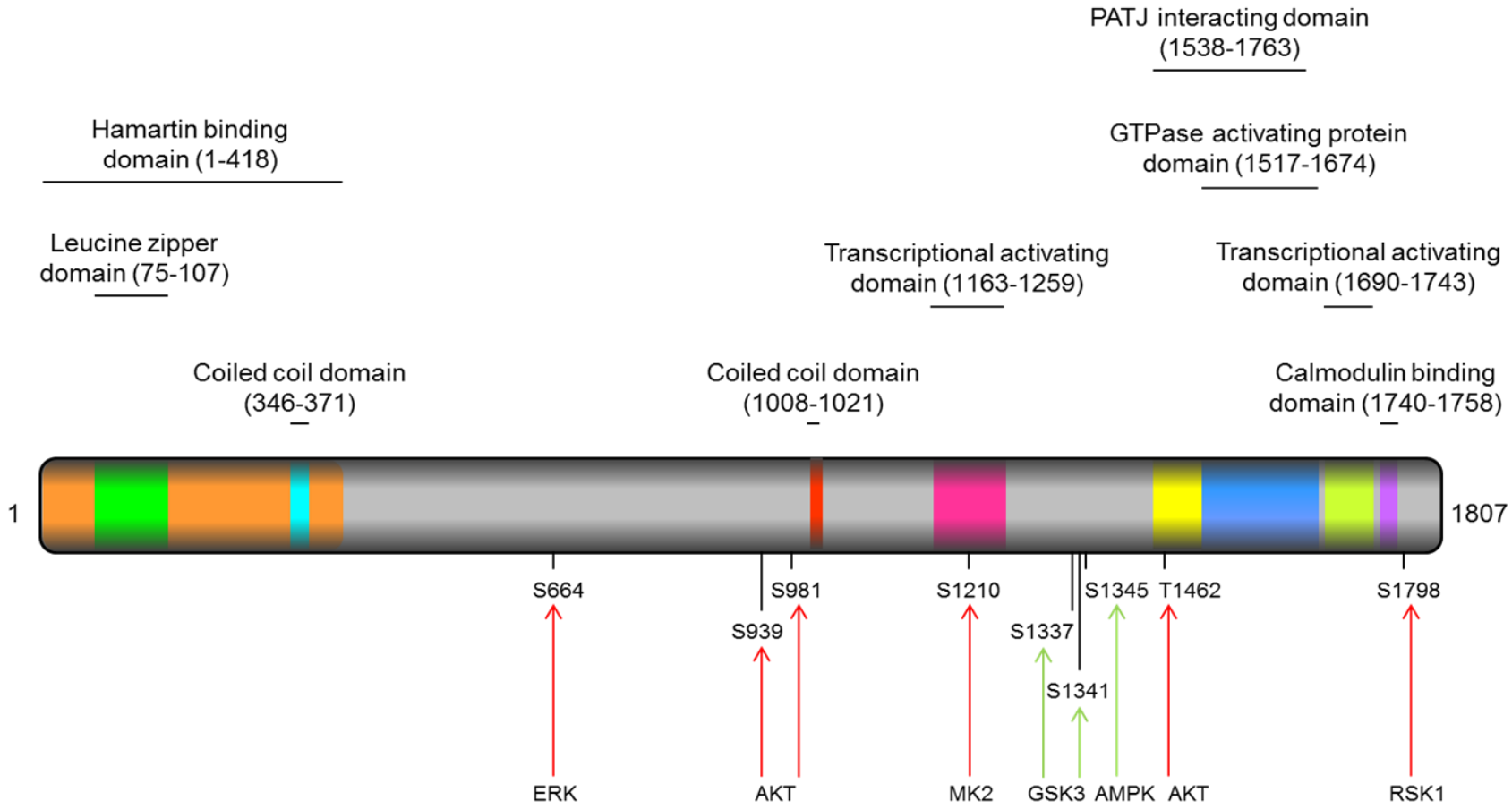

Figure 1.4 Tuberin domain structure. Tuberin is spanning 1807 aa. It is phosphorylated by AKT (residues S939, S981 and T1462), RSK1 (S1798), ERK (S664), GSK3 (S1337 and S1341), AMPK (S1345) and MK2 (S1210) kinases. The green arrows indicate activating phosphorylations and the red arrows inhibiting phosphorylations. (Rosner *et al*. 2008). The function of each domain is listed in Table 1.3.

1.2.2.2.1 The functional significance of tuberin's GAP domain

The existence of a domain at the C-terminus of tuberin which shares homology with the GTPase activating protein (GAP) Rap1GAP, suggests that tuberin acts as a GAP (The European Chromosome 16 Tuberous Sclerosis Consortium, 1993). This domain spans about 160 aa residues within exons 36-40 of the *TSC2* gene (Au *et al*. 2007, Maheshwar *et al*. 1997). The GAP domain of tuberin is a target for frequent TSC-associated mutations (Maheshwar *et al*. 1997, Niida *et al*. 1999), suggesting that it is important in tuberin's function (Jin *et al*. 1996). The GAP domain negatively regulates the activity of ras-related rab1a and rab5a however its GAP activity towards these two small G-proteins is modest (Wienecke *et al*. 1995, Xiao *et al*. 1997). This functional domain has major activity for the small GTPase Rheb, a potent regulator of mTOR signalling. Rheb is a downstream target of tuberin. Tuberin, when complexed with hamartin, exerts GAP activity toward Rheb (Inoki *et al*. 2003, Rosner *et al*. 2008) and negatively regulates Rheb-mediated mTORC1 (mammalian target of rapamycin complex 1) signalling (Tee *et al*. 2003).

1.2.2.3 The TSC1-TSC2 complex

The region encoded by aa 302-430 of hamartin (Tuberin binding domain) strongly interacts with the region encoded by aa 1-418 of tuberin (Hamartin binding domain) (Hodges *et al*. 2001). The presence of a reciprocal stabilisation mechanism is reported for tuberin and hamartin (Benvenuto *et al*. 2000). The complex blocks the ubiquitination and the consequent proteasome-dependent degradation of tuberin by preventing its interaction with the HERC1 ubiquitin ligase (Benvenuto *et al*. 2000, Chong-Kopera *et al*. 2006). Similarly, the association with tuberin stabilises hamartin and inhibits its self-aggregation and the formation of homomeric protein complexes (Nellist *et al*. 1999). Recently, Dibble *et al*. (2012) characterised Tre2-Bub2-Cdc16 1 domain family, member 7 (TBC1D7) as a stably associated and ubiquitous third core subunit of the TSC1-TSC2 complex. Loss of TBC1D7 decreased the association of TSC1 and TSC2 leading to decreased Rheb-GAP activity (Dibble *et al*. 2012).

Several kinases have been recognised to phosphorylate hamartin and tuberin at different sites leading to either their activation or inactivation. Kinase-mediated regulation may cause the disruption or the formation of the complex (Astrinidis and Henske, 2005). Through these phosphorylation events, the TSC1-TSC2 complex senses and integrates signals from various cellular pathways and acts as a molecular switchboard controlling mTORC1 activity. mTORC1 is a key mediator of cellular growth (Figure 1.5) (Huang and Manning, 2008). Tuberin displays optimal GAP activity only when it interacts with hamartin and TBC1D7 (Dibble *et al*. 2012, Tee *et al*. 2003). Regulation of the GAP activity of TSC1-TSC2-TBC1D7 complex occurs through phosphorylation of hamartin by CDK1 during the G_2/M phase of the cell cycle. CDK1-mediated phosphorylation of hamartin at three residues (Thr417, Ser584 and Thr1047) interrupts its interplay with tuberin and decrease tuberin's function (Astrinidis *et al*. 2003). In addition, phosphorylation of hamartin at residues Thr357 and Thr390 by GSK3*β* strengthens the stability of the complex (Mak *et al*. 2005). TSC1-TSC2-TBC1D7 complex inhibits Rheb by increasing its intrinsic GTPase activity. Hydrolysis of the Rheb-GTP (guanosine 5'-triphosphate) to an inactive Rheb-GDP (guanosine 5'-diphosphate) leads to Rheb inactivation (Tee *et al*. 2003). The active GTP charged form of Rheb enables activation of mTOR (Avruch *et al*. 2006) (Figure 1.5).

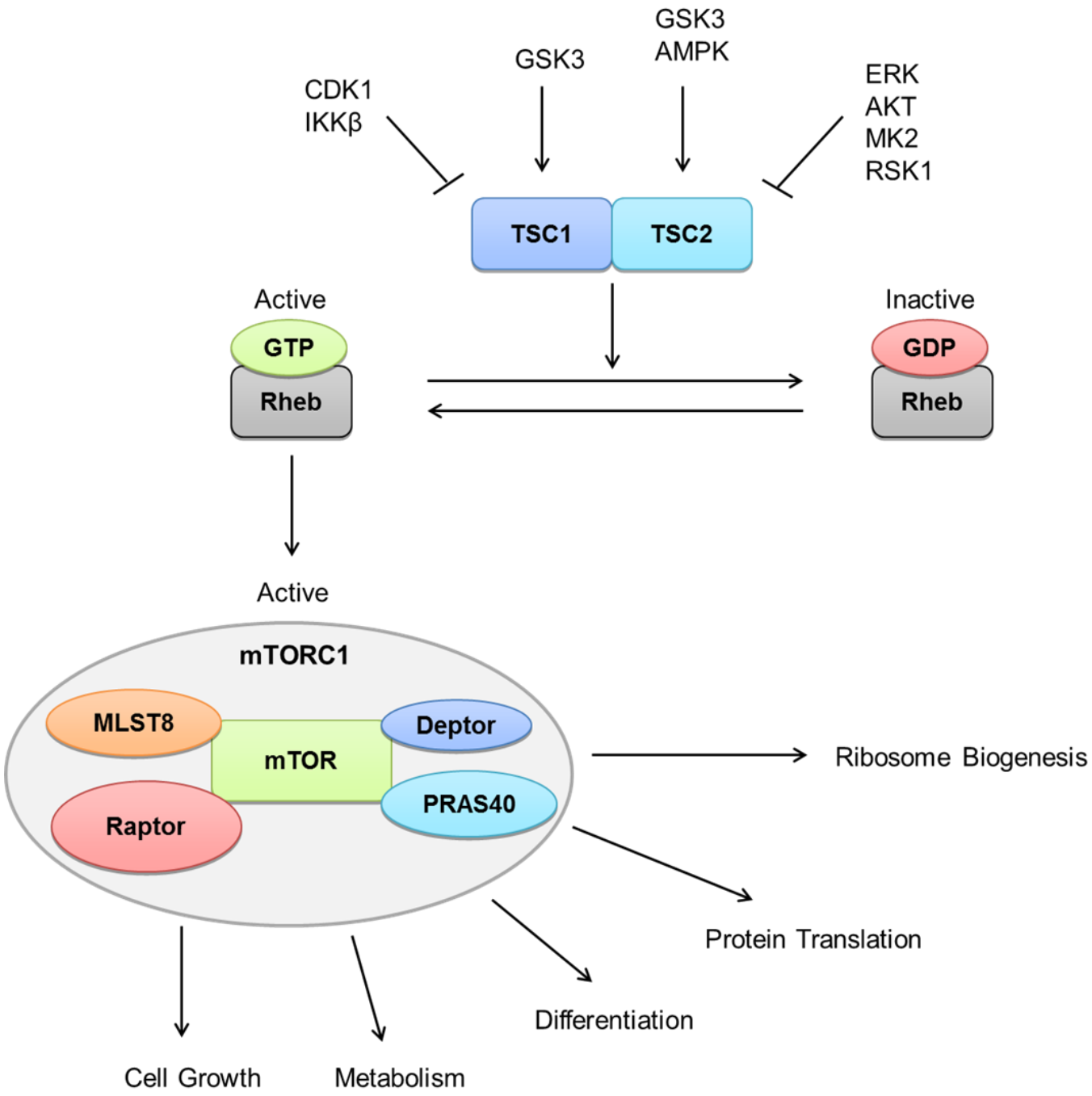

Figure 1.5 The critical role of TSC1-TSC2 complex in the modulation of mTORC1. The TSC1-TSC2 complex regulates mTORC1 activity in response to upstream signalling pathways. Under poor growth conditions, the complex blocks the activation of mTORC1 through its GAP activity towards Rheb which facilitates the conversion Rheb-GTP into Rheb-GDP. Under favourable growth conditions, GTP-bound state of Rheb activates mTORC1 signalling.

1.2.3 Mutations in *TSC1* and *TSC2*

Around 1076 and 2948 mutations have been reported in hamartin and tuberin respectively, resulting in functional inactivation of the complex. Seventy *TSC1* and 192 *TSC2* mutations have been functionally tested (updated LOVD- Variant listings at 22/01/2014). *TSC2* and *TSC1* mutations account for 74% and 26% of all TSC cases, respectively (4.2:1 ratio) (Cheadle *et al*. 2000). Sixty percent of TSC cases are sporadic (Sampson *et al*. 1989). *TSC1* mutations are seen in a minority (10-15%) and TSC2 mutations in the majority of sporadic TSC (70%) (Ali *et al*. 1998, Jones *et al*. 1997, Kwiatkowska *et al*. 1998, Niida *et al*. 1999, Van Slegtenhorst *et al*. 1997, Young *et al*. 1998). The higher incidence of *TSC2* mutations rather than *TSC1* mutations may depend on the larger size and more complex structure of *TSC2* gene. In addition, *TSC1* mutations cause a less severe phenotype and some cases may not be diagnosed. *TSC2* has longer coding region (1.5 times longer than *TSC1*) and a large number of exons and splice sites which may be prone to mutational changes (Cheadle *et al*. 2000).

The distribution of mutations varies in *TSC1* and *TSC2*. Small deletions and nonsense mutations are very common in *TSC1*. In addition, a small number of insertions and splice mutations have also been identified, and a minority of missense mutations (Figure 1.6) (Kwiatkowski *et al*. 2010). Genomic deletions or rearrangements are not common in *TSC1*. Mutations had been identified in all coding exons of *TSC1*, mainly in exons 15 (31%), 17 (14%) and 18 (13%) and rarely in exons 3, 16, 22 and 23 (Gomez *et al*. 1999).

Deletions, nonsense and missense mutations frequently affect *TSC2* whereas insertion and splice mutations are less common (Figure 1.6) (Kwiatkowski *et al*. 2010). Seventeen percent of *TSC2* mutations are genomic deletions or rearrangements, 59% small deletions, insertions, nonsense or splice mutations and 24% missense mutations (Gomez *et al*. 1999). Mutations in coding exons 16, 33 and 40 of *TSC2* are the most common, while mutational changes in exons 2, 25, 31, 41 are rare (Kwiatkowski *et al*. 2010). Missense mutations account for the majority of

mutations found in the functional GAP-related domain of *TSC2* (Maheshwar *et al*. 1997). Frequent missense in exons 36-40 encoding the GAP-related domain were reported by Au *et al*. (2007). In other study about 6% of TSC2 mutations were found in exon 16 at codon R611 which has an essential role in the regulation of the mTOR signalling pathway (Nellist *et al*. 2005).

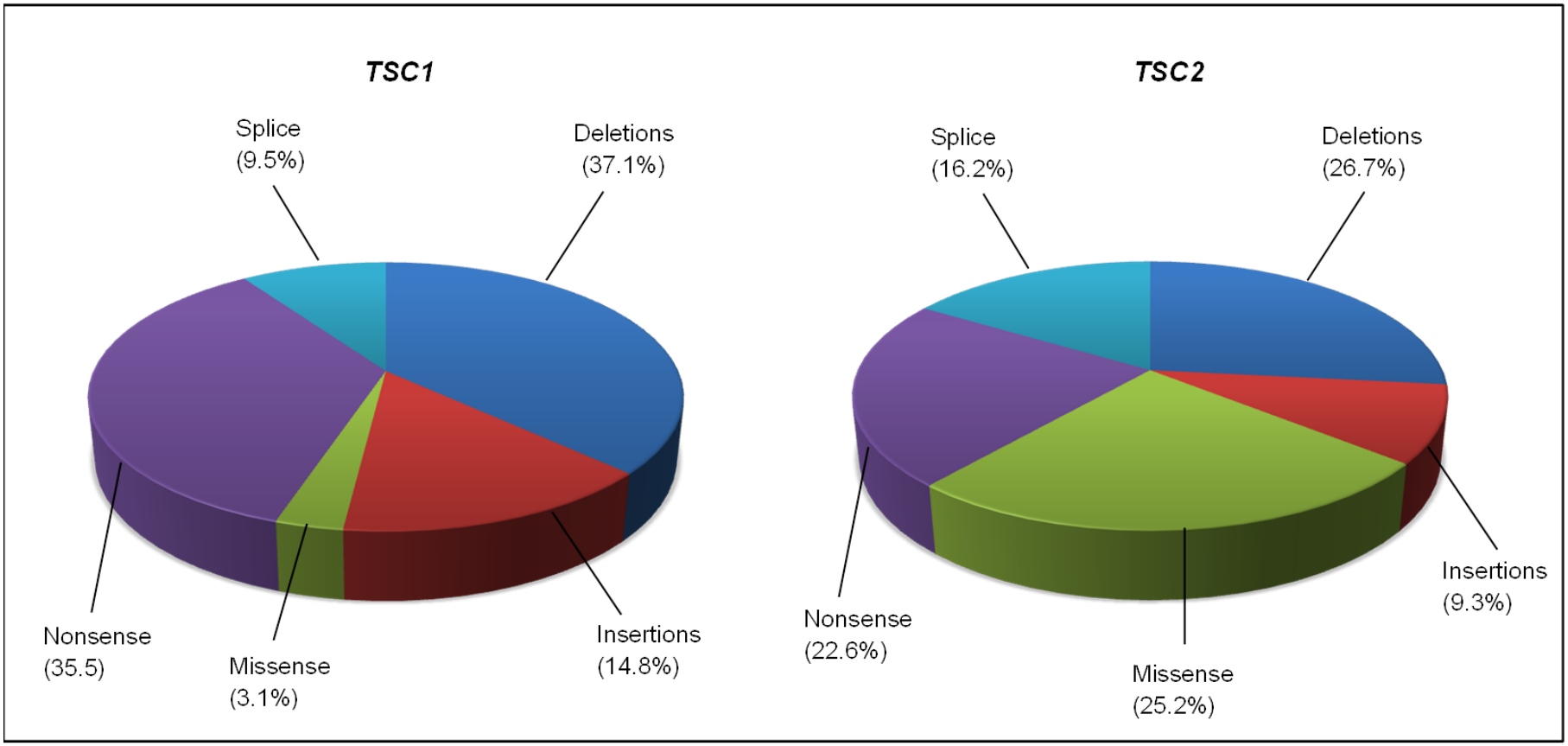

Figure 1.6 Relative frequency of the different types of small mutations found in *TSC1* and *TSC2* (adapted from Kwiatkowski *et al*. 2010).

1.2.4 Knudson's two hit hypothesis

TSC lesions develop as a result of two mutational events involving the tumour suppressor genes *TSC1* or *TSC2* (Knudson, 1971). According to Knudson's hypothesis, two 'hits' are required; an inherited germline mutation to a tumour suppressor gene in combination with a somatic second hit mutation resulting in complete inactivation of the tumour suppressor gene (biallelic inactivation) leading to tumourigenesis (Figure 1.7). Second hit mutations causing loss of heterozygosity (LOH) are usually large genomic deletions of the normal allele (Carbonara *et al*. 1994, Green *et al*. 1994). LOH is demonstrated using genetic markers (Kwiatkowski *et al*. 2010). LOH has been documented in 66% of renal AMLs (Au *et al*. 1999, Henske *et al*. 1996, Tucker and Friedman, 2002) and in CRs (Henske *et al*. 1996), TSC-associated LAM (Smolarek *et al*. 1998) and in SEGAs (Chan *et al*. 2004, Henske *et al*. 1996). Inactivation of a tumour suppressor results in inappropriate cell growth and proliferation and thus leads to tumourigenesis (Tomasoni and Mondino, 2011).

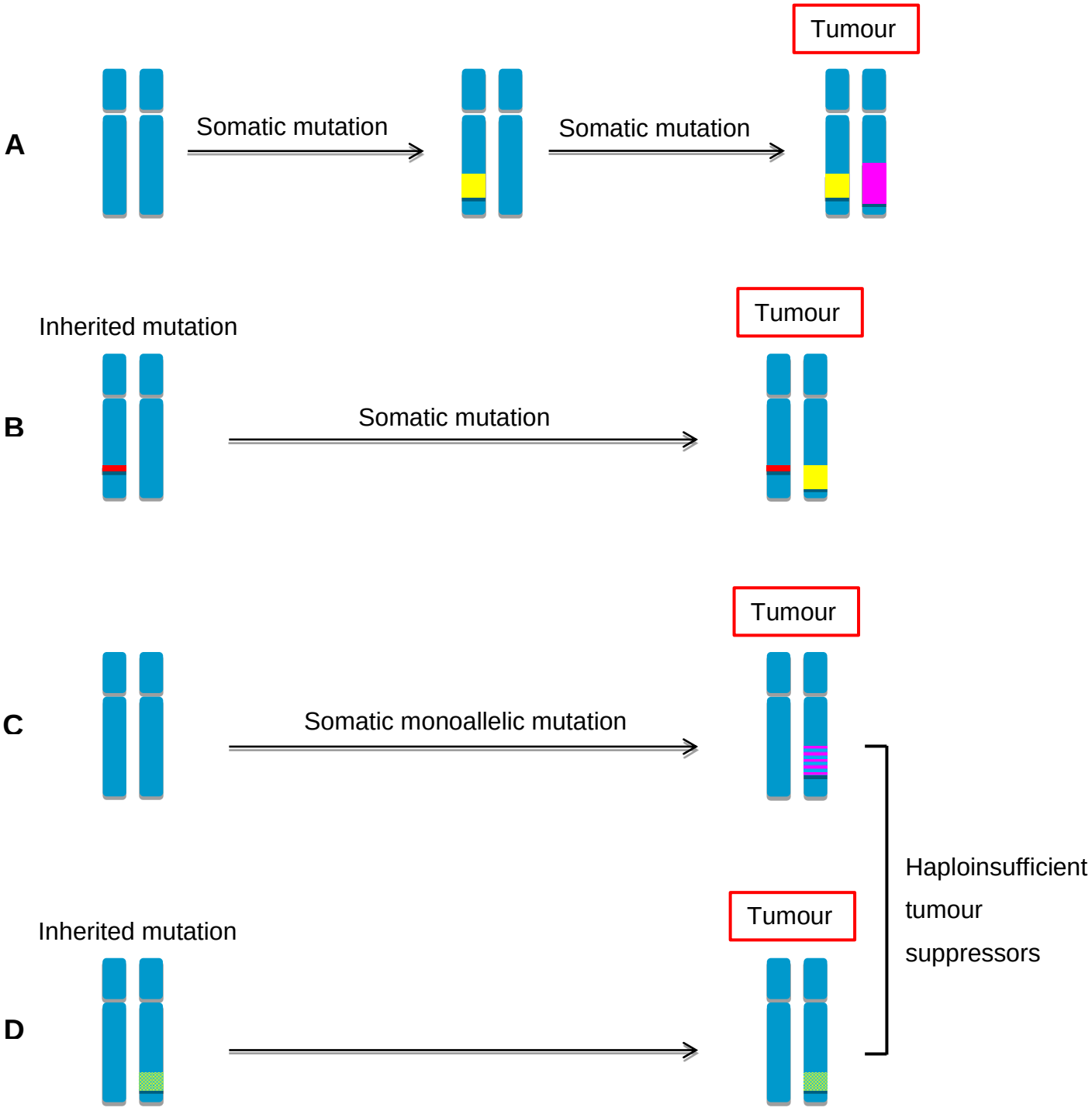

Figure 1.7 Mutational inactivation of tumour suppressor genes in cancer. **A)** Two somatic independent mutational events inactivate both alleles of the same tumour suppressor gene. **B)** Loss of the 2nd allele by a somatic mutational event complements the inactivation of the 1st allele caused by a germline inherited mutation in the same tumour suppressor gene. **C)** Inactivation of one of the two copies of the tumour suppressor gene may lead to tumour formation. **D)** A single inherited germline mutation in a tumour suppressor gene may result in tumourigenesis.

1.2.5 Mosaicism

Mosaicism refers to a mutation which is only present in a small proportion of cells rather than throughout the organism (Kwiatkowska *et al*. 1999, Roberts *et al*. 2004). Spontaneous *TSC1* or *TSC2* mutations may arise during early development in utero (Figure 1.8) (Roberts *et al*. 2004). Generalised somatic and confined gonadal (germline) mosaicism for *TSC1* and *TSC2* mutations are not uncommon in TSC (Cheadle *et al*. 2000). Germline mosaicism occurs when the mutation is only present within one of the parents germ cells, this then gets passed on to a child whilst the parents are unaffected (Rose *et al*. 1999, Yates *et al*. 1997). Somatic TSC mosaicism occurs due to the high frequency of *de novo* mutations (Gomez *et al*. 1999) and is seen in around 10% of sporadic cases of TSC (Verhoef *et al*. 1999). Sampson *et al*. (1997) described somatic mosaicism in 7 out of 27 families (26%) affected with TSC and PKD due to deletions of both the *TSC2* and *PKD1* genes. In these cases, the severity of TSC was proportional to the level of mosaicism that was present.

When mosaicism affects only a small portion of cells in an organism, there are no clinical symptoms. However, if the mutation is present in a large proportion of cells (5-50% mosaicism), the severity and the clinical manifestations of TSC may be restricted to specific organs containing the mutated cells (Gomez *et al*. 1999). Patients with mosaicism tend to present with a less severe phenotype (Dabora *et al*. 2001, Kwiatkowski, 2005; Sancak *et al*. 2005). Thirteen to 15% somatic mosaicism for a *TSC2* mutation by denaturing high performance liquid chromatography (DHPLC) was associated with mild clinical signs of TSC (Jones *et al*. 2001). A higher degree of mosaicism causes a more severe phenotype, for instance a TSC patient with 30% mosaicism for a *TSC1* mutation developed a reportedly severe TSC phenotype (Kwiatkowska *et al*. 1999).

The lack of detectable mutations in 15% of individuals with TSC may indicate the existence of a third unidentified TSC-causing gene (Kwiatkowski, 2005). Alternatively, these patients may have low levels of *TSC1* or *TSC2* mosaicism

making mutation detection difficult even in patients meeting the full diagnostic criteria (Dabora *et al*. 2001, Jones *et al*. 1999, Roberts *et al*. 2004, Sancak *et al*. 2005). In some cases, mutational analysis by automated or manual direct sequencing of polymerase chain reaction (PCR) products is inefficient in detecting TSC mutations (Jones *et al*. 2001). Qin *et al*. (2010) applied ultra-deep pyrosequencing to test for mosaicism in 38 TSC patients with no confirmed evidence of *TSC1* or *TSC2* mutations. Five non-mosaic *TSC2* mutations were detected which had been missed during the first analysis and two *TSC2* mosaic mutations were detected in two different patients.

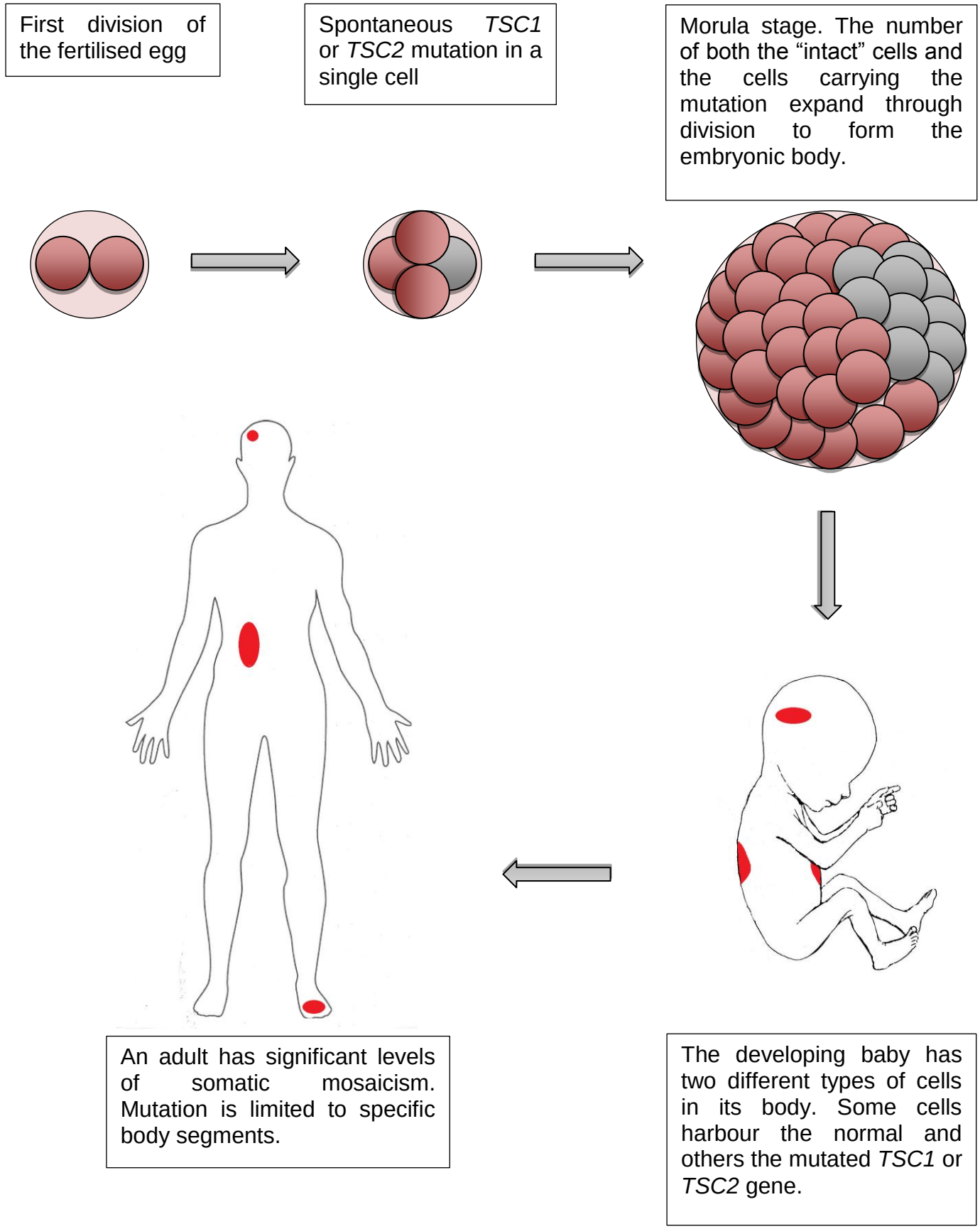

Figure 1.8 Somatic mosaicism of TSC. Sporadic *TSC1* or *TSC2* mutations arise during embryogenesis after the first division of the fertilised egg and this can result in a mosaic TSC individual. The altered *TSC1* or *TSC2* gene is present in only a fraction of cells making up an organ or tissue of an individual who developed from that embryo.

1.2.6 Genotype-phenotype correlations

1.2.6.1 Contiguous deletion syndrome

Previous studies have looked for correlation between the location or the type of different mutations with the variation in TSC phenotypes. A clear association was found between contiguous *TSC2* and *PKD1* deletions and severe renal cystic disease in TSC (Brook-Carter *et al*. 1994, Sampson *et al*. 1997). Twenty-seven patients with TSC and renal cystic disease were previously tested for mutations and 22 of them were found to have contiguous deletion syndrome. All 17 non-mosaic patients had similar clinical symptoms with enlarged cystic kidneys during infancy and radiographic features resembling advanced ADPKD (Sampson *et al*. 1997).

1.2.6.2 TSC1 versus TSC2 disease

Many comprehensive genotype-phenotype correlation studies have attempted to find correlations between TSC mutations (*TSC2* versus *TSC1* mutations) and clinical features (Au *et al*. 2007, Dabora *et al*. 2001, Jones *et al*. 1999, Sancak *et al*. 2005). Generally, patients with *TSC2* mutations tend to present with a more severe phenotype than patients with *TSC1* mutations. Patients with TSC2 mutations present with a higher incidence of renal AMLs and cysts, forehead plaques, SENs, retinal phakomas, facial angiofibromas, mental retardation and seizures than those with *TSC1* mutations (Au *et al*. 2007, Dabora *et al*. 2001, Kwiatkowski *et al*. 2010, Sancak *et al*. 2005).

1.2.6.3 Familial versus sporadic TSC patients

Differences in the severity of the disease are seen in both familial and sporadic TSC cases (Au *et al*. 2007, Dabora *et al*. 2001, Sancak *et al*. 2005). Familial TSC patients tend to present with milder phenotypes than sporadic TSC patients. Large scale meta-analysis across three studies indicated that seizures, renal AMLs, SENs and retinal phakomas are less common in cases of familial rather than sporadic TSC (Au *et al*. 2007, Dabora *et al*. 2001, Kwiatkowski *et al*. 2010, Sancak *et al*. 2005).

1.2.6.4 Male versus female TSC patients

Both Au *et al*. (2007) and Sancak *et al*. (2005) reported a higher frequency of clinical TSC features among male than female TSC patients. A meta-analysis of these two studies indicated that male patients are more prone to cortical tubers, SENs, retinal phakomas, renal cysts, ungual fibromas, mental retardation and seizures than female patients (Au *et al*. 2007, Kwiatkowski *et al*. 2010, Sancak *et al*. 2005). In addition, Smalley *et al*. (1992) reported a higher incidence of autism and learning difficulties in male than female TSC patients. The reason for this remains unknown. However it is likely that hormonal, immunologic or additional genetic events may be contributing factors (Gomez *et al*. 1999, Henske, 2005; Yu *et al*. 2004).

1.2.7 *TSC1* or *TSC2* haploinsufficiency

As stated by Knudson, mutation or LOH of tumour suppressor genes causes tumourigenesis (Knudson, 1971) (Figure 1.7). LOH was demonstrated in several lesions including SEGAs, CRs, LAM, RCCs, AMLs, and RCCs, from TSC patients (Carbonara *et al*. 1994, Green *et al*. 1994, Henske *et al*. 1995, Parry *et al*. 2001, Sepp *et al*. 2006, Smolarek *et al*. 1998). However, some TSC associated early renal cysts, cardiac (rhabdomyomas) and brain lesions (SEGAs, cortical tubers) have been reported without evidence of LOH (Henske *et al*. 1996, Niida *et al*. 2001, Wilson *et al*. 2006). In 2006, Wilson *et al*. reported somatic *TSC1* mutations in around 80% of renal cystadenomas and RCCs and in just 31.6% of renal cysts of *Tsc1*$^{+/-}$ mice. These data indicated that *TSC1* haploinsufficiency may promote renal tumourigenesis in TSC (Wilson *et al*. 2006).

TSC1 or *TSC2* haploinsufficiency reduces gene dosage and may be sufficient to diminish the function of tumour suppressor proteins, resulting in Tsc-associated tumourigenic events (Figure 1.7). It has also been reported that haploinsufficiency of some tumour suppressors such as *p27*^{Kip1}, *p53*, *MSH2*, *MAD2*, *PTEN* and *LKB1* can result in tumourigenesis (Santarosa and Ashworth, 2004). Compound haploinsufficiency may also occur when other genetic changes (oncogenic or

haploinsufficient events) cooperate with TSC1/2 haploinsufficiency gene and promote tumourigenesis (Santarosa and Ashworth, 2004).

As suggested by Henske *et al*. (1996) and Niida *et al*. (2001), some tumours may result from *TSC1* or *TSC2* haploinsufficiency and a secondary different pathogenic mechanism. In TSC-associated cardiac or brain lesions in which LOH is absent, the expression of wild-type hamartin or tuberin is normal (Jóźwiak *et al*. 2008). However, Han *et al*. (2004) reported that although hamartin and tuberin were expressed in the brain lesions, tuberin was inactivated by a post-translational mechanism. Both Akt and mitogen-activated protein kinase (MAPK) pathways were upregulated in TSC brain lesions. The single functional *TSC2* allele was present in cells, but its product was inactivated through this tissue-specific regulation (Han *et al*. 2004). In normal cells, tuberin is directly phosphorylated and inactivated by Akt, preventing its interaction with hamartin. Disruption of the TSC complex by Akt-dependent phosphorylation leads to mTOR upregulation in response to growth factors (Inoki *et al*. 2003).

1.2.8 Existence of *TSC3* gene?

Mutation analysis of *TSC1* or *TSC2* demonstrated the absence of mutations in about 15-20% patients with TSC and led to the assumption of the existence of a third TSC gene (*TSC3*) (Kwiatkowski, 2005; Kaczorowska *et al*. 2006). A third mutated protein may exist which is very closely associated with the TSC complex and is involved in the dysregulation of the downstream pathway (Jóźwiak *et al*. 2008). Recently, the third component of the TSC1-TSC2 complex was identified TBC1D7 (Dibble *et al*. 2012). However, sequencing analyses of samples from TSC patients suggested that this component is unlikely to represent TSC3. TBC1D7 is required for the proper regulation of Rheb and mTORC1 by cellular growth conditions (Dibble *et al*. 2012).

1.3 mTOR signalling pathway

The mammalian target of rapamycin or mechanistic target of rapamycin (mTOR) (Soliman, 2013), also known as FK506 binding protein 12-rapamycin associated protein (FRAP) (Brown *et al*. 1994) or rapamycin and FKBP12 target-1 protein (RAFT1) (Sabatini *et al*. 1994) is a highly conserved serine/threonine kinase of the PIKK (phosphoinositide 3-kinase-related kinase) family (Huang *et al*. 2008) and is a key mediator of cell growth, proliferation, metabolism and survival (Wullschleger *et al*. 2006). The two *Tor* (Target of rapamycin) genes, *TOR1* and *TOR2* were first identified in budding yeast *Saccharomyces cerevisiae* after the discovery of the immunosuppressive compound rapamycin. The products encoded by these genes appeared to respond to rapamycin (Heitman *et al*. 1991). mTOR is found in two functionally distinct multi-protein complexes, the mTORC1 and mTORC2. These complexes have different downstream substrates and regulate distinct pathways (Loewith *et al*. 2002, Wullschleger *et al*. 2006, Zoncu *et al*. 2011). The TSC1-TSC2 complex, through its GAP activity towards Rheb, is an important negative regulator of mTORC1.

1.3.1 mTORC1

mTORC1 is well characterised and is referred to as the rapamycin sensitive complex. mTORC1 comprises of mTOR, Raptor (regulatory associated protein of mTOR), PRAS40 (proline-rich AKT substrate 40 kDa), mLST8 (mammalian lethal with Sec-13 protein 8) and DEPTOR (DEP domain TOR-binding protein). This complex is involved in the regulation of multiple cellular processes such as growth, proliferation, angiogenesis, cell cycle progression, lipid metabolism, glucose transport, erythropoiesis and mitochondrial biogenesis (Fingar and Blenis, 2004; Hay and Sonenberg, 2004). mTORC1 mediates these processes through phosphorylation of multiple downstream substrates, with the ribosomal protein S6 kinases S6K1 and S6K2, and eukaryotic initiation factor 4E (eIF4E)-binding proteins 4E-BP1 and 4E-BP2 being the best characterised (Fingar and Blenis, 2004; Hay and Sonenberg, 2004).

mTORC1 directly phosphorylates S6K1 at the Thr389 site (Pearson *et al*. 1995). This priming phosphorylation event is critical for the phosphorylation of other sites resulting in full S6K1 activation. S6K1 together with S6K2 which is also regulated by mTORC1, are key mediators of protein synthesis. S6K1 and S6K2 are also involved in the regulation of mRNA processing and cell growth and survival. The majority of their functions are mediated through phosphorylation/activation of the downstream ribosomal protein S6 (rpS6 or S6) and eukaryotic translation initiation factor 4B (eIF4B) (Fenton and Gout, 2011; Holz *et al*. 2005, Raught *et al*. 2004; Ruvinsky and Meyuhas, 2006). S6 is activated following sequential phosphorylation of five different serine sites within its C-terminus (Ser236, Ser235, Ser240, Ser244, Ser247). Phosphorylation at the Ser240/244 residues is S6Ks-mediated (Moore *et al*. 2009). S6 is component of the ribosomal 40s subunit and is required for translation as it takes part in binding mRNA (Ruvinsky and Meyuhas, 2006). In addition, S6K1/S6K2 specifically phosphorylate eIF4B at the Ser422 residue (Raught *et al*. 2004). elF4B assists elF4A in unwinding of mRNA for translation (Rogers *et al*. 2001).

Normally, eukaryotic translation initiation factor 4G (elF4G) interacts strongly with the eukaryotic translation initiation factor 4E (elF4E) for the initiation of cap-dependent translation. Hypophosphorylated 4E-BPs supress translation initiation by competing for the eIF4G binding site on eIF4E preventing their interaction (Lin *et al*. 1994, Mader *et al*. 1995). mTORC1-mediated phosphorylation on 4E-BP releases it from the cap-bound eIF4E to initiate cap-dependent translation (Gingras *et al*. 1999). mTORC1 directly phosphorylates the translational repressor 4E-BP1 at Thr37, Thr46, Ser65 and Thr70 sites with Thr37 and Thr46 being the priming phosphorylation sites for subsequent phosphorylation of other residues (Gingras *et al*. 2001, Harris and Lawrence, 2003). mTORC1 also regulates the activation of specific transcription factors including Hypoxia-inducible factor 1α (HIF-1α), Signal transducer and activator of transcription 3 (STAT3), Sterol Regulatory Element-Binding Proteins (SREBPs), Peroxisome proliferator-activated receptor alpha (PPARα), Peroxisome proliferator-activated receptor gamma (PPARγ), Yin Yang 1 peroxisome proliferator-activated receptor gamma coactivator-1α (YY1-PGC1α) and Transcription factor EB (TFEB) (Laplante and Sabatini, 2013).

1.3.2 mTORC2

mTORC2 (mammalian target of rapamycin complex 2) consists of mTOR, Rictor (rapamycin-insensitive companion of mTOR), mSIN1 (mammalian stress-activated protein kinase-interacting protein 1), DEPTOR, PROTOR (protein observed with Rictor) and mLST8. Little is known about mTORC2 but is thought to regulate cell survival/metabolism and the actin cytoskeleton through modulation of the Rho GTPases (Jacinto *et al*. 2004) and AGC kinases (García-Martínez and Alessi, 2008; Guertin *et al*. 2006, Hresko and Mueckler, 2005; Jones *et al*. 2009, Sarbassov *et al*. 2004, Sarbassov *et al*. 2005, Yan *et al*. 2008). mTORC1 is regulated by nutrients and growth factors, while mTORC2 responds to insulin and growth factors but is considered nutrient-insensitive complex (Jacinto *et al*. 2004, Loewith *et al*. 2002, Sarbassov *et al*. 2004).

The serine-threonine kinase Akt is a direct target of mTORC2. Akt is involved in the control of cell-cycle progression, cell survival, gluconeogenesis, glucose uptake, modulating neuronal synapse activity and activation of mTORC1 (Brazil *et al*. 2004, Huang and Manning, 2009). Rictor knockout in mice indicated that mTORC2 activity and Ser473 phosphorylation of Akt are essential for the development of both embryonic and extraembryonic tissues (Shiota *et al*. 2006). Insulin and growth factors stimulate Akt activation. Akt is activated by phosphorylation of the carboxyl-terminal hydrophobic motif (at Ser473) and of the turn motif (at Thr450) by mTORC2 allowing phosphorylation at Thr308 of the activation loop by phosphoinositide-dependent kinase 1 (PDK1) (Alessi *et al*. 1996, Facchinetti *et al*. 2008, Guertin and Sabatini, 2007; Hanada *et al*. 2004, Hresko and Mueckler, 2005; Ikenoue *et al*. 2008, Manning and Cantley, 2007, Sarbassov *et al*. 2005).

mTORC2 signalling is not as well characterised as mTORC1 due to lack of mTORC2 specific inhibitors. Several studies have demonstrated that mTORC2 is insensitive to rapamycin inhibition (Jacinto *et al*. 2004, Loewith *et al*. 2002, Sarbassov *et al*. 2005). However, more recent studies suggested that prolonged treatment with rapamycin suppressed mTORC2 assembly in a subset of cells. This is believed to be due to a

reduced pool of 'free' mTOR available for mTORC2 assembly (Sarbassov *et al*. 2006, Zeng *et al*. 2007).

1.3.3 mTORC1 activation

The mTORC1 signalling pathway has been well studied in the last decade and the following discussion will focus on this pathway. mTORC1 integrates a wide range of upstream signals, including growth factors (insulin or insulin-like growth factor), nutrients (amino acids availability), cellular energy depletion and cellular oxygen levels to modulate its downstream targets (Figure 1.9) and is regulated by multiple feedback loops.

1.3.3.1 Insulin and Growth factors

Insulin and growth factors stimulate receptor-mediated activation of the PI3K-Akt pathway. Tyrosine kinase receptors become activated and auto-phosphorylated upon binding to insulin or insulin-like growth factors (IFG). Auto-phosphorylated receptors stimulate the recruitment of insulin receptor substrate adaptor proteins (IRSs) which activate PI3Ks (Phosphatidylinositide 3-kinases). Active PI3Ks are then recruited to the membrane where they convert phosphatidylinositol-4,5-bisphosphate (PIP2) to phosphatidylinositol-3,4,5-trisphosphate (PIP3) (Oldham and Hafen, 2003). The activity of PI3K is inhibited by the phosphatase and tensin homolog (PTEN) which acts as a tumour suppressor and converts PIP3 back to PIP2 (Vogt, 2001). PIP3 provides a docking site for Akt promoting its phosphorylation at Ser473 and Thr450 by mTORC2 and at Thr308 by PDK1. Akt activates mTORC1 through phosphorylation of TSC2 at Ser939 and Thr1462 blocking TSC2 GAP activity towards the mTORC1 activator Rheb (Inoki *et al*. 2002, Manning *et al*. 2002). Akt also activates PRAS40 a negative regulator of mTORC1, causing its dissociation from the complex (Haar *et al*. 2007).

In addition, Ras is also activated upon growth factor stimulation. Ras activates both PI3K-Akt and Raf/Mek1 signalling cascades. The Raf/Mek1 signalling cascade then

promotes the phosphorylation/inhibition of TSC2 on Ser540 and Ser664 by the MAPK ERK1/2 (Extracellular-signal-regulated kinases 1/2) (Ma *et al*. 2005). ERK1/2 also phosphorylates and activates p90-RSK1 (Ribosomal protein S6 kinase alpha-1) which phosphorylates TSC2 at the Ser1798 site to inactivate the complex (Roux *et al*. 2004). Furthermore, P90-RSK1 phosphorylates Raptor to increase mTORC1 kinase activity (Summy and Gallick, 2006).

1.3.3.2 Amino acid regulation

The Rag GTPases (Rag Guanosine Triphosphatases) proteins are critical in regulating amino acid signalling to mTORC1. In mammals, there are four Rag proteins called RAGA, RAGB, RAGC and RAGD. RAGA or RAGB forms a heterodimer with RAGC and RAGD (Sekiguchi *et al*. 2001). The presence of amino acids stimulates the formation of the active RAGA/B•GTP- RAGC/D•GDP complex (Jewell *et al*. 2013). Recently, a model has emerged where amino acids accumulate within the lysosome and signal to vacuolar H^+-ATPase (v-ATPase). v-ATPase promotes the GEF (Guanine Exchange Factor) activity of a complex termed 'Ragulator', resulting in the active RAG GTPase conformation. Activated RAGA/B•GTP- RAGC/D•GDP complex then binds to the mTORC1 component Raptor and recruits mTORC1 to the lysosome where Rheb is also present, leading to mTORC1 activation (Jewell *et al*. 2013). A new model was also suggested involving leucyl-tRNA synthetase (LeuRS) which functions as a direct sensor for the amino acid Leu and is implicated in the activation of mTORC1 in the cytoplasm (Bonfils *et al*. 2012, Han *et al*. 2012).

1.3.3.3 Energy sensing pathway

AMP-dependent protein kinase (AMPK) is activated by liver-kinase B1 (LKB1), in response to ATP depletion (Shaw *et al*. 2004, Lizcano *et al*. 2004) and down-regulates mTORC1 signal transduction. When intracellular ATP levels decrease, AMP levels increase and AMPK is activated. Active AMPK phosphorylates TSC2 at Ser1345 to promote formation of the TSC1/2 complex and subsequent mTORC1 inhibition (Inoki *et al*. 2003). Glycogen synthase kinase 3 beta (GSK3β) also

phosphorylates TSC2 at Ser1341 and Ser1337 (Gough *et al*. 2009). GSK3β acts synergistically with AMPK to promote TSC2 activation, as AMPK-mediated TSC2 phosphorylation is required for GSK3β-mediated TSC2 phosphorylation. This data indicates a link between Wnt signalling pathway and mTORC1 (Inoki *et al*. 2006). In addition, AMPK suppresses mTORC1 though direct phosphorylation of Raptor on Ser722 and Ser792. This stimulates the binding of the inhibitory 14-3-3 proteins to Raptor which leads to suppression of mTORC1 signal transduction (Gwinn *et al*. 2008).

1.3.3.4 Hypoxic regulation

During hypoxia, the cell compensates for the drop in oxygen levels by suppressing energy consuming processes such as protein translation. The cell also increases expression of HIFs (hypoxia-inducible factors) to promote cellular processes including angiogenesis, erythropoiesis and glucose transport (Iyer *et al*. 1998, Semenza, 1996; Wenger and Gassmann, 1997). Hypoxia causes suppression of mTORC1 to conserve energy levels via multiple mechanisms. Hypoxia rapidly decreases intracellular ATP levels and leads to inhibition of mTORC1 through AMPK activation as described in section 1.3.3.3 (Liu *et al*. 2006). In addition, oxygen depletion stimulates stabilisation of HIF-1α and up-regulation of its transcriptional target REDD1/2 (Jin *et al*. 2007). When mTORC1 is active, there is growth factor-induced association between TSC2 and the inhibitory 14-3-3 proteins (Li *et al*. 2002, Nellist *et al*. 2003). Under hypoxia, REDD1/2 promotes the suppression of mTORC1 by binding to TSC2 causing dissociation of the inhibitory 14-3-3 proteins (DeYoung *et al*. 2008).

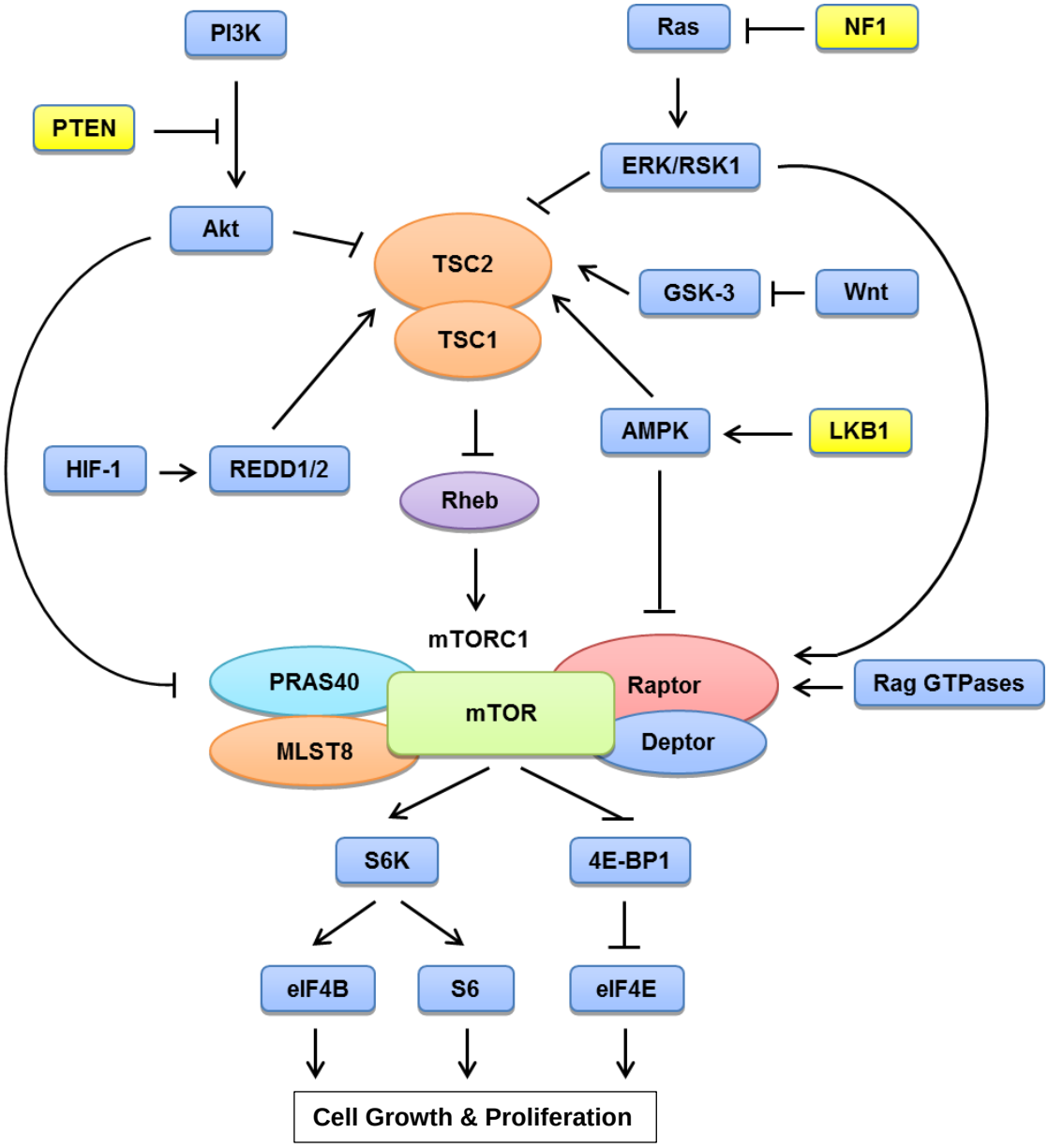

Figure 1.9 Activation of mTORC1 signalling. mTORC1 activity is regulated by several external signals including growth factors, amino acids and intracellular energy and oxygen levels. The TSC1/TSC2 tumour suppressor complex acts as a signal integration point to control cell growth and proliferation. Insulin/Growth factor stimulation activates PI3-Akt signalling and subsequently mTORC1 indirectly and directly through phosphorylation of TSC2 and PRAS40, respectively. Insulin/Growth factors also activate the Ras/Erk/Rsk1 signalling cascade. Erk and Rsk1 phosphorylate TSC2 and Raptor and activate mTORC1. Recently, the mechanism by which amino acids signal to mTORC1 is defined. Amino acid accumulation promotes the activation of Rag GTPases through Ragulator which can then recruit mTORC1 to the lysosome, leading to mTORC1 activation. Availability of energy or oxygen increases ATP levels and inhibits AMPK. Under ATP depletion, AMPK and Gsk-3 act in synergy to activate TSC2 and subsequently inhibit mTORC1. AMPK also suppresses mTORC1 through direct phosphorylation of Raptor. In case of hypoxia, the amount of HIF-1 is stabilised and the expression of REDD1/2 which sequester inhibitory 14-3-3 proteins from TSC2 is upregulated, leading to mTORC1 suppression. Functional loss of either TSC1 or TSC2 leads to mTORC1 hyperactivity. mTORC1-mediated phosphorylation of S6K and 4E-BP1 promotes cell growth and proliferation.

1.3.4 Feedback loops

S6K1, a direct substrate for mTORC1 is involved in several feedback mechanisms. S6K1 induces Ser/Thr phosphorylation on IRS (insulin receptor substrate) proteins, suppressing the response to insulin and PI3Kinase activation. This negative feedback control mechanism makes cells resistant to insulin (Zick, 2001; Um *et al*. 2004). Furthermore, when mTORC1 is active, activated S6K1 markedly reduces the expression of PDGFRα and PDGFRβ (platelet derived growth factor receptor) and this renders cells resistant to serum and platelet derived growth factor (PDGF) stimulation (Zhang *et al*. 2003). S6K1 was also indicated to inhibit mTORC2-dependent activation of Akt through phosphorylation of Rictor which is an essential component of mTORC2 (Julien *et al*. 2010, Dibble *et al*. 2009). In addition, activation of mTORC1 promotes negative feedback inhibition of PI3K through phosphorylation (at Ser501 and Ser503) and accumulation of a negative regulator of PI3K signalling, the growth factor receptor-bound protein 10 (Grb10). Overexpressed Grb10 suppresses activation of PI3K by inhibiting insulin receptor-dependent phosphorylation of IRS and its subsequent recruitment of PI3K (Yu *et al*. 2011).

Feedback mechanisms are critical in relation to therapeutic strategies for mTORC1 inhibition since they also become dysregulated when signalling pathways are manipulated. mTORC1 inhibition promotes the Ras/Raf signalling cascade while S6K1 acts to inhibit activation of the Ras/Raf signalling cascade in response to growth factors as described above. Therefore, suppression of mTORC1 by rapamycin lessens the S6K1-induced inhibition of Ras/Raf signalling (Carracedo *et al*. 2008). This may result in inappropriate activation of additional pathways downstream of Ras/Raf.

1.3.5 mTOR activation in tumour syndromes and sporadic tumours

mTOR has a central role in regulating cell growth, proliferation and metabolism, and aberrant mTOR activation is implicated in tumourigenesis. Mutations in the *TSC1* or *TSC2* tumour suppressor genes lead to aberrant mTOR activation and the development of benign hamartomas in multiple organs. Mutations in other

components of the PI3K/AKT/mTOR signalling pathway result in a group of tumour syndromes (Dazert and Hall, 2011; Guertin and Sabatini, 2007; Shaw and Cantley, 2006) (Table 1.4, adapted from Inoki *et al*. 2005). mTOR signalling pathway has also been reported to be activated in a variety of sporadic cancer such as lung adenocarcinomas breast, ovarian, colon cancers and glioblastoma (Shaw and Cantley, 2006).

Table 1.4 Hamartoma syndromes with a proven or potential link to mTOR (adapted from Inoki *et al*. 2005).

Syndromes with an established link to mTOR dysregulation		
Disease	*Gene mutated*	*Phenotype*
Tuberous Sclerosis Complex	*TSC1* *TSC2*	Hamartomas in multiple organs, hypomelanocytic macules, renal carcinomas
Peutz-Jeghers Syndrome	*STK11*	Hamartomas in the gastrointestinal tract, lentigenes
Cowden Disease	*PTEN*	Hamartomas in multiple organs, lentigenes
Bannayan-Riley-Ruvalcaba Syndrome	*PTEN*	Hamartomas in multiple organs, lentigenes
Proteus Syndrome	*PTEN*	Hamartomas in multiple organs
Lhermitte-Duclos Disease	*PTEN*	Hamartomas in brain
Autosomal dominant polycystic kidney disease	*PKD1* *PKD2*	Cysts in kidneys

Syndromes implicated with mTOR dysregulation or with clinical similarities to mTOR-related diseases		
Disease	*Gene mutated*	*Phenotype*
Neurofibromatosis type 1	*NF1*	Neurofibromas
Von Hippel-Lindau Syndrome	*VHL*	Angiomas of the retina, hemangioblastomas of the central nervous system, renal carcinomas
Carney Complex	*PRKAR1A*	Hamartomas, myxomas, lentigenes
Birt-Hogg-Dube Syndrome	*FLCN*	Hamartomas in many organs, renal carcinomas
Familial Adenomatous Polyposis	*APC*	Polyps or carcinomas in the gastrointestinal tract
Juvenile Polyposis Syndrome	*SMAD4* *BMPR1A*	Hamartomas in the gastrointestinal tract

1.4 TSC models

Genetic models of TSC are available in different species. *Drosophila* has been used as an important model system for understanding the molecular function of hamartin and tuberin tumour suppressors. Rodent models have also been invaluable in elucidating the mechanisms underlying TSC and in testing potential therapies and preventive strategies for the disease.

1.4.1 Insights from *Drosophila*

Drosophila is a powerful model system for understanding the function of disease causing genes since for 70% of human disease genes there is a counterpart gene in *Drosophila* (Rubin *et al*. 2000). Genetic and biochemical studies in *Drosophila* models have facilitated our understanding of the role of the Tsc1-Tsc2 complex (Pan *et al*. 2004). Ito and Rubin first reported the existence of TSC1 and TSC2 orthologues in *Drosophila*. They demonstrated that mutation to the *Tsc2* gene resulted in a dramatic increase in cell size (Ito and Rubin, 1999). Further work carried out independently by three groups (Gao and Pan, 2001; Tapon *et al*. 2001, Potter *et al*. 2001) showed a similar effect upon cell size after *Tsc1* mutation.

Several genetic studies have demonstrated the involvement of insulin signalling components including PI3K (Leevers *et al*. 1996), IRS (Böhni *et al*. 1999), Akt (Verdu *et al*. 1999), PTEN (Gao *et al*. 2000, Goberdhan *et al*. 1999, Huang *et al*. 1999), PDK1 (Cho *et al*. 2001, Rintelen *et al*. 2001) and S6K (Montagne *et al*. 1999) in the regulation of cell size. Mutations in the *Tsc1*, *Tsc2* or *PTEN* genes of *Drosophila* resulted in similar increase in cell size, indicating a link between TSC1-TSC2 complex and insulin signalling. It was also noted that mutations of both the *Tsc1* and *PTEN* genes caused a greater increase in cell growth compared to mutations of either gene alone (Gao and Pan, 2001).

Genetic studies of *Drosophila* also initially suggested a role for the TSC1-TSC2 complex in negatively regulating TORC1 signalling (Gao *et al*. 2002, Oldham *et al*.

2000, Zhang *et al*. 2000). Rheb was identified as a direct GTPase target of the Tsc2 GAP domain (Patel *et al*. 2003, Saucedo *et al*. 2003, Stocker *et al*. 2003). The inhibitory effect of TORC1 signalling on autophagy was shown in *Drosophila* (Scott *et al*. 2007). In 2002, Radimerski *et al*. reported that lack of TSC1-TSC2 in *Drosophila* larvae and cells, resulted in constitutive S6K activation and inhibition of Akt, suggesting a negative feedback loop between TORC1 and the insulin pathway (Radimerski *et al*. 2002) which was later confirmed. Additional studies conducted in *Drosophila* were used to characterise amino-acid-mediated TORC1 activation, leading to the discovery of the Rag GTPases (Kim *et al*. 2008, Sancak *et al*. 2008). The relationship between TSC1-TSC2 tumour suppressor complex activity and the hypoxia-induced expression of Scylla/Charybdis (the *Drosophila* homologue of REDD1/RTP801) in response to hypoxia was also uncovered using this model system (Reiling and Hafen, 2004).

1.4.2 Spontaneously mutated rat model

In 1954, a genetic animal model with a predisposition for kidney adenoma and carcinoma called Eker rat was first described (Eker, 1954). It was later discovered that spontaneous germline inactivation of a *Tsc2* allele caused this predisposition (Eker 1954, Eker *et al*. 1961, Kobayashi *et al*. 1997, Pan *et al*. 2004). This was the first rodent model of TSC. Homozygous rats for the mutated *Tsc2* exhibited embryonic lethality at approximately 10-12 days of gestation, demonstrating the essential role of *Tsc2* in development (Everitt *et al*. 1995, Hino *et al*. 1993). While Eker heterozygous rats were born viable, renal lesions including cysts, branching cysts and cyst adenomas generally developed within 12 months of age (Eker *et al*. 1981). These renal lesions derived from early pre-neoplastic lesions which first become evident at 2 months of age (Hino *et al*. 2002). Hemangiomas/hemangiosarcomas of the spleen (23-68% at 14 months- 2 years), leiomyomas/leiomyosarcomas of the uterus (47-62% of female at 14 months- 2 years) (Everitt *et al*. 1992) and pituitary adenomas (55% at 2 years) (Hino *et al*. 1994, Kubo *et al*. 1994, Kubo *et al*. 1995) developed in the heterozygous Eker rat model in addition to kidney lesions. Brain lesions including subependymal and

subcortical hamartomas (Yeung *et al*. 1997), cortical tuber and anaplastic ganglioglioma (Mizuguchi *et al*. 2000) were also observed.

The*Tsc2* gene was mapped to rat chromosome 10q12 (Yeung *et al*. 1993, Hino *et al*. 1993). Kobayashi *et al*. (1995) and Yeung *et al*. (1994) detected a germline 6.3kb retrotransposon insertion in this Eker rat gene which disrupted codon 1272 and caused aberrant RNA expression from the mutant allele, leading to an unstable, larger tuberin product. The *Pkd1* gene located adjacent to the *Tsc2* gene (as in humans) is not affected in this model (Kobayashi *et al*. 1995).

The stages of renal carcinogenesis were analysed in the Eker rat. The renal lesions initiated from altered renal tubules and were characterised by partial replacement of the tubular epithelium with larger cells exhibiting atypical nuclei. These tubules developed into foci of cells with atypical hyperplasia, then into adenomas and finally into carcinomas (Hino *et al*. 2002). These kidney lesions developed in the outer cortex and often progressed to carcinomas within the life time of the rodent. A minority of lesions became malignant and sometimes metastasised to the lungs, pancreas and liver (Eker *et al*. 1981). Even the earliest pre-neoplastic lesions arising from the kidneys of this rat model showed LOH of the wild-type *Tsc2* allele. This suggested that the second somatic mutation is a rate-limiting step for renal carcinogenesis in the Eker rat (Kobayashi *et al*. 1997). In sporadic renal cell carcinoma, 60% of rodents showed loss of the wild-type *Tsc2* allele consistent with two-hit hypothesis (Kubo *et al*. 1994). LOH was also demonstrated in renal adenomas (40-60%), uterine leiomyomas (36%) and in pituitary adenomas (35%) in rat *Tsc2*$^{+/-}$ model (Kubo *et al*. 1995, Yeung *et al*. 1995).

1.4.3 Transgenic mouse models

1.4.3.1 Conventional transgenic Tsc2$^{+/-}$ *mice*

In 1999, two *Tsc2*$^{+/-}$ mouse models were developed which exhibited identical phenotypes. *Tsc2* null (-) alleles were developed by a neomycin cassette insertion

into coding exon 2 in both models (Table 1.5) (Kobayashi *et al*. 1999, Onda *et al*. 1999) (Table 1.5). *Tsc2*$^{-/-}$ mice exhibited embryonic lethality and died *in utero* between E10.5-12.5 (Kobayashi *et al*. 1999, Onda *et al*. 1999). *Tsc2*$^{-/-}$ embryos displayed developmental delay and delay in neural tube closure in comparison with *Tsc2*$^{+/+}$ and *Tsc2*$^{+/-}$ matched littermates. The primary cause of embryonic death appeared to be severe liver hypoplasia and cardiac hypertrophy may also contribute to embryonic death (Kobayashi *et al*. 1999, Onda *et al*. 1999).

By 6-12 months, *Tsc2*$^{+/-}$ mice developed renal lesions which progressed throughout rodent's life (full penetrance by 15 months) (Kobayashi *et al*. 1999, Onda *et al*. 1999). These renal lesions, called cystadenomas, include pure cysts, cysts with papillary growth and solid adenomas (Onda *et al*. 1999). Cystadenomas were observed in the cortical region of the kidney, this is not surprising given that they developed from intercalated cells of the cortical collecting duct which share a similar gene expression profile. Renal carcinomas were also seen in 5-10% of 18 month-old *Tsc2*$^{+/-}$ mice. Strain-dependent differences in number and volume of these renal lesions were observed in *Tsc2*$^{+/-}$ mice (Onda *et al*. 1999).

By 18 months of age, 50% of *Tsc2*$^{+/-}$ mice developed liver hemangiomas characterised by smooth muscle cell proliferation and large vascular spaces. The incidence of liver hemangiomas in *Tsc2*$^{+/-}$ 129/SvJae mice was shown to be higher than in any other strains. Hemangiosarcomas of the tail, paws or mouth were noted in 5% of *Tsc2*$^{+/-}$ mice at 12 months (Kwiatkowski *et al*. 2010). LOH was revealed in 24% of renal cystadenomas and carcinomas, and 50% of liver hemangiomas. These data are consistent with the second-hit notion in tumourigenesis (Onda *et al*. 1999).

During the generation of a conditional allele for *Tsc2* as discussed below, a hypomorphic allele (*Tsc2*^{neo}) was made by a neocassette insertion into exon 1 of *Tsc2* (Table 1.5) (Hernandez *et al*. 2007). *Tsc2*$^{neo/neo}$ embryos didn't exhibit exencephaly and some of them survived until embryonic day 17, longer than the *Tsc2*$^{-/-}$ embryos. Also, renal cysts developed in *Tsc2*$^{+/neo}$ mice after the age of 1 year.

Western analysis indicated reduced tuberin expression in the *Tsc2*$^{neo/neo}$ embryo, suggesting that the *Tsc2*^{neo} allele was hypomorphic (Hernandez *et al*. 2007).

1.4.3.2 Conventional transgenic Tsc1$^{+/-}$ *mice*

Three different transgenic *Tsc1*$^{+/-}$ mouse models are now available. Kobayashi *et al*. (2001) developed a *Tsc1*$^{+/-}$ mouse model by insertion of a neocassette and deletion of exons 6, 7 and 8 of *Tsc1*. Kwiatkowski *et al*. (2002) also produced a *Tsc1*$^{+/-}$ mouse model through deletion of exons 17 and 18 (Table 1.5). Wilson *et al.* (2005) generated another *Tsc1*$^{+/-}$ mouse model by insertion of a β-Galactosidase reporter/neomycin selection cassette, partial deletion of exon 6 and complete deletion of exons 7 and 8 (Table 1.5). Homozygous *Tsc1* mice from all three groups had an embryonic lethal phenotype and were found dead by embryonic days 10.5-13.5. *Tsc1*$^{-/-}$ embryos appeared to be developmentally retarded with incomplete neural tube closure (Kobayashi *et al*. 2001, Kwiatkowski *et al*. 2002, Wilson *et al*. 2005).

Although the phenotype of the first two *Tsc1*$^{+/-}$ mouse models were very similar (Kobayashi *et al*. 2001, Kwiatkowski *et al*. 2002), Wilson's model exhibited a more severe phenotype (Wilson *et al*. 2005) (Table 1.5). The differences may be strain-dependent (Wilson *et al*. 2005). More *Tsc1*$^{+/-}$ mice on a C3H background (44%) developed macroscopically visible renal lesions in comparison with age matched (3-6 months old) *Tsc1*$^{+/-}$ mice on the Balb/c (13%) and C57BL/6 (8%) backgrounds. The incidence of renal cell carcinoma was higher (80%) in *Tsc1*$^{+/-}$ Balb/c mice compared with other strains. By 15-18 months, *Tsc1*$^{+/-}$ mice of all backgrounds exhibited microscopically visible lesions. Renal lesions were classified as cysts, atypical cysts, branching cysts, mixed cystic/solid carcinomas or solid carcinomas. It was demonstrated for the first time using this model that small cysts progress to carcinomas (Wilson *et al*. 2005). LOH analysis in the renal lesions of these *Tsc1*$^{+/-}$ mice indicated second somatic *Tsc1* mutations in around 80% of renal cystadenomas and RCCs but in just 31.6% of renal cysts suggesting that *TSC1* haploinsufficiency may promote renal cystogenesis (Wilson *et al*. 2006).

The tumours found in *Tsc1*$^{+/-}$ mice such as kidney cystadenomas and liver hemangiomas were similar to those observed in *Tsc2*$^{+/-}$ mice. However, the incidence of renal tumours was higher in *Tsc2*$^{+/-}$ than in *Tsc1*$^{+/-}$ mice of the same age (Kobayashi *et al*. 2001, Kwiatkowski *et al*. 2002). In the *Tsc1*$^{+/-}$ mouse model generated by Kwiatkowski *et al*. (2002), liver hemangiomas were more common and more severe in females than in males leading to higher mortality rate in females.

1.4.3.3 Conditional transgenic mouse models

1.4.3.3.1 Tissue-specific knockout of *Tsc1* or *Tsc2*

Conditional *Tsc1* and *Tsc2* alleles allow targeted loss of these genes in specific tissue and organs of interest. These models allow the generation of homozygous deletion of *Tsc1* or *Tsc2* genes in a given tissues and therefore provide a powerful tool to dissect gene functions (Kwiatkowski *et al*. 2010). Conditional tissue specific knockout of *Tsc1* or *Tsc2* genes may also help minimise suffering of mice compared to conventional mouse models. Meikle *et al*. (2005) used a conditional, floxed allele of *Tsc1* and a modified myosin light chain 2v allele expressing the cre recombinase (loss of exons 17 and 18) in ventricular myocytes to develop a mouse model of TSC rhabdomyomas. Mice with ventricular *Tsc1* loss had a median survival of 6 months and none of them survived longer than 8 months. These mice showed dilated cardiomyopathy and scattered foci of enlarged cardiac myocytes with apparent vacuoles. These enlarged cells increased levels of glycogen and p-S6, similar to findings in TSC patient rhabdomyoma cells (Meikle *et al*. 2005).

Mice have also been developed with conditional disruption of *Tsc2* in pancreatic *β* cells (*βTsc2*$^{-/-}$). These mice displayed decreased blood glucose levels, higher concentration of plasma insulin, increased *β* cell mass and improved glucose tolerance (Rachdi *et al*. 2008, Shigeyama *et al*. 2008). Rapamycin treatment reverted the metabolic phenotype observed in *βTsc2*$^{-/-}$ mice (Rachdi *et al*. 2008). By 40 weeks of age, however, *βTsc2*$^{-/-}$ mice exhibited progressive hyperglycemia and

hypoinsulinemia (Shigeyama *et al*. 2008). These data suggest that TSC1/TSC2/mTOR pathway has a critical role in the regulation of *β* cell mass and function, and targeting this pathway may be an effective therapy for diabetic patients. A mutant mouse model with oocyte-specific deletion of *Tsc2* (*OoTsc2*$^{-/-}$ mice) was also developed (Adhikari *et al*. 2009). Deletion of *Tsc2* in oocytes caused premature activation of all primordial follicles around the time of puberty. This deletion resulted in depletion of follicles in early adulthood, causing premature ovarian failure (POF) (Adhikari *et al*. 2009).

Meikle *et al*. (2007) generated and studied a new brain model of TSC (*Tsc*$^{c-}$*SynICre*$^{+}$ mice). *Tsc*$^{c-}$*SynICre*$^{+}$ mice displayed delayed development, median survival of 35 days, spontaneous seizures, neuropathological abnormalities including ectopic, enlarged and aberrant neurons in multiple locations and persistent hypomyelination (Meikle *et al*. 2007). In another pre-clinical study, Ehninger *et al*. (2008) developed a mouse model with homozygous conditional deletion of *Tsc1* in the neurons of the postnatal forebrain (*Tsc1*^{cc}-αCaMKII-Cre mice). These mice had a more severe phenotype than the *Tsc2*$^{+/-}$ mice and most of them died within a week of birth. Those that survived exhibited extreme macroencephaly due to neuronal hypertrophy as well as astrogliosis (Ehninger *et al*. 2008). Furthermore, astrocyte-specific *Tsc1* conditional knockout mice (*Tsc1*^{cc}-GFAP-Cre mice) generated by Uhlmann *et al*. (2002), developed epilepsy by 1 month of age, increased astrocyte proliferation by 3 weeks of age, showed abnormalities in hippocampal neuronal organisation between 3-5 weeks and typically died at 3-4 months.

Conditional knockout was also used to generate a hypomorphic *Tsc2* allele by deleting exon 3 (Table 1.5) (Pollizzi *et al*. 2009). *Tsc2*$^{del3/del3}$ embryos survived until embryonic day 13.5, longer than the *Tsc2*$^{-/-}$ embryos. They died as a result of underdevelopment of the liver, poor hematopoiesis, aberrant vascular development and haemorrhage. The development of renal lesions was markedly reduced (10-15 fold less) in the *Tsc2*$^{+/del3}$ mice in comparison with the *Tsc2*$^{+/-}$ mice. In addition, biochemical analysis of mouse embryonic fibroblast (MEF) cell lines and embryos which were homozygous for the *del3* allele, showed elevation of mTORC1 and

suppression of Akt signalling. This Tsc2-del3 mouse model appeared to be a good representative model for hypomorphic *TSC2* missense mutations found in individuals with TSC (Pollizzi *et al*. 2009).

1.4.4 Allograft mouse model

Kidney and liver pathology in transgenic TSC mouse models is age-dependent and thus the use of these models in pre-clinical studies is time-consuming. For this reason, Lee *et al*. (2005) generated a nude mouse model for TSC-related lesions by transplantation of a *Tsc2*$^{-/-}$, *Trp53*$^{-/-}$ MEF cells though subcutaneous injection. These mice developed measurable tumours between days 18-29 (Lee *et al*. 2005).

Table 1.5 *Tsc1* and *Tsc2* alleles in rodent models (adapted from Kwiatkowski *et al*. 2010).

Species	Gene	Allele name	Exon targeted/ mutation	Major features of heterozygote animals	Major references
Rat	*Tsc2*	Eker	Intracisternal A-particle (IAP) element insertion into codon 1272	Cystadenomas-carcinomas of kidney Splenic hemangiomas Uterine leiomyomas Pituitary adenomas Subependymal and subcortical hamartomas	Eker *et al*. 1981, Everitt *et al*. 1992, Hino *et al*. 1993, Yeung *et al*. 1997
Mouse	*Tsc2*	-, Kwiatkowski	Neomycin cassette insertion into exon 2	Cystadenomas of kidney Liver hemangiomas Extremity angiosarcomas	Onda *et al*. 1999
Mouse	*Tsc2*	-, Hino	Neomycin cassette insertion into exon 2, deletion of exons 2-5	Cystadenomas of kidney Liver hemangiomas	Kobayashi *et al*. 1999
Mouse	*Tsc1*	-, Hino	Neomycin cassette insertion and deletion of exons 6-8	Cystadenomas of kidney Liver hemangiomas	Kobayashi *et al*. 2001
Mouse	*Tsc1*	-, Kwiatkowski	Deletion of exons 17 and 18	Cystadenomas of kidney Liver hemangiomas	Kwiatkowski *et al*. 2002
Mouse	*Tsc1*	-, Cheadle	Deletion of exons 6-8 with insertion of neomycin cassette	Cystadenomas of kidney Liver hemangiomas Reduced survival of $Tsc1^{+/-}$ when in C57BL/6 strain $Tsc1^{+/-}$ kidney cancer in BALB/c strain	Wilson *et al*. 2005
Mouse	*Tsc2*	*neo*, Gambello	Neomycin cassette insertion into exon 1	Hypomorphic allele: renal cysts only at 20 months of age, and $Tsc2^{neo/neo}$ embryos survive to E17 in some cases	Hernandez *et al*. 2007
Mouse	*Tsc2*	*del3*, Kwiatkowski	Deletion of exon 3	Hypomorphic allele: reduced severity of renal tumours, 1-2 day longer survival of $Tsc2^{del3/del3}$ embryos	Pollizzi *et al*. 2009
Mouse	*Tsc2*	*KO*, Gambello	Deletion of exons 2-4	Cystadenomas of kidney Little published data	Hernandez *et al*. 2007
Mouse	*Tsc2*	-, Kobayashi	Deletion of exons 3-4	Little published data	Shigeyama *et al*. 2008

1.5 Molecularly targeted therapy of TSC

There is currently no cure for TSC. TSC therapy was primarily focused on the natural mTOR inhibitor rapamycin and its derivatives (Jóźwiak *et al*. 2006). Metformin might also have potential for treatment of TSC patients due to its reported anti-tumour activity and inhibitory effect on mTOR signalling (Anisimov *et al*. 2005, Gwinn *et al*. 2008, Inoki *et al*. 2003). Other agents tested for candidate therapies for TSC include statins. Statins were found to reduce the risk of colon, breast, lungs and prostate cancers (Khurana *et al*. 2005, Kochhar *et al*. 2005, Poynter *et al*. 2005, Singal *et al*. 2005). Atorvastatin was shown to selectively inhibit the proliferation of *Tsc2*$^{-/-}$ MEFs and to inhibit the phosphorylation of S6 kinase, and S6 in *Tsc2*$^{-/-}$ cells and in *Tsc2*$^{+/-}$ mice (Finlay *et al*. 2007). However, lesions in *Tsc2*$^{+/-}$ mice had no response to treatment with atorvastatin (Finlay *et al*. 2009).

1.5.1 Rapamycin

Rapamycin also called sirolimus, was isolated from the bacterium *Streptomyces hygroscopicus* from the soil of Easter Island in the 1970s (Vézina *et al*. 1975, Sehgal *et al*. 1975). It was found to have antibiotic, anti-fungal, anti-proliferative, anti-inflammatory and immunosuppressant properties. This drug has been used to prevent rejection in organ transplantation and restenosis following balloon angioplasty (Jóźwiak *et al*. 2006). It is an analogue of the macrolide antibiotic FK506 (Abraham *et al*. 1996) and binds to the intracellular receptor protein FKBP12 (FK506-binding protein 12), a member of the family of FK506-binding proteins. The FKBP12-rapamycin complex specifically binds to mTORC1 and inhibits its function (Figure 1.10) (Inoki *et al*. 2005). Since mTORC1 is a key mediator of cell growth and proliferation, rapamycin has been tried to treat different cancers. Rapamycin is an appealing therapeutic option for TSC since loss of *TSC1* or *TSC2* leads to constitutive activation of mTOR signalling pathway (Tee *et al*. 2003).

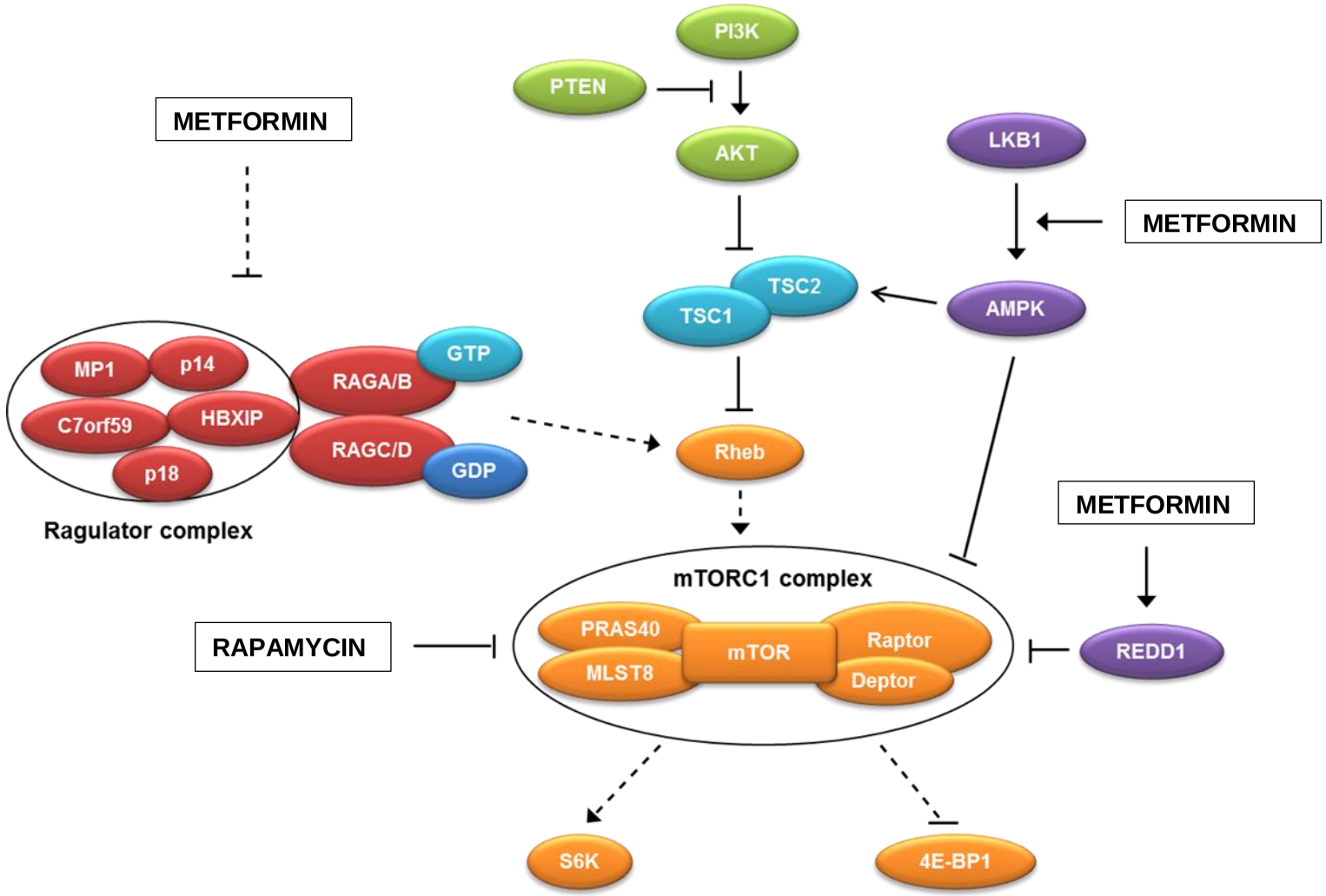

Figure 1.10 Mechanisms underlying rapamycin and metformin action. Rapamycin/FKBP12 complex binds with very high affinity to mTORC1 and inhibits it. Metformin suppress mTORC1 signalling by AMPK-dependent and -independent pathways. First, metformin activates AMPK via LKB1 leading to phosphorylation of TSC2 and Raptor, and to subsequent mTORC1 inhibition. Second, metformin inhibits mTORC1 through inactivation of the Ragulator complex. Metformin also downregulates mTORC1 through p53-mediated REDD1 upregulation.

The poor solubility of rapamycin in water, its instability and concerns regarding side-effects have led to the synthesis of three rapamycin analogues with better pharmaceutical activities: temsirolimus (CCI-779, cell cycle inhibitor-779) (Wyeth), everolimus (RAD001) (Novartis) and ridaforolimus (AP23573) (Ariad Pharmaceuticals). The efficacy of these derivatives was tested in several *in vitro* and *in vivo* systems (Clarkson *et al*. 2002, Geoerger *et al*. 2001, Schuler *et al*. 1997).

1.5.1.1 Anticancer activity of rapamycin

1.5.1.1.1 Eker rat and rapamycin treatment

Renal tumours in the Eker rat exhibited mTORC1 activation. Short-term treatment of these rats with rapamycin dramatically inhibited mTORC1 activity and cellular proliferation (Kenerson *et al*. 2002). Serial non-invasive ultrasound imaging was utilised to monitor the *Tsc2*-related renal tumour size during rapamycin treatment (Kenerson *et al*. 2005). Treatment of animals for up to 2 months resulted in significant reduction in renal tumour volume (more than 90% tumour volume regression). Histological analysis confirmed this with the appearance of “tumour scars” and clearance of the lesion tissue. Nevertheless, drug resistance was evident in a small proportion of renal tumours following prolonged treatment (Kenerson *et al*. 2005). Conversely, rapamycin did not prevent tumour development since administration of the drug at the time of tumour “initiation” (between 2-4 months of age), reduced the development of macroscopic tumours but did not affect the number of microscopic precursor lesions (Kenerson *et al*. 2005). These results suggest that, although mTOR activation is essential for lesion progression, other signalling pathways are influencing tumourigenesis. Additional beneficial effects of rapamycin treatment included increased survival of rats with pituitary tumours. Samples of pituitary tumour obtained from treated animals showed activation of apoptosis and suppression of mTORC1 activity (Kenerson *et al*. 2005).

1.5.1.1.2 TSC mouse model and rapalogue treatment

Several pre-clinical studies using TSC mouse models were carried out to evaluate the anti-tumour efficacy of rapamycin and analogues (both rapamycin and its analogues are referred to as rapalogues). Lee *et al*. (2005) reported that 3 month treatment of *Tsc2*$^{+/-}$ mice with CCI-779 significantly reduced the number of cystadenomas per kidney (62-92% reduction) compared with the untreated group. Significant reduction in tumour growth and improved survival was also seen in nude mouse models injected with *Tsc2*$^{-/-}$, *Trp53*$^{-/-}$ MEFs after CCI-779 treatment. In addition to CCI-779, Lee *et al*. (2005) tested the effects of interferon gamma (IFN-γ) since increased IFN-γ expression is associated with a lower frequency of renal tumours in TSC patients, and found similar effects to CCI-779 treatment. However, one year later, Lee *et al*. (2006) showed that although IFN-γ treatment has some advantages, it is not as effective as CCI-779 when used as a single agent to treat nude mice bearing *Tsc2*$^{-/-}$ tumours. Additionally, no significant benefit of combination therapy of CCI-779 with IFN-γ was seen compared to treatment with CCI-779 alone in *Tsc2*$^{+/-}$ mice (Messina *et al*. 2007).

Rapamycin was also reported to have significant therapeutic effects for brain and neurologic manifestations in TSC mouse models. Treatment of adult *Tsc2*$^{+/-}$ mice with rapamycin improved deficits related to two spatial learning tasks, contextual discrimination and abnormal long-term potentiation (LTP) (Ehninger *et al*. 2008). Meikle *et al*. (2008) demonstrated improvement in median survival (from 33 to >100 days), weight gain and a neurological phenotype (neurofilament abnormalities, myelination and cell enlargement) in *Tsc1*$^{null\text{-}neuron}$ mice following treatment with rapamycin or RAD001. These drugs also suppressed mTORC1 and Akt signalling in the brain, improved neurofilament abnormalities, myelination and cell enlargement but had only modest effects in dendritic spine density and length (Meikle *et al*. 2008). Zeng *et al*. (2008) used a mouse model with conditional inactivation of the *Tsc1* gene in glial fibrillary acidic protein (GFAP)-positive cells (*Tsc1*GFAP CKO mice). Rapamycin treatment inhibited the progression of astrocyte proliferation and megencephaly whilst increasing expression of astrocyte-specific glutamate transporters Glt-1 (glutamate transporter 1) and GLAST (glutamate aspartate

transporter). Early treatment with rapamycin, starting at postnatal day 14, prevented epilepsy and dramatically improved survival to greater than 6 months in comparison with untreated *Tsc1*^{GFAP} CKO (conditional knockout) mice which usually died by 3 to 4 months of age. Late rapamycin treatment, started after the onset of seizures (6 weeks of age), decreased seizures and expanded the life span of the rodents (Zeng *et al*. 2008). Lastly, Rauktys *et al*. (2008) reported improved survival and reduced growth of subcutaneous TSC-related tumours in a nude mouse model following topical application of rapamycin. These findings suggest that topical rapamycin may be effective in treating TSC skin lesions in TSC patients.

1.5.1.1.3 Use of rapalogues in TSC clinical trials

Rapalogues have been used in a number of TSC clinical trials. Oral rapamycin treatment resulted in regression of all SEGAs in a small scale MRI study involving 5 subjects (Franz *et al*. 2006). Similarly, treatment with RAD001 for three months reduced seizure frequency and volumes of SEGAs in TSC patients (Krueger *et al*. 2010). Bissler *et al*. (2008) conducted a 24 month trial to determine the efficacy of rapamycin on AMLs in TSC patients and sporadic LAM cases. MRI and CT were performed to monitor the changes in tumour volumes along with pulmonary-function tests. AMLs regressed during the 12 months of rapamycin administration but regrew following drug withdrawal. In addition, some LAM patients exhibited improvement in lung function following therapy that persisted after treatment (Bissler *et al*. 2008). In another 2 year clinical trial, involving 16 TSC patients, rapamycin caused sustained AML shrinkage in all patients (Davies *et al*. 2011). On the basis of these results, randomised control trials have been undertaken to evaluate the therapeutic efficacy of rapamycin or analogues in a range of TSC or LAM-related clinical problems (Bissler *et al*. 2013, Davies *et al*. 2010, Franz *et al*. 2013). These studies confirmed efficacy of everolimus for SEGA and AML and the drug is now approved for treatment of these tumours in TSC patients in North America and Europe

1.5.1.1.4 Adverse events associated with rapamycin treatment

However, there are several concerns regarding rapamycin treatment for TSC. Firstly, long term treatment with rapamycin is thought to be unfavourable because of its immunosuppressive properties and short term rapamycin treatment may be clinically ineffective (Franz *et al*. 2006). Second, several studies observed an increase in tumour volume once treatment was discontinued (Bissler *et al*. 2008, Franz *et al*. 2006). Thirdly, treatment with rapalogues is associated with significant side effects including diarrhoea, pyelonephritis, stomatitis, upper respiratory tract infections (Bissler *et al*. 2008) and dose related reduction in blood platelet (PLT) count (Murgia *et al*. 1996).

Another concern is that rapamycin-mediated mTOR inhibition results in a loss of negative feedback inhibition towards Akt. Treatment of *Tsc1* null and *Tsc2* null MEF cell lines with rapalogues led to upregulation of Akt due to reduced IRS-1 degradation (O'Reilly *et al*. 2006, Sarbassov *et al*. 2006, Sun *et al*. 2005, Zhang *et al*. 2003). Hyperactivation of Akt might promote tumourigenesis (Bhaskar and Hay, 2007; Manning and Cantley, 2007).

1.5.2 Metformin

Metformin is a biguanide drug, derived from the French lilac plant (*Galega officinallis*) and has been widely used for lowering blood glucose in type 2 diabetic (T2D) patients for over 40 years (Bailey and Turner, 1996; Stumvoll *et al*. 1995). Decreased hepatic glucose production (Hundal *et al*. 2000, Stumvoll *et al*. 1995) and increased skeletal myocyte glucose uptake (Galuska *et al*. 1994, Hundal *et al*. 1992) contribute to its glucose-lowering effect. This drug is also used to treat non-alcoholic fatty liver disease (NAFLD) (Kaser *et al*. 2010) and polycystic ovarian syndrome (PCOS) (Diamanti-Kandarakis *et al*. 2010). Long-term treatment with metformin is generally well tolerated in diabetic patients with minimal toxicity and no major side-effects. Studies suggest that metformin prolongs life span in experimental models that have been used for investigation of mechanism of aging (Mouchiroud *et al*.

2010, Onken and Driscoll, 2010). Increasing evidence suggests that metformin has anti-tumour activities *in vitro* and *in vivo* (Pierotti *et al*. 2013).

1.5.2.1 Anticancer activity of metformin

1.5.2.1.1 Epidemiological evidence

A recent meta-analysis combining several studies indicated an increased risk of cancer in patients with type 2 diabetes (Vigneri *et al*. 2009). However, several population-based studies reported reduced risk of cancer in diabetic patients receiving metformin than those untreated or treated with other drugs (Bowker *et al*. 2006, Evans *et al*. 2005, Landman *et al*. 2010, Libby *et al*. 2009). Metformin was also reported to decrease risk of prostate and pancreatic cancer in some clinical studies (Li *et al*. 2009, Wright and Stanford, 2009).

1.5.2.1.2 Experimental data in tumour models

Anti-tumour activity of metformin has been demonstrated using several cancer models. In a chemopreventive study, metformin treatment delayed the onset of chemically-induced mammary carcinogenesis in female Sprague-Dawley rats (Bojkova *et al*. 2009). In a pre-clinical trial, chronic metformin treatment prolonged the mean life span of transgenic female mice carrying the HER-2 oncogene. It also significantly decreased the incidence and size of mammary adenocarcinomas and delayed tumourigenesis (Anisimov *et al*. 2005). In another study, oral and intraperitoneal (i.p.) administration of metformin prevented tobacco-specific carcinogen 4-(methylnitrosamino)-1-(3-pyridyl)-1-butanone (NNK)- induced lung tumourigenesis by 40-50% (oral) and ~75% (i.p.) in A/J mice, respectively (Memmott *et al*. 2010).

In vitro experiments also suggested anti-proliferative action of metformin on breast cancer cells (Alimona *et al*. 2009, Zakikhani *et al*. 2006). Metformin treatment inhibited the growth of breast cancer cells and suppressed mTORC1 activity

(Zakikhani *et al*. 2006). Furthermore, the growth inhibitory effect of metformin was demonstrated on prostate and colon cancer cells *in vitro* through AMPK activation (Zakikhani *et al*. 2008). Liu *et al*. (2009) reported the effects of metformin upon triple negative breast cancer both *in vitro* and *in vivo* (nude mice bearing tumour xenografts of the TN line MDA-MB-231). Although TN is a very aggressive form of cancer, metformin treatment suppressed cell proliferation, colony formation and induced apoptosis (Liu *et al*. 2009). Interestingly, this drug was found to selectively target and kill cancer stem cells in four genetically different types of breast cancer. Metformin may therefore represent a potential anti-cancer therapeutic (Hirsch *et al*. 2009).

1.5.2.2 Molecular mechanisms of mTORC1 inhibition

Metformin suppresses mTORC1 activity via multiple mechanisms in both AMPK-dependent and independent manners (Figure 1.10). Previous publications showed that metformin stimulates the activity of AMPK in the presence of LKB1 tumour suppressor (Zakikhani *et al*. 2006, Zhou *et al*. 2001). LKB1 phosphorylates AMPK at Thr172 of the activation loop within the catalytic subunit promoting its activation (Hong *et al*. 2003, Woods *et al*. 2003). AMPK activation leads to attenuation of mTORC1 signalling in the presence or absence of functional TSC1-TSC2 complex, through two distinct mechanisms as described in section 1.3.3.3 (Gwinn *et al*. 2008, Inoki *et al*. 2003).

Recent evidences suggest that metformin may suppress mTORC1 activity through two additional AMPK-independent mechanisms. Ben Sahra *et al*. (2011) and Kalender *et al*. (2010) reported metformin-induced mTORC1 inhibition through p53-mediated REDD1 upregulation and through inhibition of the Rag GTPases, respectively. Metformin increases REDD1 expression which normally acts to suppress mTORC1 during hypoxia (Ben Sahra *et al*. 2011). Metformin treatment also negatively regulates mTORC1 by inhibiting the ‘Ragulator complex’ (Kalender *et al*. 2010).

1.6 Project aims

The main purpose of this project was to identify mTOR inhibitors for prevention and therapy of TSC using transgenic mouse models. Specific aims are:

- To evaluate T2 weighted MRI for assessment of renal lesions using both *Tsc1*$^{+/-}$ and *Tsc2*$^{+/-}$ mouse models by comparison with histological analysis.
- To assess the effects of continuous metformin treatment on renal lesions in a *Tsc1*$^{+/-}$ mouse model using T2 weighted MRI and histological analysis.
- To investigate the preventive effects of long term treatment with rapamycin, metformin or both on renal tumours in a *Tsc2*$^{+/-}$ mouse model using histological analysis.
- To analyse the effects of the different treatments on mTORC1 signalling by IHC and Western analysis.

CHAPTER TWO

Materials and methods

2.1 *Suppliers*

Materials and equipment used within this study were purchased from the following companies:

Abbott Laboratories Ltd, Maidenhead, UK

Abcam, Cambridgeshire, UK

Adam Equipment Co Ltd, Perth, Australia

Analyze Direct Inc., Overland Park, USA

Aperio Technologies, Oxford, UK

Applied Biosystems, Cheshire, UK

Azer Scientific, Morgantown, USA

Baxter Healthcare Ltd, Thetford, UK

Becton Dickinson, Oxford, UK

Bibby Scientific Ltd, Staffordshire, UK

Bio-Rad Laboratories Ltd, Hertfordshire, UK

Bruker, Ettlingen, Germany

Camlab Ltd, Cambridgeshire, UK

Cell Signalling Technology, Danvers, MA, USA

Charles River Laboratories, Kent, UK

Corning Life Sciences, New York, USA

DAKO, Cambridgeshire, UK

Eurogentec, Hampshire, UK

GE Healthcare Life Sciences, Buckinghamshire, UK

Grant Instruments Ltd, Cambridgeshire, UK

Greiner Bio One Ltd, Gloucestershire, UK

Invitrogen Life Sciences, Paisley, UK

Labnet International, Woodbridge, USA

Labtech International Ltd, East Sussex, UK

LC Laboratories, Woburn, USA

Leica Microsystems Ltd, Milton Keynes, UK

Merck, Darmstadt, Germany

Merz Hygiene, Frankfurt, Germany

New England Biolabs, Hertfordshire, UK

Nikon, Surrey, UK

Peco Services Ltd, Cumbria, UK

Prestige Medical Ltd, Blackburn, UK

Promega, Southampton, UK

Qiagen, West Sussex, UK

RelonChem, London, UK

SAI Inc., Stony Brook, New York, USA

Sigma-Aldrich Company Ltd, Dorset, UK

Simport, Beloeil, QC, Canada

Sony, Hampshire, UK

Stuart Scientific, Essex, UK

Swann-Morton Ltd, Sheffield, UK

Thermo Fisher Scientific, Surrey, UK

Ultra-Violet Products Ltd, Cambridgeshire, UK

VWR International, Leicestershire, UK

2.2 *Materials*

2.2.1 Animals

The *Tsc1*$^{+/-}$ mouse model was generated in the Institute of Medical Genetics, Cardiff University as previously described (Wilson *et al*. 2005) and the *Tsc2*$^{+/-}$ mouse model was provided by Dr. David J. Kwiatkowski (Onda *et al*. 1999). The wild type balb/c mice were purchased from Charles River (UK).

2.2.2 General chemicals and drugs

All standard laboratory chemicals were obtained from either Sigma-Aldrich or Thermo Fisher Scientific. Chemical Metformin was supplied by Merck (Germany) and Metformin (500 mg tablets) by RelonChem (UK). Rapamycin was provided by the LC Laboratories (USA). Polyethylene glycol 400 (PEG-400), Tween-80 and Dimethyl sulfoxide (DMSO) used for the preparation of vehicle solution were all purchased from Sigma-Aldrich.

2.2.3 DNA extraction and purification kit

Wizard® SV Genomic DNA Purification System was supplied by Promega and Proteinase K was obtained from Qiagen.

2.2.4 Polymerase chain reaction

PCR Master Mix (2X) was provided by Promega. TSC1 and TSC2 Primers were synthesized by Eurogentec. PCR tube (0.2 ml) and domed cap strips were supplied by Thermo Fisher Scientific.

2.2.5 Agarose gel electrophoresis

Agarose *(*molecular biology grade) for standard electrophoresis was obtained from Eurogentec and Ethidium bromide solution from Sigma-Aldrich. Gel Loading Dye, Blue (6X) was supplied by New England Biolabs.

2.2.6 Anaesthesia

Isoflurane used for induction of animal anaesthesia was provided from Baxter Healthcare.

2.2.7 Exsanguination

BD Plastipak 1 ml Hypodermic Syringes and BD Hypodermic 0.6 x 25 mm needles were supplied by Thermo Fisher Scientific. MiniCollect® K3EDTA 1.0 ml blood plasma tubes were obtained from Greiner Bio One.

2.2.8 Tissue collection

Isopentane used for tissue snap-freezing, Nalgene 15 ml General Long term storage cryogenic tubes and Sterilin 30 ml universal containers were provided by Thermo Fisher Scientific.

2.2.9 Antibodies

Primary antibodies used against β-actin (#4970), GAPDH (#2118), phospho-S6 ribosomal protein ($Ser^{235/236}$) (#2211), phospho-AMPKα (Thr^{172}) (#2535), phospho-Acetyl-CoA Carboxylase (Ser^{79}) (#3661), phospho-Raptor (Ser^{792}) (#2083), phospho-Akt (Ser^{473}) (#3787), phospho-4E-BP1 (Thr^{70}) (#9455) and MCM2 (#3619) were all supplied by Cell Signalling Technology. Primary antibodies used against Cyclin D1 (ab134175), Ki67 (ab16667) and MUC1 (ab15481) were supplied by Abcam. Secondary horseradish peroxidise-conjugated antibody against rabbit (#7074) was purchased from Cell Signalling Technology.

2.2.10 DNA and protein size markers

The 100 bp DNA ladder was supplied by New England Biolabs. Novex® Sharp prestained and MagicMark™ XP western protein standards were purchased from Invitrogen Life Technologies.

2.2.11 Histology

Formaldehyde Raymond Lamb tissue fixative, plastic processing cassettes, alcohol, xylene, Histoplast paraffin wax, Mayer's Haematoxylin stain, 1% w/v Aqueous Eosin stain solution, 25 x 75 x 1.0 mm polysine slides, 24 x 40 mm coverslips and DPX mountant were all provided by Thermo Fisher Scientific. Histology tissue mould and microtome blades were supplied by Leica Microsystems.

2.2.12 Immunohistochemistry

EXPOSE Rabbit Specific AP (red) Detection IHC Kit was purchased from Abcam. Xylene, DPX mounting medium and 22 x 50 mm cover glass were provided from VWR International and wax pen from DAKO. Hematoxylin solution and TWEEN® 20 viscous liquid were obtained from Sigma-Aldrich and Ethanol 99+% (GLC) absolute from Thermo Fisher Scientific.

2.2.13 Treatment of disposable Tissue Ruptor probes

RNase-free water and RNase Zap solution were supplied by VWR International and Applied Biosystems respectively. Disinfectant Pursept-A Xpress was obtained from Merz Hygiene.

2.2.14 DNA, RNA and protein extraction from tissues

AllPrep® DNA/RNA/Protein Mini Kit was supplied by Qiagen and the 14.3 M 2-Mercaptoethanol and the DL-Dithiothreitol solutions by Sigma-Aldrich.

2.2.15 Western blot

Hybond ECL Nitrocellulose Membranes and ECL Advance Western Blotting Detection Kit were purchased from GE Healthcare Life Sciences. NuPAGE® LDS Sample Buffer (4X), NuPAGE® Transfer Buffer (20X) and NuPAGE® MES SDS Running Buffer (20X) (for Bis-Tris Gels only) were supplied by Invitrogen Life Technologies and 3 MM Whatman filter paper by Thermo Fisher Scientific.

2.3 *Equipment*

2.3.1 PCR Thermal Cycler

MJ Research PTC-225 DNA Engine Tetrad Peltier Thermal Cycler was provided by Bio-Rad Laboratories.

2.3.2 Agarose gel electrophoresis apparatus

Power Source™ 300 V Power Supply and KuroGEL Mini Plus 10 Horizontal gel tanks were purchased from VWR International. BioDoc-It® Imaging System was obtained from Ultra-Violet Products and Digital UP-895MD Graphic Printer from Sony.

2.3.3 Magnetic resonance imaging system

The BioSpec 94/20 USR Preclinical MRI System was supplied by Bruker.

2.3.4 Photography

Nikon Coolpix 4500 Digital Camera was bought from Nikon UK.

2.3.5 Animal dissecting kit

Highland™ Portable Precision Balance used for animal weight measurement was provided by Adam Equipment Co Ltd. Disposable Sterile Scalpels were obtained from Swann-Morton Ltd and dissection set from VWR International. Long forceps for handling samples in freezing bath were supplied by Thermo Fisher Scientific.

2.3.6 Histology

Tissue dehydration, clearing and paraffin impregnation steps were facilitated by LEICA TP1050 tissue processor, LEICA EG1150 H and LEICA EG1150 C machines. LEICA RM2235 microtome (Leica Microsystems Ltd, UK) and Raymond Lamb Stain mate machine were supplied by Thermo Fisher Scientific.

2.3.7 Immunohistochemistry (IHC)

The Slide Staining Tray System was obtained from Azer Scientific and the EasyDip™ Slide Staining Rack from Simport. An Advanced Ergonomic System Microscope with 100W Illumination Leica DM2500 was provided by Leica.

2.3.8 Slide scanning

Histological and immunohistochemical slides were scanned to create digital slides using the Scanscope® CS slide scanner which was provided by Aperio Technologies.

2.3.9 Tissue disruption and homogenation

TissueRuptor and TissueRuptor Disposable Probes were obtained from Qiagen.

2.3.10 DNA, RNA and protein quantification

NanoDrop® 8-sample Spectrophotometer (ND8000) provided by Labtech International was used to measure DNA, RNA and protein concentration.

2.3.11 Western blot equipment

XCell *SureLock*® Mini-Cell Electrophoresis system, XCell II™ Blot Module, PowerEase® 500 Power Supply (220/240 VAC 50/60 Hz), NuPAGE® Novex 4-12% Bis-Tris Gels 1.0 mm (12-Well, 15-well, 17-well) and sponge pads for blotting were all supplied by Invitrogen Life Technologies. Stuart Orbital shaker SSM1 was obtained from Bibby Scientific Ltd. BioSpectrum® Imaging System was purchased from Ultra-Violet (UV) Products and Digital UP-895MD Graphic Printer from Sony.

2.4 *Buffers and solutions*

10X DNA agarose gel loading buffer

1.5 g Ficoll

2 ml 0.5M EDTA

1 ml 10% SDS

0.025 g Bromophenol

First dissolve Ficoll (1.5 g) in 5 ml dH_2O in 50°C (water bath) before adding other chemicals. Add dH_2O up to 10 ml.

50X TAE Buffer

To produce 1 litre solution:

242 g Tris Base (121.1 MW)

57.1 ml Glacial Acetic Acid

100 ml 0.5 M EDTA

Dissolve Tris in about 600 ml of ddH_2O and then add EDTA and Acetic Acid. Add ddH_2O up to 1 L.

Protein resuspension buffer

1 ml ALO

8 mg DTT

Add Dithiothreitol (DTT) into ALO buffer before use.

10X Tris Buffered Saline (TBS)

To produce 1 litre solution:

24.2 g 1 M Tris HCl (pH 7.6)

80 g NaCl

Add dH_2O up to 1 L (pH to 7.6 with 1N HCl).

1X TBS-T

100 ml 10X TBS

900 ml dH_2O

1 ml Tween-20 (0.1%)

10 mM sodium citrate buffer

To produce 1 litre solution:

2.94 g Tri-sodium citrate dihydrate

Add dH_2O up to 1 L (pH to 6.0 with 1N HCl)

Stripping buffer (25 ml)

175 µl 2-mercaptoethanol (MW 78.13)

5 ml 10% SDS

12.5 ml 125 mM Tris.HCl (MW 121.14)

7.325 ml dH_2O

Vehicle solution

2.5% PEG-400

2.5% Tween-80

2.5% DMSO

Rapamycin solution

Two mg/ml Rapamycin was prepared in a vehicle solution containing:

2.5% PEG-400

2.5% Tween-80

2.5% DMSO.

2.5 Methodology

2.5.1 Animal husbandry

Mice used in this study were kept under standard laboratory conditions in the Animal research facility of the School of Biosciences, Cardiff University, in open topped cages and provided with standard rodent diet and de-chlorinated water. All cages were held in a 19-23°C room temperature, 55+/- 10% room relative humidity and provided with 12 hour light and 12 hour dark cycle (8:00am- 20:00pm each day). *Tsc1*$^{+/-}$ and *Tsc2*$^{+/-}$ mouse models were backcrossed on the background of the balb/c strain at least 10 times to produce *Tsc1*$^{+/-}$ balb/c and *Tsc2*$^{+/-}$ balb/c mice respectively. All animals used in trials of this study were randomly allocated into different treatment groups with balanced sex, age and litter mates using Graphpad (http:/www.graphpad.com/welcome.htm). All animal procedures were carried out in accordance with the UK Home Office guidelines. Animals were monitored by trained technicians for animal work. Body weight of the animals was one of the major factors we look for that might be affected by treatment. Body weight was monitored every week. The animals were humanely sacrificed if additional clinical signs such as less active behaviour and piloerection appeared following treatment.

2.5.2 Genotyping

2.5.2.1 DNA extraction

DNA was extracted from mouse ear punches (1-2 mm ear punch) to determine genotype for breeding and further experiments. DNA was purified using Wizard® SV Genomic DNA Purification System. Briefly, ear punches were removed from each mouse, placed in 1.5 ml eppendorf tubes and kept frozen at -20°C. After thawing, 68.75 µl digestion solution (50 µl Nuclei Lysis solution, 12.5 µl 0.5 M EDTA pH 8.0, 5

µl 20mg/ml Proteinase K, 1.25 µl 4 mg/ml RNase A) was added into each sample. Samples were then incubated in a 55°C water bath overnight (16-18 hours). Each sample was then immersed in 62.5 µl Wizard® SV Lysis buffer and mixed. Sample lysate was subsequently transferred into a Wizard® SV Minicollumn and centrifuged at 13,000 rpm for 3 minutes (min). Three-hundred microliters of Wizard® SV Wash solution was then added to each sample and the assembly was centrifuged at 13,000 rpm for 1 min. Following centrifugation, the flow-through was discarded and three washes with 150 µl wash solution were carried out by spinning at 13,000 rpm for 1 min. The flow-through was discarded after each wash and an extra 2 min centrifugation at 13,000 rpm was performed to remove any residual wash solution. The minicolumn was finally transferred into a fresh 1.5 ml eppendorf tube along with 100 µl Nuclease-Free water, incubated for 3 min at room temperature and centrifuged at 13,000 rpm for 1 min to collect DNA samples.

2.5.2.2 Polymerase chain reaction

DNA extracted from the mouse ear punches was used for genotyping by PCR. PCR reaction was performed in a total volume of 10 µl solution containing 4.5 µl template DNA (25-50 ng), 5 µl PCR master mix (2X) (50 units/ml of *Taq* DNA polymerase pH 8.5, 400 µM dATP, 400 µM dGTP, 400 µM dCTP, 400 µM dTTP, 3 mM $MgCl_2$) and 0.5 µl 100 µM primer mix (20X). Primers used for genotyping the Tsc1 mouse model, were TSC1Intron8WT1F 5'TGGGACTACTGGGATGAGAGTT3', TSC1Intron8LoxP1F 5'TCGCCTTCTTGACGAGTTCT3' and TSC1Intron8WT1R 5'GGCAATGCTACAGCAAGACA3'. Primers for genotyping the Tsc2 mouse model, were TSC2W-F 5'AATCGCATCCGAATGATAGG3', TSC2W-R 5'GTTTAATGGGCCCTGGATCT3' and TSC2M-R 5'GGATGATCTGGAGGAAGAGC3'.

Following an initial step of 95˚C for 2 min, 35 cycles of PCR reaction was conducted at 94˚C for 30 seconds (sec) (Tsc1) or 94˚C for 40 sec (Tsc2), 52˚C for 30 sec (Tsc1) or 56˚C for 40 sec (Tsc2) and 72˚C for 30 sec (Tsc1) or 72˚C for 1 min (Tsc2) with a final extension step of 72˚C for 5 min.

2.5.2.3 Agarose gel electrophoresis

Following PCR, agarose gels of 1.5% (w/v) concentration were prepared using 1X TAE buffer to screen for the heterozygous *Tsc1*$^{+/-}$ and *Tsc2*$^{+/-}$ mice. Ethidium bromide (0.05 µg/ml) was added to gels for viewing DNA bands under UV light. Ten microliters of PCR product mixed with 2 µl Gel Loading Dye (6X) were loaded into each gel well. Gels were submerged in 1X TAE buffer and run at 80 Volts for approximately an hour. DNA products were visualised through UV exposure using BioDoc-It® Imaging System and fragment sizes were compared with 1kb DNA fragment ladder run on the same gel in a separate well. Gel images were captured using a Digital UP-895MD Graphic Printer.

2.5.3 Drug treatment

2.5.3.1 Metformin treatment

Metformin used for mouse treatment in this thesis, was either provided in drinking water or by gavage. Daily dosage of chemical metformin (Merck, Germany) in drinking water was 150-600 mg/kg body weight, assuming that a mouse consumes 15 ml water per 100 g body weight a day. Metformin solution (in drinking water) was changed every 3 days. Metformin (500 mg) tablets (RelonChem, UK) were diluted in water at 30 mg/ml and delivered by gavage. Metformin alone was given at 300 mg/kg 5 times a week.

2.5.3.2 Rapamycin treatment

R-5000 Rapamycin (LC Laboratories, USA) was prepared at 2 mg/ml in vehicle solution (2.5% PEG-400, 2.5% Tween-80 and 2.5% DMSO). Mice were treated with 5-10 mg/kg rapamycin via intra-peritoneal injection (i.p.) five times a week. Dosage was decreased accordingly if mice were found sick or rapid loss of body weight was observed. In the prevention study, rapamycin was given once a week for the last month.

2.5.3.3 Combination drug treatment

For combination drug treatment, R-5000 rapamycin was given at 2.5-4 mg/kg five times a week by intra-peritoneal injection and metformin (500 mg tablets) at 150 mg/kg five times a week by gavage. Dosage was decreased accordingly if mice were found sick or rapid loss of body weight was observed. In the prevention study, rapamycin was given once a week for the last month.

2.5.4 Magnetic resonance imaging

Magnetic resonance imaging (MRI) scans were carried out at the Experimental MRI Centre (EMRIC) at Cardiff University (http://www.cardiff.ac.uk/biosi/researchsites/emric/facilities.html) using a high-field (9.4 T) small bore (20 cm) Bruker Biospec 94/20 MRI/MRS spectrometer equipped with S116 high performance gradient insert and avance II electronics. Scans were acquired using a 72 mm id transmit/receive quadrature polarised birdcage rf coil.

Mice were anaesthetised with 5% isoflurane in a 40% O_2/air mix at 1.2 L/min, injected with 2 x 0.2 ml of 4% glucose/0.18% saline solution subcutaneously and transferred to specialist MRI bed model #T10532 (Bruker, Germany) with integrated circulating heated water and anaesthetic nose cone. Isoflurane was reduced to ~1.5 to 2% for the maintenance of anaesthesia during scanning. Body temperature, breathing rate and heart rate were monitored throughout using the Model 1025 Monitoring and Gating System (SAI Inc., New York). Body temperature was maintained during recovery in a warm air V1200 recovery chamber (Peco Services Ltd, UK) set at 27°C.

T2 weighted, respiratory gated, fat suppressed RARE scans were performed with an FOV of 10.0 x 4.0 cm, a matrix of 640 x 256, and 64 x 0.5 mm coronal slices, a TEeff of 26 ms, a TR of 4100 ms, a RARE factor of 4, a BW of 100 kHz. Proton density

weighted, respiratory gated, FLASH scan was performed with an FOV of 10.0 x 4.0 cm, a matrix of 480 x 192, and 64 x 0.5 mm coronal slices, a TR/TE of 675/4.25 ms, a FA of 30° and BW of 200 kHz, NEX 4. T2* (Proton density) weighted, respiratory gated, FLASH scan was performed with an FOV of 10.0 x 4.0 cm, a matrix of 480 x 192, and 64 x 0.5 mm coronal slices, a TR/TE of 860/7 ms, a FA of 30° and BW of 200 kHz, NEX 4.

T2 weighted MRI images obtained from the MRI scans were used to assess the renal lesions using the software Analyze 9.0 (Analyze Direct Inc., USA). All lesions detected by MRI were counted and their volumes were measured for each mouse. The total volume measurement of each lesion (mm^3) was calculated by adding lesion volumes of all slices. The lesion type (cystic, papillary and solid) was documented and whole kidney volumes were also measured. The measurement was conducted blindly in terms of treatment information. Finally, to evaluate the efficiency and the detection rate of renal lesions by T2 weighted MRI, MRI analysis was compared and confirmed with findings by histological analysis.

2.5.5 Animal dissection

2.5.5.1 Exsanguination

Mice were anaesthetised and blood was collected from the heart via exsanguination (cardiac puncture). Blood samples were obtained following the end of each drug treatment. Induction of anaesthesia was achieved by placing the animal in the inhalation chamber and by setting oxygen level at 2 L/min and Isoflurane (inhalation anaesthetic) at 5 units.

Anaesthesia was maintained by transferring the animal to the inhalation mouth adapter and by setting Isoflurane at 2.5 units. The animal was laid down on its back and pain response was tested by pinching tails and toes. If pain was detected, the inhalation level was increased. Blood was collected from heart using a 1 ml syringe with a needle (23g/1”) just behind the xiphoid cartilage and by a gentle aspiration of

the blood into the syringe. In order to reach the heart; the needle was entered at 10-30 degrees from the horizontal axis of the sternum. Around 0.5 ml of blood was collected from each mouse and kept in MiniCollect® K3EDTA 1.0 ml blood plasma tube. Blood samples were left for 2 hours at room temperature and centrifuged for 5 min at 8,000 rpm. Plasma aliquots were prepared into 50 or 100 µl and stored at -80°C.

2.5.5.2 Necropsy analysis

Following exsanguination, oxygen and Isoflurane were turned off and mice were killed by cervical dislocation, and dissected. Necropsy analysis included macroscopic examination which allowed the internal organs to be inspected. The spleen, the kidneys, the liver, the heart, the lungs and the brain were examined carefully and any signs of lesions were recorded.

2.5.5.3 Tissue collection

During dissection, half of the brain, a portion of the large lope of the liver and kidneys were harvested from each animal, fixed in 10% buffered formalin saline (pH 7.0) for 24 hours, processed and embedded in paraffin according to standard histological procedures (see details in 2.5.6.1). The rest part of the liver and brain, the heart, the lungs, the spleen and the tail, were snap frozen. Briefly, fresh tissues were placed in a 1-litre glass beaker containing cold isopentane, to prevent the formation of ice crystals in tissues. The glass beaker was embedded in a larger container filled with liquid nitrogen. The samples were left in isopentane until they became frozen and removed with long metal forceps. These frozen tissues were then stored in cryotubes at -80°C for use in further molecular analysis.

2.5.6 Histology

2.5.6.1 Tissue fixation, embedding and sectioning

Fixed tissues were placed into tissue prep cassettes for dehydration, clearing and embedding; all these processes carried out in LEICA TP1050 tissue processor. Tissues were subjected to dehydration in 70% ethanol (1 hour), 95% ethanol (1 hour), 100% ethanol (1 hour) x 2, 100% ethanol (1.5 hours) and to clearing by two changes of immersions in xylene; first immersion for 45 minutes and a second one for 1 hour. This was followed by three immersions in molten paraffin wax (60°C) for 1 hour x 2 and 1.5 hours.

During the final embedding stage, each specimen was embedded into a mold filled with molten paraffin wax, allowed to set and hardened onto a cold plate. Both processes were accomplished on LEICA EG1150 H and LEICA EG1150 C machines. The firm paraffin block was then popped out of the mould and paraffin embedded kidneys were sectioned at 5 µm (with or without interruption at 200 µm intervals) using the LEICA RM2235 microtome and then placed in a 45°C water bath and collected onto 25 x 75 x 1.0 mm polysine slides. Sections were transferred on a hot plate, allowed to dry and then moved to a 45°C oven and left overnight (12 hours).

2.5.6.2 Haematoxylin and eosin staining

Paraffin embedded kidney sections were H&E stained using the following protocol: xylene (2 min) x 3, 100% ethanol (1 min) x 3, 95% ethanol (1 min), 70% ethanol (1 min), running water (1 min), Mayer's Haematoxylin (2 min), running water (5 min), 1% Aqueous Eosin (10 min), running water (15 sec), 70% ethanol (15 sec), 95% ethanol (30 sec), 100% ethanol (1 min), 100% ethanol (2 min) x 2, xylene (2 min) x 3. Haematoxylin stained the nuclei of cells blue/black, whilst Eosin coloured cell cytoplasm and most connective tissue fibres pink. Sections were then mounted under a coverslip using DPX mountant and left to dry.

2.5.7 IHC

Slides containing paraffin embedded 5 micron thick sections of *Tsc1*$^{+/-}$ and *Tsc2*$^{+/-}$ mouse kidneys, were deparaffinised and rehydrated in xylene x 3, 100% ethanol, 70% ethanol, 50% ethanol and water for 5 min each. For pre-staining treatment, sections were placed in a plastic slide rack and boiled in a microwave oven, in a 1-litre glass beaker containing 10 mM Citrate buffer (pH 6.0) for 10 min. Slides were cooled for 10 min at room temperature and immersed in water and in 1X TBS-T x 3 for 5 min per wash. The EXPOSE Rabbit Specific AP (red) Detection IHC Kit was used to immunostain the paraffin sections. This kit contains AP Conjugate, Co-factor (Enhancer), Fast Red Chromogen, Napthol Phosphate and Protein block. Sections were circled with a wax pen and placed in a humidified chamber. Following 10 min incubation with 4 drops of Protein block at room temperature to block non-specific background staining, each section was incubated overnight with diluted primary antibody (1:200 rabbit anti-PS6 in diluted Blocking solution- 30 µl Normal blocking goat serum plus 2 ml 1X TBS-T) at 4°C according to the manufacturer's protocol. The next morning, slides were washed in 1X TBS-T for 5 min x 3, exposed to the alkaline phosphatase (AP) secondary antibody conjugate (4 drops) for 30 min at room temperature and rinsed again in 1X TBS-T buffer x 4. One hundred and fifty microliters of Enhancer was then applied to each slides and incubated for 4 min at room temperature. An equal volume of Naphthol Phosphate and Fast Red was mixed just before use. One hundred and fifty microliters of the mixture were added onto each slide with Enhancer and incubated for around 8 min at room temperature. After another 4 rinses in 1X TBS-T followed by water, slides were counter-stained with haematoxylin for 2 min and rinsed about 5 min in tap water. Sections were dehydrated and cleared in 50% ethanol, 70% ethanol, 100% ethanol and xylene for 5 min each. DPX was used to mount slides with a cover slip and sections were left to dry. Immunohistochemical slides were viewed using an Advanced Ergonomic System Microscope with 100W Illumination Leica DM2500 and scanned using a Scanscope™ CS slide scanner.

2.5.8 Slide scanning

The resulting haematoxylin and eosin (H&E) stained and IHC slides were scanned (40x magnification) using the ScanScope® CS microscope slide scanner (Aperio Technologies, UK) and the digital slides created (.svs files), were viewed using the Aperio ImageScope™.

2.5.9 Histological analysis

The digitised images of previously scanned H&E stained kidney sections using the Aperio system (http://www.aperio.com/?gclid=CNXN-_8by4aUCFcINfAods3eg1w), were used to take photographs of individual renal lesions on its maximum size with a reference scale length. Lesion photographs were subsequently exported to ImageJ (http://rsbweb.nih.gov/ij) for analysis. Each renal lesion was assessed by calculating the maximum cross-sectional whole lesion area (lesion size) and cellular area (excluding fluid filled cystic areas). In addition, lesion location and type (cystic, papillary or solid) were recorded, and total lesion number and volume per animal were measured and compared between different groups of treated mice. Histological analyses were conducted blindly in terms of treatment status of mice.

2.5.10 RNA, DNA and protein extraction from tissues

2.5.10.1 Tissue disruption and homogenation

RNA, DNA and proteins were extracted from frozen tissues using AllPrep® DNA/RNA/Protein Mini Kit (Qiagen). Briefly, samples previously stored in -80°C were cut in a sterile liquid nitrogen cold plastic dish in a mortar. Tissues were immediately transferred into a round-bottom tube containing 600 µl RLT and homogenised as quickly as possible using TissueRuptor (30-45s operation). Samples were centrifuged for 3 min at 12,000 rpm and the supernatant was stored at -80°C for future use or transferred to ALLPrep DNA spin column placed in a new 2 ml collection tube and centrifuged for 30 sec at 12,000 rpm. The ALLPrep DNA spin column was placed in a new 2 ml collection tube and stored at 4°C for later DNA purification.

2.5.10.2 RNA purification

The flow-through was combined with 430 µl 100% ethanol, mixed well and up to 700 µl of the sample was transferred to an RNeasy spin column placed in a 2 ml collection tube, centrifuged for 15 sec at 12,000 rpm and the flow-through was kept at 4°C for later protein purification (transferred into a capped tube). Successive centrifugations were carried out in the same RNeasy spin column if the sample volume exceeded 700 µl. The RNeasy spin column was placed in a fresh collection tube, where 700 µl of Buffer RW1 was added and the solution was centrifuged for 15 sec at 12,000 rpm. The filtrate was discarded and another two washes were performed to wash the spin column membrane, using 500 µl of Buffer RPE and spinning for 15 sec at 12,000 rpm. The flow-through was discarded after each wash and an extra 2 min of centrifugation at 12,000 rpm was performed to remove any residual buffer. The RNeasy spin column was placed in a new 1.5 ml collection tube and the RNA was eluted by adding 30-50 µl RNase-free water directly into the spin column membrane and by spinning for 1 min at 12,000 rpm. The last step was repeated If the expected RNA yield was >30 µg, using another 30-50 µl of RNase-free water. RNA samples were stored at -80°C.

2.5.10.3 Protein purification

One volume of Buffer APP was added to the flow-through (kept previously at 4°C) and the solution was mixed vigorously, incubated for 10 min at room temperature to precipitate proteins, and centrifuged for 10 min at full speed. The supernatants were removed carefully and 500 µl of 70% ethanol was added into the tube containing the protein pellet. Samples were centrifuged for 1 min at 12,000 rpm. Supernatants were removed again and protein pellets were dried at room temperature for 10 min. Protein pellets were resuspended in around 150 µl Buffer ALO. DTT was added to Buffer ALO before use (8 mg DTT/ 1 ml ALO). Protein solutions were incubated for 5 min at 95°C, cooled down to room temperature and centrifuged for 1 min at 13,000 rpm. Aliquots of the supernatants (10-30 µl each) were stored at -80°C and used for western analysis.

2.5.10.4 DNA purification

Five hundred microliters of Buffer AW1 was added into an ALLPre DNA spin column and the column was centrifuged for 15 sec at 12,000 rpm. The flow-through was discarded and a second wash was performed using 500 µl of Buffer AW2 and spinning for 15 sec at 12,000 rpm. The flow-through was discarded again and followed by an extra 2 min of centrifugation at full speed to remove any residual buffer from the washes. Finally, the ALLPrep DNA spin column was placed in a new 1.5 ml collection tube and the DNA was eluted in 100 µl EB Buffer (preheated to 70°C) after incubation for 2 min at room temperature and centrifugation for 1 min at 12,000 rpm. The resulting DNA samples were stored at -20°C.

2.5.11 Nucleic acid and protein quantification

Nucleic acid (ng/µl) and protein (mg/ml) concentration was determined with UV spectrophotometry at 260nm and 280nm wavelengths respectively, using the ND8000 8-sample NanoDrop Spectrophotometer.

2.5.12 Treatment of disposable Tissue Ruptor probes

Following usage of Tissue Ruptor probes, they were submersed and quickly spun twice in 500 ml fresh dH_2O using the tissue Ruptor (~30 sec operation). Probes were subsequently rinsed and washed four times in 500 ml fresh dH_2O (3 min/wash) on an orbital shaker, dipped into RNase Zap solution and rinsed with 500 ml ddH_2O x 3. Finally, they were rinsed in RNase-free H_2O, wrapped with foil, autoclaved and dried in an oven of 60 °C. Probes can be used for 5-10 times.

2.5.13 Western blot analysis

2.5.13.1 *Electrophoresis and blotting*

Electrophoresis was performed using Invitrogen Novex XCell SureLock™ Mini-Cell Electrophoresis system according to manufacturer's protocol. NuPAGE Novex 4-

12% Bis-Tris Gels (1.0 mm) of 12, 15 and 17 wells were used for the separation of small to medium sized proteins. Protein samples were diluted in distilled water if necessary, and then in NuPAGE LDS Sample Buffer (1X) in a total volume of 10 µl. These samples were briefly spun, incubated at 70°C for 10 min and briefly spun again before loading into the wells. Four-12% Bis-Tris gels were run with 1X NuPAGE MES SDS Running Buffer at 200 V constant for 35 min. Proteins were then transferred to a Hybond ECL membrane at 30V constant for 1 hour in 1X NuPAGE Transfer Buffer using the Invitrogen XCell II™ Blot Module; accordingly with manufacturer's protocol. The filter paper and the blotting pads were pre-soaked in transfer buffer before blotting. Membrane (9 cm x 8.5 cm) was firstly immersed in distilled water and equilibrated in transfer buffer for around 10 min before use.

2.5.13.2 *Blocking and incubation*

After protein blotting, the membrane was immersed into 10 ml of 1X TBS-T plus 2% (w/v) ECL Advance Blocking Agent for 1 hour at room temperature on an orbital shaker, to block any non-specific binding and rinsed with two changes of 15 ml 1X TBS-T buffer. Primary antibody was diluted (dilution factor determined empirically for each antibody) with 10 ml 1X TBS-T supplemented with 2% (w/v) ECL Advance Blocking Agent. Membranes were incubated in the diluted primary antibody for 1 hour at room temperature on an orbital shaker, rinsed with 15 ml 1X TBS-T twice and washed in 30 ml 1X TBS-T, firstly for 15 min and then for 5 min x 3 with fresh 1X TBS-T at room temperature on an orbital shaker. Membranes were then incubated in secondary antibody (conjugated with horse radish peroxidase- HRP; diluted 1:10000 in 10 ml 1X TBS-T supplemented with 2% (w/v) ECL Advance Blocking Agent) for 1 hour at room temperature on an orbital shaker. Membranes were rinsed with 15 ml 1X TBS-T twice, washed in 30 ml 1X TBS-T for 15 min and washed again for 5 min x 3 with fresh 1X TBS-T. All washes were carried out at room temperature on an orbital shaker. The ECL detection reagents were allowed to equilibrate to room temperature from 4°C. An equal volume of detection solution 1 was mixed with detection solution 2 to cover the membranes (~2 ml total volume/membrane). The washed membrane was drained well to remove any excess TBS-T, placed in a clean plastic square plate with protein side up and covered with the prepared mixture of

detection reagents. After 5 min of incubation at room temperature, the membrane was drained and wrapped with cling film. BioSpectrum Imaging System was used to visualise chemiluminescent signals and photos of scanned images were obtained using the Digital UP-895MD Graphic Printer. Different exposure settings were used (2 sec up to 5 min) to optimise the exposure conditions for data collection. Scanned images were displayed and further analysed for densitometry using the ImageJ image processing program.

2.5.14 Statistics

Wilcoxon signed-rank test, Wilcoxon rank-sum (Mann-Whitney) test and Kruskal-Wallis equality-of-populations rank test were used in MRI and Histological analyses for comparisons between different treatment groups. Two tailed Student's t-Test was used for comparison of Western analysis. $P \leq 0.05$ was considered to be statistically significant.

CHAPTER THREE

Evaluation of T2 weighted MRI for assessing renal lesions in *Tsc1*$^{+/-}$ and *Tsc2*$^{+/-}$ mouse models

3.1 Introduction

T2 weighted MRI has been used to detect renal lesions for assessment of therapeutic effects of chemicals in *Tsc2* knockout mouse models in several preclinical trials (Brown *et al*. 2005, Lee *et al*. 2005). Nevertheless, no preclinical studies have used MRI to follow-up renal lesions *in vivo* or have managed properly to assess the detection rate of renal lesions by MRI in these models. In this study, we evaluated T2 weighted small bore MRI for assessing renal lesions in both *Tsc1*$^{+/-}$ and *Tsc2*$^{+/-}$ mouse models by comparison with histological analysis.

3.2 Materials and methods

3.2.1 DNA extraction and genotyping

As outlined in section 2.5.2.1, DNA was extracted from mouse ear punches, using the Wizard® SV Genomic DNA Purification System. Briefly, ear tissues were digested in 68.75 µl digestion solution (50 µl Nuclei Lysis solution, 12.5 µl 0.5 M EDTA pH 8.0, 5 µl 20mg/ml Proteinase K, 1.25 µl 4 mg/ml RNase A) for 16-18 hours at 55˚C and samples were subsequently immersed in Wizard® SV lysis buffer, applied to a spin column, centrifuged, washed and dissolved in 100 µl nuclease-free water. Genotyping was determined by PCR as described in section 2.5.2.2. Results were visualised using gel electrophoresis on 1.5% agarose gels.

3.2.2 Animals and procedures

Five *Tsc1*$^{+/-}$ (Wilson *et al*. 2005), 4 *Tsc2*$^{+/-}$ (Onda *et al*. 1999) and 5 wild type balb/c mice were used in this trial. Both mouse models were backcrossed with the balb/c strain (Charles River, UK) at least 10 times. Mice were first scanned with MRI at the

age of 12 months followed by a second scan two months later. After the second MRI scan, mice were killed humanely (detailed protocol was outlined in section 2.5.5). Necropsy was performed involving macroscopic examination of the spleen, kidneys, liver, heart, lungs and brain in all animals. Kidney tissues were collected for further histological analysis.

3.2.3 MRI

A detailed MRI procedure is outlined in section 2.5.4. The volumes of renal lesions were measured using the software Analyze 9.0. The measurement was conducted blindly in triplicate. The lesion types were confirmed by histology.

3.2.4 Histology

Kidneys were harvested from animals and fixed in 10% buffered formalin saline (pH 7.0) for 24 hours at RT. Kidney sections were prepared as follows. Fixed kidney samples were processed for dehydration, clearing and embedding in molten paraffin wax (60°C). Paraffin embedded kidneys were sectioned at 5 μm (at 200 μm intervals) and series of microscope slides were H&E stained. H&E stained slides were scanned to create virtual slides using the Aperio ScanScope® CS scanner. Virtual slides were viewed using the Aperio ImageScope™ and used to take photographs of individual renal lesions with a reference length for subsequent scale setting. Photos were subsequently exported to ImageJ for analysis as described in section 2.5.9.

3.2.5 Statistical analysis

The Wilcoxon signed-rank test was performed for all comparisons as indicated in Tables 3.1 and 3.2 (Stata software, version 11). Student's t-test was used for comparison of total lesion number between the *Tsc1* and *Tsc2* mouse models. $P \leq 0.05$ was considered to be statistically significant. An Altman-Bland plot was used to show differences in total volumes of "follow up" lesions between the first and second

MRI scan. “Follow-up” lesions refer to those that were identified in both the first and second scans.

3.3. Results

3.3.1. Genotyping

PCR based genotyping was carried out for *Tsc1* and *Tsc2* in mice. PCR products were analysed by electrophoresis on 1.5% agarose gels followed by staining with ethidium bromide. Mutant and wild-type alleles were 283 base pairs (bp) and 352 bp for *Tsc1* and 658 bp and 849 bp for *Tsc2*, respectively (Figure 3.1).

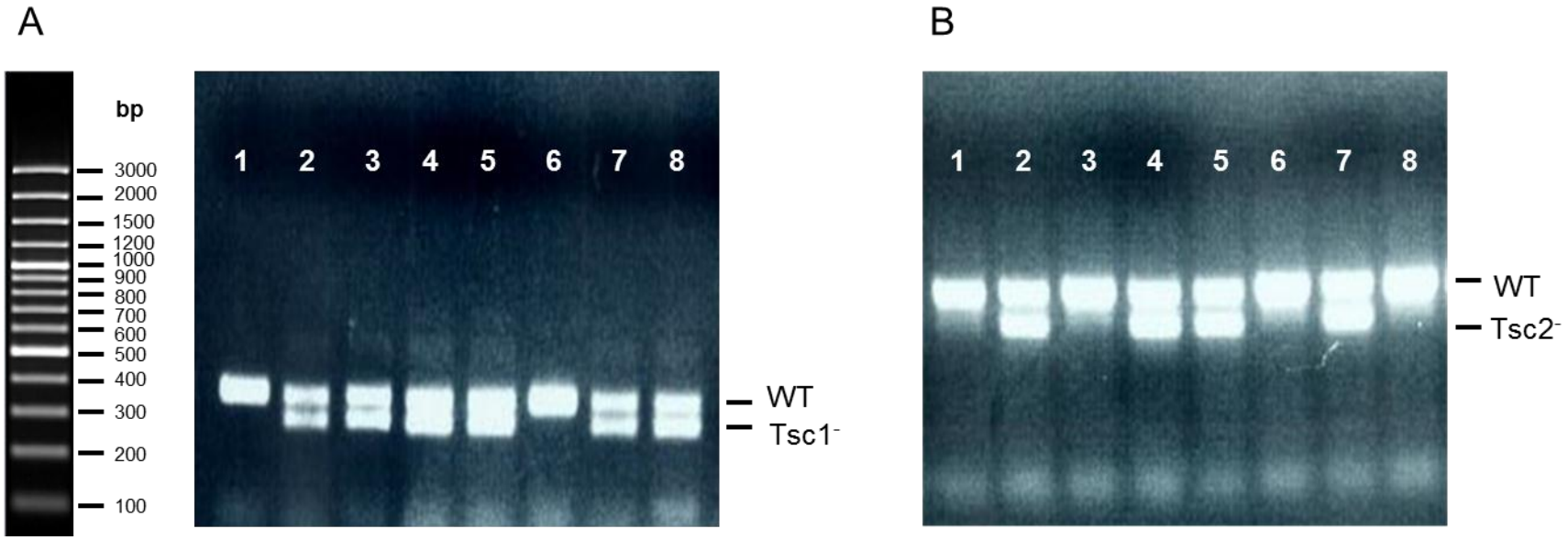

Figure 3.1 Mouse genotyping by PCR using ear DNA. PCR products were run on 1.5% agarose gels, stained with ethidium bromide and visualised on a UV scanner. One hundred bp DNA Ladder was used as a size marker. **(A)** *TSC1* genotyping. Samples in lanes 2, 3, 4, 5, 7 & 8 are heterozygous for *Tsc1*. **(B)** *TSC2* genotyping. Samples in lanes 2, 4, 5 & 7 are heterozygous for *Tsc2*.

3.3.2. T2 weighted MRI

3.3.2.1 Detection of renal lesions in vivo using T2 weighted MRI

T2 weighted small bore MRI scans were performed on 5 *Tsc1*$^{+/-}$, 5 *Tsc2*$^{+/-}$ and 5 wild type mice firstly at 12 months and then at 14 months of age. Sixty four coronal slices, 0.5 mm each, were acquired spanning each animal (Figure 3.2). The images obtained from the MRI scans were used for ascertaining the number of renal lesions and measurement of volumes of renal lesions using the Analyze 9.0 software.

Different types of renal lesions were detected after examination of the T2 weighted MRI scans. We termed these lesions cystic, papillary and solid lesions for practical purposes (Figure 3.3). Renal lesions appeared as regular/irregular spherical structures that varied from bright lesions (cysts) to bright but with grey/dark area lesions (papillary), to solid lesions. Cysts were the most easily detectable renal lesions consistent with their fluid-filled nature which had high signal intensity on T2 weighted images. Solid lesions were recognised by their darker colour or by morphological changes between the kidney tissue and the solid lesion which caused deformed kidneys. Renal lesions were detected in all *Tsc1*$^{+/-}$ and *Tsc2*$^{+/-}$ mice and varied in number, size, type, morphology and location. As expected, no renal lesions were found in wild-type balb/c mice in either the first or second MRI scan.

The type (cystic, papillary or solid lesion) and location of each renal lesion were recorded and all lesions were counted in each animal. The volume of individual lesions was measured slice by slice from MRI scans. By summing the volumes obtained from the first to the last contiguous slices containing the particular lesion, the final volume of that lesion was determined (e.g. total lesion volume detected in one of the *Tsc1*$^{+/-}$ mice (labelled as TSC1-1) by the first MRI was 8.86mm^3) (Table 3.1, Figure 3.3). The first MRI scan revealed a total number of 226 renal lesions in all 9 mice of both models (Table 3.1). The smallest lesion detected in the kidneys tissues by T2 weighted MRI was < 0.1 mm^3.

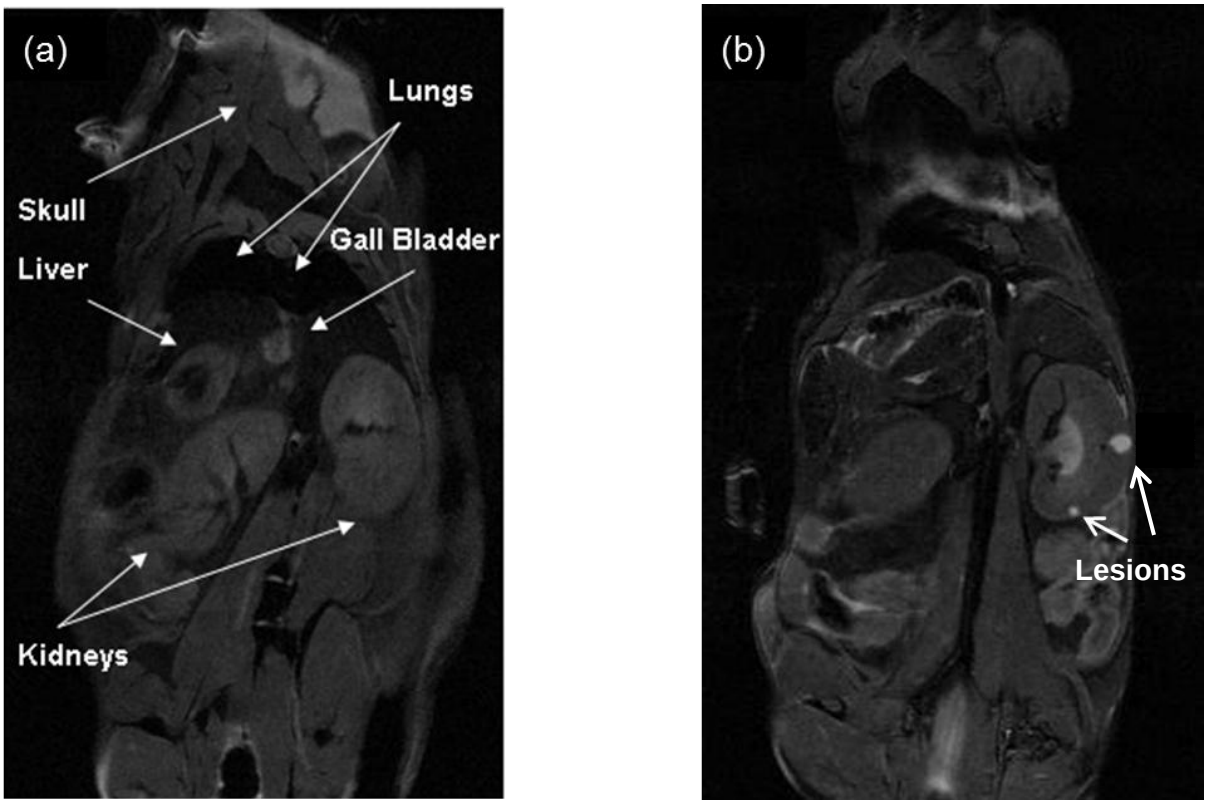

Figure 3.2 T2 weighted MRI (full length coronal views) for *Tsc1*$^{+/-}$ mice. **(a)** Anatomical landmarks. **(b)** Renal lesions detected in the right kidney of a *Tsc1*$^{+/-}$ mouse.

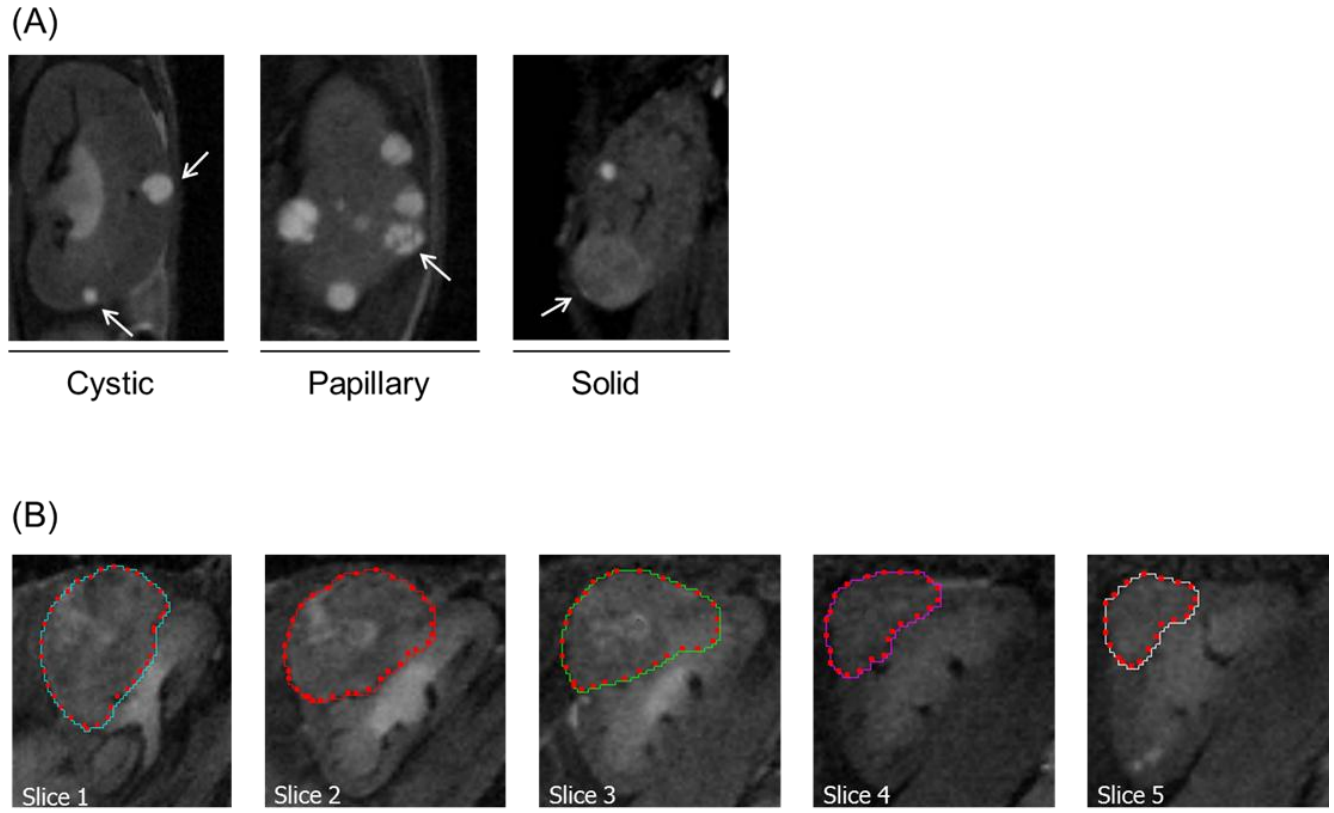

Figure 3.3 T2 weighted MRI analysis. **(A)** Different types of Tsc-associated mouse renal lesions detected by T2 weighted MRI (see arrowheads). **(B)** Contiguous 0.5 mm-thick MRI slices from anterior (Slice 1) to posterior (Slice 5), showing the volume measurement (mm^3) of a solid tumour in a Tsc mouse kidney. A total volume of a lesion is the sum of volumes measured from all individual slices containing the lesion.

Table 3.1 Analysis of mouse renal lesions and kidneys *in vivo* by T2 weighted MRI.

Mouse	Total number of lesions			Total volume of all lesions (mm^3)		Total volume of follow-up[a] lesions (mm^3)		Total volume of kidneys (mm^3)	
	1st MRI	2nd MRI	Follow-up[a]	1st MRI	2nd MRI	1st MRI	2nd MRI	1st MRI	2nd MRI
TSC1–1	14	15	12	8.86	14.17	8.69	13.6	534.79	557.9
TSC1–2	12	12	9	15.64	22.82	15.28	21.75	784.18	746.8
TSC1–3	20	32	17	11.24	19.86	11.03	15.75	794.47	796.08
TSC1–4	10	11	8	17.24	39	14.83	37.81	563.58	553.65
TSC1–5	15	22	14	21.13	46.21	20.47	45.58	439.37	483.78
TSC2–1	27	44	25	21.42	46.06	21.28	40.87	694.23	654.06
TSC2–2	70	72	56	90.31	130.84	88.78	128.36	992.33	1011.74
TSC2–3	20	23	18	114.77	128.51	114.31	127.91	930.12	826.97
TSC2–4	38	42	33	60.95	91.99	47.28	84.59	646.36	694.91
Total	226	273	192	361.56	539.46	341.95	516.22	6379.43	6325.89
Z[b]	2.61			2.66		2.66		0.06	
P[b]	0.009			0.008		0.008		0.925	

[a] "Follow-up" lesions were those that were detected in both the 1st and 2nd MRI scans with the assumption that the lesions would not disappear spontaneously between the two MRI scans.
[b] *z* and *P* values were obtained by Wilcoxon signed-rank test between the 1st and 2nd MRI.

3.3.2.2 "Following up" renal lesions using T2 weighted MRI

A second T2 weighted MRI scan was performed to test whether the lesions detected in the first scan could be re-identified ("followed up") two months later. This also allowed us to monitor any changes in lesion size and number *in vivo*. Any changes in lesion type and size such as tumour growth from the first to the second MRI scan were recorded.

Two hundred and seventy three renal lesions were detected in the second scan in all 9 *Tsc1*$^{+/-}$ and *Tsc2*$^{+/-}$ mice. One hundred and ninety two of these renal lesions were similarly detected in the first MRI scan (192/226), indicating that 85% of the renal lesions identified in the first scan were detected in the second scan (Table 3.1). "Follow up" renal lesions revealed significant differences in lesion size between the two scans (P= 0.008), with a significant lesion growth in the 9 untreated animals, from 341.95 mm^3 to 516.22 mm^3 (Figure 3.4).

In addition, there were significant differences in the total lesion number (P= 0.009) and volume (mm^3) (P= 0.008) in all mice, between the two scans (Table 3.1). The total number of all renal lesions identified in mice was increased from 226 to 273 in the second scan (Table 3.1). Furthermore, the total volume of renal lesions was considerably increased in all animals, from 361.56 mm^3 in the first scan to 539.46 mm^3 in the second scan. However, no significant differences were seen in total kidney volumes between the two scans (P= 0.925) (Table 3.1).

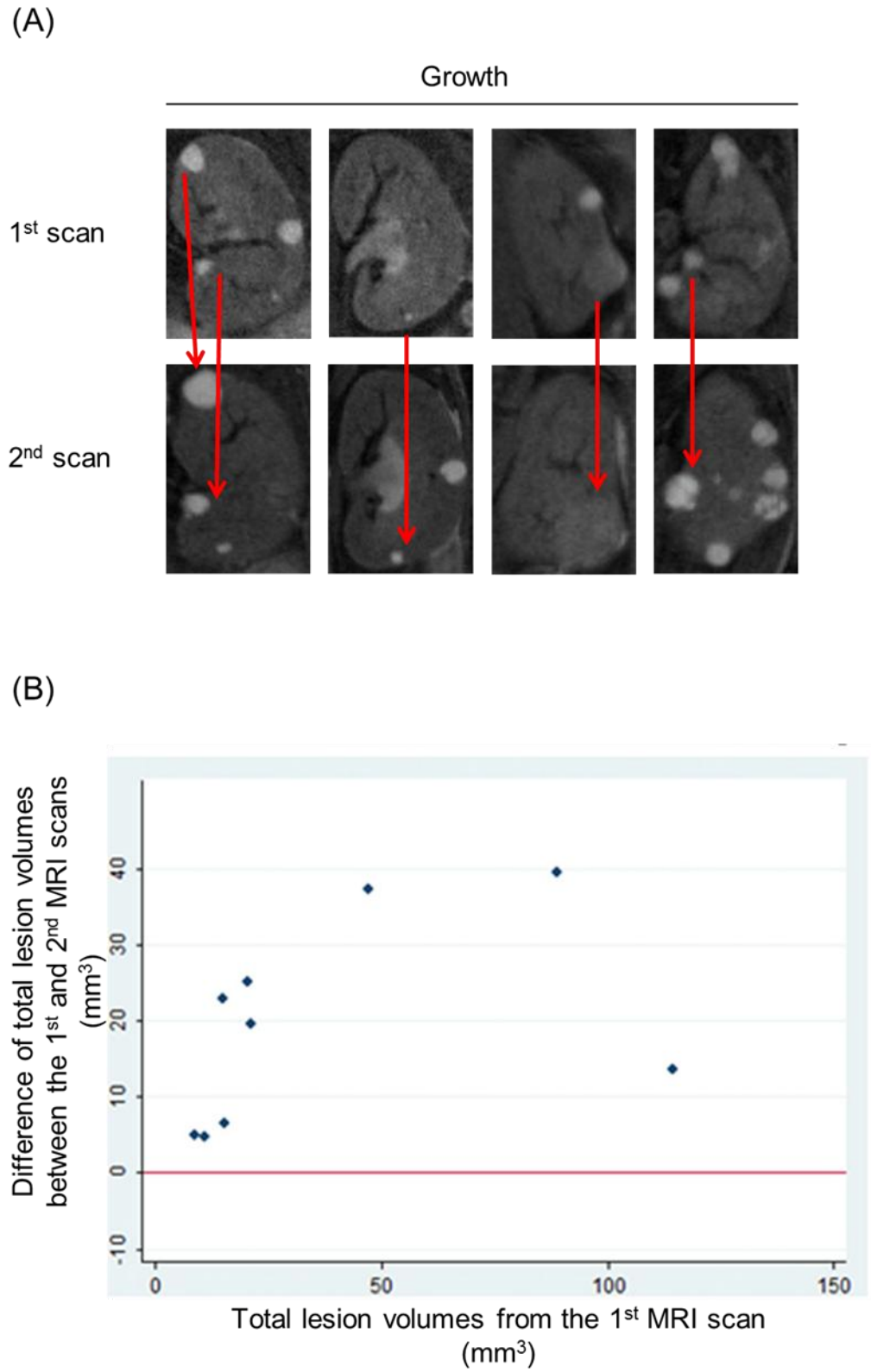

Figure 3.4 Growth of renal lesions detected by T2 weighted MRI. **(A)** T2 weighted MRI images showing lesion growth (no treatment). **(B)** Altman-Bland plot showing lesion growth in 9 animals. The total lesion volumes were obtained from "follow-up" lesions that were detected in both the first and second MRI scans (see also Table 3.1). Difference of total lesion volumes = total lesion volumes from the second MRI scan – total lesion volumes from the first MRI scan.

3.3.3 Histological analysis

3.3.3.1 Renal lesions detection by histological analysis

All animals were killed for further analysis shortly after the second MRI scan. The kidneys from all 14 months old mice were removed, fixed in 10% buffered formalin saline overnight, processed and embedded into paraffin wax for sectioning. A series of 5 µm sections were prepared with 200 µm interval from each kidney. Sections were then H&E stained. Slides were scanned to make virtual slides for image acquisition and lesion evaluation. Virtual slides were examined and used to take photographs of individual renal lesions with a reference scale length. Lesion photos were subsequently exported to ImageJ for analysis. The type and location of each renal lesion were recorded, the total lesion number was counted and the total volume was measured per animal (Table 3.2). Each renal lesion was assessed by calculating the maximum cross-sectional whole lesion area and cellular area (mm^2) (Figure 3.5).

Renal lesions identified by histology ranged from pure cysts, through papillary to solid lesions and varied in number, size, shape and location (Figure 3.6). Cystic lesions were lesions with a single epithelial cell lining (pure cysts) and papillary lesions were described as cysts with papillary projections into the lumen. Solid lesions had a more dense cellular architecture, filled with hyperplastic epithelial cells (Figure 3.6). Renal lesions with <25% of cellular content were considered as cystic, lesions with >25% and <90% cellular content as papillary and tumours with >90% cellular content as solid (Figure 3.6).

By the age of 14 months, both mouse models had developed multiple renal lesions. A total number of 444 lesions were detected on HE renal sections of all animals (n= 9) (Table 3.2). Four hundred and eleven out of the 444 renal lesions identified were either cystic or papillary and all the rest (33 lesions) were solid lesions. The total whole and cellular areas of all renal lesions were 243.58 mm^2 and 114.57 mm^2, respectively (Table 3.2). The smallest lesion identified by histological analysis was <

0.02 mm^2. None of the wild-type mice had any macroscopic or microscopic kidney lesions.

The histologic features of renal lesions identified in *Tsc1*$^{+/-}$ mice were similar to those seen in *Tsc2*$^{+/-}$ mice. However, *Tsc1*$^{+/-}$ mice had a milder renal phenotype with lower incidence of kidney tumours in comparison with age-matched *Tsc2*$^{+/-}$ mice. We found that *Tsc2*$^{+/-}$ mice (n= 4) had significantly more renal lesions (77 lesions per mouse) than *Tsc1*$^{+/-}$ mice (n= 5) (27 lesions per mouse) (*P*= 0.0078). In terms of lesion type, *Tsc2*$^{+/-}$ mice had considerably more cystic/papillary (*P*= 0.0098) and solid lesions (*P*= 0.0492) than *Tsc1*$^{+/-}$ mice. Power calculations based on histological data for different drug effect sizes are shown on Tables 3.3 and 3.4.

Table 3.2 Comparison of T2 weighted MRI and histological analysis (HA) in detection of mouse renal lesions.

Mouse	Number of cystic and papillary lesions		Number of solid lesions		Measurement of renal lesions[b]		
	MRI	HA	MRI	HA	MRI (mm^2)	HA whole (mm^2)	HA Cellular (mm^2)
TSC1–1	15	28	15	26	0	2	7.08	5.93	2.35
TSC1–2	12	20	11	19	1	1	9.73	8.92	4.37
TSC1–3	32	35	32	32	0	3	8.87	12.66	5.99
TSC1–4	11	26	9	23	2	3	13.90	12.1	8.26
TSC1–5	22	27	22	26	0	1	15.57	19.4	5.76
TSC2–1	44	53	43	50	1	3	15.53	16.61	6.98
TSC2–2	72	94	71	91	1	3	31.16	45.69	22.47
TSC2–3	23	79	19	69	4	10	30.79	66.51	40.14
TSC2–4	42	82	41	75	1	7	24.64	55.76	18.25
Total	273	444	263	411	10	33	157.26	243.58	114.57
z[c]	2.66		2.61		2.63		1.72	1.72	
P[c]	0.008		0.009		0.009		0.09	0.09	

[a] MRI refers to the 2nd MRI scan after which animals were sacrificed for histological analysis. Lesions detected by HA include "microlesions" that were <0.02 mm^2. After excluding these "microlesions", the detection rate by MRI in comparison with HA was 76%.

[b] For comparison, total volume (mm^3) obtained from the 2nd MRI scan was converted to MRI area (mm^2) (area = $3V/R/4$, where V = volumes and R = radius) with the assumption that all lesions were spherical and a maximum cross-sectional area was estimated. "HA whole" means whole areas of lesions obtained by HA; "HA cellular" means lesion areas containing cellular contents only.

[c] z and P values were obtained by Wilcoxon signed-rank test between MRI and HA.

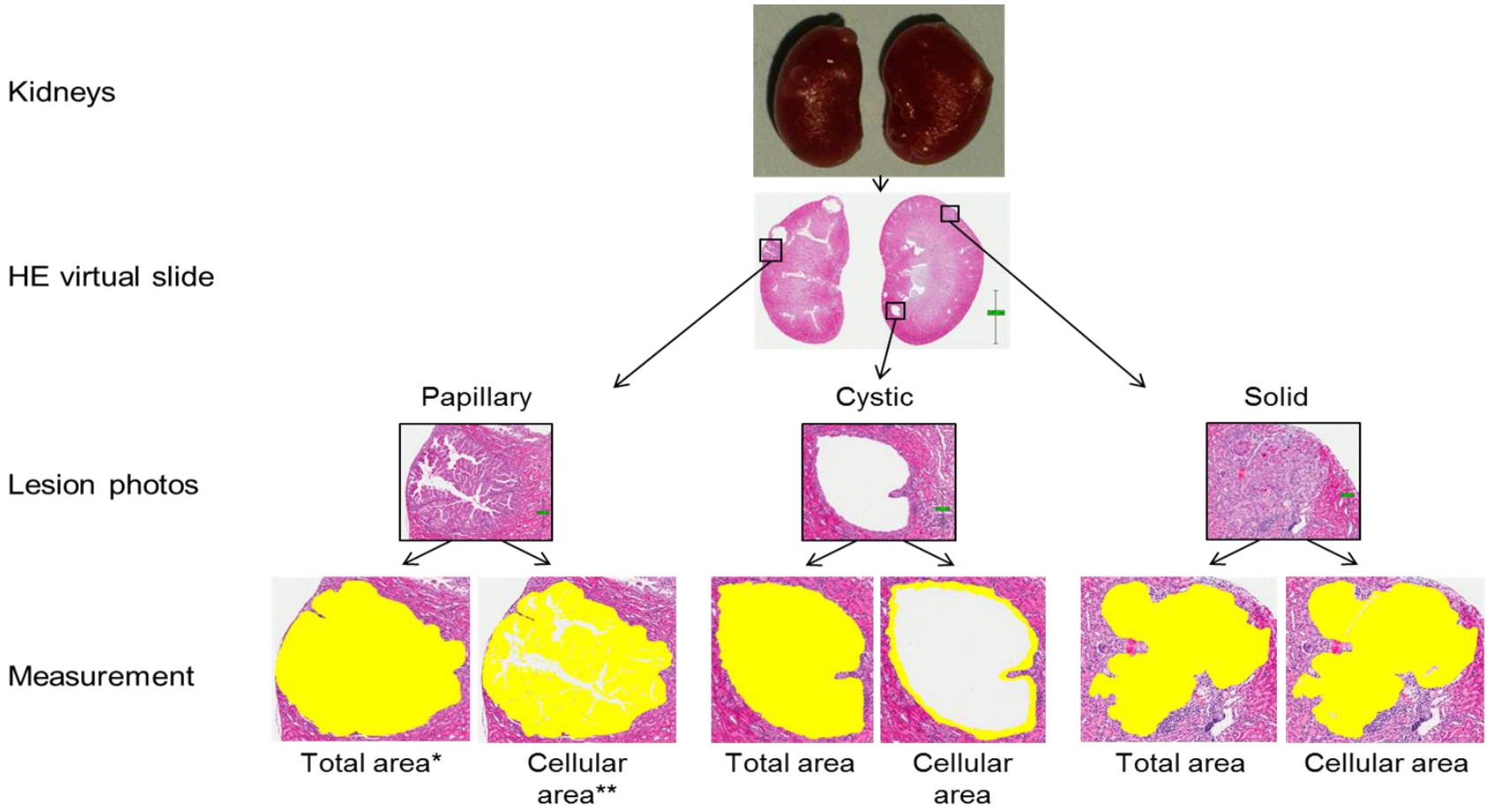

Figure 3.5 Histological analysis of mouse kidney lesions. Mouse kidneys were fixed, processed, wax-embedded and cut into 5 µm sections at 200 µm intervals. Kidney sections were H&E stained and scanned to create virtual slides that were used to assess renal lesions by calculating maximum cross-sectional whole lesion areas (lesion size) and cellular areas (excluding fluid filled cystic areas). *Total area is indicated by the yellow colour. **Cellular area= Total area-White area.

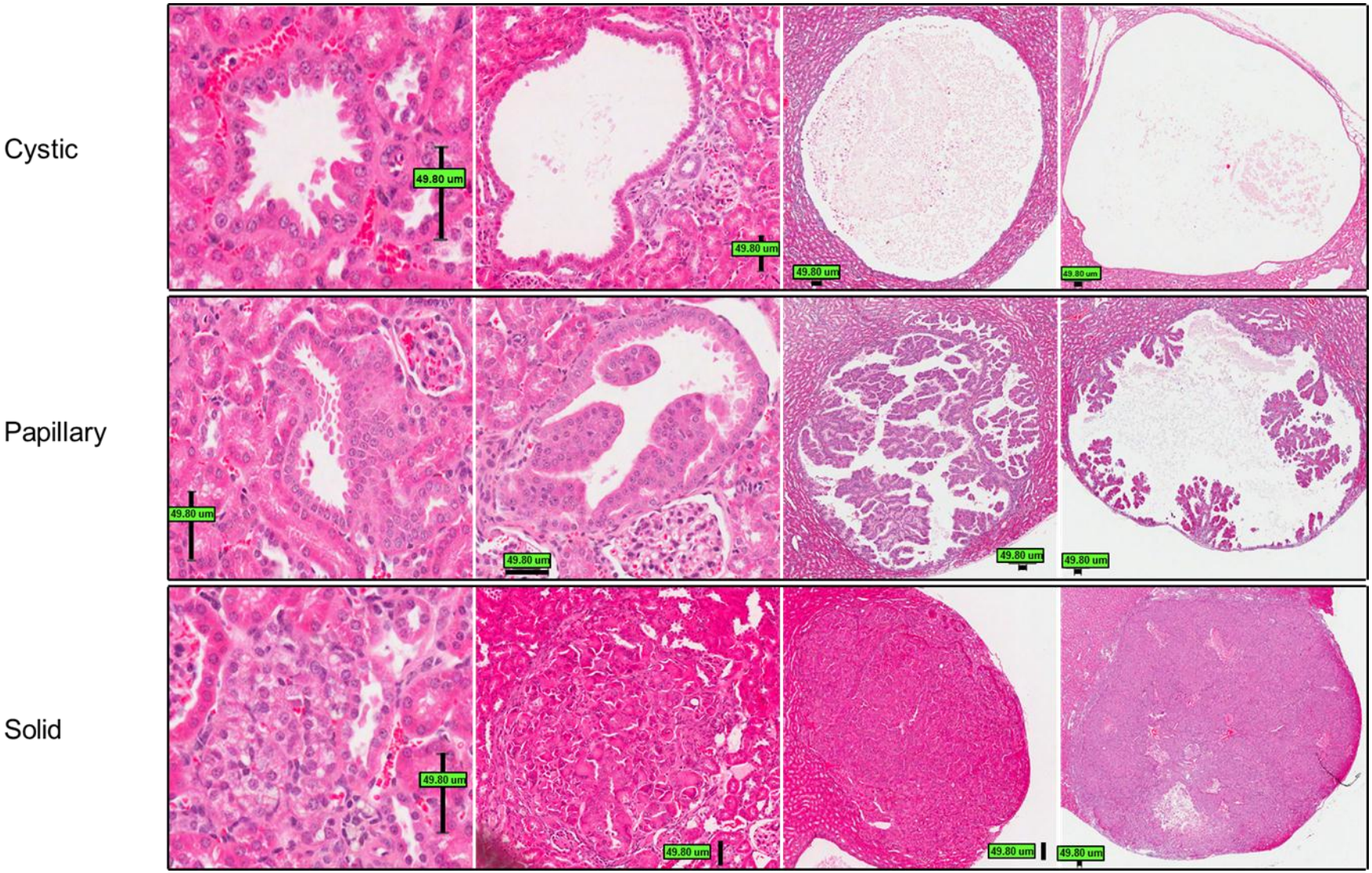

Figure 3.6 Microscopic analysis of H&E stained lesions in the kidneys of *Tsc1*$^{+/-}$ and *Tsc2*$^{+/-}$ mice. Cystic, papillary and solid lesions are shown and they are different in size. Scale bars: 49.80 µm.

Table 3.3 Estimation of sample size for metformin treatment of renal tumours using a *Tsc1*$^{+/-}$ mouse model.

Mouse	Total number of lesions[a]
TSC1-1	28
TSC1-2	20
TSC1-3	35
TSC1-4	26
TSC1-5	27

Alpha error	Statistical power	Expected mean[b]	Sample size per group
0.05	0.89	21.76	10

[a] Total number of lesions detected by HA (derived from Table 3.2).

[b] Expected mean: assuming 20% reduction in tumour number after treatment.

Table 3.4 Estimation of sample size for prevention of renal tumours using a *Tsc2*$^{+/-}$ mouse model.

Mouse	Total number of lesions[a]
TSC2-1	53
TSC2-2	94
TSC2-3	79
TSC2-4	82

Alpha error	Statistical power	Expected mean[b]	Sample size per group
0.05	0.81	61.6	10

[a] Total number of lesions detected by HA (derived from Table 3.2).

[b] Expected mean: assuming 20% reduction in tumour number after treatment.

3.3.4 Comparison of T2 weighted MRI and histological analysis in renal lesion detection

T2 weighted MRI scans provided a series of coronal slices spanning each mouse for comparison with histology. Data obtained from MRI analysis were confirmed by histological analysis (Figure 3.7). Two hundred and seventy three out of 444 renal lesions (61%) detected by histological analysis, were clearly identified by T2 weighted MRI (*P*= 0.008) (Table 3.2). MRI identified 64% of cystic/papillary (263/411, *P*= 0.009) and 30% of solid renal lesion (10/33, *P*= 0.009). All cystic lesions found on histological slides with cross sectional areas of less than 0.02 mm^2 (we termed these lesions as “microlesions”) were below the limit of resolution of T2 weighted MRI (Figure 3.8). When microlesions were excluded, the detection rate by MRI increased from 61% to 76%.

To further compare T2 weighted MRI and histological analysis, the total number of lesions detected by MRI was plotted against the total number of lesions detected by histological analysis indicating that MRI is less sensitive than histological analysis (Figure 3.9). In addition, whole lesion volumes determined by MRI were converted from mm^3 to mm^2 (area= $3V/R/4$, where *V*= volumes and *R*= radius) for subsequent comparison with histological data (mm^2) assuming that lesions were spherical. Good agreement was found between the estimated cross-sectional areas by MRI and histology for small lesions (< 20 mm^2) but not for bigger renal lesions (*P*= 0.0926) (Figure 3.9).

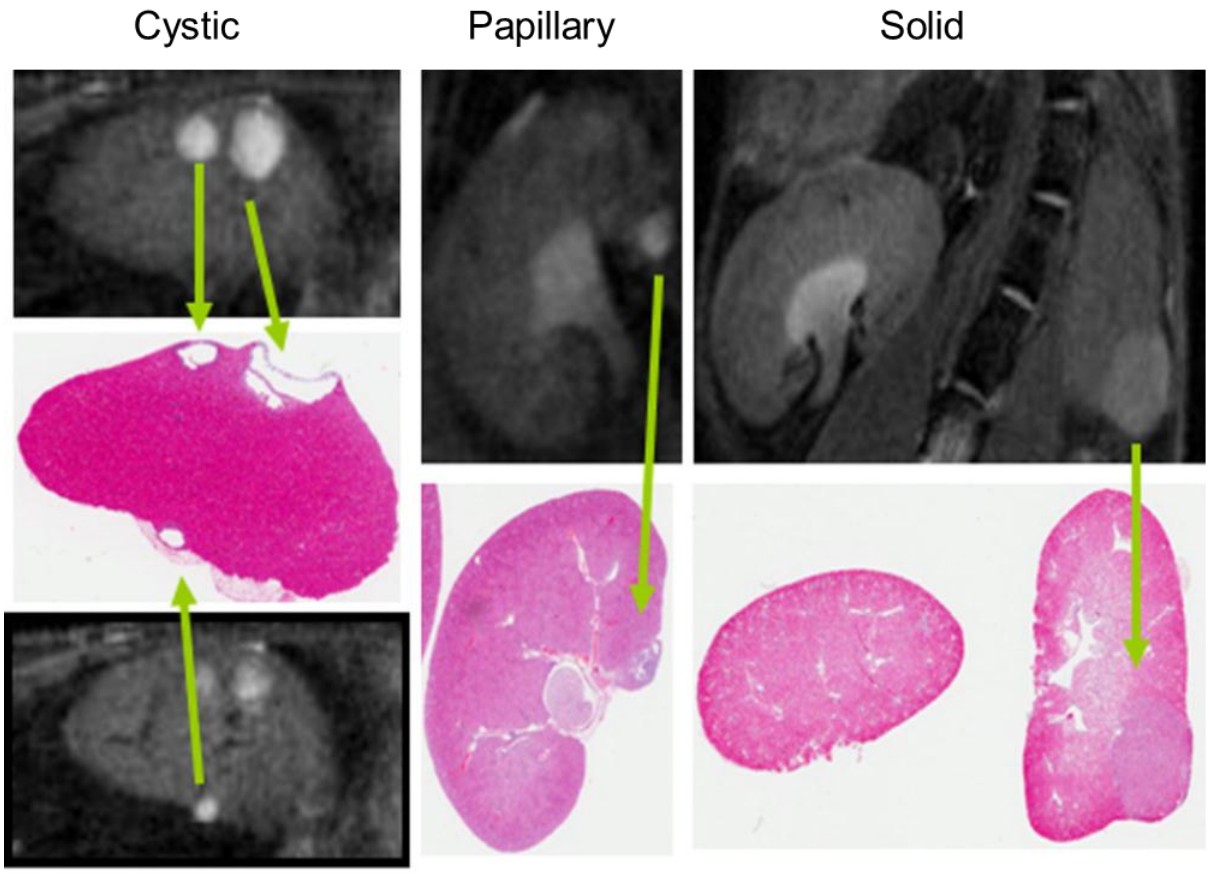

Figure 3.7 Detection of different types of mouse kidney lesions by T2 weighted MRI. Tsc mouse kidney lesions were identified *in vivo* by T2 weighted MRI and then confirmed by histological analysis as cystic, papillary and solid tumours.

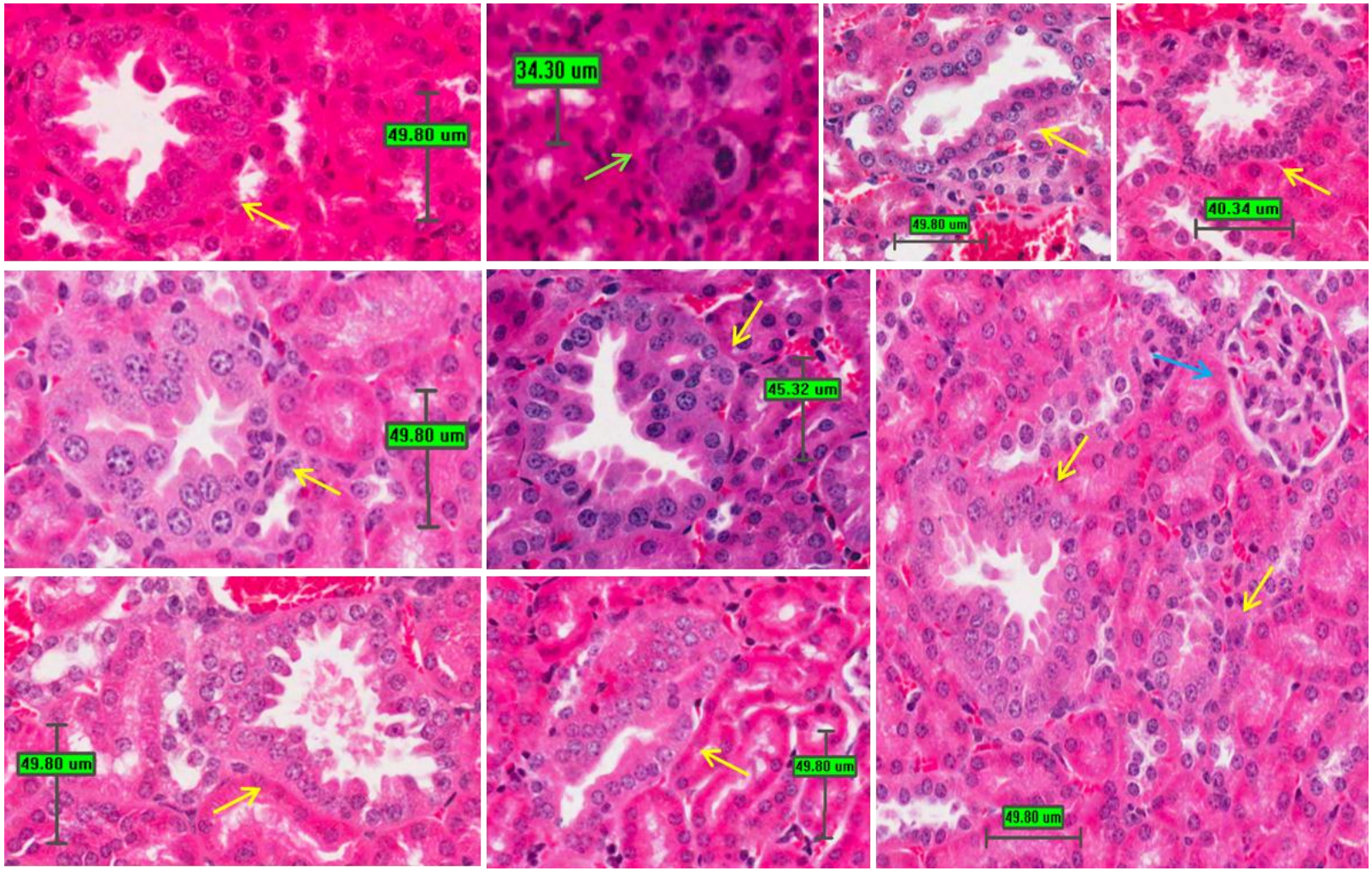

Figure 3.8 Microlesions in Tsc mouse kidneys. Small lesions of <0.02 mm^2 were seen on histological analysis but were beyond the resolution of T2 weighted MRI using current protocols. The arrows show the following: Yellow arrows, cystic microlesions; green arrow, micro dysplastic growth; blue arrow, glomerulus.

(A)

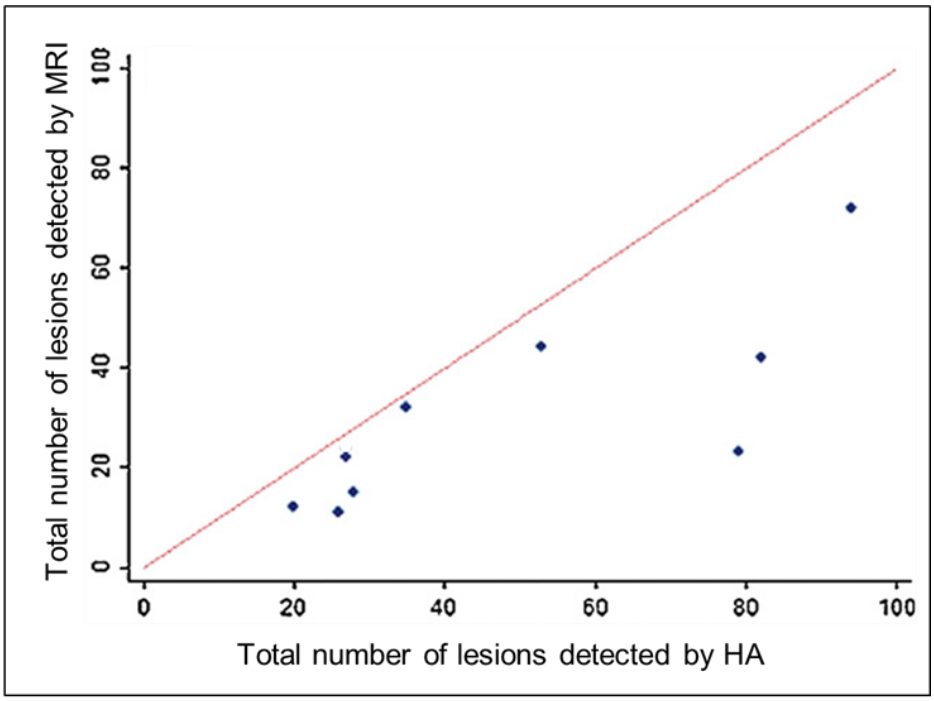

(B)

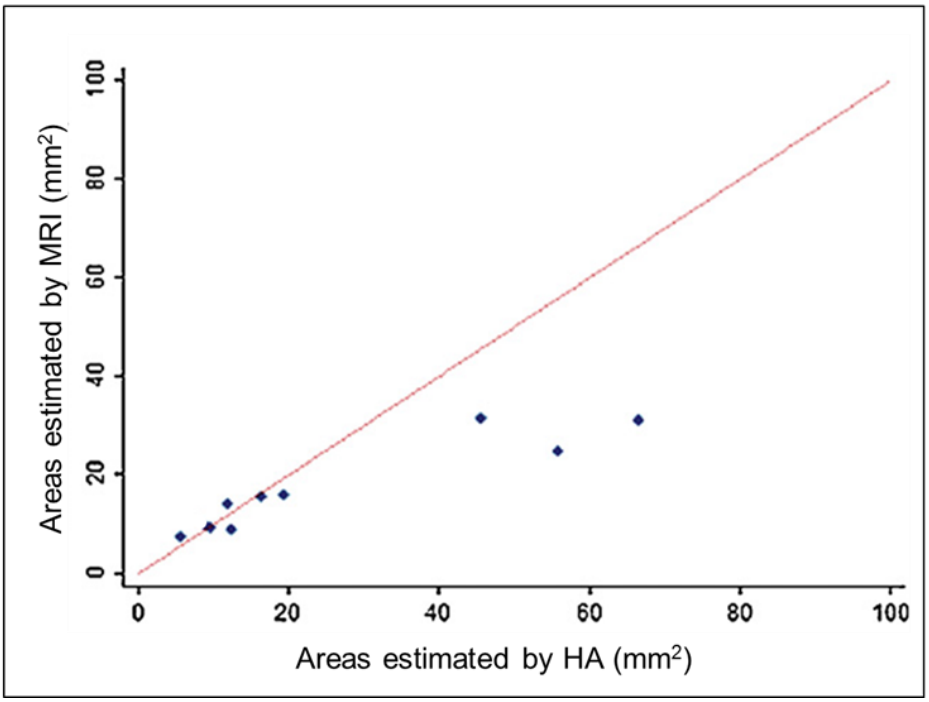

Figure 3.9 Comparison of T2 weighted MRI and histological analysis in renal lesion detection. **(A)** Total number of lesions detected by T2 weighted MRI at 14 months of age (second scan) and by histological analysis (see Table 3.2). **(B)** Maximum cross-sectional areas of renal lesions estimated by T2 weighted MRI and by histological analysis (see Table 3.2).

3.4. Discussion

MRI is a noninvasive technique that has been used for detection of tumours in animals and patients (Cha *et al*. 2003, Chalifoux *et al*. 2013). A high-field (9.4 T) Bruker Biospec 94/20 MRI/MRS spectrometer with a small diameter bore (20 cm) is suitable for small animals. Using this facility, we have evaluated T2 weighted MRI for the assessment of renal lesions in two transgenic mouse models of TSC by comparison with histological analysis. We compared MRI with histology indirectly since it was not feasible to compare directly T2 weighted MRI slices with the corresponding H&E renal sections for a number of reasons. First, the T2 weighted MRI and histological analyses had different resolutions. Second, it was difficult to match exactly the orientation of T2 weighted MRI slices obtained *in vivo* to the renal H&E sections. Third, other factors might also affect the comparison, such as the dissection and fixation of the organs.

We demonstrated that high resolution T2 weighted MRI (0.5 mm slice thickness) could detect cysts, papillary and solid tumours. Sensitivity for the detection of solid tumours was poor as only 30% of lesions found histologically were also detected by the T2 weighted MRI. In comparison MRI detected 64% of cystic and papillary lesions. Cystic and papillary renal lesions were more easily detectable due to the high contrast between normal kidney tissue and fluid-filled cysts and papillary lesions. In addition, histological analysis revealed many microscopic early lesions (area < 0.02 mm^2) that were below the resolution of the MRI modality used here, and excluding these lesions 76% of all renal lesions were detected by MRI.

Eighty five percent of lesions detected on a first MRI scan could be re-identified unambiguously in a second scan undertaken two months later, even when they had grown or shrunk. There might be a number of possible reasons for the failure to re-identify some of the lesions in the second scan in the untreated mice. First, there might be changes in lesion type from the first to the second scan; for example a cystic or papillary lesion in the first scan might have developed to be a solid lesion in the second scan that might not be detectable. Second, it is sometimes difficult to

distinguish new lesions from old ones in the second scan because of differences in animal orientation during scanning, particularly if lesions were close to one another. Finally, spontaneous shrinkage of some renal lesions following the first scan might also happen.

More lesions were identified in the second scan for both *TSC1*$^{+/-}$ and *TSC2*$^{+/-}$ mice. This indicates that either some lesions developed *de novo* during the follow-up period and/or that some lesions were too small in the first scan for detection, but big enough in the second scan. These results suggest that T2 weighted MRI could be useful for monitoring renal lesions *in vivo*.

Cross sectional areas of lesions assessed by the T2 weighted MRI and histological analysis showed good agreement for small lesions but poor agreement for large lesions. The lesion areas by T2 weighted MRI were estimated by conversion of lesion volumes with an assumption that renal lesions were spherical. Some large lesions do, however, appear to be of irregular shape. It could not be excluded that the difference in agreement for small and large lesions might be caused by the different resolutions between the T2 weighted MRI and histological analysis.

Brown *et al*. (2005) performed T2 weighted MRI (1-1.5 mm slice thickness) to detect lesions in the liver, kidneys and lungs of *Tsc2*$^{+/-}$ mice for evaluation of cell based therapy. Lee *et al*. (2005) used T2 weighted MRI (0.75 mm slice thickness) to determine the number of lesions in kidneys following treatment, using the same *Tsc2*$^{+/-}$ mouse model. While both studies showed that T2 weighted MRI could detect different types of lesions in the kidneys of *Tsc2*$^{+/-}$ mice, none of these studies performed two successive MRI scans and presented MRI follow-up data or evaluated the total volume of renal lesions. In addition, these studies have not addressed the actual detection rate of renal lesions by T2 weighted MRI properly in comparison to histological analysis (Brown *et al*. 2005, Lee *et al*. 2005). Our study is the first report of T2 MRI analysis that has presented follow-up data, evaluated total lesion volumes and the utility of MRI for assessing lesions by giving the actual

detection rate in comparison to histological findings. In a recent study that compared micro-CT (micro-computed tomography) and T2 weighted MRI for monitoring metastasis of mouse pheochromocytoma, a kidney lesion of 0.203 mm^3 was detected by T2 weighted MRI (Martiniova *et al*. 2009). In the current report, we show that the smallest T2 weighted MRI-detectable renal lesions were <0.1 mm^3 but that sensitivity of the T2 weighted scans is much better for cystic than solid lesions. Wallace *et al.* (2008) monitored the volume of PKD mouse kidneys over time by T2 weighted MRI (0.5mm slice thickness), and suggested that T2 weighted MRI can be used to evaluate the effectiveness of therapeutic agents to treat the disease. By contrast, in *Tsc1*$^{+/-}$ and *Tsc2*$^{+/-}$ mice we found that total kidney volumes did not change significantly over a period of two months while the numbers and volumes of renal lesions were significantly increased in all mice.

In conclusion, T2 weighted MRI is a potentially useful tool for assessing renal lesions in pre-clinical studies using Tsc mouse models. As measures can be repeated, T2 weighted MRI enables longitudinal studies to be undertaken *in vivo* with the potential to reduce the numbers of animals required. Technical challenges remain, notably development of protocols that will improve T2 weighted MRI sensitivity for solid renal lesions. Alternatively, MRI modalities other than T2 weighted may be explored for detecting solid renal lesions in Tsc mouse models.

CHAPTER FOUR

Effect of metformin on renal tumours and mTORC1 signalling in a *Tsc1*$^{+/-}$ mouse model

4.1 Introduction

Rapamycin and its analogues such as CCI-779, RAD001, AP23576 are potent inhibitors of mTORC1 signalling (Easton and Houghton, 2006). Clinical trials have demonstrated that rapalogues can shrink or stabilise tumours such as SEGAs (Krueger *et al*. 2010, Franz *et al*. 2006, Koenig *et al*. 2008), renal AMLs (Davies *et al*. 2011, Bissler *et al*. 2008, Dabora *et al*. 2011), LAM (Bissler *et al*. 2008, Taillé *et al*. 2007) and facial angiofibromas (Hofbauer *et al*. 2008). However, the beneficial effects on TSC-associated tumours were reversed and tumour regrowth occurred once the drug was discontinued. Additionally, treatment with these drugs is associated with frequent adverse events consistent with their known metabolic and immunosuppressive properties including respiratory infections, stomatitis, leukopenia and sinusitis. One additional concern is that rapamycin treatment is thought to promote Akt activation due to loss of negative feedback towards IRS-1 loop. This suggests that long-term treatment with rapamycin might increase tumour progression in individuals with TSC (Zakikhani *et al*. 2010).

Metformin may be a possible candidate for treatment of TSC since it is suggested to suppress mTORC1 activity via multiple mechanisms (described in detail in section 1.5.2.2). More importantly, metformin treatment not only attenuated mTORC1 activity in preclinical studies but also decreased Akt activity through AMPK phosphorylation of IRS-1Ser789, leading to greater apoptotic and anti-proliferative effect than rapamycin (Zakikhani et al. 2010).

Here, we assessed the effect of long term treatment with metformin on renal tumours using *Tsc1*$^{+/-}$ mice. Tsc mouse models have pathophysiological features that match some aspects of the disease in TSC patients. *Tsc1*$^{+/-}$ mice develop tumours in

multiple organs including the kidneys, liver and lungs and these tumours exhibit aberrant activation of mTORC1 (Chan *et al*. 2004, El-Hashemite *et al*. 2003). In chapter 3, T2 weighted MRI was demonstrated to be useful for *in vivo* examination of renal tumours. This chapter investigates therapeutic efficiency of metformin on TSC-associated renal lesions using both T2-weighted MRI and histological analysis. mTORC1 signalling was also analysed in kidney tissues and renal tumours of *Tsc1*$^{+/-}$ mice after treatment with metformin.

4.2 Materials and methods

4.2.1 DNA extraction and genotyping

As outlined in section 2.5.2.1, DNA was extracted from mouse ear punches, using the Wizard® SV Genomic DNA Purification System. Genotyping was determined by PCR as described in section 2.5.2.2. PCR products were 352 bp (wild-type) and 283 bp (mutant), and were analysed on 1.5% agarose gels.

4.2.2 Animals and procedures

All animal procedures were carried out under the UK Home Office guidelines, outlined in sections 2.5.1 to 2.5.5. The *Tsc1*$^{+/-}$ mouse model was generated by the Institute of Medical Genetics (Cardiff University) (Wilson *et al*. 2005) and backcrossed on the background of the balb/c strain (Charles River, UK) more than 10 times. Twenty *Tsc1*$^{+/-}$ mice at the age of six months were randomly allocated into two different treatment groups (n= 10 per group) with balanced sex, age and litter number using Graphpad (http:/www.graphpad.com/welcome.htm). One group was treated with metformin (Merck, Germany) in drinking water and the other as a control group with normal drinking water. The treatment lasted for 9 months and metformin was provided with a daily dosage of 150 mg/kg body weight for the first 7 months and 600 mg/kg body weight for the last two months, assuming that a mouse consumes 15 ml water per 100 g body weight a day. New metformin solution was replaced every 3 days. One of the animals treated with metformin died unexpectedly during the treatment and was excluded from this trial. Animal body weight was

checked every week. Once the treatment was finished, mice of 15 months old were scanned by T2 weighted MRI and then humanely killed for tissue collection and histological and immunohistological analyses. Necropsy was performed involving macroscopic examination of the kidneys, spleen, liver, heart, lungs and brain. Six additional 14-15 month old *Tsc1*$^{+/-}$ balb/c mice were used for further molecular analysis. Three of them were treated with 600 mg/kg body weight and the rest with drinking water for 2 weeks. At the end of the treatment all 6 mice were killed and kidney tissues and renal tumours were collected.

4.2.3 MRI

A detailed MRI procedure is outlined in section 2.5.4. The same protocol was used as in Chapter 3.

4.2.4 Histology

The same protocol was used as described in Chapter 3, section 3.2.4. The assessment was conducted blindly with respect to treatment status.

4.2.5 IHC

EXPOSE Rabbit specific AP (red) detection IHC Kit was used to stain the antigen. Briefly, paraffin-embedded mouse renal sections were deparaffinised and rehydrated. Sections were boiled for 10 min in 10 mM sodium citrate buffer (pH 6.0) to unmask antigens. After cooling down in room temperature and 3 washes in TBST, sections were blocked in 1.5% goat serum for 10 minutes at room temperature. Antigen staining was performed according to the kit supplier's instructions as described in section 2.5.7. Antibody against phosphor-S6 ribosomal protein (Ser235/236) (pS6Ser$^{235/236}$) was used in 1:200 dilutions. Virtual sections of the immunohistochemical slides were created using the Scanscope™ CS slide scanner.

4.2.6 Western analysis

Kidneys and renal tumours were harvested during dissection of *Tsc1*$^{+/-}$ mice and snap frozen. Proteins were purified from the frozen kidney and tumour samples according to the supplier's protocol using TissueRuptor and AllPrep DNA/RNA/Protein Mini Kit as described in section 2.5.10. NuPAGE Novex 4-12% Bis-Tris Gels were used for protein separation (25 µg protein loading amount) and proteins were then transferred to Hybond ECL membranes (see section 2.5.13). Membranes were blocked with 1X TBS-T plus 2% (w/v) ECL Advance Blocking Agent and incubated with primary antibodies against pS6$^{Ser235/236}$ (1:1000), phospho-AMPKα (Thr172) (pAMPK^{Thr172}) (1:1000), phospho-Acetyl-CoA Carboxylase (Ser79) (pACC^{Ser79}) (1:1000), phospho-Akt (Ser473) (pAkt^{Ser473}) (1:1000) and phospho-Raptor (Ser792) (pRaptor^{Ser792}) (1:1000). Membranes were then incubated in horseradish peroxidase-conjugated secondary antibody against rabbit (1:10000). Protein signals were detected using ECL Advance Western Detection Kit and Autochemi Imaging System (UVP). β-actin was used as loading control. Relative intensity of protein signals were obtained using ImageJ (http://rsbweb.nih.gov/ij).

4.2.7 Statistical analysis

The Wilcoxon rank-sum (Mann-Whitney) test was performed for comparisons of metformin effect on mouse renal lesions as indicated in Tables 4.1 and 4.2 using the software Stata (version 11). Two tailed Student's t-Test was used for comparison of Western analysis and mouse body weight. $P \leq 0.05$ was considered to be statistically significant.

4.3 Results

4.3.1 Metformin was well-tolerated in the *Tsc1*$^{+/-}$ mouse model

Ten 6-month old *Tsc1*$^{+/-}$ mice were treated with metformin and another 10 age matched *Tsc1*$^{+/-}$ mice with drinking water for 9 months. One of the mice treated with metformin died before the experiment was completed and was excluded from final analysis. Animals treated with metformin generally looked healthy. Mouse weight

was monitored once a week. No significant difference in body weight change was found between the metformin treated (+2.26 g) and control (+2.30 g) groups (*P*= 0.97138). These results suggest that long term metformin treatment was well-tolerated in *Tsc1*$^{+/-}$ mice.

4.3.2 Metformin had no effect on *Tsc1*-associated renal lesions

4.3.2.1 In vivo analysis of renal tumours in Tsc1$^{+/-}$ *mice by T2 weighted MRI following metformin treatment*

After 9 months of treatment with either metformin or water, all *Tsc1*$^{+/-}$ mice (n=19) were subjected to *in vivo* T2 weighted MRI and the effect of metformin on *Tsc1*-associated renal lesions was assessed (Table 4.1). MRI identified different types of renal lesions including cystic, papillary and solid lesions (Figure 4.1). Renal lesions were visible in all animals of both treatment groups and varied in number, size, morphology and location. All lesions were counted and lesion volumes (mm^3) were obtained using Analyze 9.0 software as previously described in Chapter 3, section 3.3.2.1.

No significant differences were found in total renal lesion number per mouse (*P*= 0.5927) or in type-specific renal lesion numbers per mouse (*P*= 0.3385, *P*= 0.6495, *P*= 0.3713 for cystic, papillary and solid lesions, respectively), between the two treatment groups (Figure 4.2). Likewise, no significant differences were seen in total volume of all renal lesions per mouse (*P*= 0.1025), the mean volume per lesion per mouse (*P*= 0.1025) and the sizes of type-specific lesions (*P*= 0.9025, *P*= 0.8703, *P*= 0.1334 for cystic, papillary and solid lesions, respectively), between metformin treated and control *Tsc1*$^{+/-}$ mice (Figure 4.2).

Table 4.1 T2 weighted MRI analysis of *Tsc1*-associated renal lesions.

Mouse	Treatment	Number of all lesions	Number of cysts	Number of papillary lesions	Number of solid lesions	Volume of all lesions (mm^3)	Mean volume per lesion (mm^3)	Volume of cysts (mm^3)	Volume of papillary lesions (mm^3)	Volume of solid lesions (mm^3)
PCT1-1	Water	14	10	3	1	16.10	1.15	11.41	2.42	2.27
PCT1-2	Water	10	4	3	3	93.30	9.33	10.47	2.27	80.56
PCT1-3	Water	13	11	1	1	23.13	1.78	13.70	0.58	8.85
PCT1-4	Water	9	7	2	0	24.53	2.73	17.44	7.09	0.00
PCT1-5	Water	20	13	7	0	9.35	0.47	4.34	5.01	0.00
PCT1-6	Water	10	7	3	0	4.25	0.43	3.34	0.91	0.00
PCT1-7	Water	12	8	1	3	38.95	3.25	5.90	0.04	33.01
PCT1-8	Water	16	10	6	0	15.87	0.99	14.35	1.52	0.00
PCT1-9	Water	12	4	7	1	134.17	11.18	0.29	4.54	129.34
PCT1-10	Water	22	10	11	1	88.54	4.02	5.27	12.82	70.45
Median		**12.50**	**9.00**	**3.00**	**1.00**	**23.83**	**2.25**	**8.19**	**2.35**	**5.56**
PCT1-11	Metformin	16	10	6	0	6.56	0.41	4.64	1.92	0.00
PCT1-12	Metformin	17	13	4	0	13.49	0.79	8.88	4.61	0.00
PCT1-13*	Metformin	-	-	-	-	-	-	-	-	-
PCT1-14	Metformin	16	9	6	1	30.25	1.89	6.51	20.96	2.78
PCT1-15	Metformin	9	8	1	0	5.77	0.64	5.43	0.34	0.00
PCT1-16	Metformin	20	14	6	0	12.62	0.63	4.34	8.28	0.00
PCT1-17	Metformin	13	10	3	0	11.87	0.91	10.16	1.71	0.00
PCT1-18	Metformin	11	9	2	0	6.27	0.57	5.39	0.88	0.00
PCT1-19	Metformin	13	7	4	2	10.39	0.80	6.23	3.87	0.29
PCT1-20	Metformin	13	10	0	3	91.08	7.01	18.64	0.00	65.09
Median		**13.00**	**10.00**	**4.00**	**0.00**	**11.87**	**0.79**	**6.23**	**1.92**	**0.00**
z **		**-0.535**	**-0.957**	**0.454**	**0.894**	**1.633**	**1.633**	**0.123**	**0.163**	**1.501**
P **		**0.5927**	**0.3385**	**0.6495**	**0.3713**	**0.1025**	**0.1025**	**0.9025**	**0.8703**	**0.1334**

* This mouse died before the end of the experiment.

** *z* and *P* values were obtained by Wilcoxon rank-sum (Mann-Whitney) test between water and metformin treatment.

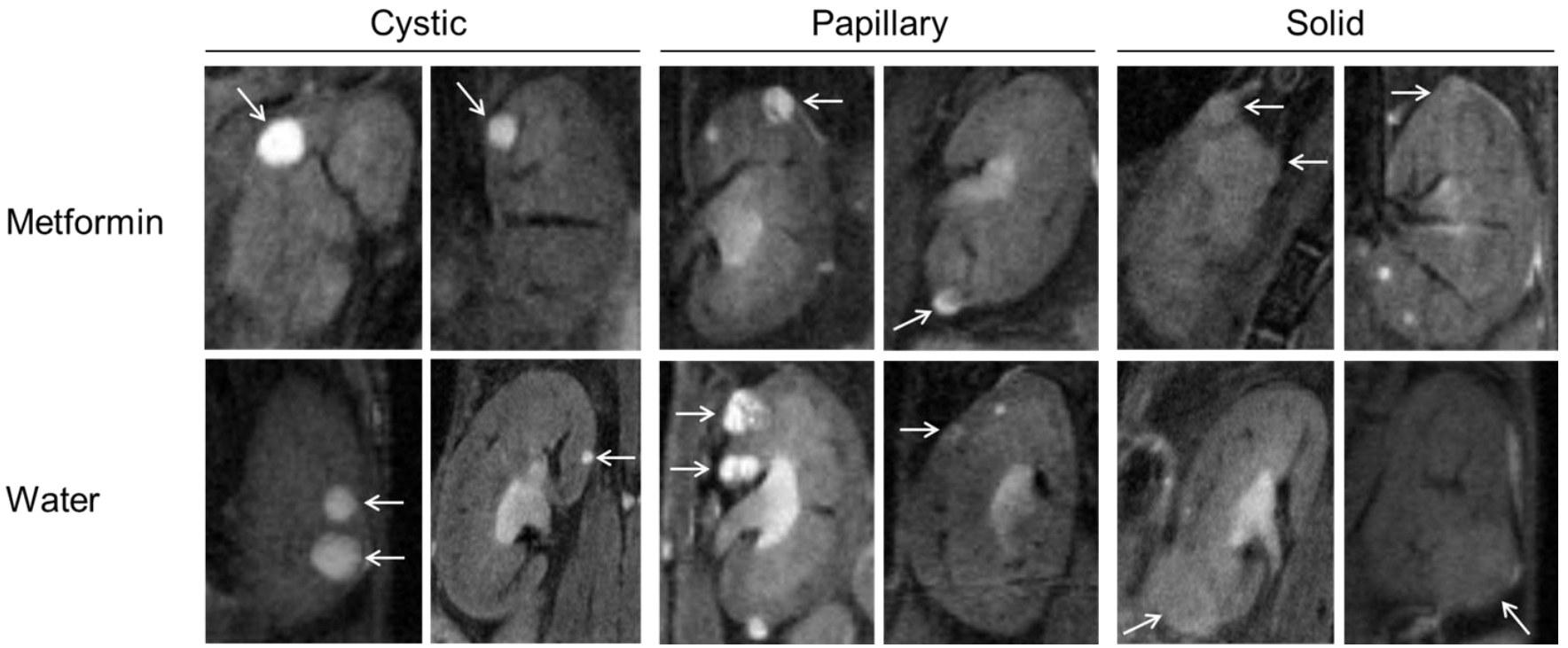

Figure 4.1 Different types of renal lesions (cystic, papillary, and solid) identified by MRI in 15 month old *Tsc1*$^{+/-}$ mice of metformin and water treatment groups.

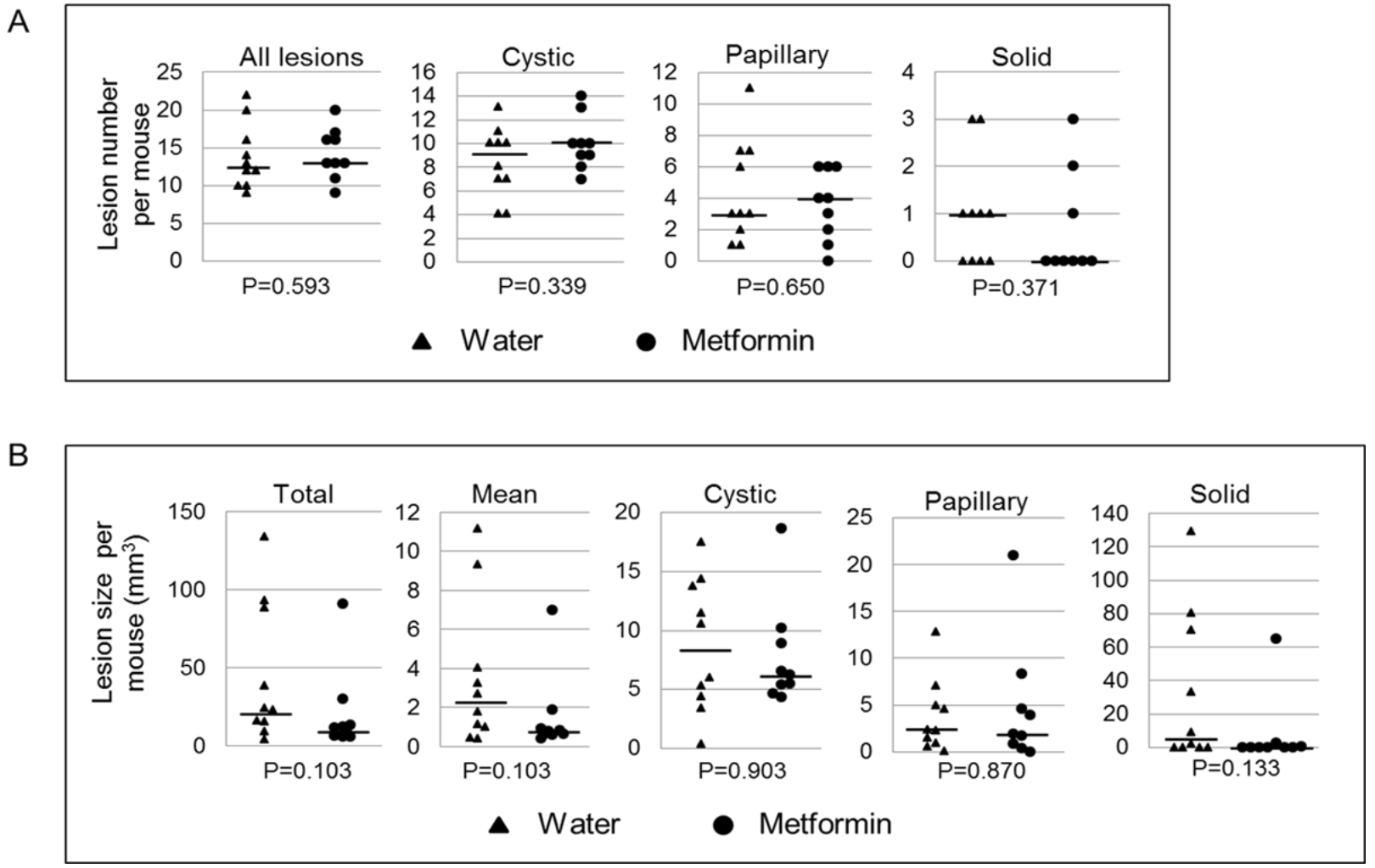

Figure 4.2 Analysis of renal lesions by MRI. *Tsc1*$^{+/-}$ mice were scanned using T2 weighted MRI after 9 months' treatment with drinking water (filled triangles) or metformin (filled circles). Renal lesion numbers and volumes were determined using the software Analyze 9.0. **(A)** Comparison of renal lesion numbers. No significant difference in lesion numbers was observed between control (drinking water) and metformin treated *Tsc1*$^{+/-}$ mice (based on Table 4.1). **(B)** Comparison of renal lesion volumes. No significant difference in lesion volumes was observed between control (drinking water) and metformin treated *Tsc1*$^{+/-}$ mice (based on Table 4.1).

4.3.2.2 Assessment of metformin effects on Tsc1-associated renal tumours by histological analysis

All animals (n=19) were humanely killed following MRI scan and an overall assessment of *Tsc1*-associated renal tumours was correspondingly performed by histological analysis (Table 4.2). Renal lesions were characterised, counted and their maximum cross-sectional whole lesion area and cellular area (mm^2) (cellular area= whole lesion area- fluid filled cystic area) were calculated using the ImageJ software as described in Chapter 3, section 3.3.3.1 (Table 4.2). Different types of mouse renal lesions were observed following H&E staining, as shown in Figure 4.3. Microscopically, all animals had multiple renal lesions by the age of 15 months that varied in size, morphology and location on the kidney. Histological features of renal lesions such as lesion size and shape identified in control $Tsc1^{+/-}$ mice were similar to those seen in metformin treated $Tsc1^{+/-}$ mice.

No significant differences were seen in total (*P*= 0.7125) or type-specific renal lesion numbers (*P*= 0.9023, *P*= 0.8683, *P*= 0.8026 for cystic, papillary and solid lesions, respectively) between the two treatment groups (Figure 4.4, Table 4.2). Similarly, there were no significant differences in the total lesion size (total whole lesion area) per mouse (*P*= 0.3691), the mean lesion size per lesion per mouse (*P*= 0.327) or lesion size of type-specific lesions per mouse (*P*= 0.568, *P*= 0.5136, *P*= 0.5118 for cystic, papillary and solid lesions, respectively) between the control and metformin treated mice (Figure 4.4). Additionally, no significant differences were found between the two groups in total cellular area of lesions per mouse (*P*= 0.4624), the mean cellular area per lesion per mouse (*P*= 0.4142), or cellular area of type-specific lesions per mouse (*P*= 0.6242, *P*= 0.5136, *P*= 0.5118 for cystic, papillary and solid lesions, respectively) (Figure 4.4). Taken together, both MRI and histological analyses, suggested that metformin appeared ineffective for treating renal lesions in $Tsc1^{+/-}$ mice.

Table 4.2 Histological analysis of renal lesions in *Tsc1*$^{+/-}$ mice treated with drinking water or metformin.

Mouse	Treatment	Number of all lesions	Number of cysts	Number of papillary lesions	Number of solid lesions	Area of all lesions (mm^2)	Mean area per lesion (mm^2)	Area of cysts (mm^2)	Area of papillary lesions (mm^2)	Area of solid lesions (mm^2)	Cellular content of all lesions (mm^2)	Mean cellular content per lesion (mm^2)	Cellular content of cysts (mm^2)	Cellular content of papillary lesions (mm^2)	Cellular content of solid lesions (mm^2)
PCT1-1	Water	34	20	10	4	5.880	0.173	3.741	1.825	0.314	2.141	0.063	0.961	0.875	0.305
PCT1-2	Water	31	17	10	4	26.556	0.857	2.961	4.406	19.188	22.503	0.726	0.579	2.940	18.983
PCT1-3	Water	24	18	4	2	9.105	0.379	4.870	0.533	3.703	4.163	0.173	0.510	0.396	3.258
PCT1-4	Water	33	24	8	1	8.600	0.261	3.563	4.890	0.147	2.185	0.066	0.609	1.431	0.145
PCT1-5	Water	25	17	8	0	6.964	0.279	3.799	3.166	0.000	2.039	0.082	0.719	1.320	0.000
PCT1-6	Water	35	27	8	0	3.922	0.112	2.859	1.063	0.000	1.185	0.034	0.531	0.655	0.000
PCT1-7	Water	29	22	3	4	13.258	0.457	4.409	0.610	8.238	9.040	0.312	0.720	0.352	7.968
PCT1-8	Water	31	22	8	1	7.307	0.236	5.949	1.266	0.092	1.500	0.048	0.714	0.694	0.091
PCT1-9	Water	25	16	8	1	34.340	1.374	0.478	2.813	31.049	30.436	1.217	0.194	1.363	28.879
PCT1-10	Water	53	34	16	3	21.024	0.397	3.081	6.450	11.493	15.954	0.301	0.539	4.045	11.370
Median		**31**	**21**	**8**	**1.5**	**8.853**	**0.329**	**3.652**	**2.989**	**0.551**	**3.174**	**0.128**	**0.594**	**1.342**	**0.545**
PCT1-11	Metformin	26	14	10	2	4.568	0.176	1.209	2.345	1.014	2.158	0.083	0.227	0.919	1.012
PCT1-12	Metformin	32	21	11	0	10.825	0.338	7.793	3.033	0.000	2.818	0.088	1.291	1.526	0.000
PCT1-13*	Metformin	-	-	-	-	-	-	-	-	-	-	-	-	-	-
PCT1-14	Metformin	30	19	10	1	12.479	0.416	4.637	7.191	0.651	5.233	0.174	0.853	3.731	0.649
PCT1-15	Metformin	23	16	7	0	2.349	0.102	2.039	0.310	0.000	0.625	0.027	0.433	0.192	0.000
PCT1-16	Metformin	44	29	14	1	13.960	0.317	5.480	8.180	0.301	5.653	0.128	0.963	4.391	0.298
PCT1-17	Metformin	44	34	7	3	6.078	0.138	4.731	0.838	0.508	1.923	0.044	0.933	0.485	0.504
PCT1-18	Metformin	44	38	4	2	3.183	0.072	2.754	0.321	0.108	0.729	0.017	0.451	0.173	0.106
PCT1-19	Metformin	27	14	6	7	7.965	0.295	3.186	1.703	3.076	3.863	0.143	0.427	0.687	2.750
PCT1-20	Metformin	33	27	4	2	22.499	0.682	6.863	0.512	15.124	16.017	0.485	0.744	0.313	14.960
Median		**32**	**21**	**7**	**2**	**7.965**	**0.295**	**4.637**	**1.703**	**0.508**	**2.818**	**0.088**	**0.744**	**0.687**	**0.504**
z **		**-0.369**	**-0.123**	**0.166**	**0.25**	**0.898**	**0.98**	**-0.57**	**0.98**	**0.492**	**0.735**	**0.816**	**-0.49**	**0.98**	**0.492**
P **		**0.7125**	**0.9023**	**0.8683**	**0.8026**	**0.3691**	**0.327**	**0.568**	**0.5136**	**0.5118**	**0.4624**	**0.4142**	**0.6242**	**0.5136**	**0.5118**

* This mouse died before the end of the experiment.

** *z* and *P* values were obtained by Wilcoxon rank-sum (Mann-Whitney) test between water and metformin treatment.

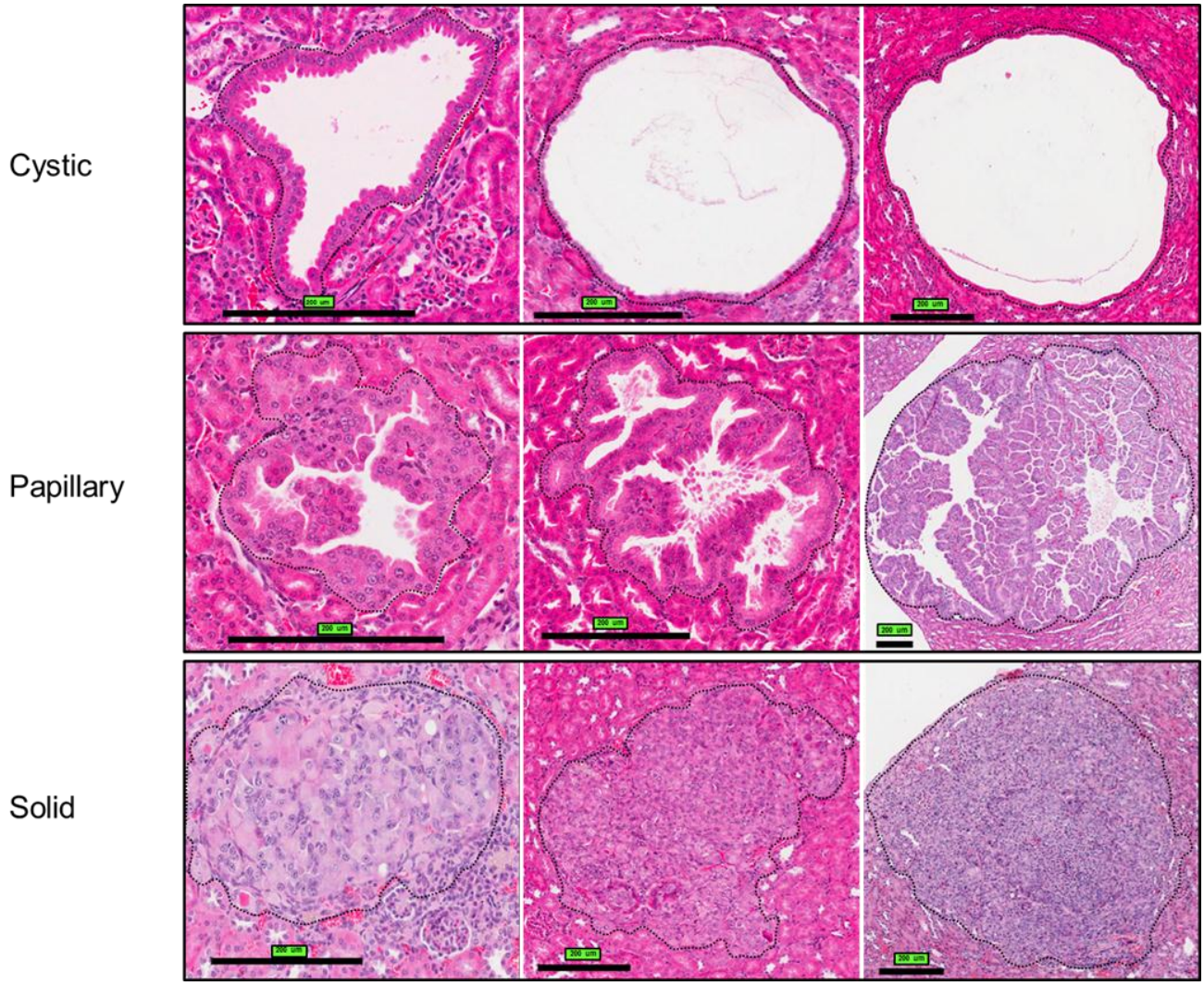

Figure 4.3 Different types of lesions (cystic, papillary, and solid) detected by histology in the kidneys of *Tsc1*$^{+/-}$ mice. Series of 5 µm coronal renal sections at 200 µm intervals were H&E stained and scanned. Scale bars: 200 µm.

A

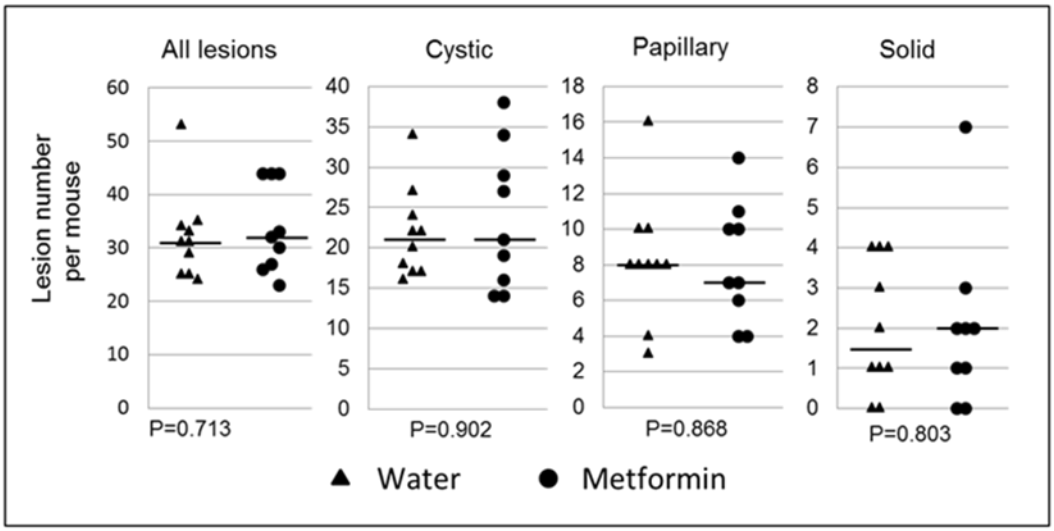
All lesions
Cystic
Papillary
Solid
Lesion number per mouse
P=0.713
P=0.902
P=0.868
P=0.803
Water
Metformin

B

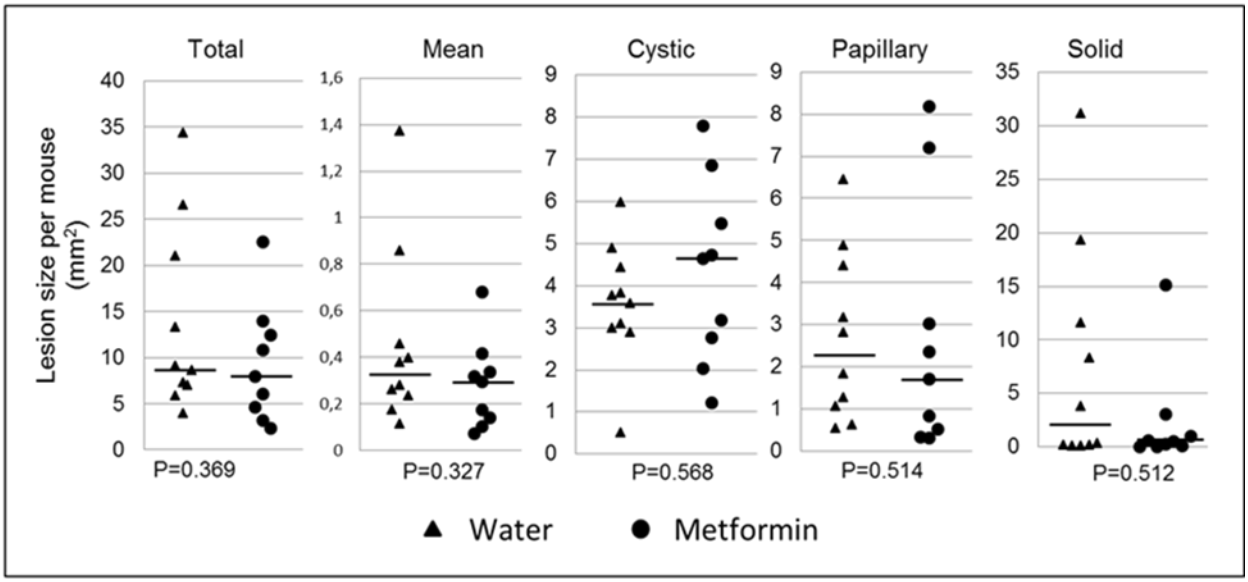
Total
Mean
Cystic
Papillary
Solid
Lesion size per mouse (mm²)
P=0.369
P=0.327
P=0.568
P=0.514
P=0.512
Water
Metformin

C

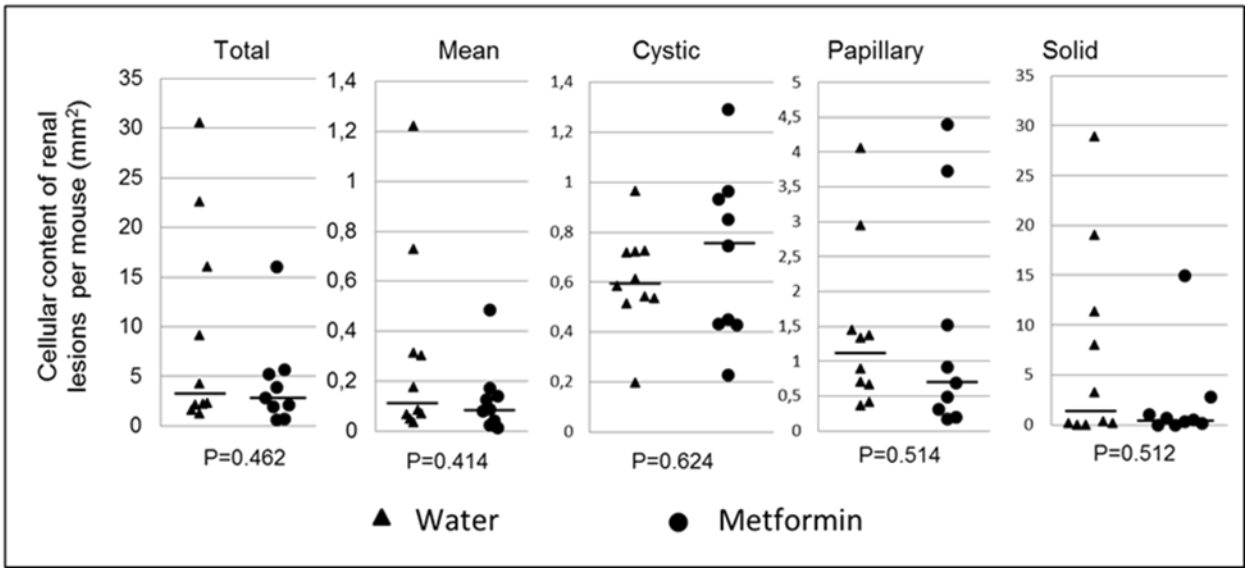
Total
Mean
Cystic
Papillary
Solid
Cellular content of renal lesions per mouse (mm²)
P=0.462
P=0.414
P=0.624
P=0.514
P=0.512
Water
Metformin

Figure 4.4 Analysis of renal lesions by histology. *Tsc1*$^{+/-}$ mice were sacrificed after an MRI scan following 9 months' treatment with drinking water (filled triangles) or metformin (filled circles). Mouse kidneys were fixed, processed and paraffin-embedded. Microscope slides were prepared with a series of 5 μm coronal sections (at 200 μm intervals), H&E stained and scanned to create virtual H&E slides. The virtual slides were used to measure the maximum cross-sectional whole area and cellular areas of renal lesions respectively with ImageJ. **(A)** Comparison of renal lesion numbers. No significant difference in lesion numbers was observed between control (drinking water) and metformin treated *Tsc1*$^{+/-}$ mice (based on Table 4.2). **(B)** Comparison of whole areas of renal lesions. No significant difference in whole areas of renal lesions was observed between control (drinking water) and metformin treated *Tsc1*$^{+/-}$ mice (based on Table 4.2). **(C)** Comparison of cellular areas of renal lesions. No significant difference in cellular areas of renal lesions was observed between control (drinking water) and metformin treated *Tsc1*$^{+/-}$ mice (based on Table 4.2).

4.3.3 Metformin suppresses mTORC1 activity in kidney tissues but not in renal lesions of *Tsc1*$^{+/-}$ mice

4.3.3.1 IHC analysis of kidney tissues and renal tumours in metformin treated and control *Tsc1*$^{+/-}$ *mice*

IHC was used to examine mTORC1 activity in kidney tissues and renal lesions of *Tsc1* mouse model. IHC was performed on 5 µm thick sections of kidney tissues and renal tumour samples of both metformin treated and control mice. The phosphorylation status of ribosomal protein S6 (Ser235/236) (rpS6$^{Ser235/236}$) was assessed as a readout for mTORC1 signalling. IHC analysis showed a slight decrease in the phosphorylation of S6$^{Ser235/236}$ in kidney tissues of mice treated with metformin in comparison to the kidney tissues of control mice (Figure 4.5). However, no obvious differences in pS6$^{Ser235/236}$ phosphorylation levels were seen in renal tumours between metformin treated and control mice (Figure 4.5). mTORC1 signalling could be quantified by quantitative immunofluorescence technique such Automated Quantitative Analysis (AQUA) (Camp RL, Chung GG, Rimm DL (2002), Automated subcellular localization and quantification of protein expression in tissue microarrays (*Nat Med* 8:1323-1327), however this was not feasible due to time limitation.

4.3.3.2 Western analysis of kidney tissues and renal tumours in metformin treated and control Tsc1$^{+/-}$ *mice*

As in IHC, we analysed the mTORC1 signalling for phosphorylated S6$^{Ser235/236}$ by Western blotting. We also investigated the phosphorylation levels of pAMPK^{Thr172}, pACC^{Ser79}, pAkt^{Ser473} and pRaptor^{Ser792} which are the main molecular targets of metformin (Gwinn *et al*. 2008, Zakikhani *et al*. 2010, Zhou *et al*. 2001). Western blot analysis showed a decrease in the phosphorylation of pS6$^{Ser235/236}$ (*P*= 0.028) and an increase in the phosphorylation of both AMPK^{Thr172} (*P*= 0.049) and ACC^{Ser79} (*P*= 0.046) in kidney tissues of metformin treated mice (Figure 4.6). However, no significant differences were seen in the phosphorylation levels of Akt^{Ser473} (*P*= 0.299) or Raptor^{Ser792} (*P*= 0.705) in the kidney tissues between metformin treated and control mice (Figure 4.6).

In contrast, no significant differences were found in the phosphorylation levels of pS6$^{Ser235/236}$ (*P*= 0.579), AMPK^{Thr172} (*P*= 0.770), ACC^{Ser79} (*P*= 0.830), Akt^{Ser473} (*P*= 0.327) and Raptor^{Ser792} (*P*= 0.794) in renal lesions of control and metformin treated groups (Figure 4.6). These results suggest that metformin can attenuate mTORC1 activity in *Tsc1*$^{+/-}$ mouse kidney tissues, but not in *Tsc1*-associated renal tumours.

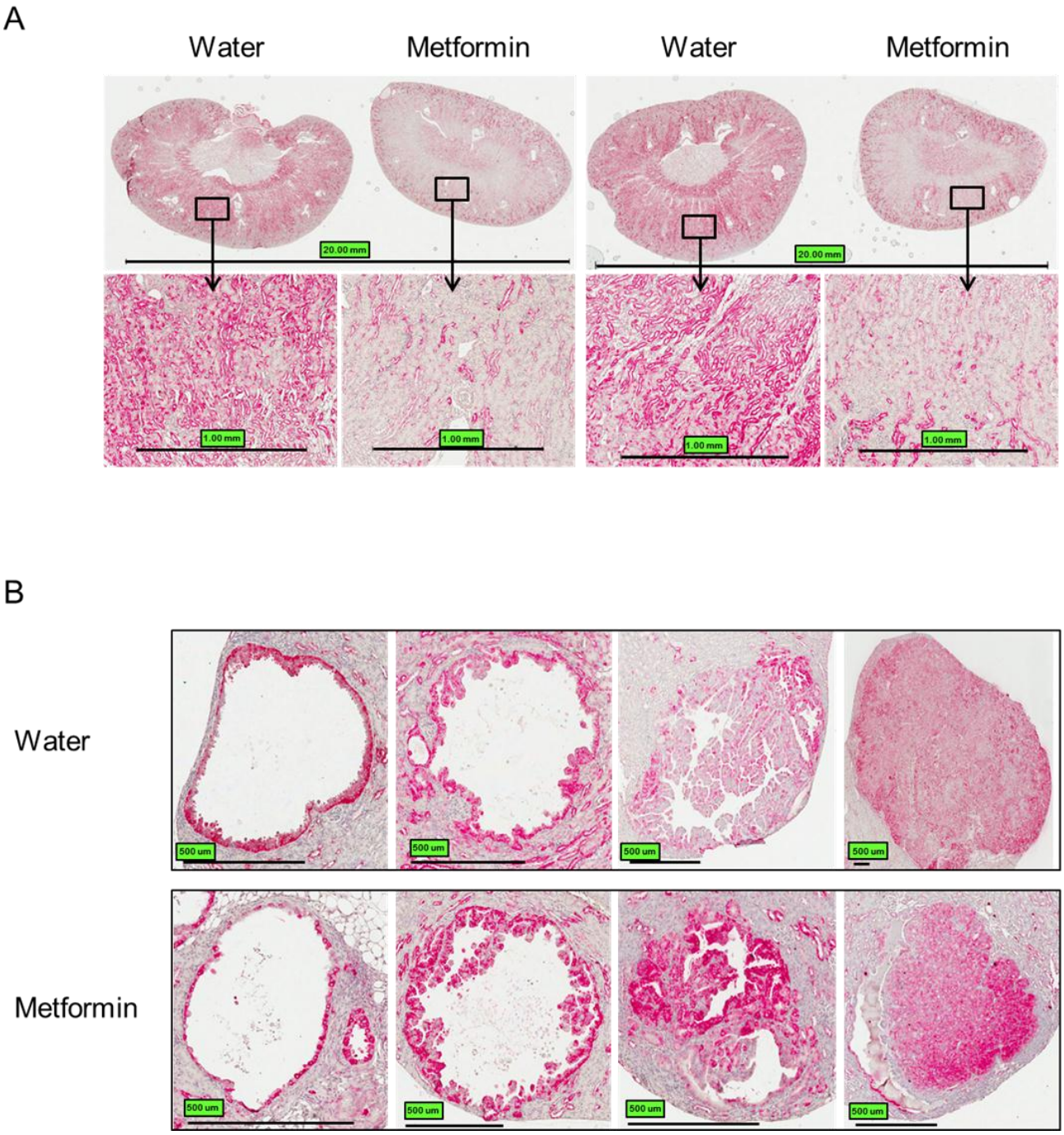

Figure 4.5 Immunohistochemical analysis of renal tissues and tumours. Paraffin-embedded sections from kidney tissues and tumours of *Tsc1*$^{+/-}$ mice were stained with an antibody against pS6$^{Ser235/236}$ using EXPOSE Rabbit specific AP detection IHC kit. **(A)** Phospho-S6$^{Ser235/236}$ (red) in kidney tissues of *Tsc1*$^{+/-}$ mice. The level of Phospho-S6$^{Ser235/236}$ is slightly lower in kidney tissues of metformin treated mice than controls. **(B)** Phospho-S6$^{Ser235/236}$ (red) in renal tumours of *Tsc1*$^{+/-}$ mice. No obvious difference was observed between control (drinking water) and metformin treated *Tsc1*$^{+/-}$ mice.

A

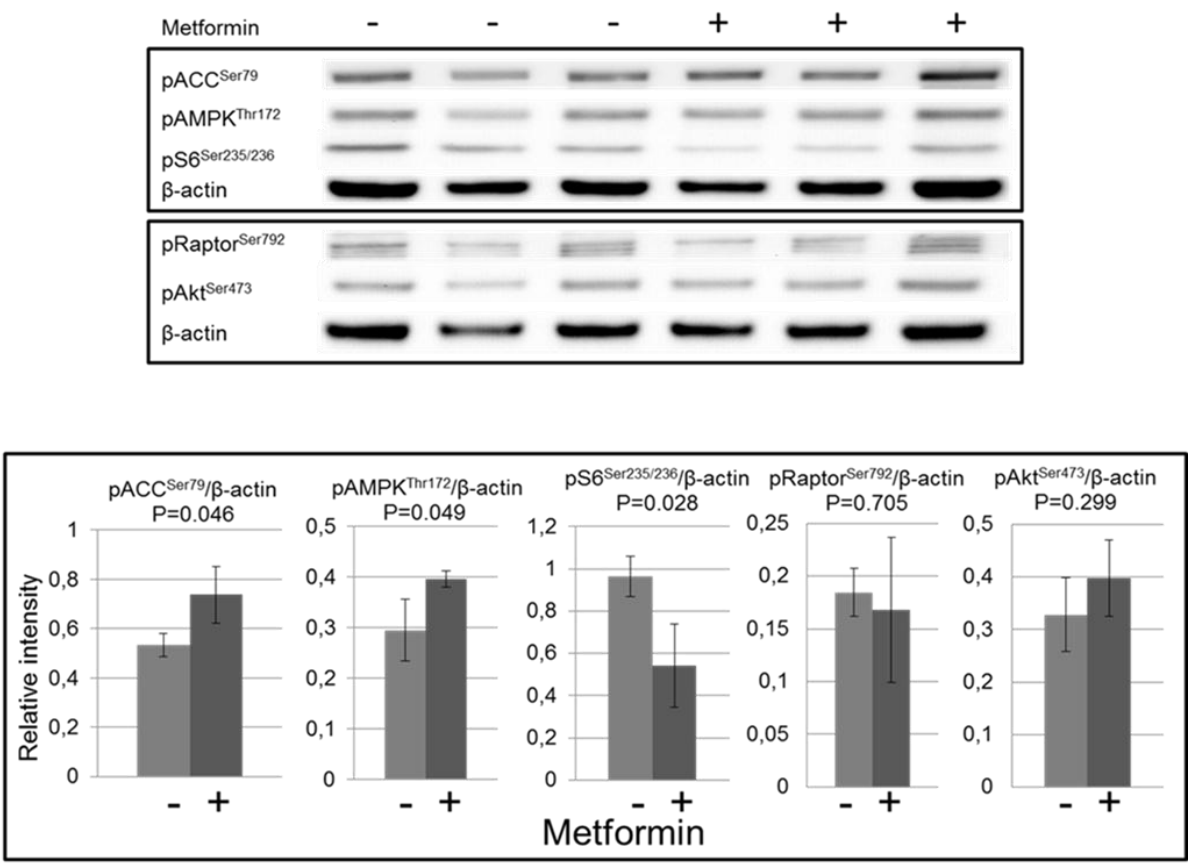
Metformin - - - + + +
pACC^Ser79
pAMPK^Thr172
pS6^Ser235/236
β-actin
pRaptor^Ser792
pAkt^Ser473
β-actin
pACC^Ser79/β-actin P=0.046
pAMPK^Thr172/β-actin P=0.049
pS6^Ser235/236/β-actin P=0.028
pRaptor^Ser792/β-actin P=0.705
pAkt^Ser473/β-actin P=0.299
Relative intensity
Metformin

B

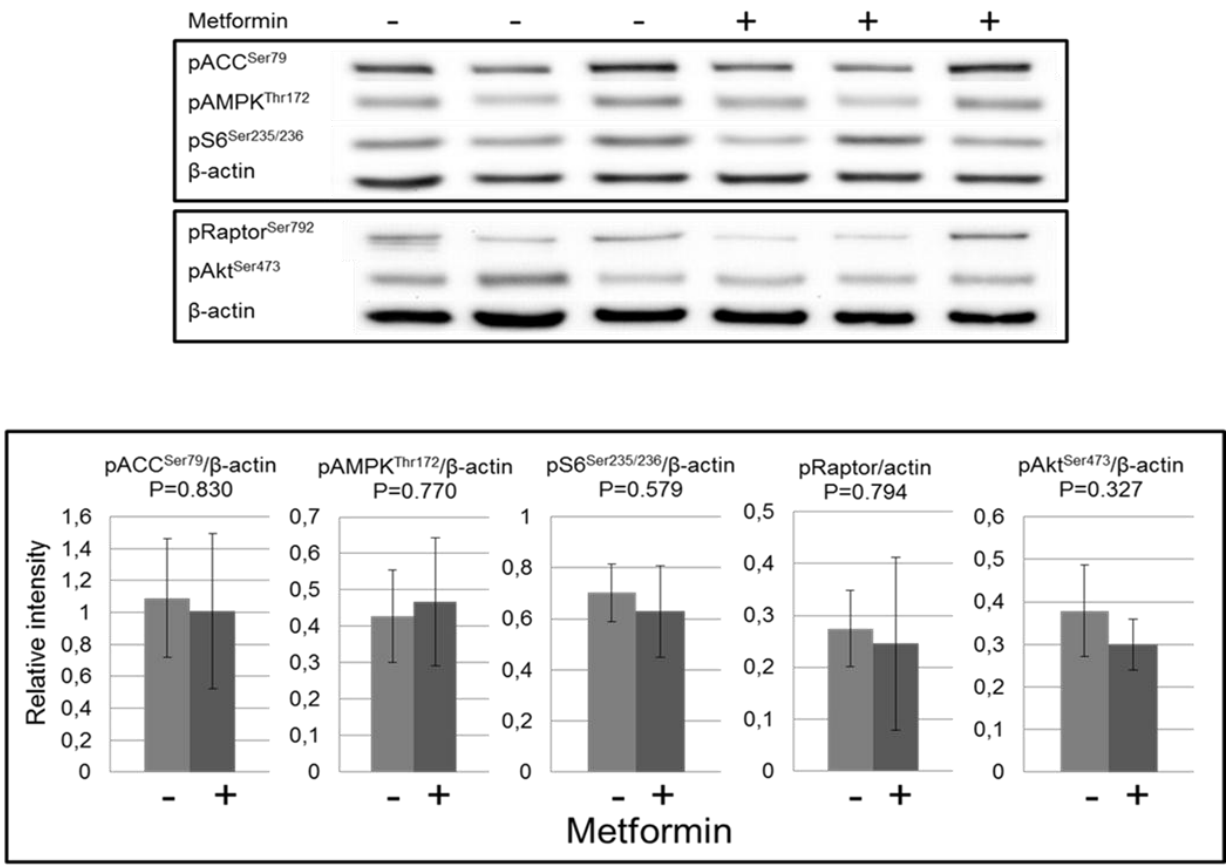
Metformin - - - + + +
pACC^Ser79
pAMPK^Thr172
pS6^Ser235/236
β-actin
pRaptor^Ser792
pAkt^Ser473
β-actin
pACC^Ser79/β-actin P=0.830
pAMPK^Thr172/β-actin P=0.770
pS6^Ser235/236/β-actin P=0.579
pRaptor/actin P=0.794
pAkt^Ser473/β-actin P=0.327
Relative intensity
Metformin

Figure 4.6 Western analysis of renal tissues and tumours. **(A)** Western analysis of renal tissues of *Tsc1*$^{+/-}$ mice. Metformin increased the phosphorylation of AMPK at Thr172 and ACC at Ser79 and decreased the phosphorylation of S6 at Ser235/236. Phosphorylation of Raptor Ser792 and Akt at Ser473 was not significantly affected by metformin. **(B)** Western analysis of renal tumours of *Tsc1*$^{+/-}$ mice. No significant difference in phosphorylation of any of the proteins at specific amino acid residuals was observed. Standard error bars are included.

4.4 Discussion

In this study, we assessed the effect of metformin on renal tumours of a *Tsc1*$^{+/-}$ mouse model. We compared lesion number, size (area by histology and volume by MRI), and cellular content (by histology) between metformin treated and control mice. Long term treatment with metformin was well tolerated in these mice. However, metformin treatment had no effect on TSC-associated renal lesions. Our results are consistent with findings reported in a recent study by Auricchio *et al*. (2012). Auricchio and colleagues used *Tsc2*$^{+/-}$ A/J mice to examine the potential benefit of metformin treatment for renal lesions. Metformin was provided to the mice in their drinking water at 300mg/kg per day for a period of 4 months (from age 1 month to age 5 months). Similar to our findings, this study reported that metformin treatment was well tolerated with no apparent toxicity but had no significant effect on renal lesions as demonstrated by quantitative tumour volume measurement. However, these results are not expected. An anti-tumour activity has been proposed for metformin, based upon epidemiological studies and preclinical data, prompting clinical trials in a variety of cancers (Jalving *et al*. 2010). Recent advances in understanding the molecular targets of metformin, particularly its inhibitory activity on mTORC1 have led to speculation that it may also be a candidate therapy for TSC. Our findings, together with those by Auricchio and colleagues, suggest, however, that metformin is not effective in the treatment of renal lesions when administered from 1 or 6 months of age for 4 or 9 months in two different mouse models on different genetic backgrounds.

We also examined the effect of metformin treatment on mTORC1 signalling in the kidney tissues and paired renal tumours of *Tsc1*$^{+/-}$ mice. Attenuation of mTORC1 signalling by metformin was observed by both IHC and Western analysis in normal *Tsc1*$^{+/-}$ mouse kidney tissues. Metformin increased the phosphorylation of AMPK^{Thr172} and ACC^{Ser79} (by Western analysis), and decreased the phosphorylation of S6$^{Ser235/236}$ (by both IHC and Western analysis) in kidney tissues. Neither method demonstrated attenuation of mTORC1 signalling in *Tsc1*-associated renal tumours. Auricchio *et al*. (2012) showed induction of AMPK activation, indicated by the increased phosphorylation levels of ACC^{Ser79} in kidney lysates and *Tsc2*-associated

tumour samples and Raptor^{Ser792} in kidney lysates in response to metformin treatment. However, no significant differences were seen in the phosphorylation levels of S6$^{Ser235/236}$ in either kidney tissues or *Tsc2*-associated renal tumours between metformin treated and control mice (Auricchio *et al*. 2012). Discrepancy between this study and Auricchio *et al.*'s might be explained by several factors, particularly differences in mouse strain and model systems used. We used *Tsc1*$^{+/-}$ mice backcrossed on balb/c background while Auricchio *et al.* used *Tsc2*$^{+/-}$ mice of the A/J strain. The A/J strain was generated by an insertion of ETn retrotransposon (5-6kb) in intron 4 of the dysferlin gene and is highly immunocompromised.

Multiple factors might contribute to the lack of efficacy by metformin treatment on Tsc-associated renal tumours. First, a functional TSC1/TSC2 complex may be required for action of metformin *in vivo*. In fact, somatic loss of the second *Tsc1* allele in renal tumours was frequently observed in this *Tsc1*$^{+/-}$ mouse model (Wilson *et al*. 2005). Consistently, metformin reduced mTORC1 activity in normal kidney tissues but not renal tumours in this study. Furthermore, Dowling *et al*. (2007) showed that treatment of *Tsc2*-deficient MEF cells *in vitro* with metformin had no effect on mTORC1 inhibition. Failure of metformin to regulate mTORC1 signalling in these cells indicates the highly important synergistic role of TSC2 in the inhibitory activity of metformin. In contrast, Kalender *et al*. (2010) have demonstrated inhibition of mTORC1 by metformin in *Tsc2* deficient MEF cells *in vitro* through a TSC1/TSC2-independent mechanism. As Kalender *et al.* (2010) suggested, density of cells in culture may affect sensitivity of mTORC1 signalling to metformin in *Tsc2*-deficient cells. Further studies are needed to clarify effect of metformin on mTORC1 in cells with different genotypes of *Tsc1* or *Tsc2*.

The treatment dose may also affect the efficacy of metformin. The daily drug dose administered in this was higher than that used for the treatment of diabetes in human patients (by over ten times in last two months of treatment). Therefore, the ineffectiveness of metformin on *Tsc1*-associated renal lesions is unlikely to be caused by low drug dose in this current trial.

Other factors affecting efficacy of metformin may include drug distribution, metabolism, uptake and excretion. Metformin is not metabolised but is cleared mainly by tubular secretion in the kidneys (Graham *et al*. 2011). Metformin is a substrate of several poly-specific organic cation transporters (OCTs) which have a highly important and critical role in the overall function of metformin (Graham *et al*. 2011). OCTs are responsible for the oral absorption, hepatic and renal uptake and renal secretion of metformin. Metformin is readily filtered at the glomerulus (Graham *et al*. 2011). SLC22A1 and SLC22A3 transport metformin between the blood supply into the liver (Chen *et al*. 2010, Sogame *et al*. 2009). ABC transporters such as ABCB1, ABCC1 and ABCG2 are usually highly expressed in the human placental tissue and are responsible for the placental disposition of oral hypoglycemic drugs including metformin. According to Hemauer *et al*. (2010), ABCBA1 and ABCG2 but not ABCC1 placental transporters are involved in the efflux of metformin in human. SLC22A2 is the major known transporter responsible for the renal uptake of metformin from blood (Graham *et al*. 2011). SLC47A1, SLC47A2 and SLC22A1 are present in the kidney and mediate the tubular secretion of metformin into the urine (Tanihara *et al*. 2007). SLC22A1 also involved in cellular uptake of metformin in the kidneys. There are species differences in the tissue distribution of different OCTs. However, the characteristics of human OCTs are to some extent similar to mouse. The tissue distribution of SLC22A1, SLC22A2, SLC22A3 and SLC47A1 is similar in both humans and mice. Slc22a3 is clustered with Slc22a1 and Slc22a2 on mouse chromosome 17 and is expressed in the kidneys. However, SLC47A2 is not expressed in mouse kidneys (Yonezawa and Inui, 2011).

Effective cellular uptake of metformin from the blood supply into the kidney and renal tumour cells is highly important for its efficient anti-cancer activity. My colleagues in our lab have extensively investigated OCTs expression in normal kidney tissues and renal tumours using quantitative polymerase chain reaction (q-PCR) (Yang *et al*. 2012). The expression of the organic cation transporter genes *Slc22a1*, *Slc22a2* and *Slc22a3* was highly suppressed in renal tumours in comparison to kidney tissues in *Tsc1*$^{+/-}$ mice. Treatment of cultured cells derived from a *Tsc1*-associated renal

tumour with 5-aza-2-deoxycytidine (5-aza-2-dC) or trichostatin A (TSA) which inhibit DNA methyltransferase and histone deacetylase, respectively, greatly increased expression of these genes. These data suggest that epigenetic suppression of the organic cation transporters responsible for cellular uptake of metformin occurs in Tsc-associated mouse renal tumours and may contribute to the lack of response to metformin treatment. This finding was also consistent with our observation that metformin appeared to attenuate mTORC1 signalling in kidney tissues but not in renal tumours of *Tsc1*$^{+/-}$ mice.

Tsc1$^{+/-}$ or *Tsc2*$^{+/-}$ mouse models share some disease features with TSC patients but both recognised and unrecognised differences are likely. Therefore, although our findings together with others' (Auricchio *et al*. 2012) suggest that metformin is not effective for treating renal lesions in *Tsc1*$^{+/-}$ balb/c or *Tsc2*$^{+/-}$ A/J mice it may be worthwhile to investigate whether metformin treatment has any effect on TSC-associated tumours in patients.

In conclusion, this study suggests that metformin is not effective for the treatment of renal cysts, papillary cyst-adenomas or solid tumours in a *Tsc1*$^{+/-}$ mouse model. Metformin did not consistently reduce mTORC1 signalling activity in *Tsc1*-associated renal tumours in this model, although some attenuation of signalling was observed in heterozygous *Tsc1* kidney tissues. It may be worthwhile to test whether metformin alone or in combination with other mTORC1 inhibitors have efficacy in prevention rather than treatment of renal lesions in further preclinical trials using Tsc mouse models.

CHAPTER FIVE

Long term inhibition of mTOR complex 1 by rapamycin prevents renal tumourigenesis

5.1 Introduction

The PI3K/Akt/mTOR signalling pathway is frequently deregulated in many human cancers due to mutations or epigenetic changes of its components (Dazert and Hall, 2011; Guertin and Sabatini, 2007). These mutations result in activation of oncogenes or loss of function of tumour suppressor genes, giving rise to tumourigenesis and providing potential targets for tumour therapy (Bjornsti and Houghton, 2004; Shaw and Cantle, 2006; Vivanco and Sawyers, 2002). As discussed before, mutations of either *TSC1* or *TSC2* tumour suppressor upstream of mTOR cause TSC (The European Chromosome 16 Tuberous Sclerosis Consortium, 1993; van Slegtenhorst *et al*. 1997). TSC-associated tumours show constitutive activation of mTORC1 signalling in both patients and animal models. Rapalogues have been shown to inhibit mTORC1 signalling and suppress the growth of TSC lesions in several clinical and preclinical trials (Bissler *et al*. 2008, Kenerson *et al*. 2005, Krueger *et al*. 2010, Lee *et al*. 2005, Pollizzi *et al*. 2009). However, rapamycin does not cause complete regression of disease in most cases, and cessation of treatment can lead to regrowth of TSC-associated tumours in addition to its side effects. Rapalogues may be effective for prevention of TSC-associated tumours. As yet, no properly designed prevention studies have been reported in TSC patients or animal models.

As stated in Chapter 4, long term treatment with metformin, a less potent mTORC1 inhibitor, had no therapeutic effect upon the renal lesions of *Tsc1*$^{+/-}$ mouse model. Nevertheless, metformin has been shown to reduce cancer risk in diabetic patients and to prevent tumourigenesis in mouse models (Evans *et al*. 2005, Huang *et al*. 2008, Memmott *et al*. 2010). It remains to be determined whether metformin can prevent tumourigenesis in TSC patients and animal models.

In this study, we tested the preventive efficacy of long term treatment with rapamycin, metformin, or both in combination, on tumourigenesis in the kidneys of *Tsc2*$^{+/-}$ mice. We also examined mTORC1 activity in renal lesions of these mice. Finally, we assessed the effect of these agents on mTORC1 signalling in normal renal and liver tissues of this animal model.

5.2 Materials and methods

5.2.1 DNA extraction and genotyping

As outlined in section 2.5.2.1, DNA was extracted from mouse ear punches, using the Wizard® SV Genomic DNA Purification System. Genotyping was determined by PCR as described in section 2.5.2.2. PCR products were 849 bp (wild-type) and 658 bp (mutant), and were analysed on 1.5% agarose gels.

5.2.2 Animals and procedures

Mice were maintained at Cardiff University (School of Biosciences) animal research facility under standard conditions (described in section 2.5.1) and all animal procedures were performed in accordance with the UK Home Office guidelines. The *Tsc2*$^{+/-}$ mice were described previously (Onda *et al*.1999) and backcrossed to balb/c strain for over 10 times. Following genotyping, 80 *Tsc2*$^{+/-}$ mice were randomly divided into 4 treatment groups: vehicle, rapamycin, metformin and rapamycin plus metformin. All treatments were started at the age of one month and continued until sacrifice at 8 months or 10 months of age. Rapamycin (LC Laboratories, Woburn, USA) was prepared at 2 mg/ml in vehicle solution (2.5% PEG-400, 2.5% Tween-80 and 2.5% DMSO). Metformin (RelonChem, London) was prepared at 30 mg/ml in water. Rapamycin alone was given at 5 mg/kg 5 times a week initially and twice a week for the last 6 weeks by i.p. injection. Metformin alone was given at 300 mg/kg 5 times a week by gavage. For combination treatment, rapamycin was given at 4 mg/kg 5 times a week and metformin at 150 mg/kg 5 times a week for the first 3 months. The rapamycin dose was then reduced to 2.5 mg/kg. Both agents were

given only twice a week for the last 6 weeks. The reductions in dosages and treatment frequency were made because of concerns over weight loss. Mouse body weight was monitored once a week. At the end of treatment, animals were humanely sacrificed for tissue collection, and subsequent histological and molecular analysis.

5.2.3 Histology

The same protocol was used as in Chapter 3, Section 3.2.4. Microscope slides were prepared with a series of 5 μm coronal sections taken with or without interruption at 200 μm intervals from each kidney. They were H&E stained and scanned to create virtual H&E slides. The virtual slides were used for lesion quantification and analysis using ImageJ. The assessment was conducted blindly with respect to treatment status.

5.2.4 IHC

Paraffin-embedded mouse kidney sections (5 μm thick) taken from the *Tsc2*$^{+/-}$ mice, were processed for IHC using the EXPOSE Rabbit specific AP detection IHC kit, according to the protocol outlined in section 2.5.7. Primary antibodies used were at the indicated dilution against: phosphor-S6 (Ser235/236) (1:200), MCM2 (1:200), Cyclin D1 (1:100), Ki67 (1:200) and MUC1 (1:100).

5.2.5 Western analysis

Western blotting was carried out as described in section 2.5.13. Primary antibodies used for Western analysis were against β-actin (1:2000 dilution), GAPDH (1:60000) phosphorylated S6 (Ser235/236) (1:1000 dilution) and 4EBP1 (T70) (1:1000 dilution). Secondary antibody was horseradish peroxidise-conjugated antibody against rabbit. Extracts of mouse liver tissues were prepared using AllPrep DNA/RNA/Protein Mini. Proteins were purified according to the kit supplier's instruction (outlined in section 2.5.10), separated on NuPAGE 4-12% Bis-Tris Gels and transferred onto Hybond ECL Membranes. Blots were analysed with ECL Advance Western Detection Kit and

signals were detected using Autochemi Imaging System. Relative intensity of blot signals was determined using ImageJ (http://rsbweb.nih.gov/ij).

5.2.6 Statistical analysis

Non-parameter statistical analysis was used for renal lesion comparison because Kurtosis tests indicated that the distribution of the lesion number and size in the *Tsc2*$^{+/-}$ mice was skewed in some treatment groups. The Wilcoxon rank-sum (Mann-Whitney) test was performed for comparison between two groups and Kruskal-Wallis equality-of-populations rank test for comparison of more than two groups using the software Stata (version 11). Two tailed unpaired Student's t-Test was used for comparison of Western analysis results. $P < 0.05$ was considered to be statistically significant.

5.3. Results

5.3.1 Renal tumourigenesis and mTORC1 signalling in a *Tsc2*$^{+/-}$ mouse model

5.3.1.1 Assessment of renal tumourigenesis in Tsc2$^{+/-}$ *mice by histological analysis*

Genetically engineered *Tsc2*$^{+/-}$ mouse models, provided by Prof David J. Kwiatkowski (Onda *et al*.1999), were backcrossed to the balb/c strain over 10 times. In order to establish the earliest time at which renal lesions develop on this genetic background, we examined by microscopy H&E stained consecutive 5 μm kidney sections from 6 mice at the age of 15 days, 30 days, 45 days and 60 days, respectively. No renal lesions were observed in *Tsc2*$^{+/-}$ mice sacrificed prior to 45 days of age. However, small cysts and microscopic solid dysplastic growths that have not been previously described were seen in mice at 60 days of age (Figure 5.1). Large cysts, papillary and solid tumours were observed in the kidney tissues of older animals (Figure 5.2).

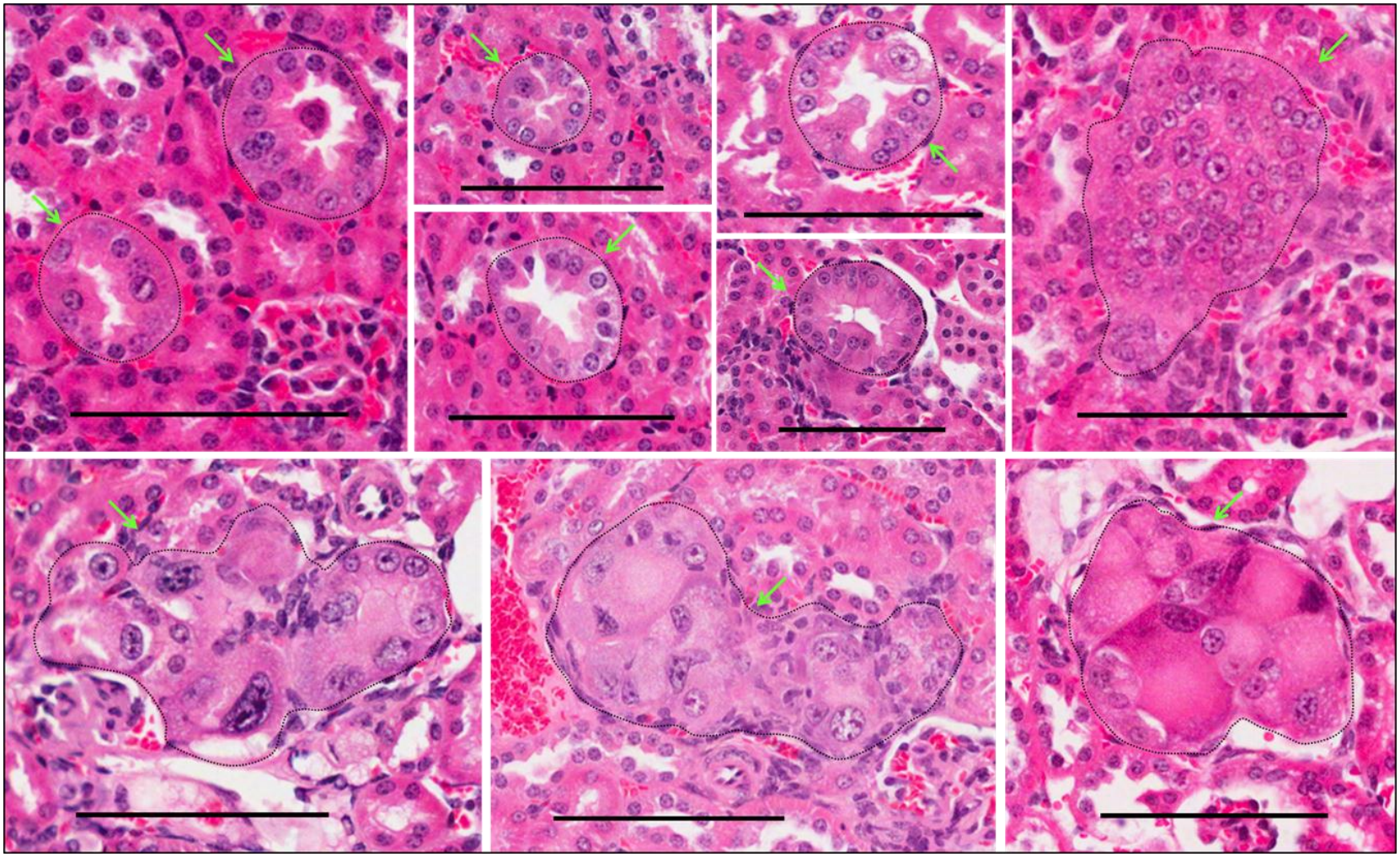

Figure 5.1 Micro renal lesions of the *Tsc2*$^{+/-}$ mice. Kidney sections were prepared from *Tsc2*$^{+/-}$ mice of 10 months old and HE-stained. Microscopic dysplasias and cysts were showed (green arrows). Scale bars: 100 μm.

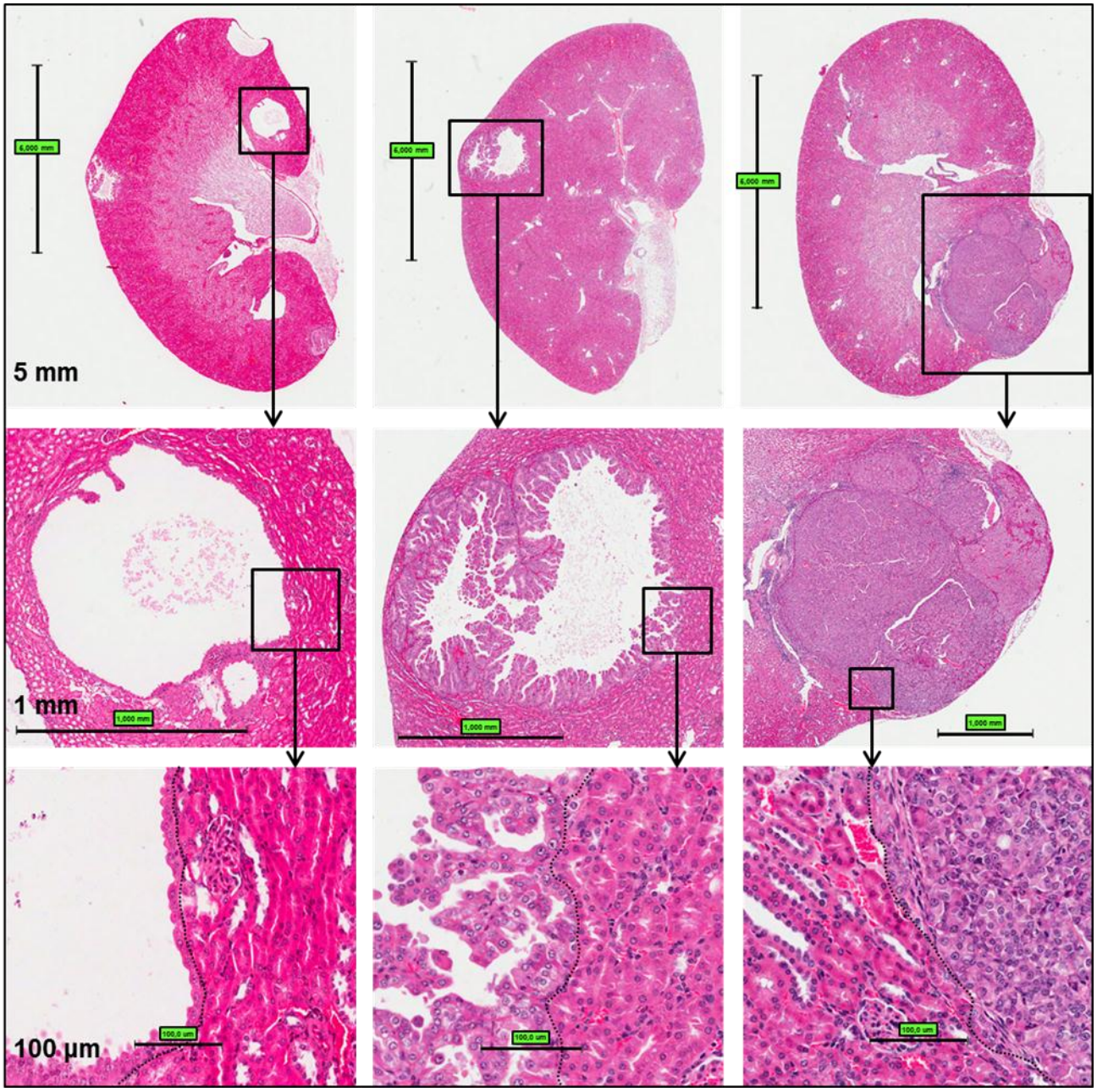

Figure 5.2 Renal lesions of the *Tsc2*$^{+/-}$ mice. Kidney sections were prepared from *Tsc2*$^{+/-}$ mice of 10 months old and HE-stained. Top panel: Gross views of kidney sections with various types of lesions. Middle panel: microscopic views of cystic, papillary and solid renal lesions from the corresponding kidney sections in the top panel. Bottom panel: magnified microscopic views showing the boundaries between the tumours and normal tissues.

5.3.1.2 Examination of mTORC1 signalling in Tsc2-associated renal lesions by IHC

IHC analysis was performed on kidney sections to determine mTORC1 activity in renal lesions of 10 month old *Tsc2*$^{+/-}$ mice. Phosphorylated ribosomal protein S6 at serine 235/236 was used as a marker of mTORC1 activation. All lesions including the smallest microscopic dysplasias and cysts showed activation of mTORC1 (Figure 5.3). These results are consistent with the notion that mTORC1 is required for renal tumourigenesis in the *Tsc2*$^{+/-}$ mouse model.

5.3.2 Increased cell proliferation in *Tsc2*-associated renal tumours

To further characterise these lesions, antibodies against Mcm2, Ki67, Cyclin D1 and Muc1 were used to determine proliferation status of renal lesions by IHC on kidney sections. All these proteins were highly expressed, indicating increased cell proliferation in renal tumours of *Tsc2*$^{+/-}$ mice (Figure 5.4).

p-S6 (Ser235/236)

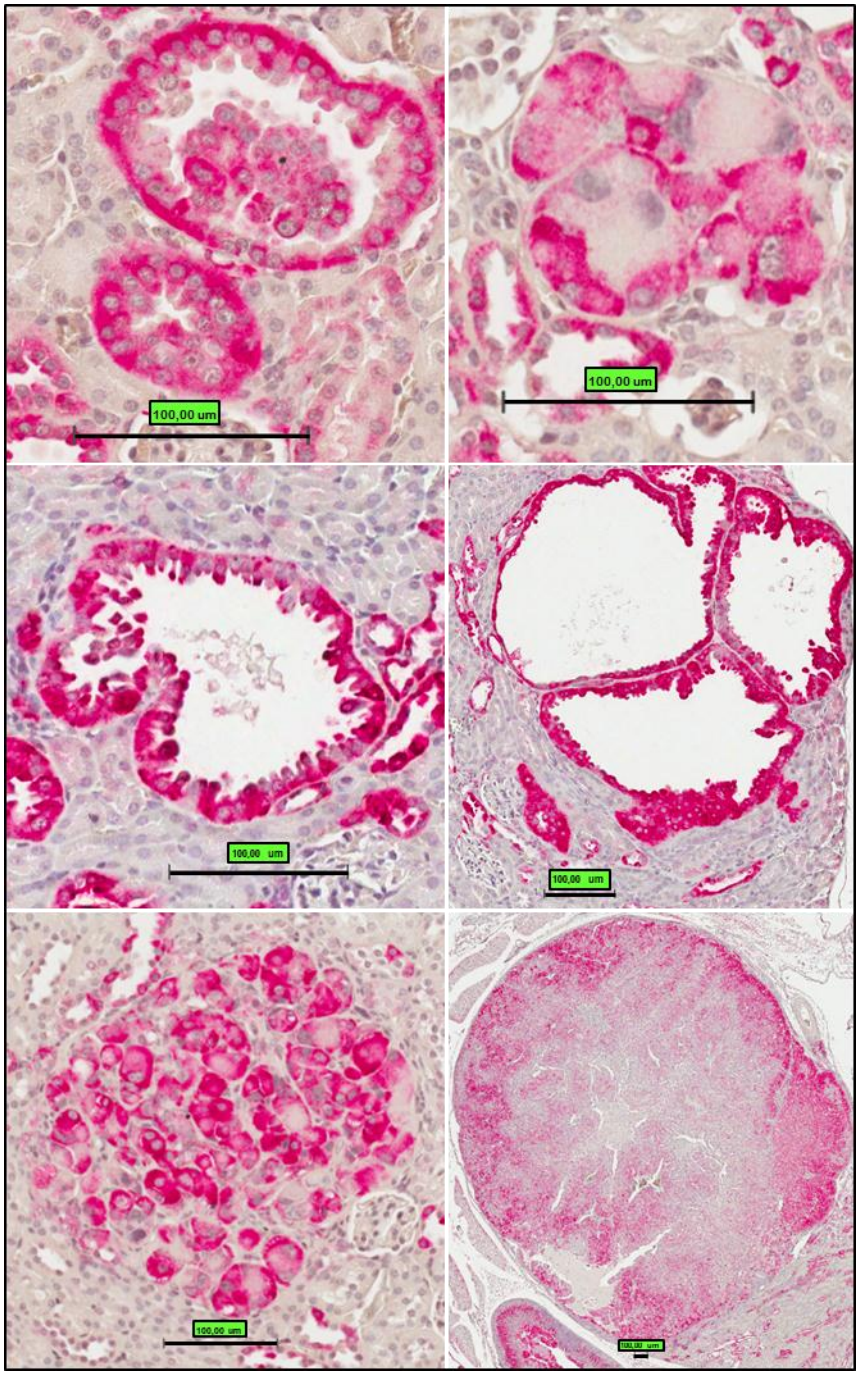

Figure 5.3 mTORC1 signalling in renal lesions of *Tsc2*$^{+/-}$ mice. Kidney sections from *Tsc2*$^{+/-}$ mice of 10 months old were prepared and stained in red with antibody against phosphorylated S6 (Ser235/2360). S6 was highly phosphorylated in all lesions. Scale bars: 100 μm.

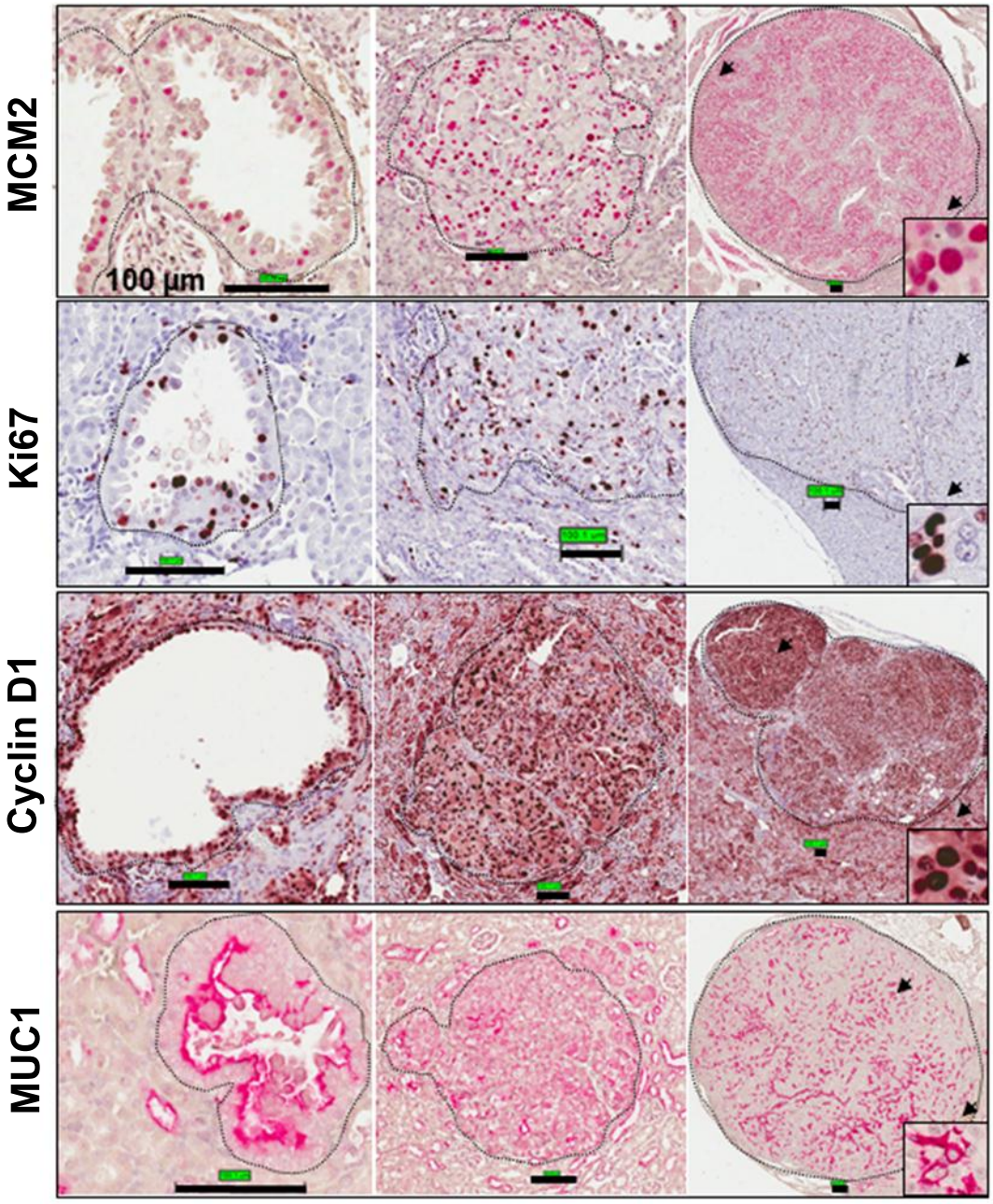

Figure 5.4 Increased cell proliferation in renal tumours of *Tsc2*$^{+/-}$ mice. Kidney sections from *Tsc2*$^{+/-}$ mice of 10 months old were prepared and stained by IHC with antibodies against MCM2, Ki67, Cyclin D1 and MUC1. Representative kidney sections were presented showing increased cell proliferation in renal tumours. Scale bars: 100.1 µm.

5.3.3 Rapamycin but not metformin alone prevents renal tumourigenesis in *Tsc2*$^{+/-}$ mice

We treated 4 groups of *Tsc2*$^{+/-}$ mice, each of 20 animals (Table 5.1). Group 1 received vehicle (control group), group 2 metformin, group 3 rapamycin and group 4 both rapamycin and metformin. All treatments were commenced at 1 month of age (+/- 1 day) and were continued until mice were sacrificed. Half of each group was sacrificed at the age of 8 months and the remainder at the age of 10 months. Three mice died unexpectedly before the end of the experiment, 1 from the rapamycin group and 2 from the rapamycin plus metformin group. No lesions were observed in kidney tissues by histological analysis. These mice were excluded from final analysis (Table 5.1). To analyse treatment efficacy, a series of coronal sections were prepared at 200 μm intervals through each whole kidney for histopathological assessment. Histological analysis was conducted blindly to treatment status and confirmed by an experienced renal pathologist, Dr David Griffiths.

All macroscopically and microscopically observed lesions were counted, characterised as cystic, papillary or solid, and quantified by measuring both their maximum cross-sectional areas (lesion size) and also the areas representing only their solid cellular components (excluding cyst lumens), as described earlier (Chapter 3, section 3.3.3). At sacrifice, the mice that had been treated with vehicle alone all had multiple bilateral renal lesions including microcystic, dysplastic, cystic, papillary and solid lesions (Figures 5.1, 5.2). Similarly, metformin treated mice also exhibited multiple renal tumours. No significant differences were found in the number (P= 0.5705 and P= 0.7620 for 7 and 9 months treatment, respectively), volume (P= 0.6501 and P= 0.3643 for 7 and 9 months treatment, respectively) and cellular content (P= 0.7055 and P= 0.2899 for 7 and 9 months treatment, respectively) of all lesions detected, between the metformin treated and control group (Tables 5.2, 5.3, Figures 5.5, 5.6). By contrast, of 9 mice treated with rapamycin alone only 1 showed 2 microscopic cysts at 8 months (P <0.0001, Table 5.2, Figure 5.5) and no lesions were seen in any of 10 mice at 10 months (P <0.0001, Table 5.3, Figure 5.6). In addition, none of the mice treated for 7 months with rapamycin plus metformin (n= 9) exhibited renal lesions (Table 5.2, Figure 5.5) and only 1 microscopic cyst was

observed among 9 mice treated with both agents for 9 months (Table 5.3, Figure 5.6). No significant differences were found in number (P= 0.3173 and P= 0.2918 for 7 and 9 months treatment, respectively), volume (P= 0.3173 and P= 0.2918 for 7 and 9 months treatment, respectively) and cellular content (P= 0.3173 and P= 0.2918 for 7 and 9 months treatment, respectively) of all lesions detected, between the rapamycin and rapamycin plus metformin treatment groups (Tables 5.2, 5.3, Figures 5.5, 5.6). These data demonstrated the effectiveness of rapamycin in blocking tumourigenesis in the kidneys of *Tsc2*$^{+/-}$ mice.

Table 5.1 Summary of animal treatment.

Treatment Group	Total number of mice	Number of males	Number of females	Treatment start age (months)	Treatment end age (months)	Number of animals died before end*
Vehicle	10	5	5	1	8	0
Metformin	10	5	5	1	8	0
Rapamycin	10	5	5	1	8	1
Rap+Met**	10	5	5	1	8	1
Vehicle	10	5	5	1	10	0
Metformin	10	5	5	1	10	0
Rapamycin	10	5	5	1	10	0
Rap+Met	10	5	5	1	10	1

*These animals were excluded from final analysis.
**Rap+Met= rapamycin plus metformin.

Table 5.2 Histological analysis of renal lesions in *Tsc2*$^{+/-}$ mice treated from one month old for 7 months with vehicle, metformin, rapamycin or rapamycin plus metformin.

Mouse	Treatment	Treatment duration (months)	Number of all lesions	Number of cysts	Number of papillary lesions	Number of solid lesions	Area of all lesions (mm^2)	Mean area per lesion (mm^2)	Area of cysts (mm^2)	Area of papillary lesions (mm^2)	Area of solid lesions (mm^2)	Cellular content of all lesions (mm^2)	Mean cellular content per lesion (mm^2)	Cellular content of cysts (mm^2)	Cellular content of papillary lesions (mm^2)	Cellular content of solid lesions (mm^2)
PCTP1-1	Vehicle	7	35	19	9	7	10.929	0.312	2.331	5.342	3.256	7.662	0.219	0.571	3.944	3.147
PCTP1-2	Vehicle	7	39	26	13	0	4.897	0.126	2.117	2.779	0.000	1.931	0.050	0.535	1.396	0.000
PCTP1-3	Vehicle	7	62	33	21	8	11.199	0.181	5.042	5.526	0.631	4.849	0.078	1.223	3.018	0.608
PCTP1-4	Vehicle	7	87	56	25	6	17.859	0.205	10.328	7.244	0.288	6.152	0.071	2.001	3.866	0.286
PCTP1-5	Vehicle	7	50	27	19	4	15.797	0.316	7.590	5.904	2.304	7.107	0.142	1.111	3.765	2.231
PCTP1-6	Vehicle	7	32	28	4	0	1.643	0.051	0.800	0.843	0.000	0.730	0.023	0.336	0.394	0.000
PCTP1-7	Vehicle	7	34	27	6	1	6.110	0.180	3.945	2.085	0.080	2.075	0.061	0.805	1.193	0.077
PCTP1-8	Vehicle	7	39	24	12	3	4.970	0.127	2.002	2.513	0.455	1.975	0.051	0.333	1.191	0.451
PCTP1-9	Vehicle	7	55	42	12	1	8.965	0.163	4.728	4.134	0.103	3.287	0.060	0.909	2.276	0.102
PCTP1-10	Vehicle	7	24	15	7	2	2.372	0.099	1.869	0.269	0.234	0.822	0.034	0.404	0.188	0.230
Median			**39.000**	**27.000**	**12.000**	**2.500**	**7.537**	**0.171**	**3.138**	**3.457**	**0.261**	**2.681**	**0.060**	**0.688**	**1.836**	**0.258**
PCTP1-11	Metformin	7	47	37	9	1	13.130	0.279	10.070	3.042	0.019	3.624	0.077	1.949	1.656	0.019
PCTP1-12	Metformin	7	48	32	12	4	22.855	0.476	4.283	6.360	12.212	15.339	0.320	1.060	3.130	11.150
PCTP1-13	Metformin	7	40	26	13	1	3.090	0.077	1.733	1.353	0.005	1.460	0.037	0.579	0.876	0.005
PCTP1-14	Metformin	7	45	26	17	2	8.233	0.183	3.453	4.749	0.031	4.214	0.094	0.802	3.383	0.029
PCTP1-15	Metformin	7	56	35	17	4	14.221	0.254	7.665	6.505	0.051	4.869	0.087	1.083	3.738	0.048
PCTP1-16	Metformin	7	18	7	10	1	4.558	0.253	1.924	2.627	0.007	1.606	0.089	0.257	1.342	0.006
PCTP1-17	Metformin	7	36	29	7	0	4.705	0.131	3.404	1.302	0.000	1.257	0.035	0.551	0.706	0.000
PCTP1-18	Metformin	7	37	27	8	2	8.997	0.243	6.831	2.149	0.018	3.402	0.092	2.147	1.237	0.018
PCTP1-19	Metformin	7	63	28	33	2	14.752	0.234	8.535	5.528	0.689	5.076	0.081	1.345	3.093	0.638
PCTP1-20	Metformin	7	62	48	13	1	8.385	0.135	2.603	5.010	0.772	5.145	0.083	0.921	3.459	0.765
Median			**46.000**	**28.500**	**12.500**	**1.500**	**8.691**	**0.239**	**3.868**	**3.896**	**0.025**	**3.919**	**0.085**	**0.991**	**2.374**	**0.024**
z***			**0.567**	**0.569**	**0.380**	**0.810**	**0.454**	**1.209**	**0.680**	**0.302**	**0.833**	**0.378**	**1.436**	**0.983**	**0.151**	**0.833**
P*			**0.5705**	**0.5694**	**0.7043**	**0.4179**	**0.6501**	**0.2265**	**0.4963**	**0.7624**	**0.4050**	**0.7055**	**0.1509**	**0.3258**	**0.8798**	**0.4050**
PCTP1-21	Rapamycin	7	0	0	0	0	0.000	0.000	0.000	0.000	0.000	0.000	0.000	0.000	0.000	0.000
PCTP1-22	Rapamycin	7	0	0	0	0	0.000	0.000	0.000	0.000	0.000	0.000	0.000	0.000	0.000	0.000
PCTP1-23	Rapamycin	7	0	0	0	0	0.000	0.000	0.000	0.000	0.000	0.000	0.000	0.000	0.000	0.000
PCTP1-24	Rapamycin	7	0	0	0	0	0.000	0.000	0.000	0.000	0.000	0.000	0.000	0.000	0.000	0.000
PCTP1-25	Rapamycin	7	2	2	0	0	0.021	0.011	0.021	0.000	0.000	0.008	0.004	0.008	0.000	0.000
PCTP1-26	Rapamycin	7	0	0	0	0	0.000	0.000	0.000	0.000	0.000	0.000	0.000	0.000	0.000	0.000
PCTP1-27	Rapamycin	7	0	0	0	0	0.000	0.000	0.000	0.000	0.000	0.000	0.000	0.000	0.000	0.000
PCTP1-28	Rapamycin	7	0	0	0	0	0.000	0.000	0.000	0.000	0.000	0.000	0.000	0.000	0.000	0.000
PCTP1-29	Rapamycin	7	0	0	0	0	0.000	0.000	0.000	0.000	0.000	0.000	0.000	0.000	0.000	0.000
PCTP1-30*	Rapamycin	7	-	-	-	-	-	-	-	-	-	-	-	-	-	-
Median			**0.000**	**0.000**	**0.000**	**0.000**	**0.000**	**0.000**	**0.000**	**0.000**	**0.000**	**0.000**	**0.000**	**0.000**	**0.000**	**0.000**
PCTP1-31	Rap+Met**	7	0	0	0	0	0.000	0.000	0.000	0.000	0.000	0.000	0.000	0.000	0.000	0.000
PCTP1-32	Rap+Met	7	0	0	0	0	0.000	0.000	0.000	0.000	0.000	0.000	0.000	0.000	0.000	0.000
PCTP1-33	Rap+Met	7	0	0	0	0	0.000	0.000	0.000	0.000	0.000	0.000	0.000	0.000	0.000	0.000
PCTP1-34	Rap+Met	7	0	0	0	0	0.000	0.000	0.000	0.000	0.000	0.000	0.000	0.000	0.000	0.000
PCTP1-35	Rap+Met	7	0	0	0	0	0.000	0.000	0.000	0.000	0.000	0.000	0.000	0.000	0.000	0.000
PCTP1-36	Rap+Met	7	0	0	0	0	0.000	0.000	0.000	0.000	0.000	0.000	0.000	0.000	0.000	0.000
PCTP1-37	Rap+Met	7	0	0	0	0	0.000	0.000	0.000	0.000	0.000	0.000	0.000	0.000	0.000	0.000
PCTP1-38	Rap+Met	7	0	0	0	0	0.000	0.000	0.000	0.000	0.000	0.000	0.000	0.000	0.000	0.000
PCTP1-39	Rap+Met	7	0	0	0	0	0.000	0.000	0.000	0.000	0.000	0.000	0.000	0.000	0.000	0.000
PCTP1-40*	Rap+Met	7	-	-	-	-	-	-	-	-	-	-	-	-	-	-
Median			**0.000**	**0.000**	**0.000**	**0.000**	**0.000**	**0.000**	**0.000**	**0.000**	**0.000**	**0.000**	**0.000**	**0.000**	**0.000**	**0.000**
z*			**1.000**	**1.000**	**NA**	**NA**	**1.000**	**1.000**	**1.000**	**NA**	**NA**	**1.000**	**1.000**	**1.000**	**NA**	**NA**
P*			**0.3173**	**0.3173**	**NA**	**NA**	**0.3173**	**0.3173**	**0.3173**	**NA**	**NA**	**0.3173**	**0.3173**	**0.3173**	**NA**	**NA**
X^2 **with ties****			**30.555**	**30.580**	**31.064**	**24.289**	**30.511**	**30.903**	**30.591**	**31.006**	**24.145**	**30.492**	**31.089**	**30.748**	**30.984**	**24.145**
P*			**0.0001**	**0.0001**	**0.0001**	**0.0001**	**0.0001**	**0.0001**	**0.0001**	**0.0001**	**0.0001**	**0.0001**	**0.0001**	**0.0001**	**0.0001**	**0.0001**

Table 5.3 Histological analysis of renal lesions in *Tsc2*$^{+/-}$ mice treated from one month old for 9 months with vehicle, metformin, rapamycin or rapamycin plus metformin.

Mouse	Treatment	Treatment duration (months)	Number of all lesions	Number of cysts	Number of papillary lesions	Number of solid lesions	Area of all lesions (mm²)	Mean area per lesion (mm²)	Area of cysts (mm²)	Area of papillary lesions (mm²)	Area of solid lesions (mm²)	Cellular content of all lesions (mm²)	Mean cellular content per lesion (mm²)	Cellular content of cysts (mm²)	Cellular content of papillary lesions (mm²)	Cellular content of solid lesions (mm²)
PCTP1-41	Vehicle	9	65	37	20	8	16.872	0.260	6.933	7.749	2.189	6.701	0.103	0.987	3.554	2.160
PCTP1-42	Vehicle	9	67	32	24	11	27.909	0.417	8.277	8.763	10.869	18.529	0.277	1.767	6.047	10.714
PCTP1-43	Vehicle	9	67	32	22	13	18.496	0.276	2.736	5.053	10.707	14.911	0.223	0.800	3.630	10.480
PCTP1-44	Vehicle	9	34	28	6	0	6.289	0.185	3.017	3.271	0.000	2.054	0.060	0.456	1.598	0.000
PCTP1-45	Vehicle	9	71	36	30	5	25.911	0.365	3.292	14.844	7.775	16.583	0.234	0.960	8.118	7.505
PCTP1-46	Vehicle	9	76	44	27	5	12.439	0.164	4.432	6.876	1.130	6.176	0.081	0.895	4.192	1.089
PCTP1-47	Vehicle	9	55	40	15	0	10.209	0.186	4.399	5.810	0.000	4.723	0.086	0.833	3.890	0.000
PCTP1-48	Vehicle	9	64	31	25	8	36.118	0.564	4.206	16.177	15.735	26.104	0.408	0.914	10.711	14.480
PCTP1-49	Vehicle	9	62	29	29	4	20.565	0.332	11.399	7.803	1.363	8.528	0.138	1.623	5.562	1.343
PCTP1-50	Vehicle	9	46	29	15	2	10.577	0.230	4.213	5.879	0.485	4.628	0.101	0.912	3.242	0.474
Median			**64.500**	**32.000**	**23.000**	**5.000**	**17.684**	**0.268**	**4.306**	**7.313**	**1.776**	**7.614**	**0.120**	**0.913**	**4.041**	**1.752**
PCTP1-51	Metformin	9	30	17	11	2	4.453	0.148	0.985	1.996	1.471	3.156	0.105	0.433	1.383	1.339
PCTP1-52	Metformin	9	90	59	24	7	20.904	0.232	13.127	5.354	2.422	8.414	0.094	2.469	3.575	2.369
PCTP1-53	Metformin	9	99	52	37	10	40.970	0.414	12.943	20.128	7.899	20.746	0.210	2.667	11.031	7.049
PCTP1-54	Metformin	9	73	41	25	7	14.412	0.197	7.032	6.255	1.125	4.691	0.064	1.072	2.519	1.100
PCTP1-55	Metformin	9	39	28	9	2	8.212	0.211	4.530	3.551	0.131	2.757	0.071	0.697	1.933	0.127
PCTP1-56	Metformin	9	54	30	21	3	25.494	0.472	5.688	5.511	14.295	18.794	0.348	1.241	3.465	14.089
PCTP1-57	Metformin	9	62	41	21	0	9.527	0.154	4.808	4.719	0.000	4.218	0.068	1.167	3.051	0.000
PCTP1-58	Metformin	9	38	29	7	2	9.568	0.252	1.072	7.739	0.758	4.306	0.113	0.443	3.137	0.726
PCTP1-59	Metformin	9	34	25	8	1	5.676	0.167	1.189	2.839	1.647	3.614	0.106	0.356	1.632	1.626
PCTP1-60	Metformin	9	73	34	31	8	22.847	0.313	6.048	11.877	4.922	13.921	0.191	1.528	7.570	4.823
Median			**58.000**	**32.000**	**21.000**	**2.500**	**11.990**	**0.221**	**5.248**	**5.432**	**1.559**	**4.499**	**0.106**	**1.119**	**3.094**	**1.483**
z***			**0.303**	**0.038**	**0.454**	**0.724**	**0.907**	**0.907**	**0.454**	**1.285**	**0.227**	**1.058**	**0.605**	**0.227**	**1.663**	**0.303**
P*			**0.7620**	**0.9698**	**0.6497**	**0.4693**	**0.3643**	**0.3643**	**0.6501**	**0.1988**	**0.8203**	**0.2899**	**0.5453**	**0.8206**	**0.0963**	**0.7620**
PCTP1-61	Rapamycin	9	0	0	0	0	0.000	0.000	0.000	0.000	0.000	0.000	0.000	0.000	0.000	0.000
PCTP1-62	Rapamycin	9	0	0	0	0	0.000	0.000	0.000	0.000	0.000	0.000	0.000	0.000	0.000	0.000
PCTP1-63	Rapamycin	9	0	0	0	0	0.000	0.000	0.000	0.000	0.000	0.000	0.000	0.000	0.000	0.000
PCTP1-64	Rapamycin	9	0	0	0	0	0.000	0.000	0.000	0.000	0.000	0.000	0.000	0.000	0.000	0.000
PCTP1-65	Rapamycin	9	0	0	0	0	0.000	0.000	0.000	0.000	0.000	0.000	0.000	0.000	0.000	0.000
PCTP1-66	Rapamycin	9	0	0	0	0	0.000	0.000	0.000	0.000	0.000	0.000	0.000	0.000	0.000	0.000
PCTP1-67	Rapamycin	9	0	0	0	0	0.000	0.000	0.000	0.000	0.000	0.000	0.000	0.000	0.000	0.000
PCTP1-68	Rapamycin	9	0	0	0	0	0.000	0.000	0.000	0.000	0.000	0.000	0.000	0.000	0.000	0.000
PCTP1-69	Rapamycin	9	0	0	0	0	0.000	0.000	0.000	0.000	0.000	0.000	0.000	0.000	0.000	0.000
PCTP1-70	Rapamycin	9	0	0	0	0	0.000	0.000	0.000	0.000	0.000	0.000	0.000	0.000	0.000	0.000
Median			**0.000**	**0.000**	**0.000**	**0.000**	**0.000**	**0.000**	**0.000**	**0.000**	**0.000**	**0.000**	**0.000**	**0.000**	**0.000**	**0.000**
PCTP1-71	Rap+Met**	9	0	0	0	0	0.000	0.000	0.000	0.000	0.000	0.000	0.000	0.000	0.000	0.000
PCTP1-72	Rap+Met	9	0	0	0	0	0.000	0.000	0.000	0.000	0.000	0.000	0.000	0.000	0.000	0.000
PCTP1-73	Rap+Met	9	0	0	0	0	0.000	0.000	0.000	0.000	0.000	0.000	0.000	0.000	0.000	0.000
PCTP1-74	Rap+Met	9	0	0	0	0	0.000	0.000	0.000	0.000	0.000	0.000	0.000	0.000	0.000	0.000
PCTP1-75	Rap+Met	9	0	0	0	0	0.000	0.000	0.000	0.000	0.000	0.000	0.000	0.000	0.000	0.000
PCTP1-76	Rap+Met	9	0	0	0	0	0.000	0.000	0.000	0.000	0.000	0.000	0.000	0.000	0.000	0.000
PCTP1-77	Rap+Met	9	1	1	0	0	0.007	0.007	0.007	0.000	0.000	0.005	0.005	0.005	0.000	0.000
PCTP1-78	Rap+Met	9	0	0	0	0	0.000	0.000	0.000	0.000	0.000	0.000	0.000	0.000	0.000	0.000
PCTP1-79	Rap+Met	9	0	0	0	0	0.000	0.000	0.000	0.000	0.000	0.000	0.000	0.000	0.000	0.000
PCTP1-80*	Rap+Met	9	-	-	-	-	-	-	-	-	-	-	-	-	-	-
Median			**0.000**	**0.000**	**0.000**	**0.000**	**0.000**	**0.000**	**0.000**	**0.000**	**0.000**	**0.000**	**0.000**	**0.000**	**0.000**	**0.000**
z*			**1.054**	**1.054**	**NA**	**NA**	**1.054**	**1.054**	**1.054**	**NA**	**NA**	**1.054**	**1.054**	**1.054**	**NA**	**NA**
P*			**0.2918**	**0.2918**	**NA**	**NA**	**0.2918**	**0.2918**	**0.2918**	**NA**	**NA**	**0.2918**	**0.2918**	**0.2918**	**NA**	**NA**
X²* with ties*			**31.686**	**31.669**	**32.295**	**25.180**	**31.890**	**31.890**	**31.706**	**32.720**	**25.094**	**31.978**	**31.753**	**31.660**	**33.059**	**25.089**
P*			**0.0001**	**0.0001**	**0.0001**	**0.0001**	**0.0001**	**0.0001**	**0.0001**	**0.0001**	**0.0001**	**0.0001**	**0.0001**	**0.0001**	**0.0001**	**0.0001**

8 months

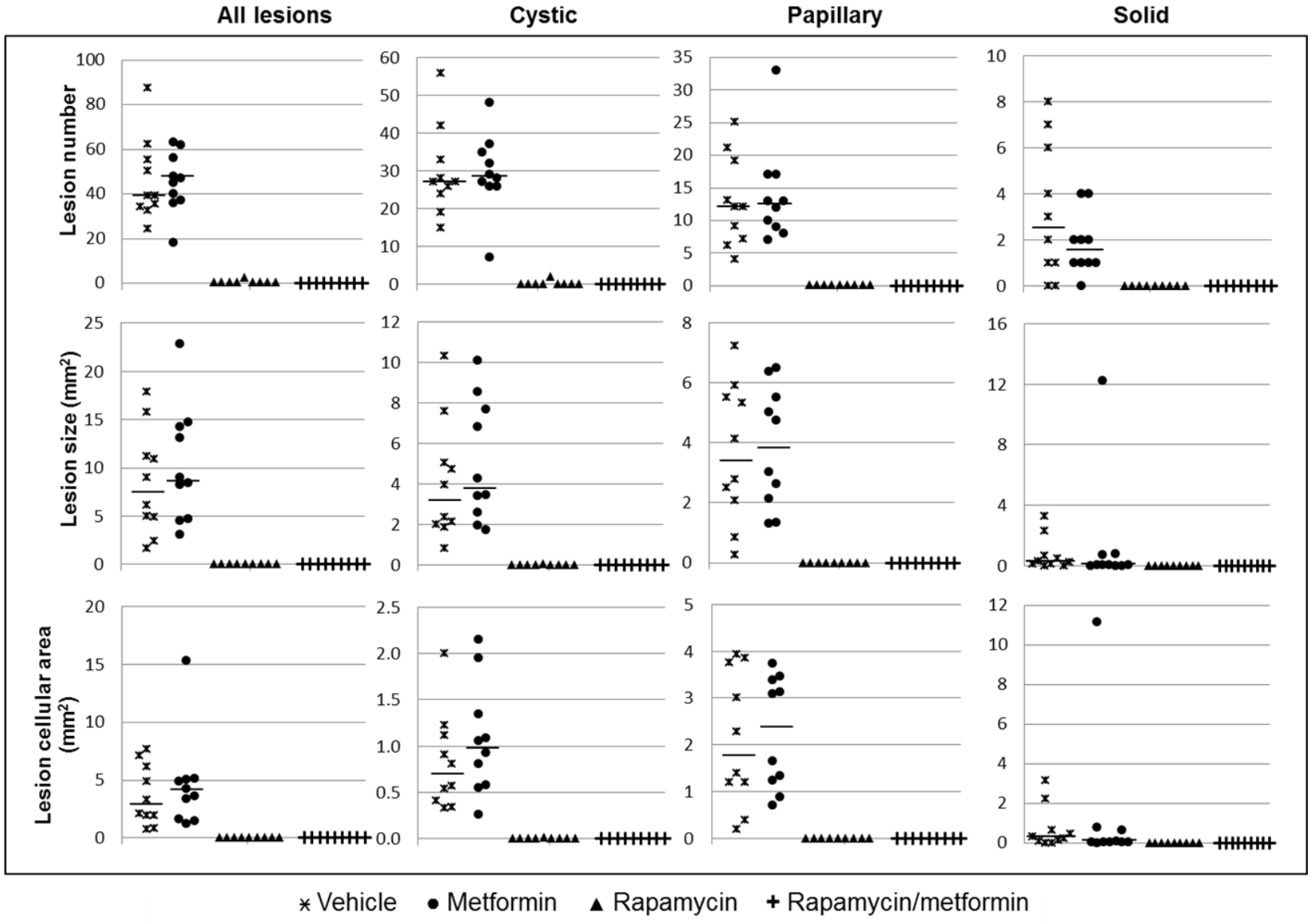
All lesions
Cystic
Papillary
Solid
Lesion number
Lesion size (mm²)
Lesion cellular area (mm²)
Vehicle
Metformin
Rapamycin
Rapamycin/metformin

Figure 5.5 Rapamycin prevents renal tumourigenesis in *Tsc2*$^{+/-}$ mice. *Tsc2*$^{+/-}$ mice were treated from one month old until sacrifice at the age of 8 months (vehicle, n=10; metformin, n=10; rapamycin, n=9; rapamycin in combination with metformin, n=9). Kidney sections were prepared for histological assessment of treatment effect. Lesion number, size (area) and cellular area were compared. All the mice treated with vehicle or metformin developed multiple lesions and no significant difference in lesion number, size or cellular area was observed between vehicle and metformin treated mice. In contrast, only two small cysts were observed in one of the rapamycin treated mice at the age of 8 months. Bars indicate a median. Detailed statistical analysis was given in Tables 5.2.

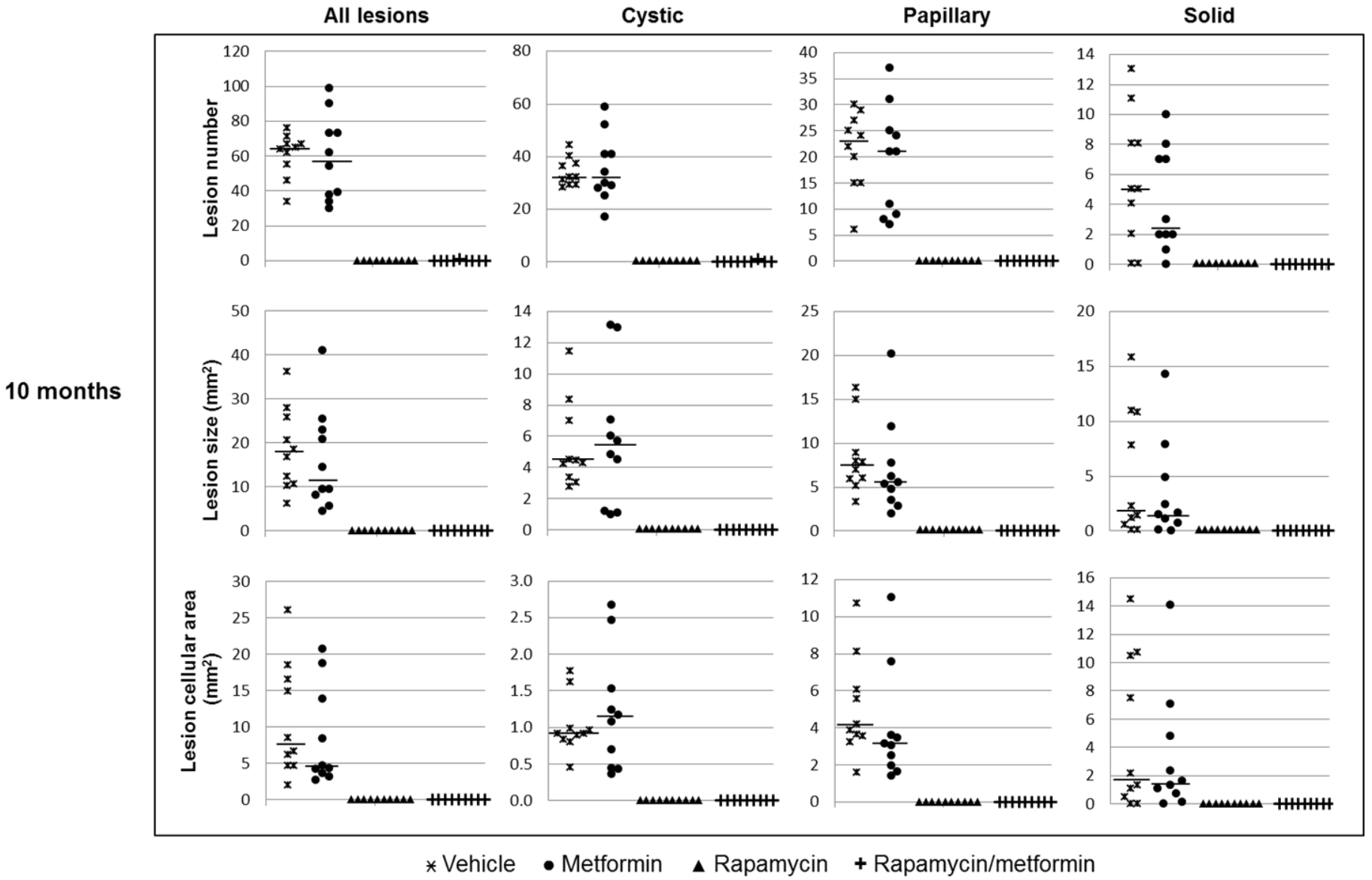
All lesions
Cystic
Papillary
Solid
10 months
Lesion number
Lesion size (mm²)
Lesion cellular area (mm²)
Vehicle
Metformin
Rapamycin
Rapamycin/metformin

Figure 5.6 Rapamycin prevents renal tumourigenesis in *Tsc2*$^{+/-}$ mice. *Tsc2*$^{+/-}$ mice were treated from one month old until sacrifice at the age of 10 months (vehicle, n=10; metformin, n=10; rapamycin, n=10; rapamycin in combination with metformin, n=9). Kidney sections were prepared for histological assessment of treatment effect. Lesion number, size (area) and cellular area were compared. All the mice treated with vehicle or metformin developed multiple lesions and no significant difference in lesion number, size or cellular area was observed between vehicle and metformin treated mice. In contrast, only one small cyst was observed in one of the mice treated with rapamycin plus metformin at the age of 10 months. Bars indicate a median. Detailed statistical analysis was given in Table 5.3.

5.3.4 Rapamycin inhibits mTORC1 in renal and liver tissues of *Tsc2*$^{+/-}$ mice

5.3.4.1 Evaluating the effects of metformin, rapamycin and rapamycin plus metformin treatments on mTORC1 signalling in kidney tissues of Tsc2$^{+/-}$ *mice by IHC*

IHC was used to demonstrate the efficacy of metformin, rapamycin and rapamycin plus metformin on mTORC1 activity in the kidney tissues of *Tsc2*$^{+/-}$ mice. The phosphorylation of S6 at Ser235/236 was tested on 5 µm thick kidney sections obtained from *Tsc2*$^{+/-}$ mice sacrificed after 9 months treatment with either one of the aforementioned treatments. IHC analysis showed a significant decrease in the phosphorylation of S6 at Ser235/236 in kidney tissues of mice treated with rapamycin or rapamycin plus metformin and a slight decrease in phosphorylated S6 at Ser235/236 in kidney tissues of metformin treated mice (Figure 5.7). These results indicate significant inhibition of mTORC1 by rapamycin or rapamycin plus metformin and a slight suppression of mTORC1 by metformin alone. mTORC1 signalling could be quantified by quantitative immunofluorescence technique such Automated Quantitative Analysis (AQUA) (Camp RL, Chung GG, Rimm DL (2002), Automated subcellular localization and quantification of protein expression in tissue microarrays (*Nat Med* 8:1323-1327), however this was not feasible due to time limitation.

5.3.4.2 Assessing the effect of rapamycin, metformin and rapamycin plus metformin treatments on mTORC1 signalling in liver tissues of Tsc2$^{+/-}$ *mice by Western analysis*

Western analysis was used to evaluate the effect of rapamycin, metformin and rapamycin plus metformin on mTORC1 activity in the liver tissues of *Tsc2*$^{+/-}$ mice sacrificed after 9 months treatment. mTORC1 activity was assessed by examining the phosphorylation levels of its downstream substrates S6 (Ser235/236) and 4EBP1 (Thr70). Densitometry analysis of Western Blotting was carried out using ImageJ software. The phosphorylation of S6 at Ser235/236 was reduced in liver tissues of mice treated with rapamycin or rapamycin plus metformin (Figure 5.8). Rapamycin plus metformin but not rapamycin alone significantly reduced phosphorylation of 4EBP1 (T70) (Figure 5.8). In contrast, metformin had no effect on phosphorylation of any of the proteins tested (Figure 5.9).

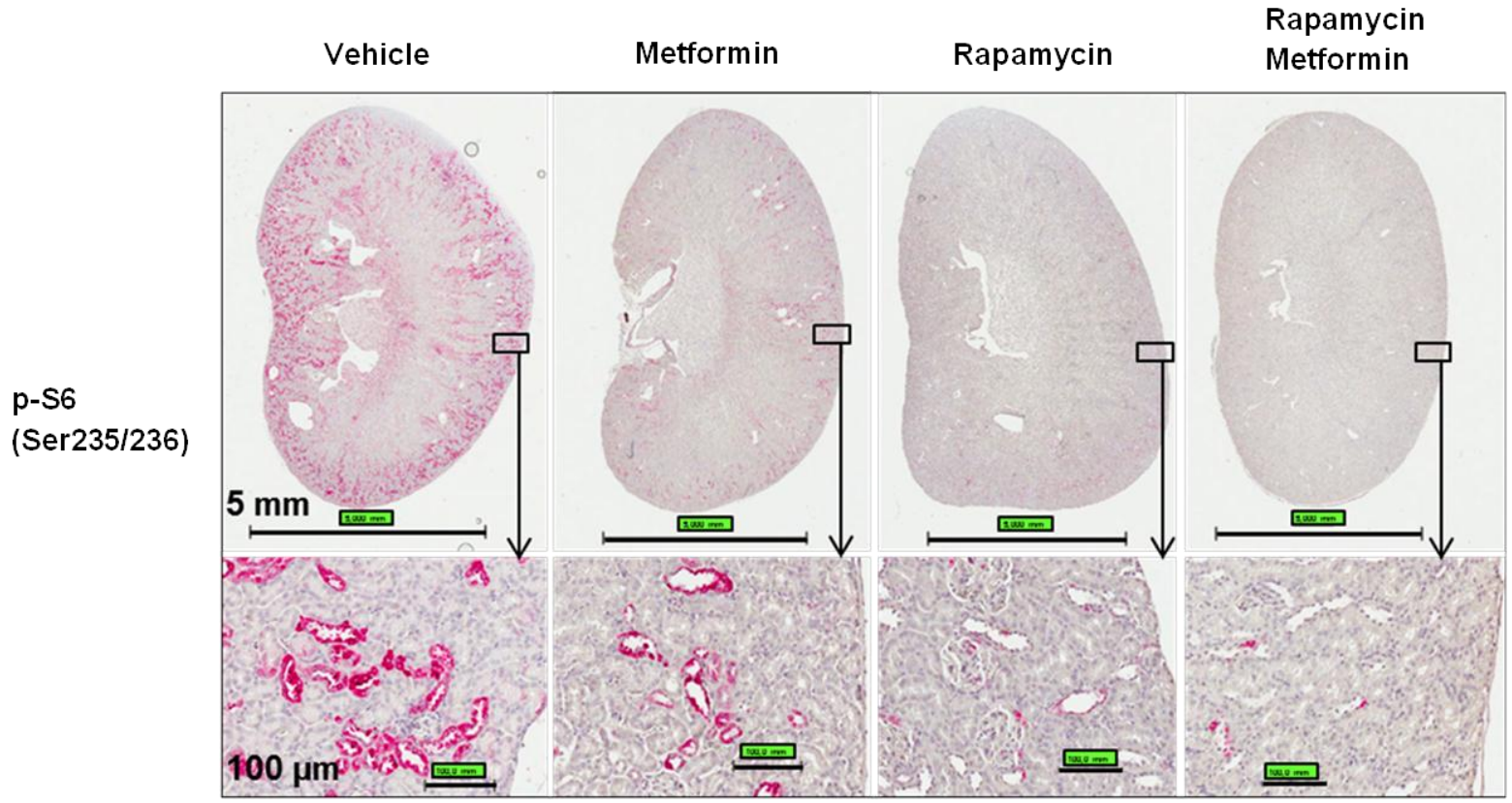

Figure 5.7 Rapamycin inhibits mTORC1 in the kidneys of *Tsc2*$^{+/-}$ mice. *Tsc2*$^{+/-}$ mice were treated from one month old for 9 months with vehicle, rapamycin, metformin or rapamycin in combination with metformin. The treated mice were sacrificed and kidney sections were prepared for IHC. Representative kidney sections stained in red with antibody against phosphor-S6 (Ser235/236) showed significant inhibition of mTORC1 by rapamycin or rapamycin plus metformin and slight inhibition of mTORC1 by metformin.

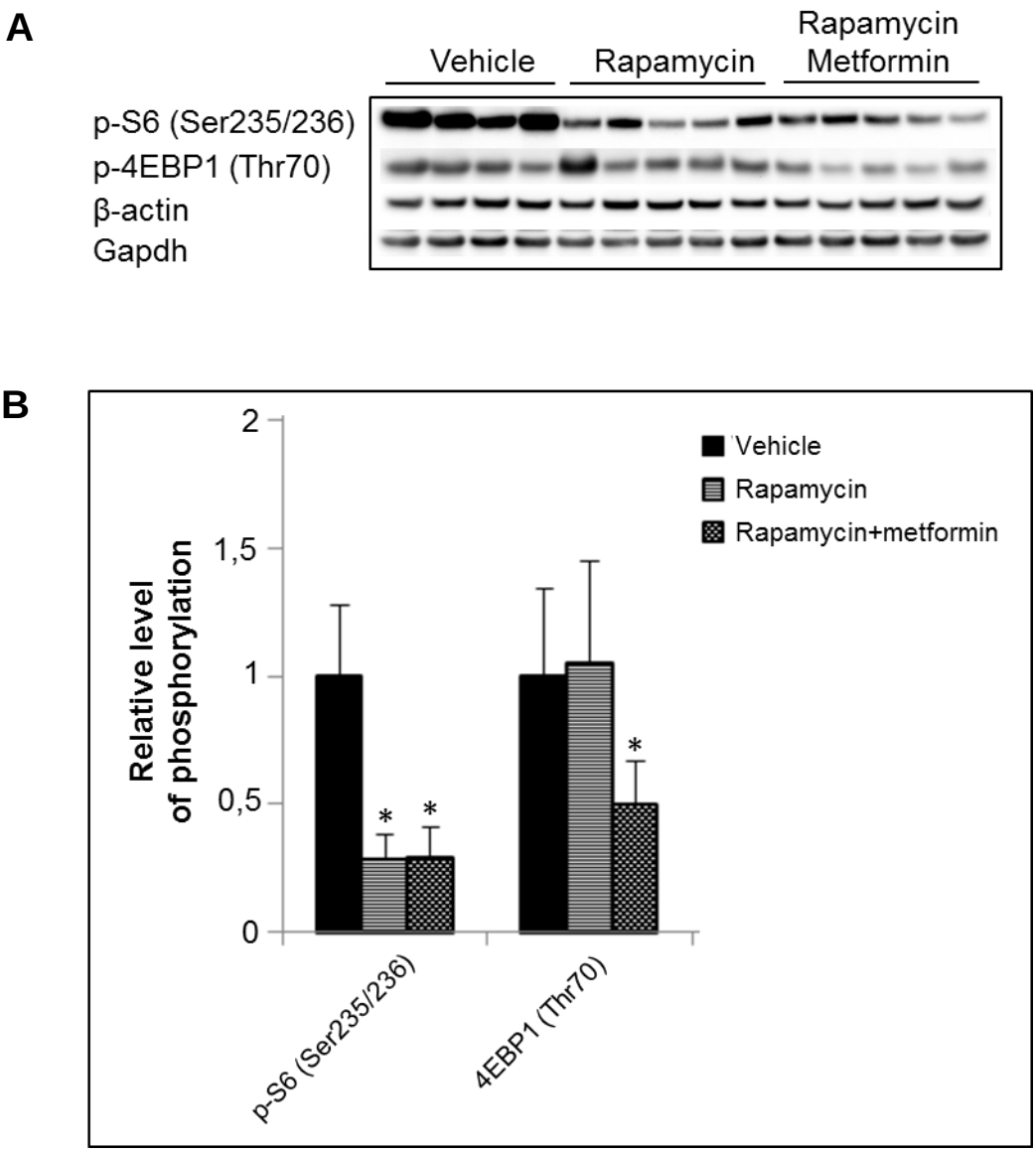

Figure 5.8 Rapamycin inhibits mTORC1 in the liver of *Tsc2*$^{+/-}$ mice. *Tsc2*$^{+/-}$ mice were treated from one month old for 9 months with vehicle (n=4), rapamycin (n=5) or rapamycin in combination with metformin (n=5). The mice were then sacrificed and liver protein was prepared for Western analysis. **(A)** Western analysis. **(B)** Relative density analysis of the p-S6 (Ser235/236) and 4EBP1 (Thr70) protein bands. Gapdh and β-actin were used as loading controls. Rapamycin or rapamycin plus metformin significantly reduced phosphorylation of S6 (Ser235/236). Rapamycin plus metformin but not rapamycin alone significantly reduced phosphorylation of 4EBP1 (Thr70).

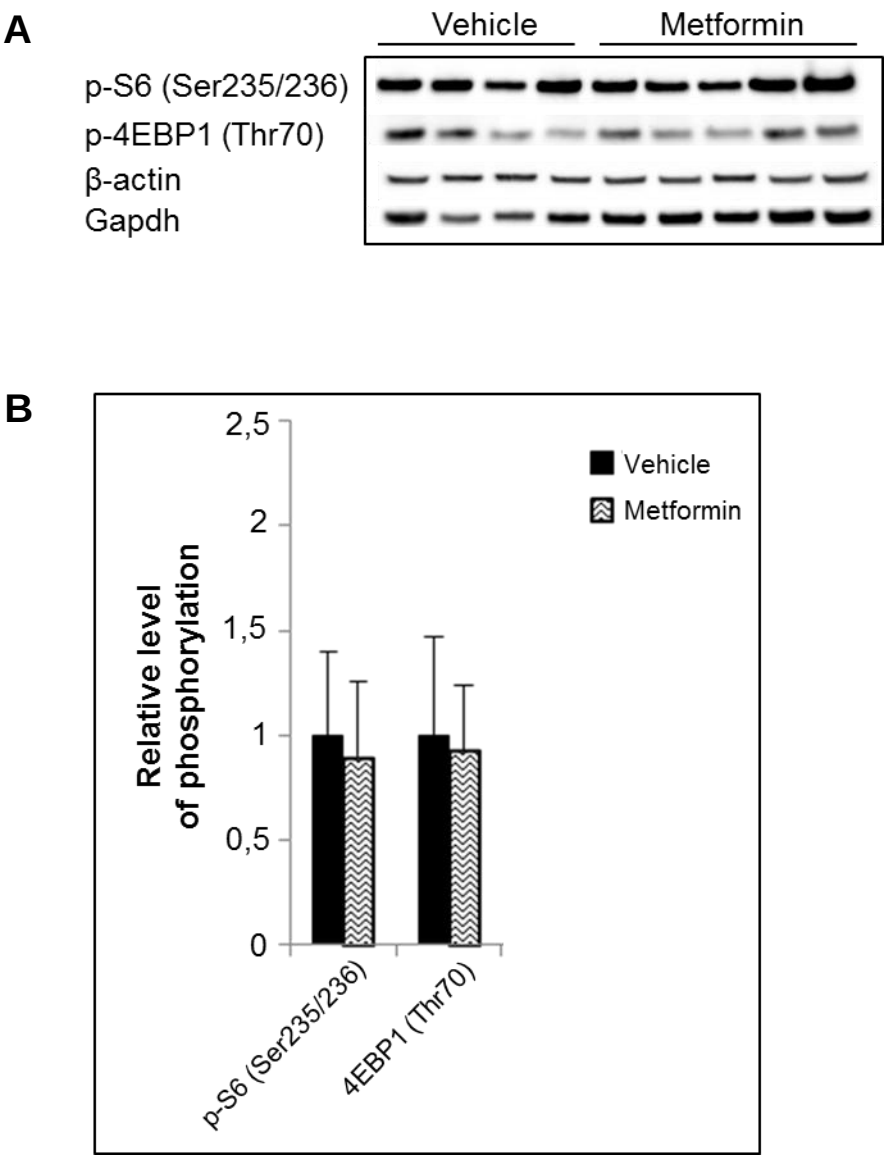

Figure 5.9 No effect of metformin on mTORC1 signalling in the liver tissues of *Tsc2*$^{+/-}$ mice. *Tsc2*$^{+/-}$ mice were treated from one month old for 9 months with vehicle (n=4) or metformin (n=5). The mice were sacrificed and liver protein was prepared for Western analysis. **(A)** Western analysis. **(B)** Relative density analysis of the p-S6 (Ser235/236) and 4EBP1 (Thr70) protein bands. Gapdh and β-actin were used as loading controls. Metformin had no effect on phosphorylation of any of the proteins tested.

5.3.5 Effect of rapamycin on body weight of *Tsc2*$^{+/-}$ mice

Mouse weight was monitored once a week. No significant difference was observed in body weight between metformin and vehicle treated mice. However, poor weight gain in the early stages of treatment and weight loss later were observed in *Tsc2*$^{+/-}$ mice treated with rapamycin or rapamycin plus metformin (Figure 5.10).

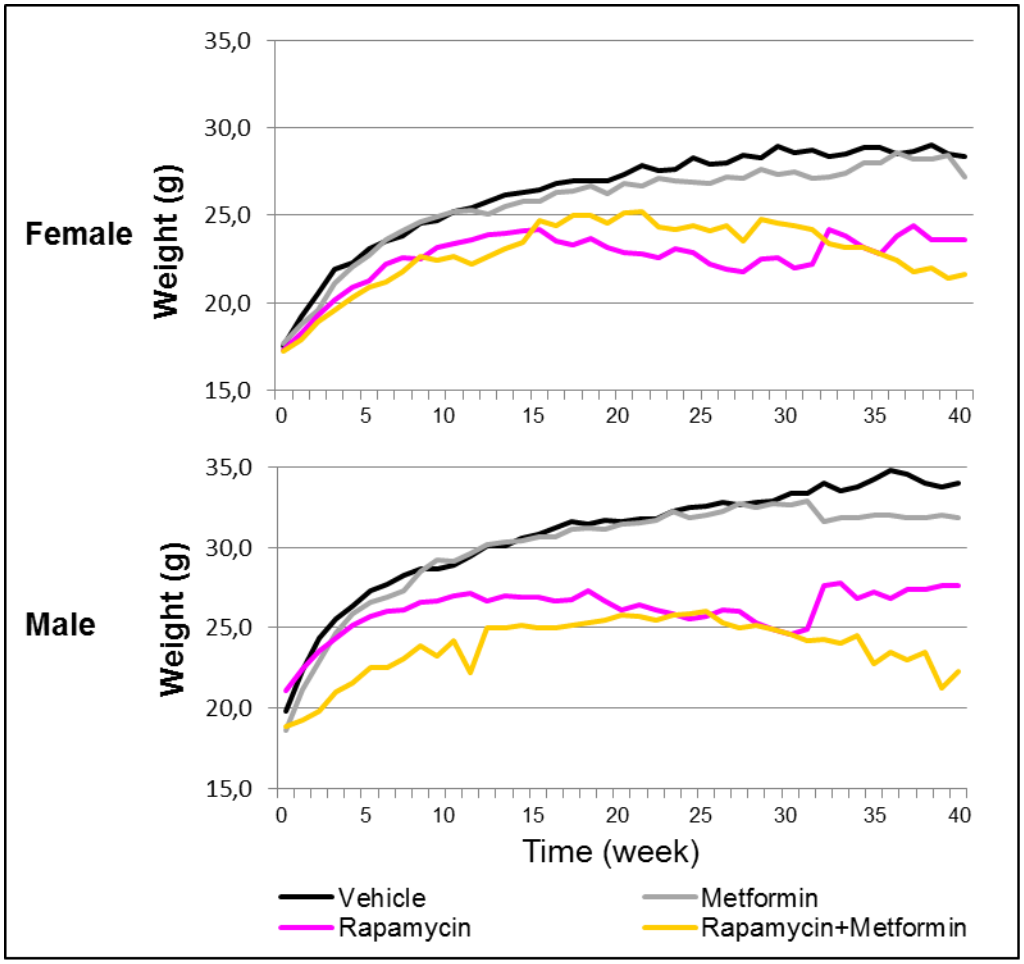

Figure 5.10 Effect of rapamycin on body weight of *Tsc2*$^{+/-}$ mice. The body weight of *Tsc2*$^{+/-}$ mice treated with vehicle or corresponding drugs was weekly monitored. Poor body weight gain in the early stage of treatment and weight loss later were observed in both rapamycin alone and rapamycin plus metformin treated mice.

5.4 Discussion

To evaluate the preventive efficacy of rapamycin, and metformin on tumourigenesis in the kidneys of the *Tsc2*$^{+/-}$ mouse model, we first established the earliest time at which renal tumourigenesis occurs on the balb/c background by histological analysis. No lesions were observed in *Tsc2*$^{+/-}$ mice until the age of 45 days. These mice started to show microscopic dysplasias and cysts at the age of 60 days. Renal tumours grew and continuously developed as dysplasias, cysts, papillary and solid lesions in the kidneys in an age dependent manner. In contrast to the usually benign features of AMLs in human TSC (Gomez *et al*. 1999), *Tsc2*$^{+/-}$ mice developed frequent renal cell carcinomas.

We have examined the mTORC1 signalling in renal lesions of *Tsc2*$^{+/-}$ mice. All of the *Tsc2*-associated mouse renal lesions, including the smallest microscopic dysplasias and cysts, showed activation of mTORC1 signalling as determined by phosphorylation of S6 at Ser235/236. Our findings suggest that aberrant activation of mTORC1 is crucial to the earliest stages of renal lesion development in *Tsc2*$^{+/-}$ mice. Consistently increased mTORC1-mediated cell proliferation was seen in all renal tumours of *Tsc2*$^{+/-}$ mice. Wilson *et al*. (2005) showed increased levels of phosphorylated mTOR and phosphorylated S6 in the renal lesions derived from *Tsc1*$^{+/-}$ mice. Likewise, Kwiatkowski *et al*. (2002) and Zhang *et al*. (2003) reported hyperphosphorylation of S6 in renal cystadenomas of *Tsc1*$^{+/-}$ and *Tsc2*$^{+/-}$ mice, respectively. In addition, Kenerson *et al*. (2002) demonstrated that primary renal tumours from the Eker rat model had elevated phosphorylation of mTOR and its effectors p70S6K, S6, 4E-BP1, and eIF4G and suggested that the mTOR pathway is activated in the primary stages of renal tumourigenesis in this rat model. mTORC1 activation have been suggested to play a role in tumourigenesis of other mouse models. In a mouse model of liver-specific *Tsc1* knockout, chronic activation of mTORC1 was sufficient to cause hepatocellular carcinoma. Rapamycin treatment blocked tumourigenesis in this liver-specific *Tsc1* knockout mouse model (Menon *et al*. 2012). In a mouse model of acute myeloid leukemia (AML) mTORC1 was essential for leukemia initiation (Hoshii *et al*. 2012).

We have demonstrated that long term treatment of *Tsc2*$^{+/-}$ mice with rapamycin from 1 month of age blocked the development of all types of kidney lesions at 8-10 months of age. However, metformin alone did not show any preventive effect compared to vehicle treated mice. These results are consistent with the suggestion that mTORC1 activity is required for tumour development in these mice. Rapalogues have been used to treat various types of cancer and TSC-associated tumours in pre-clinical and clinical trials, and show anti-tumour effect by suppressing cell proliferation and promoting apoptosis (Bissler *et al*. 2008, Krueger *et al*. 2010, Lee *et al*. 2005, Pollizzi *et al*. 2009). However, no properly designed study has been reported using rapalogues for prevention of Tsc-associated renal tumours. This study provides the first proof of concept that Tsc-associated renal tumours are preventable by rapamycin.

We have also examined the effects of different treatments on mTORC1 signalling in *Tsc2*$^{+/-}$ mouse kidneys by IHC and in the liver by Western analysis. In mice sacrificed after 9 months treatment with rapamycin or rapamycin plus metformin, mTORC1 signalling was greatly attenuated in both tissues as indicated by the decreased phosphorylation of S6 at Ser235/236. Similarly, Lamming *et al*. (2012) reported reduced phosphorylation of both S6K1 Thr389 and S6 in the livers of rapamycin-treated wild type mice. Interestingly, treatment with rapamycin plus metformin but not rapamycin alone significantly reduced phosphorylation of 4EBP1 (Thr70) in the liver tissues. Treatment with metformin alone appeared to be associated with a slight decrease in phospho-S6 staining in the kidneys but no effect could be detected by Western analysis in liver. Different effects may be a result of differences in tissue origin.

More recent studies have indicated a role of mTORC2 in tumour development. Guertin *et al*. (2009) showed that mTORC2 signalling is involved in the development of prostate cancer caused by *Pten* loss but it is not essential for non-cancerous prostate epithelial cells. Hietakangas and Cohen (2008) reported a significant role of mTORC2 in proliferation and anchorage-independent growth of MCF7 breast cancer and PC3 prostate cancer cells, and suggested that inhibition of mTORC2 may be

promising in the prevention of cancer cell proliferation and growth. Interestingly, long term treatment with rapamycin was shown not only to supress mTORC1 activity, but also mTORC2 activity in recent studies (Sarbassov *et al*. 2006*,* Zeng *et al*. 2007). However, Huang and colleagues found that TSC1/2 complex promotes the activity of mTORC2 and loss of the TSC tumour suppressors results in elevated mTORC1 signalling and attenuated mTORC2 signalling in kidney tumours from both *Tsc2*$^{+/-}$ mice and TSC patients (Huang *et al*. 2008, Huang *et al*. 2009). Our group have recently investigated the mTORC2 signalling extensively in renal tumours of *Tsc2*$^{+/-}$ mice and found that both mTORC1 and mTORC2 are activated in these lesions (unpublished data). Hyper-activation of mTOR was evidenced by increased phosphorylation of mTOR at Ser2448 and Ser2481 as well as increased phosphorylation of S6K at Thr389, S6 at Ser235/236, and 4EBP1 at Thr37/46, Ser65 and Thr70. Therefore, to confirm these findings it is worthwhile to fully investigate mTORC2 in both TSC-associated animal models and human TSC patients.

We found that the rapamycin dosage used here caused initial poor body weight gain and later weight loss. This adverse effect is likely to be a result of high rapamycin dose, long treatment duration as well as high treatment frequency. It may be worthwhile to investigate whether lower doses of rapamycin are effective in preventing renal tumourigenesis and less toxic in *Tsc2*$^{+/-}$ mice.

In conclusion, our findings showed that rapamycin or rapamycin in combination with metformin but not metformin alone is effective in preventing renal tumourigenesis in a *Tsc2*$^{+/-}$ mouse model. All renal lesions including the earliest detectable ones exhibited mTORC1 activation and long term treatment with rapamycin inhibited mTORC1 signalling consistent with the notion that mTORC1 is required for renal tumourigenesis in *Tsc2*$^{+/-}$ mice. In TSC many growth-related disease complications develop during childhood or early adult life and may be amenable to prevention by mTORC1 inhibition. Rapalogues are already in clinical use for long term immunosuppression to prevent organ rejection in transplant patients and long term or even lifetime medication with these agents may be safe and acceptable for

patients with TSC. However, it will be important to establish whether lower doses are also effective before translation to clinical trials.

CHAPTER SIX

General discussion

6.1 Mouse models for Tsc-associated tumour research

Mouse models have been widely used in cancer research and have hugely contributed to the progress made in this field (Frese and Tuveson, 2007; van Miltenburg and Jonkers, 2012; Walrath *et al*. 2010). Mouse models provide useful tools to investigate the mechanisms of tumourigenesis in ways that are impossible to do in humans. They are also useful for testing potential preventive and therapeutic interventions for cancer before translation to clinical trials. Mouse models share many molecular and pathological features of tumourigenesis with humans. The contribution of genetic backgrounds to tumour development can be analysed in mouse models more easily than in human. Tumour samples can be regularly collected from mouse models for detailed molecular and cellular analysis. However, species difference in tumourigenesis between mouse and human represent a big concern about using mouse models in cancer research. Tumours developed in mouse models do not recapitulate all aspects of those in patients (Frese and Tuveson, 2007). Some agents show anti-tumour efficacy in mice but may not have any effect on human tumours. Therefore, caution should be taken when results obtained from mouse models are interpreted.

Different types of mouse tumour models have been developed including xenograft, carcinogen-induced and genetically engineered models. Xenograft mouse models are generated by transplanting human tumours or tumour cells into immunodeficient mouse (Becher and Holland, 2006). These models are easy to use, economical and reproducible. Lesion progression can be easily monitored and treatment can be started once the lesions are of an optimal size. Xenografts develop tumours rapidly and only a small number of animals are needed in studies testing therapeutic efficacy of drugs. However, human tumours or tumour cells need to be injected into an immunodeficient mouse. Some tumour cell lines may not represent original tumours in their native state since they have been passaged in culture for years. In

addition, the microenvironment for tumours in xenograft mouse models are different from those developed spontaneously (Becher and Holland, 2006).

Carcinogens have been used to induce tumourigenesis in mice for many years (Memmott *et al*. 2010, Rosenberg *et al*. 2009). Some carcinogens can induce certain tumours rapidly and reproducibly in mice but mutations induced by carcinogens are usually widespread in the genome and some phenotypes generated may not be wanted. Technical progress in genetic engineering has allowed successful generation of mouse models with defined genetic changes for cancer research. The major advantages of these genetically engineered models (GEM) are the development of spontaneous tumours *in situ* and the knowledge of genetic lesions with a normal immune system. However, tumours in these models show heterogeneity with regards to frequency, latency and growth (Becher and Holland, 2006). The spontaneous tumours in these models also generally take longer time to develop and thus cost more.

Several mouse models of *Tsc1* and *Tsc2* have been generated using gene targeting (Kobayashi *et al*. 1999; 2001, Kwiatkowski *et al*. 2002, Onda *et al*. 1999, Wilson *et al*. 2005). One hundred percent of the *Tsc2*$^{+/-}$ mice generated by Onda *et al*. (1999) developed renal cystadenomas, 50% hepatic hemangiomas, and 32% lung adenomas by 15 months of age. Around 10% of these mice also displayed progression to renal carcinoma and extremity angiosarcomas (Onda *et al*. 1999). Sixty-four percent of the *Tsc1*$^{+/-}$ mice generated by Kobayashi *et al*. (2001) developed renal cystadenomas and 71% hepatic hemangiomas by the age of 15-18 months. The incidence of hepatic hemangiomas in *Tsc1*$^{+/-}$ mice resembled that of *Tsc2*$^{+/-}$ mice at a similar age (~80%) (Kobayashi *et al*. 1999). Wilson *et al*. (2005) generated a *Tsc1*$^{+/-}$ mouse model with a more severe renal phenotype than the *Tsc1*$^{+/-}$ models previously described (Kobayashi *et al*. 2001, Kwiatkowski *et al*. 2002). It is notable that both *Tsc1*$^{+/-}$ and *Tsc2*$^{+/-}$ mouse models frequently developed renal carcinomas on different genetic backgrounds but in TSC patients renal lesions are generally benign and renal carcinomas develop only rarely. This suggests that the mechanisms of tumourigenesis are not the same between mouse and human.

Conditional alleles of *Tsc1* and *Tsc2* have also been generated in mice and allowed targeted loss of *Tsc1* or *Tsc2* in specific organ systems or cell types to model human TSC phenotypes more accurately (Meikle *et al*. 2005, Rachdi *et al*. 2008, Shigeyama *et al*. 2008). For example, Menon *et al*. (2012) found that mice with liver-specific KO of *Tsc1* developed sporadic hepatocellular carcinoma. Xenograft mouse models were also generated by transplantation of a $Tsc2^{-/-}$, $Trp53^{-/-}$ MEF cells (Lee *et al*. 2005). Most of these Tsc models have been used to test therapeutic agents in pre-clinical trials (Lee *et al*. 2005, Meikle *et al*. 2008, Messina *et al*. 2007, Rauktys *et al*. 2008, Zeng *et al*. 2008).

$Tsc1^{+/-}$ mice showed milder phenotype in terms of renal tumour development than that in $Tsc2^{+/-}$ mice on the same genetic background (Kobayashi *et al*. 2001, Kwiatkowski *et al*. 2002). Similarly, we found that our $Tsc1^{+/-}$ mice experienced a milder renal phenotype with lower incidence of renal tumours in comparison with age-matched $Tsc2^{+/-}$ mice. Differences in the severity of the disease are also seen between TSC patients associated with *TSC1* and *TSC2* mutations. For example, Dabora *et al*. (2001) reported that patients with *TSC1* mutations had milder disease in comparison with patients with *TSC2* mutations.

Genetic background is one of the major factors affecting tumourigenesis. Hunter (2012) reported that different genetic backgrounds display significantly different susceptibilities to cancer. The $Tsc1^{+/-}$ mice on the balb/c and C57BL/6 backgrounds had a less dramatic phenotype of renal lesions in comparison with the C3H background (Wilson *et al*. 2005). In addition, $Tsc1^{+/-}$ mice on a C3H background had significantly more cystic lesions compared to mice on a C57BL/6 background. The $Tsc1^{+/-}$ mice on a balb/c background also had significantly more solid lesions compared to mice on C3H or C57BL/6 backgrounds (Wilson *et al*. 2005). In this study, we have chosen to use $Tsc1^{+/-}$ and $Tsc2^{+/-}$ balb/c mice as they frequently develop renal tumours with an otherwise relatively healthy condition. Recently, Auricchio *et al*. (2012) used $Tsc2^{+/-}$ A/J mice to examine the therapeutic effect of

metformin and bortezomib on renal lesions. The *Tsc2*$^{+/-}$ A/J mice develop tumours rapidly and may represent a cost-effective mouse model but this strain displays abnormal phenotypes in multiple systems including the immune system (Auricchio *et al*. 2012, Woodrum *et al*. 2010). These additional abnormalities may further complicate the interpretation of results obtained in preclinical trials.

In the future, more defined conditional mouse models of TSC with simultaneous multiple genes disruption should be very useful in elucidating mechanisms of tumourigenesis in the kidneys. For example, by conditional knockout of both *Tsc1* and *rictor* in the kidneys, we could investigate whether mTORC2 is essential to the initiation and progression of renal lesions *in vivo*.

6.2 In vivo imaging of renal lesions in TSC associated mouse models by MRI

Several techniques for *in vivo* imaging of tumours in mouse models have been developed such as MRI, positron emission tomography (PET), single photon emission computed tomography (SPECT), bioluminescence imaging (BLI), fluorescence imaging, computed tomography (CT), ultrasound and intra-vital microscopy (Lyons, 2005). These techniques are particularly useful in anti-tumour pre-clinical trials and help reduce the numbers of animals used significantly.

Each imaging modality has certain strengths and limitations as shown in Table 6.1 (Lyons, 2005). Micro-CT and MRI are the most widely used methods with high spatial resolution and whole anatomical picture of the internal mouse body in pre-clinical trials. However, micro-CT requires contrast agents to provide adequate intra-organ contrast, high doses of radiation exposure (70-220mSv per scan) and longer scanning periods up to 20-30 minutes per scan (Martiniova *et al*. 2009, Weber *et al*. 2004). In serial micro-CT imaging studies, high radiation exposure might cause secondary effects in animals which might interfere with results in a treatment study. In addition, longitudinal studies using micro-CT must be carefully carried out as the time of contrast excretion needs to be considered in order to avoid any influence on

signal intensities (Suckow and Stout, 2008). In contrast, the use of MRI in small animals poses fewer challenges. MRI has higher resolution with shorter scanning time up to 5-7 minutes per scan, no exposure of the animals to ionising radiation and no requirement of intravenous contrast media in many cases (Martiniova *et al*. 2009). Martiniova *et al*. (2009) described that T2 weighted MRI appeared to be more sensitive than micro-CT in detecting lung, adrenal, ovarian and renal lesions in a mouse model of metastatic cancer.

We have used a high-field (9.4 T) small bore MRI/MRS spectrometer to detect renal lesions in *Tsc1*$^{+/-}$ and *Tsc2*$^{+/-}$ mouse models. Before initiating this investigation, a pilot study was performed to test different MRI protocols in the detection of mouse kidney lesions such as T1 weighted, T2 weighted, T2* weighted and proton density weighted MRI sequences. T2 weighted MRI with long TR (repetition time) and long TE (echo time) sequence was found to be the most consistent protocol in terms of resolution and specificity in detecting renal lesions in the *Tsc1*$^{+/-}$ and *Tsc2*$^{+/-}$ mice. T2 weighted MRI has been successfully used in a variety of mouse models for *in vivo* detection of tumours in various locations such as the brain (Cha *et al*. 2003), breast (Galiè *et al*. 2004), prostate (Arbab *et al*. 2011), colon (Zhang *et al.* 2013) and kidneys (Flores *et al*. 2013), as well as metastatic tumours (Gauvain *et al*. 2005, Pandit *et al*. 2013).

Brown *et al*. (2005) evaluated the efficiency of T2 weighted MRI in detecting spontaneous lesions in a *Tsc2*$^{+/-}$ mouse model for subsequent assessment of cell-based gene therapy. Using T2 weighted MRI, these authors detected renal cystadenomas and renal cell carcinomas in 100% of the *Tsc2*$^{+/-}$ mice. They also detected hepatic hemangiosarcomas and lung adenocarcinomas in 75% and 33% of the *Tsc2*$^{+/-}$ mice respectively. Lee *et al*. (2005) used T2 weighted MRI to quantitate renal cystadenomas in the same mouse model for assessment of treatment efficacy with CCI-779 or IFN-γ. However, neither study reported T2 weighted MRI follow-up data or measured total volumes of renal lesions. Furthermore, previously published data have not addressed the detection rate of renal lesions by T2 weighted MRI appropriately in comparison to histological analysis in Tsc mouse models.

In this project, we have evaluated T2 weighted MRI for the assessment of renal lesions in both *Tsc1*$^{+/-}$ and *Tsc2*$^{+/-}$ mouse models. We also used T2 weighted MRI to monitor tumour growth or shrinkage. T2 weighted MRI is a potentially useful tool for assessing renal lesions in pre-clinical studies using Tsc mouse models. However, technological advances are required to improve T2 weighted MRI sensitivity for solid renal lesions. As at present no single imaging modality provides all features, a combination of two imaging modalities may improve detection sensitivity, particularly for solid lesions. For example, T2 weighted MRI might be used in combination with PET for detection of renal lesions in Tsc mouse models. In addition, MRI modalities other than T2 weighted may be modified and explored for detection of Tsc-associated solid lesions in these mouse models.

Table 6.1 Imaging modalities for *in vivo* detection of tumours in mice (adapted from Lyons, 2005).

Modality (and basis)	Reagents	Resolution	Main advantages	Main disadvantages
PET (high-energy γ rays)	^{18}F, ^{11}C, ^{13}N, ^{15}O labelled probes or substrates for reporter transgenes (eg HSV-TK)	1-2 mm	High sensitivity; provides quantitative measure of tumour cell metabolism; variety of probes and strategies confers a high degree of versatility	Cyclotron required to generate short-lived radioisotopes; low resolution; unincorporated substrate can increase noise
SPECT (low-energy γ -rays)	^{99m}Tc, ^{111}In, ^{125}I labelled probes	1-2 mm	Multiple probes can be detected simultaneously; radioisotopes have longer half-lives than those used in PET	Between 10- and 100-fold less sensitive than PET
MRI (radiowaves)	Paramagnetic cation probes (for contrast enhancement)	25-100 µm	High spatial resolution; provides both anatomical detail and functional information	Low sensitivity, long acquisition and image process times, so relatively low throughput
CT (X-rays)	Iodine (for contrast enhancement)	50 µm	Morphological detection of tumours and metastases in lung and bone	Relatively poor soft-tissue contrast
BLI (visible light)	Luciferase and substrate (Firefly luc: luciferin, *Renilla* luc: coelenterazine)	1-10 mm–dependent on tissue depth	High sensitivity; provides relative measure of cell viability or cell function; high throughput; transgene-based approach confers versatility	Low anatomic resolution; light emission prone to attenuation with increased tissue depth
Whole-body fluorescence imaging (visible and near-infrared light)	Fluorescent proteins, fluorescent dyes, and quantum dots (CdSe or CdTe nanocrystals)	1-10 mm–dependent on tissue depth	Multiple reporter wavelengths enables multiplex imaging; highly compatible with a range of *ex vivo* analysis methodologies; transgene-based approach confers versatility	Excitation and emission light <600 nm prone to attenuation with increased tissue depth; autofluorescence of non-labelled cells increases noise
Intra-vital microscopy (visible and near-infrared light)	Fluorescent proteins, fluorescent dyes, and quantum dots	Single cell	Microscopic resolution; potential for multiplex imaging; enables real-time imaging and tracking of labelled cell populations	Surgery required to implant tissue window; small field of view; limited to relatively superficial tissues
Ultrasound (high-frequency sound)	Microbubbles (for contrast enhancement)	50 µm	Images morphology and physiology of tissue relatively close to the surface of the mouse in real time	Limited ability to image through bone or lungs

6.3 Targeting mTOR signalling pathway for prevention and therapy of TSC

Tumours from TSC patients demonstrate aberrant activation of mTOR signalling including renal AMLs (El-Hashemite *et al*. 2003), SEGAs (Chan *et al*. 2004), skin hamartomas (Li *et al*. 2008), LAM (Yu and Henske, 2010) and RCCs (Kenerson *et al*. 2002). Tsc-associated tumours from the Eker rat model and mouse models also demonstrate aberrant activation of mTOR signalling such as renal cystadenomas and RCC (Kwiatkowski *et al*. 2002, Wilson *et al*. 2005). In addition, *Tsc1* and *Tsc2* null MEF cells showed activation of mTOR (Kwiatkowski *et al*. 2002) and rapamycin could inhibit mTOR signalling in these cells (Zhang *et al*. 2003). Rapalogues were used to treat Tsc-associated tumours in several preclinical studies using TSC rodent models and were very effective in blocking tumour growth (Kenerson *et al*. 2002, Kenerson *et al*. 2005, Lee *et al*. 2005, Meikle *et al*. 2008, Messina *et al*. 2007, Pollizzi *et al*. 2009, Rauktys *et al*. 2008, Zeng *et al*. 2008). Clinical trials have also demonstrated that rapalogues have anti-tumour effects in TSC patients. By inhibiting mTOR signalling these drugs result in shrinkage or stabilisation of renal AMLs (Bissler *et al*. 2008, Herry *et al*. 2007, Wienecke *et al*. 2006), SEGAs (Franz *et al*. 2006, Koenig *et al*. 2008, Krueger *et al*. 2010), facial angiofibromas (Hofbauer *et al*. 2008) and LAM (Bissler *et al*. 2008, Morton *et al*. 2008, Taillé *et al*. 2007). Rapalogues suppress tumour growth by inhibiting cell proliferation and promoting apoptosis (Kenerson *et al*. 2002).

However, TSC-associated tumours including AMLs and SEGAs exhibit only partial and reversible responses to rapamycin and everolimus (Bissler *et al*. 2008, Krueger *et al*. 2010, Lee *et al*. 2005, Pollizzi *et al*. 2009, Wienecke *et al*. 2006). Furthermore, the tumours tended to re-grow after drug withdrawal. A number of factors may affect the treatment efficacy of these mTOR inhibitors. For example, rapalogues normally inhibit mTORC1 but not mTORC2 and thus lead to limited anti-tumour efficacy (Jacinto *et al*. 2004, Loewith *et al*. 2002, Sarbassov *et al*. 2004). Rapalogues may also cause a loss of negative feedback inhibition of Akt and activated Akt may promote tumour cell survival, proliferation and growth (Harrington *et al*. 2005, Manning, 2004; O'Reilly *et al*. 2006). Nevertheless, prolonged treatment with rapamycin has been shown to inhibit Akt in tumour cells in a cell type dependent

manner, and inhibition of Akt may contribute to its anti-tumour effect *in vivo* (Sarbassov *et al*. 2006). Many dual inhibitors of mTORC1 and mTORC2 have been developed and extensive test of these inhibitors are needed in Tsc mouse models to determine their anti-tumour effects *in vivo* by overcoming the problem caused by loss of feedback inhibition when rapalogues are used.

Recent studies have reported that metformin attenuates mTORC1 signalling in the presence or absence of a functional TSC1/TSC2 complex through multiple mechanisms (Ben Sahra *et al*. 2011, Gwinn *et al*. 2008, Inoki *et al*. 2003, Kalender *et al*. 2010) (described in Chapter 1, section 1.5.2.2). The anti-tumourigenic effect of metformin has been demonstrated in several *in vitro* and *in vivo* studies on many mouse models of cancer such as endometrial (Cantrell *et al*. 2010), ovary (Gotlieb *et al*. 2008), pancreatic (Kisfalvi *et al*. 2009), lung (Memmott *et al*. 2010), prostate (Ben Sahra *et al*. 2008), breast (Zakikhani *et al*. 2006) and colon cancer (Buzzai *et al*. 2007), acute myeloid leukemia (Green *et al*. 2010) and glioma (Isakovic *et al*. 2007). These observations suggest that metformin could have therapeutic potential for TSC. In this study, we assessed the therapeutic effects of metformin on renal lesions of *Tsc1*$^{+/-}$ mouse model using both T2 weighted MRI and histological analysis. Nine-month metformin treatment was well tolerated but had no effect on renal lesions. We also examined the effect of metformin treatment on mTORC1 signalling in *Tsc1*$^{+/-}$ kidney tissues and *Tsc1*-associated renal tumours. Although metformin appeared to attenuate mTORC1 signalling in normal *Tsc1*$^{+/-}$ kidney tissues, it had no significant effect on *Tsc1*-associated renal tumours. These results are consistent with findings reported by Auricchio *et al.* (2012) who treated *Tsc2*$^{+/-}$ mice with metformin for up to 4 months and found no significant difference in renal tumour size compared to controls. A functional Tsc1/Tsc2 complex may be required for full action of metformin on mTORC1 signalling and loss of the complex in *Tsc1*-associated tumours may compromise the treatment efficacy (Dowling *et al*. 2007). More recently epigenetic suppression of the OCTs, *Slc22a1*, *Slc22a2* and *Slc22a3*, responsible for cellular uptake of metformin was observed in *Tsc1*-associated mouse renal tumours in our group (Yang *et al*. 2012), probably partly contribute to the lack of treatment response to metformin.

Rapalogues may be more effective for prevention of TSC-associated tumours than therapy. In this project, we have demonstrated that long term treatment with rapamycin from 1 month of age inhibits mTORC1 and effectively blocks the development of all types of kidney lesions at 8-10 months of age in a *Tsc2*$^{+/-}$ mouse model. Rapamycin greatly attenuated mTORC1 signalling in both kidney and liver tissues of *Tsc2*$^{+/-}$ mice as indicated by the decreased phosphorylation of S6 at Ser235/236. We also tested whether metformin alone or in combination with rapamycin was effective in prevention of Tsc-associated renal lesions. We observed that 9 month treatment with metformin had no preventive effect. Metformin slightly decreased phosphorylation of S6 at Ser235/236 in the kidneys but had no effect in the liver. In contrast, 9 month treatment with rapamycin plus metformin prevented the development of renal tumours in *Tsc2*$^{+/-}$ mice and attenuated mTORC1 signalling in both tissues as determined by decreased phosphorylation of S6 at Ser235/236 and 4EBP1 at Thr70. These results strongly suggest that Tsc-associated tumours may be preventable by inhibiting mTORC1 using rapalogues. It is notable that the high dose of rapamycin used in the current study caused initial poor weight gain and later weight loss. Further preclinical trials are needed to test whether low doses of rapalogues alone or in combination with less potent inhibitors (more discussion in section 6.4 of this chapter) can effectively prevent Tsc-associated tumours but with no significant adverse effect.

Our work provided the first proof of the concept that Tsc-associated tumours are preventable by inhibiting mTORC1. No preclinical or clinical trials for prevention of TSC had been documented when we started the project. Kotulska *et al*. (2013) have recently reported that early mTOR inhibition in TSC patients may prevent the development of TSC lesions. They treated one of monozygotic twin sisters affected with TSC2 with everolimus for two years from 4 years old and left the other without treatment. They found a significant reduction of SEGA volume and absence of facial angiofibromas and renal AMLs in the everolimus treated patient while her untreated sister developed significant facial angiofibromas and renal AMLs in addition to a

stable brain tumour. These results are very promising but more defined clinical trials are required to confirm these results for prevention of TSC using rapalogues.

6.4 Development of new mTOR inhibitors for prevention and therapy of TSC

Rapalogues provide the first generation of inhibitors of mTOR signalling. Although these drugs are still useful, their limitations as described above have triggered huge efforts to develop new agents and strategies for prevention and therapy of TSC. Farnesyltransferase inhibitors (FITs) and angiogenesis inhibitors were considered as possible treatments for TSC (Kwiatkowski, 2003). FITs are attractive agents since they are capable of supressing mTOR by inhibiting Rheb. FITs were shown to inhibit constitutive activation of mTOR/S6K signalling and block the growth of *Tsc1*$^{-/-}$ *and* *Tsc2*$^{-/-}$ MEF cells derived from *Tsc1* and *Tsc2* knockout mice respectively (Gau *et al*. 2005). Angiogenesis inhibitors could be valuable since TSC hamartomas are characterised by aberrant vascular channels, likely associated with increased expression of vascular endothelial growth factor (VEGF) (El-Hashemite *et al*. 2003, Kwiatkowski, 2003). Angiogenesis inhibitors can be used alone or in combination with mTOR inhibitors for the treatment of TSC-related tumours. Woodrum *et al*. (2010) reported that angiogenesis inhibitors, sunitinib and bevacizumab, reduced tumour growth in *Tsc2*$^{-/-}$ subcutaneous tumour mouse model although these drugs were not as effective as rapamycin. Lee *et al*. (2009) showed that the combination of sorabenib and rapamycin was more effective than either agent alone in *Tsc2*$^{-/-}$ subcutaneous tumour mouse model. Lee *et al*. (2006) showed that combination therapy with rapamycin analogue CCI-779 and IFN-γ was more effective than single agent therapy in reducing tumour growth and improving survival in a *Tsc2*$^{-/-}$ tumour-bearing nude mouse model (Lee *et al*. 2006). However, in another trial from the same group later, short term treatment of CCI-779 plus IFN-γ did not signficiantly decrease kidney disease in *Tsc2*$^{+/-}$ mice (Messina *et al*. 2007).

Many new ATP-competitive mTOR inhibitors have recently been developed such as Torin1, PP242, PP30, Ku-0063794, WAY-600, WYE-687, WYE-354, INK128, AZD8055, and OSI-027. These chemicals inhibit both mTORC1 and mTORC2 by

targeting the mTOR kinase domain and competing with ATP *in vitro* (Feldman *et al*. 2009). Some of these inhibitors have been tested in mouse cancer models. For example, in U87-MG glioblastoma and A549 lung cancer mouse xenografts, AZD8055 reduced phosphorylation of S6 at Ser225/236 and AKT at Ser473 and inhibited tumour growth (Chresta *et al*. 2010). AZD8055 also resulted in significant growth inhibition and/or regression in other tumour xenograft mouse models (Chresta *et al*. 2010). Similarly, OSI-027 was well tolerated *in vivo* and showed robust anti-tumour activity in several tumour xenograft mouse models (Bhagwat *et al*. 2011). More importantly, OSI-027 demonstrated greater inhibition of tumour growth in COLO 205 and GEO colon cancer xenograft mouse models than rapamycin (Bhagwat *et al*. 2011). In a recent phase 1 clinical trial, OSI-027 has been used to treat advanced solid tumours and lymphoma and were well tolerated in patients (Tan *et al*. 2010). However, these mTOR inhibitors have not been used for any clinical trials for TSC patients and only one (INK128) was tested in an A/J *Tsc2*$^{+/-}$ mouse model (Guo and Kwiatkowski, 2013). Compared to rapamycin, INK128 appeared to have similar therapeutic benefit in suppressing renal tumour development in these mice despite its inhibitory effect on both mTORC1 and mTORC2 (Guo and Kwiatkowski, 2013).

Efforts have also made to develop ATP-competitive dual inhibitors of PI3K and mTOR such as PI-103, GNE-477, NVP-BEZ235, BGT226, XL765, SF-1126, and WJD008. PI3K/mTOR dual inhibitors simultaneously target the ATP binding sites of PI3K and mTOR (Heffron *et al*. 2010, Li *et al*. 2010, Maira *et al*. 2008, Molckovsky and Siu, 2008; Zou *et al*. 2009). PI-103 was well tolerated and was highly effective in blocking tumour growth in a glioma xenograft mouse model (Fan *et al*. 2006). In BT474 H1047R breast cancer xenografts, NVPBEZ235 had potent anti-tumour activity (Serra *et al*. 2008). Pollizzi *et al*. (2009) reported that NVP-BEZ235 and RAD001 showed equivalent anti-tumour effects although NVP-BEZ235 reduced activity of both mTORC1 and Akt in a *Tsc2*$^{+/-}$ mouse model.

These new inhibitors, ether dual inhibitors of PI3K/mTOR or mTORC1/mTORC2, are expected to be more effective in blocking tumourigenesis since they could overcome

the potential problem caused by loss of negative feedback after rapamycin treatment (Yu *et al*. 2009, Zhang *et al*. 2011, Zhou and Huang, 2012). However, these chemicals may also cause more severe adverse effects partly by inhibiting multiple kinases at therapeutic concentration (Zhang *et al*. 2011). For example, PI-103 was used to treat melanoma in a mouse model and was found to promote immunosuppression and tumour growth (López-Fauqued *et al*. 2010). The use of PI3K/mTOR dual inhibitors could lead to metabolic disturbances such as hyperglycemia and glucose intolerance (Ihle and Powis, 2009; Yap *et al*. 2008). Extensive investigation of these inhibitors is, therefore, required to determine whether they are useful for treating and preventing TSC-associated tumours in animals and patients.

Combinational treatment using two or more medicines can be an attractive strategy for cancer prevention and therapy (Al-Lazikani *et al*. 2012). Combinational therapy may also be considered for treating Tsc-associated tumours. As mentioned above, combination of CCI-779 and IFN-γ was used to treat renal tumours in *Tsc2* mouse models but obtained contradicted results (Lee *et al*. 2006, Messina *et al*. 2007). We used rapamycin and metformin to prevent tumourigenesis in the kidneys of a *Tsc2*$^{+/-}$ mouse model (Chapter 5). Treatment with either rapamycin alone or rapamycin with metformin nearly completely blocked renal tumourigenesis. These results indicate that the high efficacy of rapamycin might mask a potential synergistic effect or that the combination did not add more anti-tumour effects. However, Western analysis demonstrated that combination of rapamycin and metformin but not rapamycin alone reduced phosphorylation of 4E-BP1 at Thr70. This may allow use of lower dosage of rapamycin, thus being less toxic when combination of rapamycin and metformin is used *in vivo*. Rapalogues or ATP-competitive inhibitors may also be combined for treating Tsc-associated tumours with less potent mTOR inhibitors. Resveratrol and curcumin are natural polyphenols well known for their anticancer effects, roles in extension of life span and low toxicity. These polyphenols exert pleiotropic actions with multiple potential beneficial effects via modulating diverse signalling pathways (Corson and Crews, 2007; Smoliga *et al*. 2011). They have been recently found to inhibit both mTORC1 and mTORC2 (Liu *et al*. 2010, Sun *et al*. 2011). Combinational treatment using these polyphenols with more specific mTOR inhibitors may help

minimise adverse effects while achieving satisfactory preventive and therapeutic efficacy for TSC.

Publications resulting from this work

Kalogerou, M., Zhang, Y., Yang, J., Garrahan, N., Paisey, S., Tokarczuk, P., Stewart, A., Gallacher, J., Sampson, J.R., and Shen, M.H. (2012) T2 weighted MRI for assessing renal lesions in transgenic mouse models of tuberous sclerosis. *Eur. J. Radiol*., 81: 2069-2074.

Yang, J., Kalogerou, M., Gallacher, J., Sampson, J.R., Shen, M.H. (2012) Renal tumours in a *Tsc1*$^{+/-}$ mouse model show epigenetic suppression of organic cation transporters Slc22a1, Slc22a2 and Slc22a3, and do not respond to metformin. *Eur. J. Cancer*., 49: 1479-1490.

Yang, J., Kalogerou, M., Samsel, P.A., Yang, J., Griffiths, D.F.R., Gallacher, J., Sampson, J.R., Shen, M.H. (2014) Renal tumours in a *Tsc2*$^{+/-}$ mouse model do not show feedback inhibition of Akt and are effectively prevented by rapamycin. *Oncogene*. In press.

References

Abraham, R.T., Wiederrecht, G.J. (1996) Immunopharmacology of rapamycin. *Annu Rev Immunol.*, 14: 483-510.

Adhikari, D., Flohr, G., Gorre, N., Shen, Y., Yang, H., Lundin, E., Lan, Z., Gambello, M.J., Liu, K. (2009) Disruption of Tsc2 in oocytes leads to overactivation of the entire pool of primordial follicles. *Molecular Human Reproduction, Mol Hum Reprod*., 15: 765-770.

Alessi, D.R., Andjelkovic, M., Caudwell, B., Cron, P., Morrice, N., Cohen, P., Hemmings, B.A. (1996) Mechanism of activation of protein kinase B by insulin and IGF-1. *EMBO Journal*, 15: 6541-6551.

Ali, J.B., Sepp, T., Ward, S., Green, A.J., Yates, J.R. (1998) Mutations in the TSC1 gene account for a minority of patients with tuberous sclerosis. *J Med Genet.*, 35: 969-972.

Alimova, I.N., Liu, B., Fan Z., Edgerton, S.M., Dillon, T., Lind, S.E., Thor, A.D. (2009) Metformin inhibits breast cancer cell growth, colony formation and induces cell cycle arrest in vitro*. Cell cycle*, 8: 909-915.

Al-Lazikani, B., Banerji, U., Workman, P. (2012) Combinatorial drug therapy for cancer in the post-genomic era. *Nat Biotechnol*., 30: 679-692.

Al-Saleem, T., Wessner, L.L., Scheithauer, B.W., Patterson, K., Roach, E.S., Dreyer, S.J., Fujikawa, K., Bjornsson, J., Bernstein, J., Henske, E.P. (1998) Malignant

tumors of the kidney, brain, and soft tissues in children and young adults with the tuberous sclerosis complex. *Cancer*, 83: 2208-2216.

Anisimov, V.N., Berstein, L.M., Egormin, P.A., Piskunova, T.S., Popovich, I.G., Zabezhinski, M.A., Kovalenko, I.G., Poroshina, T.E., Semenchenko, A.V., Provinciali, M., Re, F., Franceschi, C . (2005) Effect of metformin on life span and on the development of spontaneous mammary tumors in HER-2/neu transgenic mice. *Exp Gerontol*., 40: 685-693.

Arbab, A.S., Shankar, A., Varma, N.R., Deeb, D., Gao, X., Iskander, A.S., Janic, B., Ali, M.M., Gautam, S.C. (2011) MRI to assess chemoprevention in transgenic adenocarcinoma of mouse prostate (TRAMP). *BMC Med Imaging*., 11: 21.

Astrinidis, A., Cash, T.P., Hunter, D.S., Walker, C.L., Chernoff, J., Henske, E.P. (2002) Tuberin, the tuberous sclerosis complex 2 tumor suppressor gene product, regulates Rho activation, cell adhesion and migration. *Oncogene*, 21: 8470-8476.

Astrinidis, A., Senapedis, W., Coleman, T.R., Henske, E.P. (2003) Cell Cycle-regulated Phosphorylation of Hamartin, the Product of the Tuberous Sclerosis Complex 1 Gene, by Cyclin-dependent Kinase 1/Cyclin B. *J Biol Chem.*, 278: 51372-51379.

Astrinidis, A., Henske, E.P. (2005) Tuberous sclerosis complex: Linking growth and energy signaling pathways with human disease. *Oncogene*, 24: 7475-7481.

Astrinidis, A., Senapedis, W., Henske, E.P. (2006) Hamartin, the tuberous sclerosis complex 1 gene product, interacts with polo-like kinase 1 in a phosphorylation-dependent manner. *Hum Mol Genet.*, 15: 287-297.

Au, K.S., Hebert, A.A., Roach, E.S., Northrup, H. (1999) Complete inactivation of the TSC2 gene leads to formation of hamartomas*. Am J Hum Genet.*, 65: 1790-1795.

Au, K.S., Williams, A.T., Roach, E.S., Batchelor, L., Sparagana, S.P., Delgado, M.R., Wheless, J.W., Baumgartner, J.E., Roa, B.B., Wilson, C.M., Smith-Knuppel, T.K., Cheung, M.Y., Whittemore, V.H., King, T.M., Northrup, H. (2007) Genotype/phenotype correlation in 325 individuals referred for a diagnosis of tuberous sclerosis complex in the United States. *Genet Med*., 9: 88-100.

Aubry, M.C., Myers, J.L., Ryu, J.H., Henske, E.P., Logginidou, H., Jalal, S.M., Tazelaar, H.D. (2000) Pulmonary lymphangioleiomyomatosis in a man. *Am J Respir Crit Care Med.*, 162: 749-752.

Auricchio, N., Malinowska, I., Shaw, R., Manning, B.D., Kwiatkowski, D. (2012) Therapeutic Trial of Metformin and Bortezomib in a Mouse Model of Tuberous Sclerosis Complex (TSC). *PLoS One.*, 7: e31900.

Avruch, J., Hara, K., Lin, Y., Liu, M., Long, X., Ortiz-Vega, S., Yonezawa, K. (2006) Insulin and amino-acid regulation of mTOR signaling and kinase activity through the Rheb GTPase. *Oncogene*, 25: 6361-6372.

Bailey, C.J., Turner, R.C. (1996) Metformin. *N Engl J Med,* 334: 574-579.

Balzer, F., Menetrier, P. (1885) Etude sur un cas d'adénomes sébacés de la face et du cuir chevelu. *Arch. Physiol. Norm. Pathol. (série III)*, 6: 564-576.

Bardazzi, F., Neri, I., Fanti, P.A., Patrizi, A. (1996) Pachydermodactyly in two young girls. *Pediatric Dermatology*, 13: 288-291.

Bass, J.L., Breningstall, G.N., Swaiman, K.F. (1985) Echocardiographic incidence of cardiac rhabdomyoma in tuberous sclerosis. *Am J Cardiol.*, 55: 1379-1382.

Becher, O.J., Holland, E.C. (2006) Genetically engineered models have advantages over xenografts for preclinical studies. *Cancer Res*., 66: 3355-3359.

Ben Sahra, I., Laurent, K., Loubat, A., Giorgetti-Peraldi, S., Colosetti, P., Auberger, P., Tanti, J.F., Le Marchand-Brustel, Y., Bost, F. (2008) The antidiabetic drug metformin exerts an antitumoral effect in vitro and in vivo through a decrease of cyclin D1 level. *Oncogene*, 27: 3576-3586.

Ben Sahra, I., Regazzetti, C., Robert, G., Laurent, K., Le Marchand-Brustel, Y., Auberger, P., Tanti, J., Giorgetti-Peraldi, S., Bost, F. (2011) Metformin, independent of AMPK, induces mTOR inhibition and cell-cycle arrest through REDD1. *Cancer Res.,* 71: 4366-4372.

Benvenuto, G., Li, S., Brown, S.J., Braverman, R., Vass, W.C., Cheadle, J.P., Halley, D.J., Sampson, J.R., Wienecke, R., DeClue, J.E. (2000) The tuberous sclerosis-1 (TSC1) gene product hamartin suppresses cell growth and augments the expression of the TSC2 product tuberin by inhibiting its ubiquitination. *Oncogene*, 19: 6306-6316.

Berg, H. (1913) Vererbung der tuberösen Sklerose durch zwei bzw. Drei Generationen. *Z. Ges. Neurol. Psychiatri*., 19: 528-539.

Bernstein, J., Robbins, T.O., Kissane, J.M. (1986) The renal lesions of tuberous sclerosis. *Semin Diagn Pathol.*, 3: 97-105.

Bernstein, J., Robbins, T.O. (1991) Renal involvement in tuberous sclerosis. *Ann N Y Acad Sci.*, 615: 36-49.

Bhagwat, S.V., Gokhale, P.C., Crew, A.P., Cooke, A., Yao, Y., Mantis, C., Kahler, J., Workman, J., Bittner, M., Dudkin, L., Epstein, D.M., Gibson, N.W., Wild, R., Arnold, L.D., Houghton, P.J., Pachter, J.A. (2011) Preclinical characterization of OSI-027, a potent and selective inhibitor of mTORC1 and mTORC2: distinct from rapamycin. *Mol Cancer Ther*., 10: 1394-406.

Bhaskar, P.T., Hay, N. (2007) The Two TORCs and Akt. *Dev Cell.*, 12: 487-502.

Bissler, J.J., Racadio, J., Donnelly, L.F., Johnson, N.D. (2002) Reduction of postembolization syndrome after ablation of renal angiomyolipoma. *Am J Kidney Dis.*, 39: 966-971.

Bissler, J.J., Kingswood, J.C. (2004) Renal angiomyolipomata. *Kidney Int*., 66: 924-934.

Bissler, J.J., McCormack, F.X., Young, L.R., Elwing, J.M., Chuck, G., Leonard, J.M., Schmithorst, V.J., Laor., T., Brody, A.S., Bean, J., Salisbury, S., Franz, D.N. (2008) Sirolimus for angiomyolipoma in tuberous sclerosis complex or lymphangioleiomyomatosis. *N Engl J Med*., 358: 140-151.

Bissler, J.J., Kingswood, J.C., Radzikowska, E., Zonnenberg, B.A., Frost, M., Belousova, E., Sauter, M., Nonomura, N., Brakemeier, S., de Vries, P.J., Whittemore, V.H., Chen, D., Sahmoud, T., Shah, G., Lincy, J., Lebwohl, D., Budde, K. (2013) Everolimus for angiomyolipoma associated with tuberous sclerosis

complex or sporadic lymphangioleiomyomatosis (EXIST-2): a multicentre, randomised, double-blind, placebo-controlled trial. *Lancet*., 381: 817-24.

Bjornsson, J., Short, M.P., Kwiatkowski, D.J., Henske, E.P. (1996) Tuberous sclerosis-associated renal cell carcinoma: Clinical, pathological, and genetic features. *Am J Pathol.*, 149: 1201-1208.

Bjornsti, M.A., Houghton, P.J. (2004) The TOR pathway: a target for cancer therapy. *Nat Rev Cancer*, 4: 335-348.

Böhni, R., Riesgo-Escovar, J., Oldham, S., Brogiolo, W., Stocker, H., Andruss, B.F., Beckingham, K., Hafen, E. (1999) Autonomous control of cell and organ size by CHICO, a Drosophila homolog of vertebrate IRS1-4. *Cell*, 97: 865-875.

Bojkova, B., Orendas, P., Garajova, M., Kassayova, M., Kutna, V., Ahlersova, E., Ahlers, I. (2009) Metformin in chemically-induced mammary carcinogenesis in rats. *Neoplasma*, 56: 269-274.

Bolton, P.F., Park, R.J., Higgins, J.N.P., Griffiths, P.D., Pickles, A. (2002) Neuro-epileptic determinants of autism spectrum disorders in tuberous sclerosis complex. *Brain*, 125: 1247-1255.

Bonfils, G., Jaquenoud, M., Bontron, S., Ostrowicz, C., Ungermann, C., De Virgilio, C. (2012) Leucyl-tRNA synthetase controls TORC1 via the EGO complex. *Mol Cell*., 46: 105-110.

Bourneville, D.M. (1880) Sclérose tubéreuse des circonvolutions cérébrales: idiotie et épilepsie hémiplégique. *Arch. Neurol. (Paris)*, 1: 81-91.

Bourneville, D.M., Brissaud, E. (1881) Encéphalite ou sclérose tubéreuse des circonvolutions cérébrales. *Arch. Neurol*.,1: 390-410.

Bowker, S.L., Majumdar, S.R., Veugelers, P., Johnson, J.A. (2006) Increased cancer-related mortality for patients with type 2 diabetes who use sulfonylureas or insulin. *Diabetes Care*, 29: 254-258.

Brazil, D.P., Yang, Z.Z., Hemmings, B.A. (2004) Advances in protein kinase B signalling: AKTion on multiple fronts. *Trends Biochem Sci.*, 29: 233-242.

Breysem, L., Nijs, E., Proesmans, W., Smet, M.H. (2002) Tuberous sclerosis with cystic renal disease and multifocal renal cell carcinoma in a baby girl. *Pediatr Radiol.*, 32: 677-680.

Brook-Carter, P.T., Peral, B., Ward, C.J., Thompson, P., Hughes, J., Maheshwar, M.M., Nellist, M., Gamble, V., Harris, P.C., Sampson, J.R. (1994) Deletion of the TSC2 and PKD1 genes associated with severe infantile polycystic kidney disease - A contiguous gene syndrome. *Nat Genet.*, 8: 328-332.

Brown, A.B., Mahmood, U., Cortes, M.L., Tang, Y., Dai, G., Stemmer-Rachamimov, A., Prabhakar, S., Leishear, K., Onda, H., Kwiatkowski, D., Weissleder, R., Breakefield, X. (2005) Magnetic resonance imaging and characterization of spontaneous lesions in a transgenic mouse model of tuberous sclerosis as a model for endothelial cell-based transgene delivery. *Hum Gene Ther.*, 16: 1367-1376.

Brown, E.J., Albers, M.W., Shin, T.B., Ichikawa, K., Keith, C.T., Lane, W.S., Schreiber, S.L. (1994) A mammalian protein targeted by G1-arresting rapamycin-receptor complex. *Nature*, 369: 756-758.

Brown, E.J., Albers, M.W., Shin, T.B., Ichikawa, K., Keith, C.T., Lane, W.S., Schreiber, S.L., Brushfield, T., Wyatt, W., (1926) Epiloia. *Br. J. Child Dis.*, 23: 178-185.

Buckle, V.J., Higgs, D.R., Wilkie, A.O.M., Super, M., Weatherall, D.J. (1988) Localisation of human α globin to 16p13.3→pter. *J Med Genet.*, 25: 847-849.

Buzzai, M., Jones, R.G., Amaravadi, R.K., Lum, J.J., DeBerardinis, R.J., Zhao, F., Viollet, B., Thompson, C.B. (2007) Systemic treatment with the antidiabetic drug metformin selectively impairs p53-deficient tumor cell growth. *Cancer Res*., 67: 6745–6752.

Cantrell, L.A., Zhou, C., Mendivil, A., Malloy, K.M., Gehrig, P.A., Bae-Jump, V.L. (2010) Metformin is a potent inhibitor of endometrial cancer cell proliferation-implications for a novel treatment strategy. *Gynecol Oncol*., 116: 92-98.

Carbonara, C., Longa, L., Grosso, E., Borrone, C., Garrè, M.G., Brisigotti, M., Migone, N. (1994) 9q34 loss of heterozygosity in a tuberous sclerosis astrocytoma suggests a growth suppressor-like activity also for the TSC1 gene. *Hum Mol Genet.,* 3: 1829-1832.

Cares, R.M. (1958) Tuberous sclerosis complex. *J. Neuropathol. Exp. Neurol.*, 17: 247-254.

Carracedo, A., Ma, L., Teruya-Feldstein, J., Rojo, F., Salmena, L., Alimonti, A., Egia, A., Sasaki, A.T., Thomas, G., Kozma, S.C., Papa, A., Nardella, C., Cantley, L.C., Baselga, J., Pandolfi, P.P. (2008) Inhibition of mTORC1 leads to MAPK pathway activation through a PI3K-dependent feedback loop in human cancer. *J Clin Invest.*, 118: 3065-3074.

Castro, M., Shepherd, C.W., Gomez, M.R., Lie, J.T., Ryu, J.H. (1995) Pulmonary tuberous sclerosis. *Chest*, 107: 189-195.

Cha, S., Johnson, G., Wadghiri, Y.Z., Jin, O., Babb, J., Zagzag, D., Turnbull, D.H. (2003) Dynamic, contrast-enhanced perfusion MRI in mouse gliomas: correlation with histopathology. *Magn Reson Med*., 49: 848-855.

Chalifoux, J.R., Perry, N., Katz, J.S., Wiggins, G.C., Roth, J., Miles, D., Devinsky, O., Weiner, H.L., Milla, S.S. (2013) The ability of high field strength 7-T magnetic resonance imaging to reveal previously uncharacterized brain lesions in patients with tuberous sclerosis complex. *J Neurosurg Pediatr*., 11: 268-273.

Chan, J.A., Zhang, H., Roberts, P.S., Jozwiak, S., Wieslawa, G., Lewin-Kowalik, J., Kotulska, K., Kwiatkowski, D.J. (2004) Pathogenesis of tuberous sclerosis subependymal giant cell astrocytomas: biallelic inactivation of TSC1 or TSC2 leads to mTOR activation. *J Neuropathol Exp Neurol*., 63: 1236-1242.

Cheadle, J.P., Reeve, M.P., Sampson, J.R., Kwiatkowski, D.J. (2000) Molecular genetic advances in tuberous sclerosis. *Hum Genet.*, 107: 97-114.

Chen, L., Pawlikowski, B., Schlessinger, A., More, S.S., Stryke, D., Johns, S.J., Portman, M.A., Chen, E., Ferrin, T.E., Sali, A., Giacomini, K.M. (2010) Role of Organic Cation Transporter 3 (SLC22A3) and Its Missense Variants in the Pharmacologic Action of Metformin. *Pharmacogenet Genomics*, 20: 687-699.

Chesa Ponce, N., Artiles Hernández, J.L., Ponce Socorro, J.M., del Rosario Medina, J., Castro López-Torrella, V., Betancort de León, R. (1995) Wunderlich's syndrome as the first manifestation of a renal angiomyolipoma. *Archivos Espanoles de Urologia*, 48: 305-308.

Cho, K.S., Lee, J.H., Kim, S., Kim, D., Koh, H., Lee, J., Kim, C., Kim, J., Chung, J. (2001) Drosophila phosphoinositide-dependent kinase-1 regulates apoptosis and growth via the phosphoinositide 3-kinase-dependent signaling pathway. *Proc Natl Acad Sci U S A.*, 98: 6144-6149.

Chong, D.Y., Hirunwiwatkul, P., McKeever, P.E., Trobe, J.D. (2007) Papilledema in obstructive hydrocephalus caused by giant cell astrocytoma of tuberous sclerosis. *J Neuroophthalmol.*, 27: 50-54.

Chong-Kopera, H., Inoki, K., Li, Y., Zhu, T., Garcia-Gonzalo, F.R., Rosa, J.L., Guan, K.L. (2006) TSC1 stabilizes TSC2 by inhibiting the interaction between TSC2 and the HERC1 ubiquitin ligase. *J Biol Chem.*, 281: 8313-8316.

Chresta, C.M., Davies, B.R., Hickson, I., Harding, T., Cosulich, S., Critchlow, S.E., Vincent, J.P., Ellston, R., Jones, D., Sini, P., James, D., Howard, Z., Dudley, P., Hughes, G., Smith, L., Maguire, S., Hummersone, M., Malagu, K., Menear, K., Jenkins, R., Jacobsen, M., Smith, G.C., Guichard, S., Pass, M. (2010) AZD8055 is a potent, selective, and orally bioavailable ATP-competitive mammalian target of rapamycin kinase inhibitor with in vitro and in vivo antitumor activity. *Cancer Res*., 70: 288-298.

Clackson, T., Metcalf, C.A. III, Rozamus, L.W. (2002) Regression of tumor xenografts in mice after oral administration of AP23573, a novel mTOR inhibitor that induces tumor starvation. *Proc Am Assoc Cancer Res.*, 43: 95.

Clarke, A., Hancock, E., Kingswood, C., Osborne, J.P. (1999) End-stage renal failure in adults with the tuberous sclerosis complex. *Nephrol Dial Transplant.*, 14: 988-991.

Corson, T.W., Crews, C.M. (2007) Molecular Understanding and Modern Application of Traditional Medicines: Triumphs and Trials. *Cell.*,130: 769-774.

Crino, P.B., Nathanson, K.L., Henske, E.P. (2006) The tuberous sclerosis complex. *N. Engl.J.Med*., 355: 1345-1356.

Critchley, M., Earl, CJC. (1932) Tuberose sclerosis and allied conditions. *Brain*, 55: 311-346.

Crome, L. (1960) The brain and mental retardation. *Br Med J.*, 1: 897-904.

Curatolo, P. (2003) Tuberous Sclerosis Complex From Basic Science to Clinical Phenotypes *Ed*. By Paolo Curatolo. Mac Keith press, London, UK.

Czechowski, J., Langille, E.L., Varady, E. (2000) Intracardiac tumour and brain lesions in tuberous sclerosis: A case report of antenatal diagnosis by ultrasonography. *Acta Radiologica*, 41: 371-374.

Dabora, S.L., Jozwiak, S., Franz, D.N., Roberts, P.S., Nieto, A., Chung, J., Choy, Y.S., Reeve, M.P., Thiele, E., Egelhoff, J.C., Kasprzyk-Obara, J., Domanska-Pakiela, D., Kwiatkowski, D.J. (2001) Mutational analysis in a cohort of 224 tuberous

sclerosis patients indicates increased severity of TSC2, compared with TSC1, disease in multiple organs. *Am J Hum Genet.*, 68: 64-80.

Dabora, S.L., Franz, D.N., Ashwal, S., Sagalowsky, A., Dimario, F.J., Jr., Miles, D. Culter, D., Krueger, D., Uppot, R.N, Rabenou, R., Camposano, S., Paolini, J., Fennessy, F., Lee, N., Woodrum, C., Manola, J., Garber, J., Thiele, E.A. (2011) Multicenter Phase 2 Trial of Sirolimus for Tuberous Sclerosis: Kidney Angiomyolipomas and Other Tumors Regress and VEGF- D Levels Decrease. *PLoS One*, 6: e23379.

Davies, D.M., Johnson, S.R., Tattersfield, A.E., Kingswood, J.C., Cox, J.A., McCartney, D.L., Doyle, T., Elmslie, F., Saggar, A., de Vries, P.J., Sampson, J.R. (2008) Sirolimus therapy in tuberous sclerosis or sporadic lymphangioleiomyomatosis. *N Engl J Med.*, 358: 200-203.

Davies, D.M., Sampson, J.R. (2010) Small-molecule signal-transduction inhibitors: Targeted therapeutic agents for single-gene disorders. *J Med Genet.*, 47: 145-149.

Davies, D.M., de Vries, P.J., Johnson, S.R., McCartney, D.L., Cox, J.A., Serra, A.L., Watson, P.C., Howe, C.J., Doyle, T., Pointon, K., Cross, J.J., Tattersfield, A.E., Kingswood, J.C., Sampson, J.R. (2011) Sirolimus therapy for angiomyolipoma in tuberous sclerosis and sporadic lymphangioleiomyomatosis: a phase 2 trial. *Clin Cancer Res*., 17**:** 4071-4081.

Dawson, J. (1954) Pulmonary tuberous sclerosis and its relation to other forms of the disease. *Q. J. Med*., 23: 113-145.

Dazert E, Hall MN. (2011) mTOR signaling in disease. *Curr Opin Cell Biol*., 23: 744-755.

De Vries, P.J., Gardiner, J., Bolton, P.F. (2009) Neuropsychological attention deficits in tuberous sclerosis complex (TSC). *Am J Med Genet A.,* 149: 387-395.

Deyoung, M.P., Horak, P., Sofer, A., Sgroi, D., Ellisen, L.W. (2008) Hypoxia regulates TSC1/2-mTOR signaling and tumor suppression through REDD1-mediated 14-3-3 shuttling. *Genes Dev.*, 22: 239-251.

Diamanti-Kandarakis, E., Economou, F., Palimeri, S., Christakou, C. (2010). Metformin in polycystic ovary syndrome. *Ann N Y Acad Sci.,* 1205**:** 192-198.

Dibble, C.C., Asara, J.M., Manning, B.D. (2009) Characterization of Rictor phosphorylation sites reveals direct regulation of mTOR complex 2 by S6K1. *Mol Cell Biol.*, 29: 5657-5670.

Dibble, C.C., Elis, W., Menon, S., Qin, W., Klekota, J., Asara, J.M., Finan, P.M., Kwiatkowski, D.J., Murphy, L.O., Manning, B.D. (2012) TBC1D7 Is a Third Subunit of the TSC1-TSC2 Complex Upstream of mTORC1. *Mol Cell.,* 47: 535-546.

Dickinson, M., Ruckle, H., Beaghler, M., Hadley, H.R. (1998) Renal angiomyolipoma: Optimal treatment based on size and symptoms. *Clin Nephrol*., 49: 281-286.

Donegani G. Gratarolla FR. Wildi E. (1972) Tuberous sclerosis. In: Vinken PJ. Bruyn GW, eds. *Handbook of clinical neurology. The phakomatoses*. Amsterdam: Elsevier, 14: 340-389.

Dowling, R.J., Zakikhani, M., Fantus, I.G., Pollak, M., Sonenberg, N. (2007) Metformin inhibits mammalian target of rapamycin-dependent translation initiation in breast cancer cells. *Cancer Res.*, 67: 10804-10812.

Easton, J.B., Houghton, P.J. (2006) mTOR and cancer therapy. *Oncogene*, 25: 6436-6446.

Eble, J.N., Hull, M.T. (1984) Morphologic features of renal oncocytoma: A light and electron microscopic study. *Hum Pathol.*, 15: 1054-1061.

Eble, J.N., Amin, M.B., Young, R.H. (1997) Epithelioid angiomyolipoma of the kidney: A report of five cases with a prominent and diagnostically confusing epithelioid smooth muscle component. *Am J Surg Pathol.*, 21: 1123-1130.

Eble, J.N. (1998) Angiomyolipoma of kidney. *Semin Diagn Pathol.*, 15: 21-40.

Ehninger, D., Han, S., Shilyansky, C., Zhou, Y., Li, W., Kwiatkowski, D.J., Ramesh, V., Silva, A.J. (2008) Reversal of learning deficits in a Tsc2+/- mouse model of tuberous sclerosis. *Nat Med.*, 14: 843-848.

Ehninger, D., de Vries, P.J., Silva, A.J. (2009) From mTOR to cognition: Molecular and cellular mechanisms of cognitive impairments in tuberous sclerosis. *J Intellect Disabil Res*., 53: 838-851

Eker, R. (1954) Familial renal adenomas in Wistar rats. *Acta Pathol Microbiol Scand*., 34: 554-562.

Eker, R., Mossige, J. (1961) A dominant gene for renal adenomas in the rat. *Nature*, 189: 858-859.

Eker, R., Mossige, J., Vincents Johannessen, J., Aars, H. (1981) Hereditary renal adenomas and adenocarcinomas in rats. *Diagn Histopathol.*, 4: 99-110.

El-Hashemite, N., Walker, V., Zhang, H., Kwiatkowski, D.J. (2003) Loss of Tsc1 or Tsc2 induces vascular endothelial growth factor production through mammalian target of rapamycin. *Cancer Res.*, 63: 5173-5177.

El-Hashemite, N., Zhang, H., Henske, E.P., Kwiatkowski, D.J. (2003) Mutation in TSC2 and activation of mammalian target of rapamycin signalling pathway in renal angiomyolipoma. *Lancet,* 361: 1348-1349.

European Polycystic Kidney Disease Consortium (1994) The polycystic kidney disease 1 gene encodes a 14 kb transcript and lies within a duplicated region on chromosome 16. *Cell*, 77: 881-894.

Evans, J.M., Donnelly, L.A., Emslie-Smith, A.M., Alessi, D.R., Morris, A.D. (2005) Metformin and reduced risk of cancer in diabetic patients. *Bmj.,* 330: 1304-1305.

Everitt, J.I., Goldsworthy, T.L., Wolf, D.C., Walker, C.L. (1992) Hereditary renal cell carcinoma in the Eker rat: A rodent familial cancer syndrome. *J Urol.*, 148: 1932-1936.

Everitt, J.I., Goldsworthy, T.L., Wolf, D.C., Walker, C.L. (1995) Hereditary renal cell carcinoma in the Eker rat: A unique animal model for the study of cancer susceptibility. *Toxicol Lett.*, 82-83: 621-625.

Ewalt, D.H., Sheffield, E., Sparagana, S.P., Delgado, M.R., Roach, E.S. (1998) Renal lesion growth in children with tuberous sclerosis complex. *J Urol.*, 160: 141-145.

Facchinetti, V., Ouyang, W., Wei, H., Soto, N., Lazorchak, A., Gould, C., Lowry, C., Newton, A.C., Mao, Y., Miao, R.Q., Sessa, W.C., Qin, J., Zhang, P., Su, B., Jacinto, E. (2008) The mammalian target of rapamycin complex 2 controls folding and stability of Akt and protein kinase C. *EMBO Journal*, 27: 1932-1943.

Fan, Q.W., Knight, Z.A., Goldenberg, D.D., Yu, W., Mostov, K.E., Stokoe, D., Shokat, K.M., Weiss, W.A. (2006) A dual PI3 kinase/mTOR inhibitor reveals emergent efficacy in glioma. *Cancer Cell*. , 9: 341-349.

Farrow, G.M., Harrison Jr., E.G., Utz, D.C., Jones, D.R. (1968) Renal angiomyolipoma. A clinicopathologic study of 32 cases. *Cancer*, 22: 564-570.

Feldman, M.E., Apsel, B., Uotila, A., Loewith, R., Knight, Z.A., Ruggero, D., Shokat, K.M. (2009) Active-site inhibitors of mTOR target rapamycin-resistant outputs of mTORC1 and mTORC2. *PLoS Biol*., 7: e38.

Fenton, T.R., Gout, I.T. (2011) Functions and regulation of the 70 kDa ribosomal S6 kinases. *Int J Biochem Cell Biol.*, 43: 47-59.

Feriz, H. (1930) Ein Beitrag zur histopathologie der tuberösen Sklerose. *Virchows Arch. Pathol*. *Anat*., 278: 690-769.

Ferraro, A., Doolittle, G.J. (1936) Tuberous sclerosis (diffuse neurospongioblastosis). *Psychiatr. Q*., 10: 365-416.

Fingar, D.C., Blenis, J. (2004) Target of rapamycin (TOR): An integrator of nutrient and growth factor signals and coordinator of cell growth and cell cycle progression. *Oncogene*, 23: 3151-3171.

Finlay, G.A., Malhowski, A.J., Liu, Y., Fanburg, B.L., Kwiatkowski, D.J., Toksoz, D. (2007) Selective inhibition of growth of tuberous sclerosis complex 2 null cells by atorvastatin is associated with impaired Rheb and Rho GTPase function and reduced mTOR/S6 kinase activity. *Cancer Res*., 67: 9878-9886.

Finlay, G.A., Malhowski, A.J., Polizzi, K., Malinowska-Kolodziej, I., Kwiatkowski, D.J. (2009) Renal and liver tumors in *Tsc2*$^{+/-}$ mice, a model of tuberous sclerosis complex, do not respond to treatment with atorvastatin, a 3-hydroxy-3-methylglutaryl coenzyme A reductase inhibitor. *Mol Cancer Ther*., 8: 1799-1807.

Fischer, W. (1911) Die niereutemoren bi der tuberosen hirsklerose. *Beitr. Z path. Anat u z allg Path*., 1: 235.

Fitzpatrick, T.B. (1991) History and significance of white macules, earliest visible sign of tuberous sclerosis. *Ann N Y Acad Sci.*, 615: 26-35.

Fleury, P., Smits, N., van Baal, S. (1987) The incidence of hepatic hamartomas in tuberous sclerosis. Evaluation by ultrasonography. *RoFo*., 146: 694-696.

Flores II, L.G., Yeh, H.H., Soghomonyan, S., Young, D., Bankson, J., Hu, Q., Alauddin, M., Huff, V., Gelovani, J.G. (2013) Monitoring therapy with MEK inhibitor U0126 in a novel Wilms tumor model in Wt1 knockout Igf2 transgenic mice using 18F-FDG PET with dual-contrast enhanced CT and MRI: Early metabolic response without inhibition of tumor growth. *Mol Imaging Biol.*, 15: 175-185.

Franz, D.N., Brody, A., Meyer, C., Leonard, J., Chuck, G., Dabora, S., Sethuraman, G., Colby, T.V., Kwiatkowski, D.J., McCormack, F.X. (2001) Mutational and radiographic analysis of pulmonary disease consistent with lymphangioleiomyomatosis and micronodular pneumocyte hyperplasia in women with tuberous sclerosis. *Am J Respir Crit Care Med.*, 164: 661-668.

Franz, D.N. (2004) Non-neurologic manifestations of tuberous sclerosis complex. *J Child Neurol.*, 19: 690-698.

Franz, D.N., Leonard, J., Tudor, C., Chuck, G., Care, M., Sethuraman, G., Dinopoulos, A., Thomas, G., Crone, K.R. (2006) Rapamycin causes regression of astrocytomas in tuberous sclerosis complex. *Ann Neurol.,* 59: 490-498.

Franz, D.N., Belousova, E., Sparagana, S., Bebin, E.M., Frost, M., Kuperman, R., Witt, O., Kohrman, M.H., Flamini, J.R., Wu, J.Y., Curatolo, P., de Vries, P.J., Whittemore, V.H., Thiele, E.A., Ford, J.P., Shah, G., Cauwel, H., Lebwohl, D., Sahmoud, T., Jozwiak, S. (2013) Efficacy and safety of everolimus for subependymal giant cell astrocytomas associated with tuberous sclerosis complex (EXIST-1): a multicentre, randomised, placebo-controlled phase 3 trial. *Lancet*., 381: 125-132.

Frese, K.K., Tuveson, D.A. (2007) Maximizing mouse cancer models. *Nat Rev Cancer*., 7: 645-58.

Fricke, B.L., Donnelly, L.F., Casper, K.A., Bissler, J.J. (2004) Frequency and Imaging Appearance of Hepatic Angiomyolipomas in Pediatric and Adult Patients with Tuberous Sclerosis. *AJR Am J Roentgenol.*, 182: 1027-1030.

Fryer, A.E., Chalmers, A.H., Connor, J.M., Fraser, I., Povey, S., Yates, A.D., Yates, J.R., Osborne, J.P. (1987) Evidence that the gene for tuberous sclerosis is on chromosome 9. *Lancet*., 1: 659-661.

Fryer, A.E., Osborne, J.P., Schutt, W. (1987) Forehead plaque: A presenting skin sign in tuberous sclerosis. *Arch Dis Child*., 62: 292-293.

Fukuda, T., Kobayashi, T., Momose, S., Yasui, H., Hino, O. (2000) Distribution of Tsc1 protein detected by immunohistochemistry in various normal rat tissues and the renal carcinomas of Eker rat: Detection of limited colocalization with Tsc1 and Tsc2 gene products in vivo. *Lab Invest.*, 80: 1347-1359.

Galiè, M., D'Onofrio, M., Calderan, L., Nicolato, E., Amici, A., Crescimanno, C., Marzola, P., Sbarbati, A. (2004) In vivo mapping of spontaneous mammary tumors in transgenic mice using MRI and ultrasonography. *J Magn Reson Imaging*., 19: 570-579.

Galuska, D., Nolte, L.A., Zierath, J.R., Wallberg-Henriksson, H. (1994) Effect of metformin on insulin-stimulated glucose transport in isolated skeletal muscle obtained from patients with NIDDM. *Diabetologia*, 37:826-832.

Gao, X., Neufeld, T.P., Pan, D. (2000) Drosophila PTEN regulates cell growth and proliferation through PI3K- dependent and -independent pathways. *Dev Biol.*, 221: 404-418.

Gao, X., Pan, D. (2001) TSC1 and TSC2 tumor suppressors antagonize insulin signaling in cell growth. *Genes Dev.*, 15: 1383-1392.

Gao, X., Zhang, Y., Arrazola, P., Hino, O., Kobayashi, T., Yeung, R.S., Ru, B., Pan, D. (2002) Tsc tumour suppressor proteins antagonize amino-acid-TOR signalling. *Nat Cell Biol.,* 4: 699-704.

García-Martínez, J.M., Alessi, D.R. (2008) mTOR complex 2 (mTORC2) controls hydrophobic motif phosphorylation and activation of serum- and glucocorticoid-induced protein kinase 1 (SGK1). *Biochem J.*, 416: 375-385.

Gastaut, H., Roger, J., Soulayrol, R., Salamon, G., Regis, H., Lob, H. (1965) Encéphalopathie myoclonique infantile avec hypsarythmie (syndrome de West) et sclérose tubéreuse de Bourneville. *J Neurol Sci.*, 2: 140-160.

Gau, C.L., Kato-Stankiewicz, J., Jiang, C., Miyamoto, S., Guo, L., Tamanoi, F. (2005) Farnesyltransferase inhibitors reverse altered growth and distribution of actin filaments in Tsc-deficient cells via inhibition of both rapamycin-sensitive and -insensitive pathways. *Mol Cancer Ther.*, 4: 918-926

Gauvain, K.M., Garbow, J.R., Song, S.K., Hirbe, A.C., Weilbaecher, K. (2005) MRI detection of early bone metastases in b16 mouse melanoma models. *Clin Exp Metastasis*., 22: 403-411.

Geist, R.T., Gutmann, D.H. (1995) The tuberous sclerosis 2 gene is expressed at high levels in the cerebellum and developing spinal cord. *Cell Growth Differ.*, 6: 1477-1483.

Geoerger, B., Kerr, K., Tang, C.B., Fung, K.M., Powell, B., Sutton, L.N., Phillips, P.C., Janss, A.J. (2001) Antitumor activity of the rapamycin analog CCI-779 in

human primitive neuroectodermal tumor/medulloblastoma models as single agent and in combination chemotherapy. *Cancer Res.*, 61: 1527-1532.

Gingras, A.C., Gygi, S.P., Raught, B., Polakiewicz, R.D., Abraham, R.T., Hoekstra, M.F., Aebersold, R., Sonenberg, N. (1999) Regulation of 4E-BP1 phosphorylation: A novel two step mechanism. *Genes Dev.*, 13: 1422-1437.

Gingras, A.C., Raught, B., Gygi, S.P., Niedzwiecka, A., Miron, M., Burley, S.K., Polakiewicz, R.D., Wyslouch-Cieszynska A, Aebersold R, Sonenberg, N. (2001) Hierarchical phosphorylation of the translation inhibitor 4E-BP1. *Genes Dev.*, 15: 2852-2864.

Goberdhan, D.C., Paricio, N., Goodman, E.C., Mlodzik, M., Wilson, C. (1999) Drosophila tumor suppressor PTEN controls cell size and number by antagonizing the Chico/PI3-kinase signaling pathway. *Genes Dev.*, 13: 3244-3258.

Goh, S., Butler, W., Thiele, E.A. (2004) Subependymal giant cell tumors in tuberous sclerosis complex. *Neurology*, 63: 1457-1461.

Goh, S.G., Ho, J.M., Chuah, K.L., Tan, P.H., Poh, W.T., Riddell, R.H. (2001) Leiomyomatosis-like lymphangioleiomyomatosis of the colon in a female with tuberous sclerosis. *Mod Pathol.*, 14: 1141-1146.

Gomez, M.R. (1979) *Tuberous Sclerosis*. New York: Raven Press.

Gomez, M.R. (1988) *Tuberous Sclerosis*, Second Edition. Raven Press, Ltd., New York.

Gomez, M.R., Sampson, J.R., Whittemore, V.H. (1999) The *Tuberous Sclerosis Complex*, Third Edition. Oxford University Press, Oxford, UK.

Gotlieb, W.H., Saumet, J., Beauchamp, M.C., Gu, J., Lau, S., Pollak, M.N., Bruchim, I. (2008) In vitro metformin anti-neoplastic activity in epithelial ovarian cancer. *Gynecol Oncol*., 110: 246-250.

Gough, D.J., Corlett, A., Schlessinger, K., Wegrzyn, J., Larner, A.C., Levy, D.E. (2009) Mitochondrial STAT3 supports RasDependent oncogenic transformation. *Science*, 324: 1713-1716.

Gould, S.R. (1991) Hamartomatous rectal polyps are common in tuberous sclerosis. *Ann N Y Acad Sci.*, 615: 71-80.

Graham, G.G., Punt, J., Arora, M., Day, R.O., Doogue, M.P., Duong, J.K., Furlong, T.J., Greenfield, J.R., Greenfield, L.C., Kirkpatrick, C.L., Ray, J.E., Timmins, P., Williams, K.M. (2011) Clinical Pharmacokinetics of metformin. *Clin Pharmacokinet.,* 50: 81-98.

Green, A.J., Johnson, P.H., Yates, J.R. (1994) The tuberous sclerosis gene on chromosome 9q34 acts as a growth suppressor. *Hum Mol Genet.*, 3: 1833-1834.

Green, A.J., Smith, M., Yates, J.R. (1994) Loss of heterozygosity on chromosome 16p13.3 in hamartomas from tuberous sclerosis patients. *Nat Genet.*, 6: 193-196.

Green, A.S., Chapuis, N., Maciel, T.T., Willems, L., Lambert, M., Arnoult, C., Boyer, O., Bardet, V., Park, S., Foretz, M., Viollet, B., Ifrah, N., Dreyfus, F., Hermine, O., Moura, I.C., Lacombe, C., Mayeux, P., Bouscary, D., Tamburini, J. (2010) The LKB1/ AMPK signaling pathway has tumor suppressor activity in acute myeloid leukemia through the repression of mTOR-dependent oncogenic mRNA translation. *Blood*, 116: 4262-4273.

Guertin, D.A., Stevens, D.M., Thoreen, C.C., Burds, A.A., Kalaany, N.Y., Moffat, J., Brown, M., Fitzgerald, K.J., Sabatini, D.M. (2006) Ablation in Mice of the mTORC Components raptor, rictor, or mLST8 Reveals that mTORC2 Is Required for Signaling to Akt-FOXO and PKCα, but Not S6K1. *Dev Cell.*, 11: 859-871.

Guertin, D.A., Sabatini, D.M. (2007) Defining the Role of mTOR in Cancer. *Cancer Cell*, 12: 9-22.

Guertin, D.A., Stevens, D.M., Saitoh, M., Kinkel, S., Crosby, K., Sheen, J.H., Mullholland, D.J., Magnuson, M.A., Wu, H., Sabatini, D.M. (2009) mTOR Complex 2 Is Required for the Development of Prostate Cancer Induced by Pten Loss in Mice. *Cancer Cell*, 15: 148-159

Gunther, M., Penrose, L.S. (1935) The genetics of epiloia. *J. Genet*., 31: 413-430.

Guo, Y., Kwiatkowski, D.J. (2013) Equivalent benefit of rapamycin and a potent mTOR ATP-competitive inhibitor, MLN0128 (INK128), in a mouse model of tuberous sclerosis. *Mol Cancer Res*., 11: 467-473.

Gushiken, B.J., Callen, P.W., Silverman, N.H. (1999) Prenatal diagnosis of tuberous sclerosis in monozygotic twins with cardiac masses. *J Ultrasound Med.,* 18: 165-168.

Gwinn, D.M., Shackelford, D.B., Egan, D.F., Mihaylova, M.M., Mery, A., Vasquez, D.S., Turk, B.E., Shaw, R.J. (2008) AMPK phosphorylation of raptor mediates a metabolic checkpoint. *Mol Cell,* 30: 214-226.

Haar, E.V., Lee, S.I., Bandhakavi, S., Griffin, T.J., and Kim, D.H. (2007) Insulin signalling to mTOR mediated by the Akt/PKB substrate PRAS40. *Nat. Cell Biol*., 9: 316-323.

Haddad, L.A., Smith, N., Bowser, M., Niida, Y., Murthy, V., Gonzalez-Agosti, C., Ramesh, V. (2002) The TSC1 tumor suppressor hamartin interacts with neurofilament-L and possibly functions as a novel integrator of the neuronal cytoskeleton. *J Biol Chem.*, 277: 44180-44186.

Haines, J.L., Short, M.P., Kwiatkowski, D.J., Jewell, A., Andermann, E., Bejjani, B., Yang, C.H., Gusella, J.F., Amos, J.A. (1991) Localization of one gene for tuberous sclerosis witihin 9q32-9q34, and further evidence for heterogeneity. *Am J Hum Genet.*, 49: 764-772.

Hallervorden, J., Krucke, W. (1956) Die tuberöse Hirnklerose. In: *Handbuch der speziellen psthologisdhen Anatomie and Histologie*. XIII/4. Berlin: Springer; 602-663.

Han, J.M., Jeong, SJ, Park MC, Kim G, Kwon NH, Kim HK, Ha SH, Ryu SH, Kim S. (2012) Leucyl-tRNA synthetase is an intracellular leucine sensor for the mTORC1-signaling pathway. *Cell*. 149: 410-424.

Han, S., Santos, T.M., Puga, A., Roy, J., Thiele, E.A., McCollin, M., Stemmer-Rachamimov, A., Ramesh, V. (2004) Phosphorylation of Tuberin as a Novel

Mechanism for Somatic Inactivation of the Tuberous Sclerosis Complex Proteins in Brain Lesions. *Cancer Res.*, 64: 812-816.

Hanada, M., Feng, J., Hemmings, B.A. (2004) Structure, regulation and function of PKB/AKT - A major therapeutic target. *Biochimica et Biophysica Acta - Proteins and Proteomics*, 1697: 3-16.

Hardman, J.A., McNicholas, T.A., Kirkham, N., Fletcher, M.S. (1993) Recurrent renal angiomyolipoma associated with renal carcinoma in a patient with tuberous sclerosis. *Br J Urol.*, 72: 983-984.

Harrington, L.S., Findlay, G.M., Lamb, R.F. (2005) Restraining PI3K: mTOR signalling goes back to the membrane. *Trends Biochem Sci*., 30: 35-42.

Harris, T.E., Lawrence Jr., J.C. (2003) TOR signaling. Science's STKE: signal transduction knowledge environment. *Sci STKE*, re15.

Harrison, J.E., O'Callaghan, F.J., Hancock, E., Osborne, J.P., Bolton, P.F. (1999) Cognitive deficits in normally intelligent patients with tuberous sclerosis. *Am J Med Genet*, 88: 642-646.

Hartdegen, A. (1881) Ein Fall von multipler Verhärtung des Grosshirns nebst histologisch eigenartigen harten Geschwülsten der Seitenventrikel ("Glioma gangliocellulare") bei einem Neugeborenen. *Archiv für Psychiatrie und Nervenkrankheiten*, 11: 117-131.

Hata, T., Yan, F., Dai, S.Y., Kanenishi, K., Yanagihara, T. (2007) Real-time 3-dimensional echocardiographic features of fetal cardiac tumor. *J Clin Ultrasound*, 35: 338-340.

Hay, N., Sonenberg, N. (2004) Upstream and downstream of mTOR. *Genes Dev.*, 18: 1926-1945.

Heffron, T.P., Berry, M., Castanedo, G., Chang, C., Chuckowree, I., Dotson, J., Folkes, A., Gunzner, J., Lesnick, J.D., Lewis, C., Mathieu, S., Nonomiya, J., Olivero, A., Pang, J., Peterson, D., Salphati, L., Sampath, D., Sideris, S., Sutherlin, D.P., Tsui, V., Wan, N.C., Wang, S., Wong, S., Zhu, B.Y. (2010) Identification of GNE-477, a potent and efficacious dual PI3K/mTOR inhibitor. *Bioorg Med Chem Lett*., 20: 2408-2411.

Heitman, J., Movva, N.R., Hall, M.N. (1991) Targets for cell cycle arrest by the immunosuppressant rapamycin in yeast. *Science*, 253: 905-909.

Hemauer, S.J., Patrikeeva, S.L., Nanovskaya, T.N., Hankins, G.D., Ahmed, M.S. (2010) Role of human placental apical membrane transporters in the efflux of glyburide, rosiglitazone, and metformin. *Am J Obstet Gynecol.,* 202: 383.e1-7.

Henske, E.P., Neumann, H.P., Scheithauer, B.W., Herbst, E.W., Short, M.P., Kwiatkowski, D.J. (1995) Loss of heterozygosity in the tuberous sclerosis (TSC2) region of chromosome band 16p13 occurs in sporadic as well as TSC-associated renal angiomyolipomas. *Genes Chromosomes and Cancer*, 13: 295-298.

Henske, E.P., Scheithauer, B.W., Short, M.P., Wollmann, R., Nahmias, J., Hornigold, N., Van Slegtenhorst, M., Welsh, C.T., Kwiatkowski, D.J. (1996) Allelic loss is

frequent in tuberous sclerosis kidney lesions but rare in brain lesions. *Am J Hum Genet.*, 59: 400-406.

Henske, E.P. (2005) Tuberous sclerosis and the kidney: From mesenchyme to epithelium, and beyond. *Pediatr Nephrol*., 20: 854-857.

Hernandez, O., Way, S., McKenna III, J., Gambello, M.J. (2007) Generation of a conditional disruption of the Tsc2 gene. *Genesis*, 45: 101-106.

Herry, I., Neukirch, C., Debray, M.P., Mignon, F., Crestani, B. (2007) Dramatic effect of sirolimus on renal angiomyolipomas in a patient with tuberous sclerosis complex. *Eur J Intern Med*., 18: 76-77.

Hietakangas, V., Cohen, S.M. (2008) TOR complex 2 is needed for cell cycle progression and anchorage-independent growth of MCF7 and PC3 tumor cells. *BMC Cancer*, 8: art. no. 282.

Hino, O., Mitani, H., Nishizawa, M., Katsuyama, H., Kobayashi, E., Hirayama, Y. (1993) A novel renal cell carcinoma susceptibility gene maps on chromosome 10 in the Eker rat. *Jpn. J. Cancer Res*., 84: 1106-1109.

Hino, O., Mitani, H., Katsuyama, H., Kubo, Y. (1994) A novel cancer predisposition syndrome in the Eker rat model. *Cancer Letters*, 83: 117-121.

Hino, O., Mitani, H., Sakaurai, J. (2002) “Second hit” of Tsc2 gene in radiation induced renal tumors of Eker rat model. *International Congress Series*, 1236: 163-174.

Hirsch, H.A., Iliopoulos, D., Tsichlis, P.N., Struhl, K. (2009) Metformin selectively targets cancer stem cells, and acts together with chemotherapy to block tumor growth and prolong remission. *Cancer Res.,* 69: 7507-7511.

Hizawa, K., Iida, M., Matsumoto, T., Tominaga, M., Hirota, C., Yao, T., Fujishima, M. (1994) Gastrointestinal involvement in tuberous sclerosis: Two case reports. *J Clin Gastroenterol.*, 19: 46-49.

Hodges, A.K., Li, S., Maynard, J., Parry, L., Braverman, R., Cheadle, J.P., DeClue, J.E., Sampson, J.R. (2001) Pathological mutations in TSC1 and TSC2 disrupt the interaction between hamartin and tuberin. *Hum Mol Genet.*, 10: 2899-2905.

Hofbauer, G.F., Marcollo-Pini, A., Corsenca, A., Kistler, A.D., French, L.E., Wüthrich, R.P., Serra, A.L. (2008) The mTOR inhibitor rapamycin significantly improves facial angiofibroma lesions in a patient with tuberous sclerosis. *Br J Dermatol*.,159: 473-475.

Holz, M.K., Ballif, B.A., Gygi, S.P., Blenis, J. (2005) mTOR and S6K1 mediate assembly of the translation preinitiation complex through dynamic protein interchange and ordered phosphorylation events. *Cell*, 123: 569-580.

Hong, S.P., Leiper, F.C., Woods, A., Carling, D., and Carlson, M. (2003). Activation of yeast Snf1 and mammalian AMP-activated protein kinase by upstream kinases. *Proc. Natl. Acad. Sci. USA*, 100: 8839-8843.

Hoshii, T., Tadokoro, Y., Naka, K., Ooshio, T., Muraguchi, T., Sugiyama, N., Soga, T., Araki, K., Yamamura, K., Hirao, A. (2012) mTORC1 is essential for leukemia propagation but not stem cell self-renewal. *J Clin Invest*., 122: 2114-2129.

Hosoya, M., Naito, H., Nihei, K. (1999) Neurological prognosis correlated with variations over time in the number of subependymal nodules in tuberous sclerosis. *Brain Dev*. 21: 544-547.

Houser, O.W., Nixon, J.R. (1988) Central nervous system imaging. In: Gomez, M.R., ed. *Tuberous Sclerosis*. New York: Raven Press; 51-62.

Hresko, R.C., Mueckler, M. (2005) mTOR·RICTOR is the Ser473 kinase for Akt/protein kinase B in 3T3-L1 adipocytes. *J Biol Chem.*, 280: 40406-40416

Huang, H., Potter, C.J., Tao, W., Li, D.M., Brogiolo, W., Hafen, E., Sun, H., Xu, T. (1999) PTEN affects cell size, cell proliferation and apoptosis during Drosophila eye development. *Development*, 126: 5365-5372.

Huang, J., Dibble, C.C., Matsuzaki, M., Manning, B.D. (2008) The TSC1-TSC2 complex is required for proper activation of mTOR complex 2. *Mol Cell Biol.*, 28: 4104-4115.

Huang, J., Manning, B.D. (2008) The TSC1–TSC2 complex: a molecular switchboard controlling cell growth. *Biochem J*., 412: 179-190.

Huang, J., Manning, B.D. (2009) A complex interplay between Akt, TSC2 and the two mTOR complexes. *Biochem Soc Trans*., 37: 217-22.

Huang, J., Wu, S., Wu, C.L., Manning, B.D. (2009) Signaling events downstream of mammalian target of rapamycin complex 2 are attenuated in cells and tumors

deficient for the tuberous sclerosis complex tumor suppressors. *Cancer Res*., 69: 6107-6114.

Huang, X., Wullschleger, S., Shpiro, N., McGuire, V.A., Sakamoto, K., Woods, Y.L., McBurnie, W., Fleming, S., Alessi, D.R. (2008) Important role of the LKB1-AMPK pathway in suppressing tumorigenesis in PTEN-deficient mice. *Biochem J*., 412: 211-221.

Huber, C., Treutner, K.H., Steinau, G., Schumoelick, V. (1996) Ruptured hepatic angiolipoma in tuberous sclerosis complex. *Langenbecks Archiv fur Chirurgie*, 381: 7-9.

Hundal, H.S., Ramlal, T., Reyes, R., Leiter, L.A., and Klip, A. (1992) Cellular mechanism of metformin action involves glucose transporter translocation from an intracellular pool to the plasma membrane in L6 muscle cells. *Endocrinology*, 131:1165-1173.

Hundal, R.S., Krssak, M., Dufour, S., Laurent, D., Lebon, V., Chandramouli, V., Inzucchi, S.E., Schumann, W.C., Petersen, K.F., Landau, B.R., Shulman, G.I. (2000) Mechanism by which metformin reduces glucose production in type 2 diabetes. *Diabetes*, 49: 2063-2069.

Hunt, A. (1983) Tuberous sclerosis: a survey of 97 cases. II: Physical findings. *Dev Med Child Neurol.*, 25: 350-352.

Hunt, A., Lindenbaum, R.H. (1984) Tuberous sclerosis: A new estimate of prevalence within the Oxford region. *J Med Genet.*, 21: 272-277.

Hunter, K.W. (2012) Mouse models of cancer: does the strain matter? *Nat Rev Cancer*., 12: 144-149.

Hyman, M.H., Whittemore, V.H. (2000) National institutes of health consensus conference: Tuberous sclerosis complex. *Arch Neurol.*, 57: 662-665.

Ihle, N.T., Powis, G. (2009) Take your PIK: phosphatidylinositol 3-kinase inhibitors race through the clinic and toward cancer therapy. *Mol Cancer Ther*., 8: 1-9.

Ikenoue, T., Inoki, K., Yang, Q., Zhou, X., Guan, K.L. (2008) Essential function of TORC2 in PKC and Akt turn motif phosphorylation, maturation and signalling. *EMBO Journal*, 27: 1919-1931.

Inglis, K. (1950) Neurilemmoblastosis: The Influence of Intrinsic Factors in Disease When Development of the Body is Abnormal. *Am. J. pathol*., 26: 521-536.

Inoki, K., Li, Y., Zhu, T., Wu, J., Guan, K.L. (2002) TSC2 is phosphorylated and inhibited by Akt and suppresses mTOR signalling, *Nat. Cell Biol*., 4: 648-657.

Inoki, K., Li, Y., Xu, T., Guan, K.L. (2003) Rheb GTpase is a direct target of TSC2 GAP activity and regulates mTOR signalling. *Genes Dev.*, 17: 1829-1834.

Inoki, K., Zhu, T., Guan, K.L. (2003) TSC2 mediates cellular energy response to control cell growth and survival. *Cell*, 115: 577-590.

Inoki, K., Corradetti, M.N., Guan, K.L. (2005) Dysregulation of the TSC-mTOR pathway in human disease. *Nat Genet.*, 37: 19-24.

Inoki, K., Ouyang, H., Zhu, T., Lindvall, C., Wang, Y., Zhang, X., Yang. Q., Bennett, C., Harada, Y., Stankunas, K., Wang, C.Y., He, X., MacDougald, O.A., You, M., Williams, B.O., Guan, K.L. (2006) TSC2 integrates Wnt and energy signals via a coordinated phosphorylation by AMPK and GSK3 to regulate cell growth. *Cell*, 126: 955-968.

Isakovic, A., Harhaji, L., Stevanovic, D., Markovic, Z., Sumarac-Dumanovic, M., Starcevic, V., Micic, D., Trajkovic, V. (2007) Dual antiglioma action of metformin: cell cycle arrest and mitochondriadependent apoptosis. *Cell Mol Life Sci*., 64: 1290-1302.

Ito, N., Rubin, G.M. (1999) gigas, a Drosophila homolog of tuberous sclerosis gene product-2, regulates the cell cycle. *Cell*, 96: 529-539.

Iyer, N.V., Kotch, L.E., Agani, F., Leung, S.W., Laughner, E., Wenger, R.H., Gassmann, M., Gearhart, J.D., Lawler, A.M., Yu, A.Y., Semenza, GL. (1998) Cellular and developmental control of O2 homeostasis by hypoxia-inducible factor-1a. *Genes Dev*., 12: 149–162.

Jacinto, E., Loewith, R., Schmidt, A., Lin, S., Rüegg, M.A., Hall, A., Hall, M.N. (2004) Mammalian TOR complex 2 controls the actin cytoskeleton and is rapamycin insensitive. *Nat Cell Biol.*, 6: 1122-1128.

Jalving, M., Gietema, J.A., Lefrandt, J.D., de Jong, S., Reyners, A.K., Gans, R.O., de Vries, E.G. (2010). Metformin: taking away the candy for cancer? *Eur J Cancer*, 46: 2369-2380.

Janssen, B., Sampson, J., Van Der Est, M., Deelen, W., Verhoef, S., Daniels, I., Hesseling, A., Brook-Carter, P., Nellist, M., Lindhout, D., Sandkuijl, L., Halley, D. (1994) Refined localization of TSC1 by combined analysis of 9q34 and 16p13 data in 14 tuberous sclerosis families. *Hum Genet.*, 94: 437-440.

Janssen, L.A., Sandkuyl, L.A., Merkens, E.C., Maat-Kievit, J.A., Sampson, J.R., Fleury, P., Hennekam, R.C., Grosveld, G.C., Lindhout, D., Halley, D.J. (1990) Genetic heterogeneity in tuberous sclerosis. *Genomics*, 8: 237-242.

Jewell, J.L., Russell, R.C., Guan, K.L. (2013) Amino acid signalling upstream of mTOR. *Nat Rev Mol Cell Biol*., 14: 133-139.

Jimbow, K. (1997) Tuberous sclerosis and guttate leukodermas. *Semin Cutan Med Surg.*, 16: 30-35.

Jimenez, R.E., Eble, J.N., Reuter, V.E., Epstein, J.I., Folpe, A.L., De Peralta-Venturina, M., Tamboli, P., Ansell, I.D., Grignon, D.J., Young, R.H., Amin, M.B. (2001) Concurrent angiomyolipoma and renal cell neoplasia: A study of 36 cases. *Mod Pathol.*, 14: 157-163.

Jin, F., Wienecke, R., Xiao, G.H., Maize Jr., J.C., DeClue, J.E., Yeung, R.S. (1996) Suppression of tumorigenicity by the wild-type tuberous sclerosis 2 (Tsc2) gene and its C-terminal region. *Proc. Natl Acad. Sci. USA*, 93: 9154-9159.

Jin, H.O., An, S., Lee, H.C., Woo, S.H., Seo, S.K., Choe, T.B., Yoo, D.H., Lee, S.B., Um, H.D., Lee, S.J., Park, M.J., Kim, J.I., Hong, S.I., Rhee, C.H., Park, I.C. (2007) Hypoxic condition- and high cell density-induced expression of Redd1 is regulated by activation of hypoxia-inducible factor-1α and Sp1 through the phosphatidylinositol 3-kinase/Akt signaling pathway. *Cell Signal.*, 19: 1393-1403.

Johnson, M.W., Kerfoot, C., Bushnell, T., Li, M., Vinters, H.V. (2001) Hamartin and tuberin expression in human tissues. *Mod Pathol.*, 14: 202-210.

Joinson, C., O'Callaghan, F.J., Osborne, J.P., Martyn, C., Harris, T., Bolton, P.F. (2003) Learning disability and epilepsy in an epidemiological sample of individuals with tuberous sclerosis complex. *Psychol Med.*, 33: 335-344.

Jones, A.C., Daniells, C.E., Snell, R.G., Tachataki, M., Idziaszczyk, S.A., Krawczak, M., Sampson, J.R., Cheadle, J.P. (1997) Molecular genetic and phenotypic analysis reveals differences between TSC1 and TSC2 associated familial and sporadic tuberous sclerosis. *Hum Mol Genet.*, 6: 2155-2161.

Jones, A.C., Shyamsundar, M.M., Thomas, M.W., Maynard, J., Idziaszczyk, S., Tomkins, S., Sampson, J.R., Cheadle, J.P. (1999) Comprehensive mutation analysis of Tsc1 and Tsc2 and phenotypic correlations in 150 families with tuberous sclerosis. *Am J Hum Genet.*, 64: 1305-1315.

Jones, A.C., Sampson, J.R., Cheadle, J.P. (2001) Low level mosaicism detectable by DHPLC but not by direct sequencing. *Hum Mutat.*, 17: 233-234.

Jones, K.T., Greer, E.R., Pearce, D., Ashrafi, K. (2009) Rictor/torc2 regulates Caenorhabditis elegans fat storage, body size, and development through sgk-1. *PLoS Biology*, 7: 0604-0615.

Jóźwiak, J., Jóźwiak, S., Oldak, M. (2006) Molecular activity of sirolimus and its possible application in tuberous sclerosis treatment. *Med Res Rev*., 26: 160-180.

Jóźwiak, J., Jóźwiak, S., Wlodarski, P. (2008) Possible mechanisms of disease development in tuberous sclerosis. *Lancet Oncol*., 9: 73-79.

Jóźwiak, S., Pedich, M., Rajszys, P., Michalowicz, R. (1992) Incidence of hepatic hamartomas in tuberous sclerosis. *Arch Dis Child.*, 67: 1363-1365.

Jóźwiak, S., Schwartz, R.A., Janniger, C.K., Michałowicz, R., Chmielik, J. (1998) Skin lesions in children with tuberous sclerosis complex: Their prevalence, natural course, and diagnostic significance. *Int J Dermatol.*, 37: 911-917.

Jóźwiak, S., Schwartz, R.A., Janniger, C.K., Bielicka-Cymerman, J. (2000) Usefulness of diagnostic criteria of tuberous sclerosis complex in pediatric patients. *J Child Neurol.*, 15: 652-659.

Jóźwiak, S., Kotulska, K., Kasprzyk-Obara, J., Domańska-Pakieła, D., Tomyn-Drabik, M., Roberts, P., Kwiatkowski, D. (2006) Clinical and genotype studies of cardiac tumors in 154 patients with tuberous sclerosis complex. *Pediatrics*, 118: e1146-1151.

Julien, L.A., Carriere, A., Moreau, J., Roux, P.P. (2010) mTORC1-activated S6K1 phosphorylates rictor on threonine 1135 and regulates mTORC2 signaling. *Mol Cell Biol.*, 30: 908-921.

Kaczorowska, M., Borkowska, J., Domańska-Pakieła, D., Kasprzyk-Obara, J., Roberts, P.S., Dabora, S.L., Kwiatkowski, D.J., Jóźwiak, S. (2006) Clinical characteristics of tuberous sclerosis complex in patients with no TSC1 or TSC2 mutations identified. *Neurol Dziec*., 30: 15-20.

Kalender, A., Selvaraj, A., Kim, S.Y., Gulati, P., Brule, S., Viollet, B., Kemp, B.E., Bardeesy, N., Dennis, P., Schlager, J.J., Marette, A., Kozma, S.C., Thomas, G. (2010). Metformin, independent of AMPK, inhibits mTORC1 in a rag GTPase-dependent manner. *Cell Metab.,*11: 390-401.

Kandt, R.S., Haines, J.L., Smith, M., Northrup, H., Gardner, R.J., Short, M.P., Dumars, K., Roach, E.S., Steingold, S., Wall, S., Blanton, S.H., Flodman, P., Kwiatkowski, D.J., Jewell, A., Weber, J.L., Roses, A.D., Pericak-Vance, M.A. (1992) Linkage of an important gene locus for tuberous sclerosis to a chromosome 16 marker for polycystic kidney disease. *Nature Genet*., 2: 37-41.

Karbowniczek, M., Yu, J., Henske, E.P. (2003) Renal angiomyolipomas from patients with sporadic lymphangiomyomatosis contain both neoplastic and non-neoplastic vascular structures. *Am J Pathol.*, 162: 491-500.

Kaser, S., Ebenbichler, C.F., Tilg, H. (2010) Pharmacological and non pharmacological treatment of non-alcoholic fatty liver disease. *Int J Clin Pract.,* 64: 968-983.

Kenerson, H., Dundon, T.A., Yeung, R.S. (2005) Effects of rapamycin in the eker rat model of tuberous sclerosis complex. *Pediatr Res.*, 57: 67-75.

Kenerson, H.L., Aicher, L.D., True, L.D., Yeung, R.S. (2002) Activated mammalian target of rapamycin pathway in the pathogenesis of tuberous sclerosis complex renal tumors. *Cancer Res*., 62: 5645-5650.

Kennelly, M.J., Grossman, H.B., Cho, K.J. (1994) Outcome analysis of 42 cases of renal angiomyolipoma. *J Urol.*, 152: 1988-1991.

Khurana, V., Kochhar, R., Bejjanki, R., Caldito, G., Fort, C. (2005) Statins reduce the incidence of lung cancer: a study of half a million US veterans. *J Clin Oncol*., 23: 1006.

Kiaffas, M.G., Powell, A.J., Geva, T. (2002) Magnetic resonance imaging evaluation of cardiac tumor characteristics in infants and children. *Am J Cardiol.*, 89: 1229-1233.

Kim, B.K., Kim II, Y., Kim, W.H. (2000) Hamartomatous gastric polyposis in a patient with tuberous sclerosis. *J Korean Med Sci.,* 15: 467-470.

Kim, E., Goraksha-Hicks, P., Li, L., Neufeld, T.P., Guan, K.L. (2008) Regulation of TORC1 by Rag GTPases in nutrient response. *Nat Cell Biol.*, 10: 935-945.

Kim, N.R., Chung, M.P., Park, C.K., Lee, K.S., Han, J. (2003) Pulmonary lymphangioleiomyomatosis and multiple hepatic angiomyolipomas in a man. *Pathol Int.*, 53: 231-235.

Kim, S.K., Wang, K.C., Cho, B.K., Jung, H.W., Lee, Y.J., Chung, Y.S., Lee, J.Y., Park, S.H., Kim, Y.M., Choe, G., Chi, J.G. (2001) Biological behavior and tumorigenesis of subependymal giant cell astrocytomas. *J Neurooncol.*, 52: 217-225.

Kirpicznik, J. (1910) Ein Fall von tuberöser Sklerose und gleichzeitigen multiplen Nierengeschwülsten. *Virchows Arch. F. Path Anat*., 202: 358.

Kisfalvi, K., Eibl, G., Sinnett-Smith, J., Rozengurt, E. (2009) Metformin disrupts crosstalk between G protein-coupled receptor and insulin receptor signaling systems and inhibits pancreatic cancer growth. *Cancer Res*., 69: 6539-6545.

Knudson Jr., A.G. (1971) Mutation and cancer: statistical study of retinoblastoma. *Proc Natl Acad Sci U S A.*, 68: 820-823.

Kobayashi, T., Hirayama, Y., Kobayashi, E., Kubo, Y., Hino, O. (1995) A gemline insertion in the tuberous sclerosis (Tsc2) gene gives rise to the Eker rat model of dominantly inherited cancer, *Nat. Genet*., 9: 70-74.

Kobayashi, T., Urakami, S., Hirayama, Y., Yamamoto, T., Nishizawa, M., Takahara, T., Kubo, Y., Hino, O. (1997) Intragenic Tsc2 somatic mutations as Knudson's second hit in spontaneous and chemically induced renal carcinomas in the Eker rat model. *Jpn J Cancer Res.*, 88: 254-261.

Kobayashi, T., Minowa, O., Kuno, J., Mitani, H., Hino, O., and Noda, T. (1999) Renal carcinogenesis, hepatic hemangiomatosis, and embryonic lethality caused by a germ-line Tsc2 mutation in mice. *Cancer Res.*, 59: 1206-1211.

Kobayashi, T., Minowa, O., Sugitani, Y., Takai, S., Mitani, H., Kobayashi, E., Noda, T., and Hino, O. (2001) A germ-line Tsc1 mutation causes tumor development and embryonic lethality that are similar, but not identical to, those caused by Tsc2 mutation in mice. *Proc Natl Acad Sci USA*, 98: 8762-8767.

Kochhar, R., Khurana, V., Bejjanki, H., Caldito, G., Fort, C. (2005) Statins reduce breast cancer risk: a case control study in US female veterans. *J Clin Oncol*., 23: 514.

Koenig, M.K., Butler, I.J., Northrup, H. (2008) Regression of subependymal giant cell astrocytoma with rapamycin in tuberous sclerosis complex. *J Child Neurol*., 23: 1238-1239.

Kotulska, K., Borkowska, J., Jozwiak, S. (2013) Possible prevention of tuberous sclerosis complex lesions. *Pediatrics*., 132: e239-242.

Krueger, D.A., Care, M.M., Holland, K., Agricola, K., Tudor, C., Mangeshkar, P., Wilson, K.A., Byars, A., Sahmoud, T., Franz, D.N. (2010) Everolimus for subependymal giant-cell astrocytomas in tuberous sclerosis. *N Engl J Med.,* 363: 1801-1811.

Kubo, Y., Mitani, H., Hino, O. (1994) Allelic loss at the predisposing gene locus in spontaneous and chemically induced renal cell carcinomas in the Eker rat. *Cancer Res.*, 54: 2633-2635.

Kubo, Y., Kikuchi, Y., Mitani, H., Kobayashi, E., Kobayashi, T., Hino, O. (1995) Allelic loss at the tuberous sclerosis (Tsc2) gene locus in spontaneous uterine

leiomyosarcomas and pituitary adenomas in the Eker rat model. *Jpn J Cancer Res.,* 86: 828-832.

Kwiatkowska, J., Jozwiak, S., Hall, F., Henske, E.P., Haines, J.L., McNamara, P., Braiser, J., Wigowska-Sowinska, J., Kasprzyk-Obara, J., Short, M.P., Kwiatkowski, D.J. (1998) Comprehensive mutational analysis of the TSC1 gene: Observations on frequency of mutation, associated features, and nonpenetrance. *Ann Hum Genet.*, 62: 277-285.

Kwiatkowska, J., Wigowska-Sowinska, J., Napierala, D., Slomski, R., Kwiatkowski, D.J. (1999) Mosaicism in tuberous sclerosis as a potential cause of the failure of molecular diagnosis. *N Engl J Med*, 340: 703-707.

Kwiatkowski, D. (2005) TSC1, TSC2, TSC3? or mosaicism? *Eur J Hum Genet.*, 13: 695-696.

Kwiatkowski, D.J. (1996) A dense str map 1.5Mb region of 9q34: small reduction in the TSC1 critical region. In: Abstracts of the 5th International Chromosome 9 workshop; Oxford, UK. 17.

Kwiatkowski, D.J., Zhang, H., Bandura, J.L., Heiberger, K.M., Glogauer, M., el-Hashemite, N., and Onda, H. (2002) A mouse model of TSC1 reveals sex-dependent lethality from liver hemangiomas, and up-regulation of p70S6 kinase activity in Tsc1 null cells. *Hum Mol Genet.*, 11: 525-534.

Kwiatkowski, D.J. (2003) Rhebbing up mTOR: New insights on TSC1 and TSC2, and the pathogenesis of tuberous sclerosis. *Cancer Biol Ther.*, 2: 471-476.

Kwiatkowski, D.J., Whittemore, V.H., Thiele, E.A. (2010) Tuberous sclerosis complex: genes, clinical features and therapeutics. First edition, Wiley-Blackwell, Germany.

Lagos, J. C. and Gomez, M. R. (1967) Tuberous sclerosis: reappraisal of a clinical entity. *Mayo. Clin. Proc*., 42: 26-49.

Lamb, R.F., Roy, C., Diefenbach, T.J., Vinters, H.V., Johnson, M.W., Jay, D.G., Hall, A. (2000) The TSC1 tumour suppressor hamartin regulates cell adhesion through ERM proteins and the GTPase Rho. *Nat Cell Biol.*, 2: 281-287.

Lamming, D.W., Ye, L., Katajisto, P., Goncalves, M.D., Saitoh, M., Stevens, D.M., Davis, J.G., Salmon, A.B., Richardson, A., Ahima, R.S., Guertin, D.A., Sabatini, D.M., Baur, J.A. (2012) Rapamycin-induced insulin resistance is mediated by mTORC2 loss and uncoupled from longevity. *Science*, 335: 1638-1643.

Landman, G.W., Kleefstra, N., van Hateren, K.J., Groenier, K.H., Gans, R.O., Bilo, H.J. (2010) Metformin associated with lower cancer mortality in type 2 diabetes: ZODIAC-16. *Diabetes Care*, 33: 322-326.

Landschulz, W. H., Johnson, P. F., and McKnight, S. L. (1988). The leucine zipper: a hypothetical structure common to a new class of DNA binding proteins. *Science*, 240: 1759-1764.

Laplante, M., Sabatini, D.M. (2013) Regulation of mTORC1 and its impact on gene expression at a glance. *J Cell Sci*., 126: 1713-1719.

Leclerc, I., Woltersdorf, W.W., da Silva Xavier, G., Rowe, R.L., Cross, S.E., Korbutt, G.S., Rajotte, R.V., Smith, R., Rutter, G.A. (2004) Metformin, but not leptin, regulates AMP-activated protein kinase in pancreatic islets: impact on glucose-stimulated insulin secretion. *Am J Physiol Endocrinol Metab.,* 286: e1023-1031.

Lee, D.F., Kuo, H.P., Chen, C.T., Hsu, J.M., Chou, C.K., Wei, Y., Sun, H.L., Li, L.Y., Ping, B., Huang, W.C., He, X., Hung, J.Y., Lai, C.C., Ding, Q., Su, J.L., Yang, J.Y., Sahin, A.A., Hortobagyi, G.N., Tsai, F.J., Tsai, C.H., Hung, M.C. (2007) IKKb suppression of TSC1 links inflammation and tumor angiogenesis via the mTOR pathway, *Cell*, 130: 440-455.

Lee, L., Sudentas, P., Donohue, B., Asrican, K., Worku, A., Walker, V., Sun, Y., Schmidt, K., Albert, M.S., El-Hashemite, N., Lader, A.S., Onda, H., Zhang, H., Kwiatkowski, D.J., Dabora, S.L. (2005) Efficacy of a rapamycin analog (CCI-779) and IFN-γ in tuberous sclerosis mouse models. *Genes Chromosomes and Cancer*, 42: 213-227.

Lee, L., Sudentas, P., Dabora, S.L. (2006) Combination of a rapamycin analog (CCI-779) and interferon-gamma is more effective than single agents in treating a mouse model of tuberous sclerosis complex. *Genes Chromosomes Cancer*, 45: 933-944.

Lee, N., Woodrum, C.L., Nobil, A.M., Rauktys, A.E., Messina, M.P., Dabora, S.L. (2009) Rapamycin weekly maintenance dosing and the potential efficacy of combination sorafenib plus rapamycin but not atorvastatin or doxycycline in tuberous sclerosis preclinical models. *BMC Pharmacol*., 9: 8.

Leevers, S.J., Weinkove, D., MacDougall, L.K., Hafen, E., Waterfield, M.D. (1996) The drosophila phosphoinositide 3-kinase Dp 110 promotes cell growth. *EMBO Journal*, 15: 6584-6594.

Lemaitre, L., Robert, Y., Dubrulle, F., Claudon, M., Duhamel, A., Danjou, P., Mazeman, E. (1995) Renal angiomyolipoma: Growth followed up with CT and/or US. *Radiology*, 197: 598-602.

Lendvay, T.S., Broecker, B., Smith, E.A. (2002) Renal cell carcinoma in a 2-year-old child with tuberous sclerosis. *J Urol.*, 168: 1131-1132.

Levine, D., Barnes, P., Korf, B., Edelman, R. (2000) Tuberous sclerosis in the fetus: Second-trimester diagnosis of subependymal tubers with ultrafast MR imaging. *AJR Am J Roentgenol.*, 175: 1067-1069.

Li, D., Yeung, S.C., Hassan, M.M., Konopleva, M., Abbruzzese, J.L. (2009) Antidiabetic therapies affect risk of pancreatic cancer. *Gastroenterology*, 137:482-488.

Li, S., Takeuchi, F., Wang, J.A., Fan, Q., Komurasaki, T., Billings, E.M., Pacheco-Rodriguez, G., Moss, J., Darling, T.N. (2008) Mesenchymal-epithelial interactions involving epiregulin in tuberous sclerosis complex hamartomas. *Proc Natl Acad Sci U S A*., 105: 3539-3544.

Li, T., Wang, J., Wang, X., Yang, N., Chen, S.M., Tong, L.J., Yang, C.H., Meng, L.H., Ding, J. (2010) WJD008, a dual phosphatidylinositol 3-kinase (PI3K)/mammalian target of rapamycin inhibitor, prevents PI3K signaling and inhibits the proliferation of transformed cells with oncogenic PI3K mutant. *J Pharmacol Exp Ther.,* 334: 830-838.

Li, Y., Inoki, K., Yeung, R., Guan, K.L. (2002) Regulation of TSC2 by 14-3-3 binding. *J Biol Chem.*, 277: 44593-44596.

Li, Y., Inoki, K., Vacratsis, P., Guan, K.L. (2003) The p38 and MK2 kinase cascade phosphorylates tuberin, the tuberous sclerosis 2 gene product, and enhances its interaction with 14-3-3. *J. Biol. Chem*., 278: 13663-13671.

Libby, G., Donnelly, L.A., Donnan, P.T., Alessi, D.R., Morris, A.D., Evans, J.M. (2009) New users of metformin are at low risk of incident cancer: a cohort study among people with type 2 diabetes. *Diabetes Care*, 32: 1620-1625.

Lie, J.T. (1991) Cardiac, pulmonary, and vascular involvements in tuberous sclerosis. *Ann N Y Acad Sci.*, 615: 58-70.

Lin, C.N., Chiang, H.S., Hsu, S.I., Huang, A.H., Chuang, S.S. (1994) Renal angiomyolipoma with a prominent angiomatous component and extramedullary hematopoiesis: a case report. *Zhonghua yi xue za zhi Chinese medical journal; Free China ed, 53*: 185-187.

Lin, T.A., Kong, X., Haystead, T.A., Pause, A., Belsham, G., Sonenberg, N., Lawrence Jr., J.C. (1994) PHAS-I as a link between mitogen-activated protein kinase and translation initiation. *Science*, 266: 653-656.

Liu, B., Fan, Z., Edgerton, S.M., Deng, X.S., Alimova, I.N., Lind, S.E. Thor, A.D. (2009) Metformin induces unique biological and molecular responses in triple negative breast cancer cells. *Cell Cycle*, 8: 2031-2040.

Liu, L., Cash, T.P., Jones, R.G., Keith, B., Thompson, C.B., Simon, M.C. (2006) Hypoxia-induced energy stress regulates mRNA translation and cell growth. *Mol Cell.*, 21: 521-531.

Liu, M., Wilk, S.A., Wang, A., Zhou, L., Wang, R.H., Ogawa, W., Deng, C., Dong, L.Q., Liu, F. (2010) Resveratrol inhibits mTOR signaling by promoting the interaction between mTOR and DEPTOR. *J Biol Chem*., 285: 36387-36394.

Lizcano, J.M., Goransson, O., Toth, R., Deak, M., Morrice, N.A., Boudeau, J., Hawley, S.A., Udd, L., Makela, T.P., Hardie, D.G., Alessi, D.R. (2004) LKB1 is a master kinase that activates 13 kinases of the AMPK subfamily, including MARK/PAR-1. *The EMBO Journal*, 23: 833-843.

Lo, W.L., Wong, C.K. (1993) Localized pachydermodactyly in tuberous sclerosis. *Clin Exp Dermatol.*, 18: 146-147.

Loewith, R., Jacinto, E., Wullschleger, S., Lorberg, A., Crespo, J.L., Bonenfant, D., Oppliger, W., Jenoe, P., and Hall, M.N. (2002). Two TOR complexes, only one of which is rapamycin sensitive, have distinct roles in cell growth control. *Mol. Cell*, 10: 457-468.

López-Fauqued, M., Gil, R., Grueso, J., Hernandez-Losa, J., Pujol, A., Moliné, T., Recio, J.A. (2010) The dual PI3K/mTOR inhibitor PI-103 promotes immunosuppression, in vivo tumor growth and increases survival of sorafenib-treated melanoma cells. *Int J Cancer*., 126: 1549-1561.

Lou, D., Griffith, N., Noonan, D.J. (2001) The tuberous sclerosis 2 gene product can localize to nuclei in a phosphorylation-dependent manner. *Mol Cell Biol Res Commun.*, 4: 374-380.

Lyons, S.K. (2005) Advances in imaging mouse tumour models in vivo. *J Pathol.,* 205: 194-205.

Ma, L., Chen, Z., Erdjument-Bromage, H., Tempst, P., Pandolfi, P.P. (2005) Phosphorylation and functional inactivation of TSC2 by Erk: implications for tuberous sclerosisand cancer pathogenesis. *Cell*, 121: 179-193.

Mader, S., Lee, H., Pause, A., Sonenberg, N. (1995) The translation initiation factor eIF-4E binds to a common motif shared by the translation factor eIF-4γ and the translational repressors 4E-binding proteins. *Mol Cell Biol.*, 15: 4990-4997.

Maheshwar, M.M., Cheadle, J.P., Jones, A.C., Myring, J., Fryer, A.E., Harris, P.C., Sampson, J.R. (1997) The GAP-related domain of tuberin, the product of the TSC2 gene, is a target for missense mutations in tuberous sclerosis. *Hum Mol Genet.*, 6: 1991-1996.

Maira, S.M., Stauffer, F., Brueggen, J., Furet, P., Schnell, C., Fritsch, C., Brachmann, S., Chène, P., De Pover, A., Schoemaker, K., Fabbro, D., Gabriel, D., Simonen, M., Murphy, L., Finan, P., Sellers, W., García-Echeverría, C. (2008) Identification and characterization of NVP-BEZ235, a new orally available dual phosphatidylinositol 3-kinase/mammalian target of rapamycin inhibitor with potent in vivo antitumor activity. *Mol Cancer Ther*., 7: 1851-1863.

Mak, B.C., Kenerson, H.L., Aicher, L.D., Barnes, E.A., Yeung, R.S. (2005) Aberrant β-catenin signaling in tuberous sclerosis. *Am J Pathol.*, 167: 107-116.

Manning, B.D., Tee, A.R., Logsdon, M.Nicole, Blenis, J., Cantley, L.C. (2002) Identification of the tuberous sclerosis complex-2 tumor suppressor gene product tuberin as a target of the phosphoinositide 3-kinase/Akt pathway. *Mol Cell.*, 10: 151-162.

Manning, B.D. (2004) Balancing Akt with S6K: implications for both metabolic diseases and tumorigenesis. *J. Cell Biol*. 167: 399-403.

Manning, B.D., Cantley, L.C. (2007) AKT/PKB Signaling: Navigating Downstream. *Cell*, 129: 1261-1274.

Martiniova, L., Kotys, M.S., Thomasson, D., Schimel, D., Lai, E.W., Bernardo, M., Merino, M.J., Powers, J.F., Ruzicka, J., Kvetnansky, R., Choyke, P.L., Pacak, K. (2009) Noninvasive monitoring of a murine model of metastatic pheochromocytoma: a comparison of contrast-enhanced microCT and nonenhanced MRI. *J Magn Reson Imaging*, 29: 685-691.

Massey-Harroche, D., Delgrossi, M.H., Lane-Guermonprez, L., Arsanto, J.P., Borg, J.P., Billaud, M., Le Bivic, A. (2007) Evidence for a molecular link between the tuberous sclerosis complex and the Crumbs complex. *Hum Mol Genet.*, 16: 529-536.

McWilliam, R.C., Stephenson, J.B. (1978) Depigmented hair. The earliest sign of tuberous sclerosis. *Arch Dis Child.*, 53: 961-963.

Meikle, L., McMullen, J.R., Sherwood, M.C., Lader, A.S., Walker, V., Chan, J.A., Kwiatkowski, D.J. (2005) A mouse model of cardiac rhabdomyoma generated by loss of Tsc1 in ventricular myocytes. *Hum Mol Genet*.14: 429-435.

Meikle, L., Talos, D.M., Onda, H., Pollizzi, K., Rotenberg, A., Sahin, M., Jensen, F.E., Kwiatkowski, D.J. (2007) A mouse model of tuberous sclerosis: neuronal loss of Tsc1 causes dysplastic and ectopic neurons, reduced myelination, seizure activity, and limited survival. *J Neurosci.,* 27: 5546-5558.

Meikle, L., Pollizzi, K., Egnor, A., Kramvis, I., Lane, H., Sahin, M., Kwiatkowski, D.J. (2008) Response of a neuronal model of tuberous sclerosis to mammalian target of rapamycin (mTOR) inhibitors: Effects on mTORC1 and Akt signaling lead to improved survival and function. *J Neurosci*., 28: 5422-5432.

Memmott, R.M., Mercado, J.R., Maier, C.R., Kawabata, S., Fox, S.D., Dennis, P.A. (2010) Metformin prevents tobacco carcinogen-induced lung tumorigenesis. *Cancer Prev Res (Phila),* 3: 1066-1076.

Mencía-Gutiérrez, E., Gutiérrez-Díaz, E., Ricoy, J.R., Sánez-Madrazo, N. (2004) Eyelid and cutaneous lesions as the sole indicators of tuberous sclerosis. *Arch Soc Esp Oftalmol.*, 79: 401-404.

Mennel, S., Meyer, C.H., Peter, S., Schmidt, J.C., Kroll, P. (2007) Current treatment modalities for exudative retinal hamartomas secondary to tuberous sclerosis: Review of the literature. *Acta Ophthalmol Scand.*, 85: 127-132.

Menon, S., Yecies, J.L., Zhang, H.H., Howell, J.J., Nicholatos, J., Harputlugil, E., Bronson, R.T., Kwiatkowski, D.J., Manning, B.D. (2012) Chronic activation of mTOR

complex 1 is sufficient to cause hepatocellular carcinoma in mice. *Sci Signal*., 5: ra24.

Messina, M.P., Rauktys, A., Lee, L., Dabora, S.L. (2007) Tuberous sclerosis preclinical studies: Timing of treatment, combination of a rapamycin analog (CCI-779) and interferon-gamma, and comparison of rapamycin to CCI-779. *BMC Pharmacol.*, 7: art. no. 14.

Miller, I.D., Gray, E.S., Lloyd, D.L. (1989) Unilateral cystic disease of the neonatal kidney: A rare presentation of tuberous sclerosis. *Histopathology*, 14: 529-532.

Miyake, M., Tateishi, U., Maeda, T., Kusumoto, M., Satake, M., Arai, Y., Sugimura, K. (2005) Pulmonary lymphangioleiomyomatosis in a male patient with tuberous sclerosis complex. *Radiat Med.*, 23: 525-527.

Mizuguchi, M., Takashima, S., Yamanouchi, H., Nakazato, Y., Mitani, H., Hino, O. (2000) Novel cerebral lesions in the Eker rat model of tuberous sclerosis: Cortical tuber and anaplastic ganglioglioma. *J Neuropathol Exp Neurol.*, 59: 188-196.

Mizuguchi, M., Takashima, S. (2001) Neuropathology of tuberous sclerosis. *Brain Dev.*, 23: 508-515.

Molckovsky, A., Siu, L.L. (2008) First-in-class, first-in-human phase I results of targeted agents: highlights of the 2008 American society of clinical oncology meeting. *J Hematol Oncol*., 1: 20.

Montagne, J., Stewart, M.J., Stocker, H., Hafen, E., Kozma, S.C., Thomas, G. (1999) Drosophila S6 kinase: A regulator of cell size. *Science*, 285: 2126-2129.

Moolten, S.E. (1942) Hamartial nature of the tuberous sclerosis complex and its bearing on the tumor problem: report of one case with tumor anomaly of the kidney and adenoma sebaceum. *Arch. Intern. Med*., 69: 589-623.

Moore, C.E., Xie, J., Gomez, E., Herbert, T.P. (2009) Identification of cAMP-Dependent Kinase as a Third in Vivo Ribosomal Protein S6 Kinase in Pancreatic β-Cells. *J Mol Biol*., 389: 480-494.

Morton, J.M., McLean, C., Booth, S.S., Snell, G.I., Whitford, H.M. (2008) Regression of pulmonary lymphangioleiomyomatosis (PLAM)-associated retroperitoneal angiomyolipoma post-lung transplantation with rapamycin treatment. *J Heart Lung Transplant.*, 27: 462-465.

Moss, J.G., Hendry, G.M. (1988) The natural history of renal cysts in an infant with tuberous sclerosis: Evaluation with ultrasound. *Br J Radiol.*, 61:1074-1076.

Mouchiroud, L., Molin, L., Dalliere, N., Solari, F. (2010) Life span extension by resveratrol, rapamycin, and metformin: The promise of dietary restriction mimetics for an healthy aging. *Biofactors,* 36: 377-382.

Muir, T.E., Leslie, K.O., Popper, H., Kitaichi, M., Gagné, E., Emelin, J.K., Vinters, H.V., Colby, T.V. (1998) Micronodular pneumocyte hyperplasia. *Am J Surg Pathol.*, 22: 465-472.

Murgia, M.G., Jordan, S., Kahan, B.D. (1996) The side effect profile of sirolimus: A phase I study in quiescent cyclosporine-prednisone-treated renal transplant patients. *Kidney Int.*, 49: 209-216.

Nellist, M., Van Slegtenhorst, M.A., Goedbloed, M., Van Den Ouweland, A.M., Halley, D.J., Van Der Sluijs, P. (1999) Characterization of the cytosolic tuberin-hamartin complex. Tuberin is a cytosolic chaperone for hamartin. *J Biol Chem.*, 274: 35647-35652.

Nellist, M., Goedbloed, M.A., Halley, D.J. (2003) Regulation of tuberous sclerosis complex (TSC) function by 14-3-3 proteins. *Biochem Soc Trans.*, 31: 587-591.

Nellist, M., Sancak, O., Goedbloed, M.A., Rohe, C., van Netten, D., Mayer, K., Tucker-Williams, A., van den Ouweland, A.M., Halley, D.J. (2005) Distinct effects of single amino-acid changes to tuberin on the function of the tuberin-hamartin complex. *Eur J Hum Genet.*, 13: 59-68.

Nevin, N.C., Pearce, W.G. (1968) Diagnostic and genetical aspects of tuberous sclerosis. *J Med Genet.*, 5: 273-280.

Nickel, W.R., Reed, W.B. (1962) Tuberous sclerosis. Special reference to the microscopic alterations in the cutaneous hamartomas. *Arch Dermatol.*, 85: 209-226.

Niida, Y., Lawrence-Smith, N., Banwell, A., Hammer, E., Lewis, J., Beauchamp, R.L., Sims, K., Ramesh, V., and Ozelius, L. (1999). Analysis of both TSC1 and TSC2 for germline mutationsin 126 unrelated patients with tuberous sclerosis. *Hum. Mutat*., 14: 412-422.

Niida, Y., Stemmer-Rachamimov, A.O., Logrip, M., Tapon, D., Perez, R., Kwiatkowski, D.J., Sims, K., MacCollin, M., Louis, D.N., Ramesh, V. (2001) Survey of somatic mutations in tuberous sclerosis complex (TSC) hamartomas suggests different genetic mechanisms for pathogenesis of TSC lesions. *Am J Hum Genet.*, 69: 493-503.

Nir, A., Tajik, A.J., Freeman, W.K., Seward, J.B., Offord, K.P., Edwards, W.D., Mair, D.D., Gomez, M.R. (1995) Tuberous sclerosis and cardiac rhabdomyoma. *Am J Cardiol.*, 76: 419-421.

Nojima, H., Tokunaga, C., Eguchi, S., Oshiro, N., Hidayat, S., Yoshino, K., Hara, K., Tanaka, N., Avruch, J., and Yonezawa, K. (2003) The mammalian target of rapamycin (mTOR) partner, raptor, binds the mTOR substrates p70 S6 kinase and 4E-BP1 through their TOR signaling (TOS) motif. *J. Biol. Chem*., 278: 15461-15464.

Noonan, D.J., Lou, D., Griffith, N., Vanaman, T.C. (2002) A calmodulin binding site in the tuberous sclerosis 2 gene product is essential for regulation of transcription events and is altered by mutations linked to tuberous sclerosis and lymphangioleiomyomatosis. *Arch Biochem Biophys.*, 398: 132-140.

Northrup, H., Beaudet, A.L., O'Brien, W.E., Herman, G.E., Lewis, R.A., Pollack, M.S. (1987) Linkage of tuberous sclerosis to ABO blood group. *Lancet*., 2: 804-805.

Northrup, H., Kwiatkowski, D.J., Roach, E.S., Dobyns, W.B., Lewis, R.A., Herman, G.E., Rodriguez Jr., E., Daiger, S.P., Blanton, S.H. (1992) Evidence for genetic heterogeneity in tuberous sclerosis: One locus on chromosome 9 and at least one locus elsewhere. *Am J Hum Genet.*, 51: 709-720.

O'Callaghan, F.J., Shiell, A.W., Osborne, J.P., Christopher, N. Martyn, C.N. (1998) Prevalence of tuberous sclerosis estimated by capture-recapture analysis. *The Lancet*, 351: 1490.

Oldham, S., Montagne, J., Radimerski, T., Thomas, G., Hafen, E. (2000) Genetic and biochemical characterization of dTOR, the Drosophila homolog of the target of rapamycin *Genes Dev*., 14: 2689-2694.

Oldham, S., Hafen, E. (2003) Insulin/IGF and target of rapamycin signaling: A TOR de force in growth control. *Trends Cell Biol.*, 13: 79-85.

Onda, H., Lueck, A., Marks, P.W., Warren, H.B., Kwiatkowski, D.J. (1999) Tsc2 (+/-) mice develop tumors in multiple sites that express gelsolin and are influenced by genetic background. *J Clin Invest.*, 104: 687-695.

Onken, B., Driscoll, M. (2010) Metformin induces a dietary restriction-like state and the oxidative stress response to extend C. elegans Healthspan via AMPK, LKB1, and SKN-1. *PLoS One,* 5: e8758.

O'Reilly, K.E., Rojo, F., She, Q.B., Solit, D., Mills, G.B., Smith, D., Lane, H., Hofmann, F., Hicklin, D.J., Ludwig, D.L., Baselga, J., Rosen, N. (2006) mTOR inhibition induces upstream receptor tyrosine kinase signaling and activates Akt. *Cancer Res.*, 66: 1500-1508.

Orlova, K.A., Crino, P.B. (2010) The tuberous sclerosis complex. *Ann N Y Acad Sci.*, 1184: 87-105.

Osborne, J.P., Fryer, A., Webb, D. (1991) Epidemiology of tuberous sclerosis. *Ann. N. Y. Acad. Sci.*, 615: 125-127.

Ou, Y.C., Wu, H.C., Yang, C.R., Chang, C.L., Hwang, T.I., Chang, C.H. (1991) Renal angiomyolipoma: experience of 23 patients. *Zhonghua yi xue za zhi Chinese medical journal; Free China ed.,* 48: 217-223.

Pan, D., Dong, J., Zhang, Y., Gao, X. (2004) Tuberous sclerosis complex: From Drosophila to human disease. *Trends Cell Biol.*, 14: 78-85.

Pandit, P., Johnston, S.M., Qi, Y., Story, J., Nelson, R., Johnson, G.A. (2013) The Utility of Micro-CT and MRI in the Assessment of Longitudinal Growth of Liver Metastases in a Preclinical Model of Colon Carcinoma. *Acad Radiol*., 20: 430-439.

Park, S.H., Pepkowitz, S.H., Kerfoot, C., De Rosa, M.J., Poukens, V., Wienecke, R., DeClue, J.E., Vinters, H.V. (1997) Tuberous sclerosis in a 20-week gestation fetus: Immunohistochemical study. *Acta Neuropathol.*, 94: 180-186.

Parry, L., Maynard, J.H., Patel, A., Clifford, S.C., Morrissey, C., Maher, E.R., Cheadle, J.P., Sampson, J.R. (2001) Analysis of the TSC1 and TSC2 genes in sporadic renal cell carcinomas. *Br J Cancer.,* 85, 1226-1230.

Patel, P.H., Thapar, N., Guo, L., Martinez, M., Maris, J., Gau, C.L., Lengyel, J.A., Tamanoi, F. (2003) Drosophila Rheb GTPase is required for cell cycle progression and cell growth. *J Cell Sci.*, 116: 3601-3610.

Paulson, G.W., Lyle, C.B. (1966) Tuberous sclerosis. *Dev Med Child Neurol*., 8: 571-586.

Pearson, R.B., Dennis, P.B., Man, J.W., Williamson, N.A., Kozma, S.C., Wettenhall, R.E., Thomas, G. (1995) The principal target of rapamycin-induced p70s6k

inactivation is a novel phosphorylation site within a conserved hydrophobic domain. *EMBO J.*, 14: 5279-5287.

Pellizzi, G.B., (1901) Contributo all'istologia ed alla patogenesi dei tumori di tessuto nervosa. Rivista *Sperimentale di Freniatria*.

Penrose, L.S. (1938) *A clinical and Genetic study of 1280 Cases of Mental Defect*. Monograph No 229. London: His Majesty's Stationery Office; 159.

Perusini, G. (1905) Über einen Fall von Sclerosis tuberosa hypertrophica.(Istioatipia corticale disseminata von Pellizzi.), *Mschr Psychiat Neurol*.,17: 352-367.

Pierotti, M.A, Berrino, F., Gariboldi, M., Melani, C., Mogavero, A., Negri, T., Pasanisi, P., Pilotti, S. (2013) Targeting metabolism for cancer treatment and prevention: metformin, an old drug with multi-faceted effects. *Oncogene*, 32: 1475-1487.

Plank, T.L., Yeung, R.S., Henske, E.P. (1998) Hamartin, the product of the tuberous sclerosis 1 (TSC1) gene, interacts with tuberin and appears to be localized to cytoplasmic vesicles. *Cancer Res.*, 58: 4766-4770.

Pollizzi, K., Malinowska-Kolodziej, I., Doughty, C., Betz, C., Ma, J., Goto, J., Kwiatkowski, D.J. (2009) A hypomorphic allele of Tsc2 highlights the role of TSC1/TSC2 in signaling to AKT and models mild human TSC2 alleles. *Hum Mol Genet.*, 18: 2378-2387.

Pollizzi K., Malinowska-Kolodziej I, Stumm M, Lane H, Kwiatkowski D. (2009) Equivalent benefit of mTORC1 blockade and combined PI3K-mTOR blockade in a mouse model of tuberous sclerosis. *Mol Cancer*. 8: 38.

Potter, C.J., Huang, H., Xu, T. (2001) Drosophila Tsc1 functions with Tsc2 to antagonize insulin signaling in regulating cell growth, cell proliferation, and organ size. *Cell*, 105: 357-368.

Povey, S., Burley, M.W., Attwood, J., Benham, F., Hunt, D., Jeremiah, S.J., Franklin, D., Gillett, G., Malas, S., Robson, E.B., Tippett, P., Edwards, J.H., Kwiatkowski, D.J., Super, M., Mueller, R., Fryer, A., Clarke, A., Webb, D., Osborne, J. (1994) Two loci for Tuberous Sclerosis: One on 9q34 and one on 16p13. *Ann Hum Genet.*, 58: 107-127.

Poynter, J.N., Gruber, S.B., Higgins, P.D., Almog, R., Bonner, J.D., Rennert, H.S., Low, M., Greenson, J.K., Rennert, G. (2005) Statins and the risk of colorectal cancer. *N Engl J Med*., 352: 2184-2192.

Prather, P., de Vries, P.J. (2004) Behavioral and cognitive aspects of tuberous sclerosis complex. *J Child Neurol.*, 19: 666-674.

Pringle, J.J. (1890) A case of congenital adenoma sebaceum. *Br. J. Dermatol.* 2: 1-14.

Qin, W., Kozlowski, P., Taillon, B.E., Bouffard, P., Holmes, A.J., Janne, P., Camposano, S., Thiele, E., Franz, D., Kwiatkowski, D.J. (2010) Ultra deep sequencing detects a low rate of mosaic mutations in tuberous sclerosis complex. *Hum Genet.*, 127: 573-582.

Rachdi, L., Balcazar, N., Osorio-Duque, F., Elghazi, L., Weiss, A., Gould, A., Chang-Chen, K.J., Gambello, M.J., Bernal-Mizrachi, E. (2008) Disruption of Tsc2 in

pancreatic beta cells induces beta cell mass expansion and improved glucose tolerance in a TORC1-dependent manner. *Proc Natl Acad Sci U S A*., 105: 9250-9255.

Radimerski, T., Montagne, J., Hemmings-Mieszczak, M., Thomas, G. (2002) Lethality of Drosophila lacking TSC tumor suppressor function rescued by reducing ds6K signalling. *Genes Dev.*, 16: 2627-2632.

Rakowski, S.K., Winterkorn, E.B., Paul, E., Steele, D.J., Halpern, E.F., Thiele, E.A. (2006) Renal manifestations of tuberous sclerosis complex: Incidence, prognosis, and predictive factors. *Kidney Intl*., 70: 1777-1782.

Raught, B., Peiretti, F., Gingras, A.C., Livingstone, M., Shahbazian, D., Mayeur, G.L., Polakiewicz, R.D., Sonenberg, N., Hershey, J.W. (2004) Phosphorylation of eucaryotic translation initiation factor 4B Ser422 is modulated by S6 kinases. *EMBO J.*, 23: 1761-1769.

Rauktys, A., Lee, N., Lee, L., Dabora, S.L. (2008) Topical rapamycin inhibits tuberous sclerosis tumor growth in a nude mouse model. *BMC Dermatol*., 8:1.

Rayer, P.F.O. (1835) *Traité théorique et pratique des maladies de la peau*, 2nd edn, JB Baillière, Paris.

Reeders, S.T., Breuning, M.H., Davies, K.E., Nicholls, R.D., Jarman, A.P., Higgs, D.R., Pearson, P.L., Weatherall, D.J. (1985) A highly polymorphic DNA marker linked to adult polycystic kidney disease on chromosome 16. *Nature*, 317: 542-544.

Reiling, J.H., Hafen, E. (2004) The hypoxia-induced paralogs Scylla and Charybdis inhibit growth by down-regulating S6K activity upstream of TSC in Drosophila. *Genes Dev.*, 18: 2879-2892.

Ridley, A. J., Hall, A. (1992) The small GTP-binding protein rho regulates the assembly of focal adhesions and actin stress fibers in response to growth factors. *Cell*, 70: 389-399.

Rintelen, F., Stocker, H., Thomas, G., Hafen, E. (2001) PDK1 regulates growth through Akt and S6K in Drosophila. *Proc Natl Acad Sci U S A.*, 98: 15020-15025.

Roach, E.S., Smith, M., Huttenlocher, P., Bhat, M., Alcorn, D., Hawley, L. (1992) Report of the Diagnostic Criteria Committee of the National Tuberous Sclerosis Association. *J Child Neurol.*, 7: 221-224.

Roach, E.S., Gomez, M.R., Northrup, H., (1998) Tuberous sclerosis complex consensus conference: revised clinical diagnostic criteria. *J Child Neurol.,* 13: 624-628.

Roach, E.S., Sparagana, S.P. (2004) Diagnosis of tuberous sclerosis complex. *J Child Neurol*., 19: 643-649.

Roberts, P.S., Dabora, S., Thiele, E.A., Franz, D.N., Jozwiak, S., Kwiatkowski, D.J. (2004) Somatic mosaicism is rare in unaffected parents of patients with sporadic tuberous sclerosis. *J Med Genet.*, 41: e69.

Robertson, D.M. (1991) Ophthalmic manifestations of tuberous sclerosis. *Ann N Y Acad Sci.*, 615: 17-25.

Robertson, F.M., Cendron, M., Klauber, G.T., Harris, B.H. (1996) Renal cell carcinoma in association with tuberous sclerosis in children. *J Pediatr Surg.*, 31: 729-730.

Rogers, G.W. Jr., Richter, N.J., Lima, W.F., Merrick, W.C. (2001) Modulation of the helicase activity of eIF4A by eIF4B, eIF4H, and eIF4F. J. *Biol. Chem*., 276: 30914-30922.

Rose, V.M., Au, K.S., Pollom, G., Roach, E.S., Prashner, H.R., Northrup, H. (1999) Germ-line mosaicism in tuberous sclerosis: How common? *Am J Hum Genet.*, 64: 986-992.

Rosenberg, D.W., Giardina, C., Tanaka, T. (2009) Mouse models for the study of colon carcinogenesis. *Carcinogenesis*, 30: 183-196.

Rosner, M., Hanneder, M., Siegel, N., Valli, A., Hengstschläger, M. (2008) The tuberous sclerosis gene products hamartin and tuberin are multifunctional proteins with a wide spectrum of interacting partners. *Mutat Res.*, 658: 234-246.

Ross, A.T., Dickerson, W.W. (1943) Tuberous sclerosis. *Arch. Neurol. Psychiatry*., 50: 233-257.

Rosser, T., Panigrahy, A., McClintock, W. (2006) The Diverse Clinical Manifestations of Tuberous Sclerosis Complex: A Review. *Semin Pediatr Neurol.*, 13: 27-36.

Roux, P.P., Ballif, B.A., Anjum, R., Gygi, S.P., Blenis, J. (2004). Tumor-promoting phorbol esters and activated Ras inactivate the tuberous sclerosis tumor suppressor complex via p90 ribosomal S6 kinase. *Proc. Natl. Acad. Sci. USA*, 101: 13489-13494.

Rowley, S.A., O'Callaghan, F.J., Osborne, J.P. (2001) Ophthalmic manifestations of tuberous sclerosis: A population based study. *Br J Ophthalmol.*, 85: 420-423.

Rubin, G.M., Yandell, M.D., Wortman, J.R., Gabor Miklos, G.L., Nelson, C.R., Hariharan, I.K., Fortini, M.E., Li, P.W., Apweiler, R., Fleischmann, W., Cherry, J.M., Henikoff, S., Skupski, M.P., Misra, S., Ashburner, M., Birney, E., Boguski, M.S., Brody, T., Brokstein, P., Celniker, S.E., Chervitz, S.A., Coates, D., Cravchik, A., Gabrielian, A., Galle, R.F., Gelbart, W.M., George, R.A., Goldstein, L.S., Gong, F., Guan, P., Harris, N.L., Hay, B.A., Hoskins, R.A., Li, J., Li, Z., Hynes, R.O., Jones, S.J., Kuehl, P.M., Lemaitre, B., Littleton, J.T., Morrison, D.K., Mungall, C., O'Farrell, P.H., Pickeral, O.K., Shue, C., Vosshall, L.B., Zhang, J., Zhao, Q., Zheng, X.H., Lewis, S. (2000) Comparative genomics of the eukaryotes. *Science*, 287: 2204-2215.

Ruvinsky, I., Meyuhas, O. (2006) Ribosomal protein S6 phosphorylation: from protein synthesis to cell size. *Trends Biochem Sci.*, 31: 342-348.

Sabatini, D.M., Erdjument-Bromage, H., Lui, M., Tempst, P., Snyder, S.H. (1994) RAFT1: A mammalian protein that binds to FKBP12 in a rapamycin-dependent fashion and is homologous to yeast TORs. *Cell*, 78: 35-43.

Saguem, M.H., Laarif, M., Remadi, S., Bozakoura, C., Cox, J.N. (1992) Diffuse bilateral glomerulocystic disease of the kidneys and multiple cardiac rhabdomyomas in a newborn. Relationship with tuberous sclerosis and review of the literature. *Pathol Res Pract.*, 188: 367-373.

Sampson, J.R., Scahill, S.J., Stephenson, J.B., Mann, L., Connor, J.M. (1989) Genetic aspects of tuberous sclerosis in the west of Scotland. *J Med Genet.*, 26: 28-31.

Sampson, J.R., Janssen, L.A., Sandkuijl, L.A. (1992) Linkage investigation of three putative tuberous sclerosis determining loci on chromosomes 9q, 11q, and 12q. *J Med Genet.*, 29: 861-866.

Sampson, J.R., Maheshwar, M.M., Aspinwall, R., Thompson, P., Cheadle, J.P., Ravine, D., Roy, S., Haan, E., Bernstein, J., Harris, P.C. (1997) Renal cystic disease in tuberous sclerosis: Role of the polycystic kidney disease 1 gene. *Am J Hum Genet.*, 61: 843-851.

Sancak, O., Nellist, M., Goedbloed, M., Elfferich, P., Wouters, C., Maat-Kievit, A., Zonnenberg, B., Verhoef, S., Halley, D., van den Ouweland, A. (2005) Mutational analysis of the TSC1 and TSC2 genes in a diagnostic setting: Genotype-phenotype correlations and comparison of diagnostic DNA techniques in tuberous sclerosis complex. *Eur J Hum Genet.*, 13: 731-741.

Sancak, Y., Peterson, T.R., Shaul, Y.D., Lindquist, R.A., Thoreen, C.C., Bar-Peled, L., Sabatini, D.M. (2008) The rag GTPases bind raptor and mediate amino acid signaling to mTORC1. *Science*, 320: 1496-1501.

Santarosa, M., Ashworth, A. (2004) Haploinsufficiency for tumour suppressor genes: When you don't need to go all the way. *Biochim Biophys Acta.*, 1654: 105-122.

Sarbassov, D.D., Ali, S.M., Kim, D.H., Guertin, D.A., Latek, R.R., Erdjument-Bromage, H., Tempst, P., Sabatini, D.M. (2004) Rictor, a novel binding partner of mTOR, defines a rapamycin-insensitive and raptor-independent pathway that regulates the cytoskeleton. *Curr Biol*., 14: 1296-302.

Sarbassov, D.D., Guertin, D.A., Ali, S.M., Sabatini, D.M. (2005) Phosphorylation and regulation of Akt/PKB by the rictor-mTOR complex. *Science*, 307: 1098-1101.

Sarbassov, D.D., Ali, S.M., Sengupta, S., Sheen, J.H., Hsu, P.P., Bagley, A.F., Markhard, A.L., Sabatini, D.M. (2006) Prolonged Rapamycin Treatment Inhibits mTORC2 Assembly and Akt/PKB. *Molecular Cell*, 22: 159-168.

Saucedo, L.J., Gao, X., Chiarelli, D.A., Li, L., Pan, D., Edgar, B.A. (2003) Rheb promotes cell growth as a component of the insulin/TOR signalling network. *Nat Cell Biol.,* 5: 566-571.

Schillinger, F., Montagnac, R. (1996) Chronic renal failure and its treatment in tuberous sclerosis. *Nephrol Dial Transplant.*, 11: 481-485.

Schuler, W., Sedrani, R., Cottens, S., Häberlin, B., Schulz, M., Schuurman, H.J., Zenke, G., Zerwes, H.G., Schreier, M.H. (1997) SDZ RAD, a new rapamycin derivative: Pharmacological properties in vitro and in vivo. *Transplantation*, 64: 36-42.

Scott, R.C., Juhász, G., Neufeld, T.P. (2007) Direct Induction of Autophagy by Atg1 Inhibits Cell Growth and Induces Apoptotic Cell Death. *Curr Biol.*, 17: 1-11.

Sehgal, S.N., Baker, H., Vézina, C. (1975) Rapamycin (AY-22,989), a new antifungal antibiotic. II. Fermentation, isolation and characterization. *J Antibiot (Tokyo)*. 28: 727-732.

Sekiguchi, T., Hirose, E., Nakashima, N., Ii, M., Nishimoto, T. (2001) Novel G proteins, Rag C and Rag D, interact with GTP-binding proteins, Rag A and Rag B. *J Biol Chem*. 276: 7246-7257.

Semenza, G. L. (1996) Transcriptional regulation by hypoxia-inducible factor-1. *Trends Cardiovasc. Med*. 6: 151-157.

Sepp, T., Yates, J.R., Green, A.J. (1996) Loss of heterozygosity in tuberous sclerosis hamartomas. *J Med Genet.*, 33: 962-964.

Serra, V., Markman, B., Scaltriti, M., Eichhorn, P.J., Valero, V., Guzman, M., Botero, M.L., Llonch, E., Atzori, F., Di Cosimo, S., Maira, M., Garcia-Echeverria, C., Parra, J.L., Arribas, J., Baselga, J. (2008) NVP-BEZ235, a dual PI3K/mTOR inhibitor, prevents PI3K signaling and inhibits the growth of cancer cells with activating PI3K mutations. *Cancer Res*., 68: 8022-8030.

Shami, M.J., Benedict, W.L., Myers, M. (1993) Early manifestation of retinal hamartomas in tuberous sclerosis. *Am J Ophthalmol.*, 115: 539-540.

Shaw, R.J., Bardeesy, N., Manning, B.D., Lopez, L., Kosmatka, M., DePinho, R.A., Cantley, L.C. (2004) The LKB1 tumor suppressor negatively regulates mTOR signalling. *Cancer Cell*, 6: 91-99.

Shaw, R.J., Cantley, L.C. (2006) Ras, PI(3)K and mTOR signalling controls tumour cell growth. *Nature*. 441: 424-430.

Shepherd, C.W., Beard, C.M., Gomez, M.R., Kurland, L.T., Whisnant, J.P. (1991) Tuberous sclerosis complex in Olmsted County, Minnesota, 1950-1989. *Arch Neurol.*, 48: 400-401.

Shepherd, C.W., Gomez, M.R., Lie, J.T., Crowson, C.S. (1991) Causes of death in patients with tuberous sclerosis. *Mayo Clin Proc.,* 66: 792-796.

Shepherd, C.W., Scheithauer, B.W., Gomez, M.R., Altermatt, H.J., Katzmann, J.A. (1991) Subependymal giant cell astrocytoma: A clinical, pathological, and flow cytometric study. *Neurosurgery*, 28: 864-868.

Shigeyama, Y., Kobayashi, T., Kido, Y., Hashimoto, N., Asahara, S., Matsuda, T., Takeda, A., Inoue, T., Shibutani, Y., Koyanagi, M., Uchida, T., Inoue, M., Hino, O., Kasuga, M., Noda, T. (2008) Biphasic response of pancreatic beta-cell mass to ablation of tuberous sclerosis complex 2 in mice. *Mol Cell Biol*., 28: 2971-2979.

Shiota, C., Woo, J.T., Lindner, J., Shelton, K.D., Magnuson, M.A. (2006) Multiallelic Disruption of the rictor Gene in Mice Reveals that mTOR Complex 2 Is Essential for Fetal Growth and Viability. *Dev Cell.*, 11: 583-589.

Simmers, R.N., Mulley, J.C., Hyland, V.J., Callen, D.F., Sutherland, G.R. (1987) Mapping the human α globin gene complex to 16p13.2→pter. *J Med Genet.*, 24: 761-766.

Singal, R., Khurana, V., Caldito, G., Fort, C. (2005) Statins and prostate cancer risk. *J Clin Oncol*., 23: 1004.

Singer, K. (1971) Genetic aspects of tuberous sclerosis in a Chinese population. *Am J Hum Genet.*, 23: 33-40.

Siracusano, S., Zanon, M., D'Aloia, G., Plaino, F., Trombetta, C., Bussani, R. (1998) Rare association of renal angiomyolipoma and oncocytoma. *Urology*, 51: 837-839.

Smalley, S.L., Tanguay, P.E., Smith, M., Gutierrez, G. (1992) Autism and tuberous sclerosis. *J Autism Dev Disord.*, 22: 339-355.

Smalley, S.L. (1998) Autism and tuberous sclerosis. *J Autism Dev Disord*., 28: 407-414.

Smith, H.C., Watson, G.H., Patel, R.G., Super, M. (1989) Cardiac rhabdomyomata in tuberous sclerosis: Their course and diagnostic value. *Arch Dis Child.*, 64: 196-200.

Smolarek, T.A., Wessner, L.L., McCormack, F.X., Mylet, J.C., Menon, A.G., Henske, E.P. (1998) Evidence that lymphangiomyomatosis is caused by TSC2 mutations: Chromosome 16p13 loss of heterozygosity in angiomyolipomas and lymph nodes from women with lymphangiomyomatosis. *Am J Hum Genet.*, 62: 810-815.

Smoliga, J.M., Baur, J.A., Hausenblas, H.A. (2011) Resveratrol and health--a comprehensive review of human clinical trials. *Mol Nutr Food Res*., 55: 1129-1141.

Sogame, Y., Kitamura, A., Yabuki, M., Komuro, S., (2009) A comparison of uptake of metformin and phenformin mediated by hOCT1 in human hepatocytes. *Biopharm Drug Dispos.,* 30: 476-484.

Soliman, G.A. (2013) The role of mechanistic target of rapamycin (mTOR) complexes signaling in the immune responses. *Nutrients*. 5: 2231-2257.

Sparling, J.D., Hong, C.H., Brahim, J.S., Moss, J., Darling, T.N. (2007) Oral findings in 58 adults with tuberous sclerosis complex. *J Am Acad Dermatol.*, 56: 786-790.

Steiner, M.S., Goldman, S.M., Fishman, E.K., Marshall, F.F. (1993) The natural history of renal angiomyolipoma. *J Urol.*, 150: 1782-1786.

Stevenson, A.C., Fischer, O.D. (1956) Frequency of epiloia in Northern Ireland. *Br. J. Prev. Soc. Med*., 10: 134-135.

Stocker, H., Radimerski, T., Schindelholz, B., Wittwer, F., Belawat, P., Daram, P., Breuer, S., Thomas, G., Hafen, E. (2003) Rheb is an essential regulator of S6K in controlling cell growth in Drosophila. *Nat Cell Biol.*, 5: 559-565.

Stumvoll, M., Nurjhan, N., Perriello, G., Dailey, G., Gerich, J.E., (1995) Metabolic effects of metformin in non insulindependent diabetes mellitus. *N Engl J Med*., 333: 550-554.

Su, AI., Wiltshire, T., Batalov, S., Lapp, H., Ching, K.A., Block, D., Zhang, J., Soden, R., Hayakawa, M., Kreiman, G., Cooke, M.P., Walker, J.R., Hogenesch, J.B. (2004) A gene atlas of the mouse and human protein-encoding transcriptomes. *Proc Natl Acad Sci U S A*., 101: 6062-6067.

Suckow, C.E., Stout, D.B. (2008) MicroCT liver contrast agent enhancement over time, dose, and mouse strain. *Mol Imaging Biol*., 10: 114-120.

Summy, J.M., Gallick, G.E. (2006) Treatment for advanced tumors: Src reclaims center stage. *Clin Cancer Res.*, 12: 1398-1401.

Sun, S.Y., Rosenberg, L.M., Wang, X., Zhou, Z., Yue, P., Fu, H., Khuri, F.R. (2005) Activation of Akt and eIF4E survival pathways by rapamycin-mediated mammalian target of rapamycin inhibition. *Cancer Res.*, 65: 7052-7058.

Sun, Z.J., Chen, G., Zhang, W., Hu, X., Liu, Y., Zhou, Q., Zhu, L.X., Zhao, Y.F. (2011) Curcumin dually inhibits both mammalian target of rapamycin and nuclear factor-κB pathways through a crossed phosphatidylinositol 3-kinase/Akt/IκB kinase complex signaling axis in adenoid cystic carcinoma. *Mol Pharmacol*., 79: 106-118.

Taillé, C., Debray, M.P., Crestani, B. (2007) Sirolimus treatment for pulmonary lymphangioleiomyomatosis*. Ann Intern Med*., 146: 687-688.

Tan, D.S., Dumez, H., Olmos, D., Sandhu, S.K., Hoeben, A., Stephens, A.W., Poondru, S., Gedrich, R., Kaye, S.B., Schoffski, P. (2010) First-in-human phase I study exploring three schedules of OSI-027, a novel small molecule TORC1/TORC2 inhibitor, in patients with advanced solid tumors and lymphoma. *J Clin Oncol*., 28: no. 15

Tanihara, Y., Masuda, S., Sato, T., Katsura, T., Ogawa, O., Inui, K., (2007) Substrate specificity of MATE1 and MATE2-K, human multidrug and toxin extrusions/H(+)-organic cation antiporters. *Biochem Pharmacol*., 74: 359-371.

Tapon, N., Ito, N., Dickson, B.J., Treisman, J.E., Hariharan, I.K. (2001) The Drosophila tuberous sclerosis complex gene homologs restrict cell growth and cell proliferation. *Cell*, 105: 345-355.

Taylor, J.R., Ryu, J., Colby, T.V., Raffin, T.A. (1990) Lymphangioleiomyomatosis: Clinical course in 32 patients. *N Engl J Med.*, 323: 1254-1260.

Tee, A.R., Manning, B.D., Roux, P.P., Cantley, L.C., Blenis, J. (2003) Tuberous Sclerosis Complex gene products, Tuberin and Hamartin, control mTOR signaling by acting as a GTPase-activating protein complex toward Rheb. *Curr Biol.*, 13: 1259-1268.

The European Chromosome 16 Tuberous Sclerosis Consortium (1993). Identification and characterization of the tuberous sclerosis gene on chromosome 16. *Cell*, 75: 1305-1315.

Tomasoni, R., Mondino, A. (2011) The tuberous sclerosis complex: Balancing proliferation and survival. *Biochem Soc Trans.*, 39: 466-471.

Torres, V.E., Björnsson, J., King, B.F., Kumar, R., Zincke, H., Edell, E.S., Wilson, T.O., Hattery, R.R., Gomez, M.R. (1995) Extrapulmonary lymphangioleiomyomatosis and lymphangiomatous cysts in tuberous sclerosis complex. *Mayo Clin Proc.*, 70: 641-648.

Tsuchiya, H., Orimoto, K., Kobayashi, T., Hino, O. (1996) Presence of potent transcriptional activation domains in the predisposing tuberous sclerosis (Tsc2) gene product of the Eker rat model. *Cancer Res.*, 56: 429-433.

Tucker, T., Friedman, J.M. (2002) Pathogenesis of hereditary tumors: Beyond the "two-hit" hypothesis. *Clin Genet.*, 62: 345-357.

Tweedale, D.N., Dawe, C.J., McDonald, J.R., Culp, O.S. (1955) Angiolipoleiomyoma of the kidney. Report of a case with observations on histogenesis. *Cancer*, 8: 764-770.

Tworetzky, W., McElhinney, D.B., Margossian, R., Moon-Grady, A.J., Sallee, D., Goldmuntz, E., van der Velde, M.E., Silverman, N.H., Allan, L.D. (2003) Association between cardiac tumors and tuberous sclerosis in the fetus and neonate. *Am J Cardiol.*, 92: 487-489.

Uhlmann, E.J., Wong, M., Baldwin, R.L., Bajenaru, M.L., Onda, H., Kwiatkowski, D.J., Yamada, K., Gutmann, D.H. (2002) Astrocyte-specific TSC1 conditional knockout mice exhibit abnormal neuronal organization and seizures. *Ann Neurol*., 52: 285-296.

Um, S.H., Frigerio, F., Watanabe, M., Picard, F., Joaquin, M., Sticker, M., Fumagalli, S., Allegrini, P.R., Kozma, S.C., Auwerx, J., Thomas, G. (2004) Absence of S6K1 protects against age- and diet-induced obesity while enhancing insulin sensitivity. *Nature*, 431: 200-205.

Urban, T., Kuttenn, F., Gompel, A., Marsac, J., Lacronique, J. (1992) Pulmonary lymphangiomyomatosis: follow-up and long-term outcome with antiestrogen therapy; a report of eight cases. *Chest*, 102: 472-476.

Uzzo, R.G., Libby, D.M., Vaughan Jr., E.D., Levey, S.H. (1994) Coexisting lymphangioleiomyomatosis and bilateral angiomyolipomas in a patient with tuberous sclerosis. *J Urol.*, 151: 1612-1615.

van der Hoeve J. (1920) Eye symptoms in tuberous sclerosis of the brain. *Trans. Ophthalmol. Soc. UK*, 20: 329-334.

van Miltenburg, M.H., Jonkers, J. (2012) Using genetically engineered mouse models to validate candidate cancer genes and test new therapeutic approaches. *Curr Opin Genet Dev*., 22: 21-27.

van Slegtenhorst, M., de Hoogt, R., Hermans, C., Nellist, M., Janssen, B., Verhoef, S., Lindhout, D., van den Ouweland, A., Halley, D., Young, J., Burley, M., Jeremiah, S., Woodward, K., Nahmias, J., Fox, M., Ekong, R., Osborne, J., Wolfe, J., Povey, S., Snell, R.G., Cheadle, J.P., Jones, A.C., Tachataki, M., Ravine, D., Sampson, J.R., Reeve, M.P., Richardson, P., Wilmer, F., Munro, C., Hawkins, T.L., Sepp, T., Ali, J.B., Ward, S., Green, A.J., Yates, J.R., Kwiatkowska, J., Henske, E.P., Short, M.P., Haines, J.H., Jóźwiak, S., Kwiatkowski, D.J. (1997). Identification of the tuberous sclerosis gene TSC1 on chromosome 9q34. *Science*, 277: 805-808.

van Slegtenhorst, M., Nellist, M., Nagelkerken, B., Cheadle, J., Snell, R., van den Ouweland, A., Reuser, A., Sampson, J., Halley, D., van der Sluijs, P. (1998) Interaction between hamartin and tuberin, the TSC1 and TSC2 gene products. *Hum Mol Genet.*, 7: 1053-1057.

Verdu, J., Buratovicht, M.A., Wilder, E.L., Birnbaum, M.J. (1999) Cell-autonomous regulation of cell and organ growth in Drosophila by Akt/PKB. *Nat Cell Biol.*, 1: 500-506.

Verhoef, S., Vrtel, R., Van Essen, T., Bakker, L., Sikkens, E., Halley, D., Lindhout, D., Van Den Ouweland, A. (1995) Somatic mosaicism and clinical variation in tuberous sclerosis complex. *Lancet*, 345: 202.

Verhoef, S., van Diemen-Steenvoorde, R., Akkersdijk, W.L., Bax, N.M., Ariyurek, Y., Hermans, C.J., van Nieuwenhuizen, O., Nikkels, P.G., Lindhout, D., Halley, D.J., Lips, K., van den Ouweland, A.M. (1999) Malignant pancreatic tumour within the spectrum of tuberous sclerosis complex in childhood. *Eur J Pediatr.*, 158: 284-287.

Vézina, C., Kudelski, A., Sehgal, S.N. (1975) Rapamycin (AY-22,989), a new antifungal antibiotic. I. Taxonomy of the producing streptomycete and isolation of the active principle. *J Antibiot (Tokyo)*. 28: 721-726.

Vigneri, P., Frasca, F., Sciacca, L., Pandini, G., Vigneri, R. (2009) Diabetes and cancer. *Endocr. Relat. Cancer*. 16: 1103-1123.

Vinters, H.V. and Miyata, H. (2006) Neuropathologic features of tuberous sclerosis, in Russell and Rubinstein's Pathology of Tumors of the Nervous System, 7th edn (eds R.E. McLendon, M.K. Rosenblum, and D.D. Bigner), Hodder Arnold, London, UK, pp. 955-969.

Vivanco, I., Sawyers, C.L. (2002) The phosphatidylinositol 3-kinase-AKT pathway in human cancer. *Nat Rev Cancer.*, 2: 489-501.

Vogt, H. (1908) Diagnostik der tuberosen sklerose. *Zeitschrift fur die Erforschung und Behandlung des jugendlichen Schwachsinns auf Wissenschaftlicher Grundlage*, 2: 1-16.

Vogt, H. (1908) Pathologie und pathologischen Anatomie der verschiedenen Idiotieform. *Monatsschr. Psychiatr. Neurol*. 24: 106-150.

Vogt, P.K. (2001) PI 3-kinase, mTOR, protein synthesis and cancer. *Trends Mol Med.*, 7: 482-484.

Von Recklinghausen F. (1862) Ein Herz von einem Neugeborenen welches mehrere Theils nach aussen, Theils nach den hohlen prominirende Tumoren (Myomen) trug. Verb Ges Geburtsh 25 Marz, *Monatsschr Geburskd*, 20: 1-2.

Wallace, D.P., Hou, Y.P., Huang, Z.L., Nivens, E., Savinkova, L., Yamaguchi, T., Bilgen, M. (2008) Tracking kidney volume in mice with polycystic kidney disease by magnetic resonance imaging. *Kidney Int.,* 73: 778-781.

Walrath, J.C., Hawes, J.J., Van Dyke, T., Reilly, K.M. (2010) Genetically engineered mouse models in cancer research. *Adv Cancer Res*., 106: 113-164.

Webb, D.W., Clarke, A., Fryer, A., Osborne, J.P. (1996) The cutaneous features of tuberous sclerosis: A population study. *Br J Dermatol.*, 135: 1-5.

Webb, D.W., Fryer, A.E., Osborne, J.P. (1996) Morbidity associated with tuberous sclerosis: A population study. *Dev Med Child Neurol.*, 38: 146-155.

Weber, S.M., Peterson, K.A., Durkee, B., Qi, C., Longino, M., Warner, T., Lee, F.T. Jr., Weichert, J.P. (2004) Imaging of murine liver tumor using microCT with a hepatocyte-selective contrast agent: accuracy is dependent on adequate contrast enhancement. *J Surg Res*., 119: 41-45.

Weiner, D.M., Ewalt, D.H., Roach, E.S., Hensle, T.W. (1998) The tuberous sclerosis complex: A comprehensive review. *J Am Coll Surg*., 187: 548-561.

Wenger, R. H., Gassmann, M. (1997) Oxygen(s) and the hypoxia-inducible factor-1. *Biol. Chem*., 378: 609-616.

Wiederholt, W.C., Gomez, M.R., Kurland, L.T. (1985) Incidence and prevalence of tuberous sclerosis in Rochester, Minnesota, 1950 through 1982. *Neurology*, 35: 600-603.

Wienecke, R., Konig, A., DeClue, J.E. (1995) Identification of tuberin, the tuberous sclerosis-2 product tuberin. Possesses specific Rap1GAP activity. *J Biol Chem.*, 270: 16409-16414.

Wienecke, R., Maize, J.C. Jr, Shoarinejad, F., Vass, W.C., Reed, J., Bonifacino, J.S., Resau, J.H., de Gunzburg, J., Yeung, R.S., DeClue, J.E. (1996) Co-localization of the TSC2 product tuberin with its target Rap1 in the Golgi apparatus. *Oncogene*, 13: 913-923.

Wienecke, R., Fackler, I., Linsenmaier, U., Mayer, K., Licht, T., Kretzler, M. (2006) Antitumoral activity of rapamycin in renal angiomyolipoma associated with tuberous sclerosis complex. *Am J Kidney Dis*., 48: e27-29.

Wilson, C., Idziaszczyk, S., Parry, L., Guy, C., Griffiths, D.F., Lazda, E., Bayne, R.A., Smith, A.J., Sampson, J.R., and Cheadle, J.P. (2005) A mouse model of tuberous sclerosis 1 showing background specific early post-natal mortality and metastatic renal cell carcinoma. *Hum. Mol. Genet*., 14: 1839-1850.

Wilson, C., Bonnet, C., Guy, C., Idziaszczyk, S., Colley, J., Humphreys, V., Maynard, J., Sampson, J.R., Cheadle, J.P. (2006) Tsc1 haploinsufficiency without mammalian target of rapamycin activation is sufficient for renal cyst formation in Tsc1+/- mice. *Cancer Res.,* 66: 7934-7938.

Wong, A.L., McGeorge, A., Clark, A.H. (1981) Renal angiomyolipoma: a review of the literature and a report of 4 cases. *Br J Urol.*, 53: 406-411.

Woodrum, C., Nobil, A., Dabora, S.L. (2010) Comparison of three rapamycin dosing schedules in A/J Tsc2+/- mice and improved survival with angiogenesis inhibitor or asparaginase treatment in mice with subcutaneous tuberous sclerosis related tumors. *J Transl Med*., 8: 14.

Woods, A., Johnstone, S.R., Dickerson, K., Leiper, F.C., Fryer, L.G., Neumann, D., Schlattner, U., Wallimann, T., Carlson, M., Carling, D. (2003) LKB1 is the upstream kinase in the AMP-activated protein kinase cascade. *Curr Biol*., 13: 2004-2008.

Wortmann, S.B., Reimer, A., Creemers, J.W., Mullaart, R.A. (2008) Prenatal diagnosis of cerebral lesions in Tuberous sclerosis complex (TSC). Case report and review of the literature. *Eur J Paediatr Neurol.*, 12: 123-126.

Wright, J.L., Stanford, J.L. (2009) Metformin use and prostate cancer in Caucasian men: results from a population-based case-control study. *Cancer Causes Control*, 20: 1617-1622.

Wullschleger S, Loewith R, Hall MN. (2006) TOR signaling in growth and metabolism. *Cell*. 124: 471-484.

Xiao, G.H., Shoarinejad, F., Jin, F., Golemis, E.A., Yeung, R.S. (1997) The tuberous sclerosis 2 gene product, tuberin, functions as a Rab5 GTPase activating protein (GAP) in modulating endocytosis. *J Biol Chem.*, 272: 6097-6100.

Yamakado, K., Tanaka, N., Nakagawa, T., Kobayashi, S., Yanagawa, M., Takeda, K. (2002) Renal angiomyolipoma: Relationships between tumor size, aneurysm formation, and rupture. *Radiology*, 225: 78-82.

Yan, L., Mieulet, V., Lamb, R.F. (2008) mTORC2 is the hydrophobic motif kinase for SGK1. *Biochem J.*, 416: e19-21.

Yang, B., Chen, W.H., Shi, P.Z., Xiang, J.J., Xu, R.J., Liu, J.H. (2008) Coincidence of hepatocelluar carcinoma and hepatic angiomyolipomas in tuberous sclerosis complex: A case report. *World J Gastroenterol.*, 14: 812-814.

Yang, J., Kalogerou, M., Gallacher, J., Sampson, J.R., Shen, M.H. (2012) Renal tumours in a *Tsc1*$^{+/-}$ mouse model show epigenetic suppression of organic cation transporters Slc22a1, Slc22a2 and Slc22a3, and do not respond to metformin. *Eur J Cancer.,* 49: 1479-1490.

Yap, T.A., Garrett, M.D., Walton, M.I., Raynaud, F., de Bono, J.S., Workman, P. (2008) Targeting the PI3K-AKT-mTOR pathway: progress, pitfalls, and promises. *Curr Opin Pharmacol*., 8: 393-412.

Yates, J.R., Van Bakel, I., Sepp, T., Payne, S.J., Webb, D.W., Nevin, N.C., Green, A.J. (1997) Female germline mosaicism in tuberous sclerosis confirmed by molecular genetic analysis. *Hum Mol Genet.*, 6: 2265-2269.

Yates, J.R. (2004) Tuberous sclerosis. *Eur. J. Hum. Genet*., 14: 1065-1073.

Yeung, R.S., Buetow, K.H., Testa, J.R., Knudson, A.G. Jr. (1993) Susceptibility to renal carcinoma in the Eker rat involves a tumor suppressor gene on chromosome 10, *Proc. Natl. Acad. Sci. U. S. A*., 90: 8038-8042.

Yeung, R. S., Xiao, G.H., Jin, F., Lee, W.C., Testa, J. R., Knudson, A.G. (1994) Predisposition to renal cell carcinoma in the Eker rat is determined by germline mutation ofthe tuberous sclerosis 2 (TSC2) gene. *Proc. NatI. Acad. Sci. USA*, 91: 11413-11416.

Yeung, R.S., Xiao, G.H., Everitt, J.I., Jin, F., Walker, C.L. (1995) Allelic loss at the tuberous sclerosis 2 locus in spontaneous tumors in the Eker rat. *Mol Carcinog.*, 14: 28-36.

Yeung, R.S., Katsetos, C.D., Klein-Szanto, A. (1997) Subependymal astrocytic hamartomas in the Eker rat model of tuberous sclerosis. *Am J Pathol*., 151: 1477-1486.

Yonezawa, A., Inui, K. (2011) Importance of the multidrug and toxin extrusion MATE/SLC47A family to pharmacokinetics, pharmacodynamics/toxicodynamics and pharmacogenomics. *Br J Pharmacol.*, 164: 1817-1825.

Young, J.M., Burley, M.W., Jeremiah, S.J., Jeganathan, D., Ekong, R., Osborne, J.P., Povey, S. (1998) A mutation screen of the TSC1 gene reveals 26 protein truncating mutations and 1 splice site mutation in a panel of 79 tuberous sclerosis patients. *Ann Hum Genet.*, 62: 203-213.

Yu, J., Astrinidis, A., Howard, S., Henske, E.P. (2004) Estradiol and tamoxifen stimulate LAM-associated angiomyolipoma cell growth and activate both genomic and nongenomic signaling pathways. *Am J Physiol Lung Cell Mol Physiol.*, 286: L694-700.

Yu, J., Henske, E.P. (2010) mTOR activation, lymphangiogenesis, and estrogen-mediated cell survival: the "perfect storm" of pro-metastatic factors in LAM pathogenesis. *Lymphat Res Biol*., 8: 43-49.

Yu, K., Toral-Barza, L., Shi, C., Zhang, W.G., Lucas, J., Shor, B., Kim, J., Verheijen, J., Curran, K., Malwitz, D.J., Cole, D.C., Ellingboe, J., Ayral-Kaloustian, S., Mansour, T.S., Gibbons, J.J., Abraham, R.T., Nowak, P., Zask, A. (2009) Biochemical, cellular, and in vivo activity of novel ATP-competitive and selective inhibitors of the mammalian target of rapamycin. *Cancer Res*., 69: 6232-6240.

Yu,Y., Yoon, S.O., Poulogiannis, G., Yang, Q. (2011) Phosphoproteomic analysis identifies Grb10 as an mTORC1 substrate that negatively regulates insulin signalling. *Science*, 332: 1322-1326.

Zakikhani, M., Dowling, R., Fantus, I.G., Sonenberg, N., Pollak, M., (2006) Metformin is an AMP kinase-dependent growth inhibitor for breast cancer cells. *Cancer Res*., 66: 10269-10273.

Zakikhani, M., Dowling, R.J., Sonenberg, N., Pollak, M.N. (2008) The effects of adiponectin and metformin on prostate and colon neoplasia involve activation of AMPactivated protein kinase. *Cancer Prev Res (Phila)*, 1: 369-375.

Zakikhani, M., Blouin, M.J., Piura, E., Pollak, M.N. (2010) Metformin and rapamycin have distinct effects on the AKT pathway and proliferation in breast cancer cells. *Breast Cancer Res Treat.,* 123: 271-279.

Zaremba, J. (1968) Tuberous sclerosis: a clinical and genetical investigation. *J Ment Defic Res.*, 12: 63-80.

Zeng, L.H., Xu, L., Gutmann, D.H., Wong, M. (2008) Rapamycin prevents epilepsy in a mouse model of tuberous sclerosis complex. *Ann Neurol.*, 63: 444-453.

Zeng, Z., Sarbassov, D.D., Samudio, I.J., Yee, K.W., Munsell, M.F., Jackson, C.E., Giles, F.J., Sabatini, D.M., Andreeff, M., Konopleva, M. (2007) Rapamycin derivatives reduce mTORC2 signaling and inhibit AKT activation in AML. *Blood*, 109: 3509-3512.

Zerban, H., Nogueira, E., Riedasch, G., Bannasch, P. (1987) Renal oncocytoma: Origin from the collecting duct. *Virchows Arch B Cell Pathol Incl Mol Pathol.*, 52: 375-387.

Zhang, H., Stallock, J.P., Ng, J.C., Reinhard, C., Neufeld, T.P. (2000) Regulation of cellular growth by the Drosophila target of rapamycin dTOR. *Genes Dev.*, 14: 2712-2724.

Zhang, H., Cicchetti, G., Onda, H., Koon, H.B., Asrican, K., Bajraszewski, N., Vazquez, F., Carpenter, C.L., Kwiatkowski, D.J. (2003) Loss of Tsc1/Tsc2 activates mTOR and disrupts PI3K-Akt signaling through downregulation of PDGFR. *J Clin Invest*, 112: 1223-1233.

Zhang, Y.J., Duan, Y., Zheng, X.F. (2011) Targeting the mTOR kinase domain: the second generation of mTOR inhibitors. *Drug Discov*., 16: 325-331.

Zhang, Z., Li, W., Blatner, N.R., Dennis, K.L., Procissi, D., Khazaie, K., Larson, A.C. (2013) Quantitative magnetic resonance imaging in the transgenic APC δ468 mouse model of hereditary colon cancer. *Mol Imaging.*, 12: 59-66

Zhou, G., Myers, R., Li, Y., Chen, Y., Shen, X., Fenyk-Melody, J., Wu, M., Ventre, J., Doebber, T., Fujii, N., Musi, N., Hirshman, M.F., Goodyear, L.J., Moller, D.E., (2001) Role of AMP-activated protein kinase in mechanism of metformin action. *J Clin Invest*., 108: 1167-1174.

Zhou, H.Y., Huang, S.L. (2012) Current development of the second generation of mTOR inhibitors as anticancer agents. *Chin J Cancer*., 31: 8-18.

Zick, Y. (2001) Insulin resistance: A phosphorylation-based uncoupling of insulin signalling. *Biochem Soc Trans.*, 11: 437-441.

Zoncu, R., Efeyan, A., Sabatini, D.M. (2011) MTOR: From growth signal integration to cancer, diabetes and ageing. *Nat Rev Mol Cell Biol.*, 12: 21-35.

Zou, Z.Q., Zhang, X.H., Wang, F., Shen, Q.J., Xu, J., Zhang, L.N., Xing, W.H., Zhuo, R.J., Li, D. (2009) A novel dual PI3Kalpha/mTOR inhibitor PI-103 with high antitumor activity in non-small cell lung cancer cells. *Int J Mol Med*., 24: 97-101.